Electronic control of a semiconductor laser for an optical fibre packet LAN

Abdelkader, Hamid Ibrahim

Award date:
1988

Awarding institution:
University of Bath

ELECTRONIC CONTROL OF A SEMICONDUCTOR LASER FOR AN OPTICAL FIBRE PACKET LAN

Submitted by Hamid Ibrahim Abdelkader

for the degree of Ph.D. of the

University of Bath

May 1988

ProQuest LLC
789 East Eisenhower Parkway
P.O. Box 1346
Ann Arbor, MI 48106-1346

ACKNOWLEDGMENTS

I would like to express my deep gratitude to Mr. J. D. Martin for his continuous guidance, support, help, invaluable contribution and supervision. Also, I would like to express my thanks to Professor T. Rozzi, Dr. R. F. Ormondroyd, Dr. J. Sarma, Dr. E. Whipp, and the technical staff in the Department of Electrical Engineering for their co-operation.

Finally, I express my sincere gratitude to the Egyptian Government for granting me the scholarship and to the ORS committee for awarding me the ORS grant.

SUMMARY

The aim of this work is to control the optical output power emitted from a semiconductor laser, when used as a light source for an optical fibre Local Area Network (LAN). The work is divided into three main stages. In the first stage a laser diode drive circuit which modulates the laser in packet form at bit rates up to 250 Mbit/s has been designed, implemented and tested.

In the second stage a circuit has been implemented to control the average temperature of the laser diode and used to draw the light–current characteristics of a laser at different temperatures. A novel practical method has been used to measure the rise in temperature of the laser diode during the packet duration, its thermal rise time has been estimated and the results obtained experimentally have been compared with the theoretical values.

In the last stage a new strategy has been presented, analysed and used to control the optical output power of the laser diode against the effects of temperature variations and ageing, when operated in a burst mode. The control strategy is based on using two feedback control loops to stabilise the average and maximum values of optical output power during the packet duration. The control circuitry has been implemented and tested, control has been exerted and the results discussed.

CONTENTS

Page No.

PRINCIPAL SYMBOLS

η	Efficiency of photodiode
R	Responsivity of the photodiode
λ_0	Zero dispersion wavelength
υ	Frequency of light
S/N	The signal to noise ratio
I_p	Photodiode current
P_{min}	The minimum detectable optical power
I_m	LD modulation current
I_{th}	LD threshold current
η_1	LD spontaneous slope efficiency
η_2	LD stimulated slope efficiency
L_{min}	The minimum optical power of the LD
L_{av}	The average optical power of the LD
L_{max}	The maximum optical power of the LD
$\bar{\Delta T}$	Average rise in temperature of the laser chip during the packet duration
V_{br}	The reference voltage in the average power control loop
V_{mr}	The reference voltage in the maximum power control loop

CHAPTER 1

OPTICAL FIBRE COMMUNICATION SYSTEMS

1.1 Optical Fibre Communication

Many forms of communication system have appeared over the years, the principal motivation behind each new one was either to improve the transmission fidelity, to increase the data rate so that more information could be sent, or to increase the transmission distance between relay stations.

The amount of information that can be transmitted is directly related to the frequency range over which the carrier wave operates. Increasing the carrier frequency theoretically increases the available transmission bandwidth and consequently provides a larger information capacity; so employing a higher frequency carrier offers a corresponding increase in bandwidth. The high frequency of the optical region, which is in the range of $5x10^{11}$ Hz, can be utilised to increase transmission capacity. Lightwave systems have therefore an information capacity which exceeds that of microwave by a factor of 10^5, which encourages the use of the optical region in communication, although it will be some time before these large capacities can be realised. With the development of the laser, atmospheric optical communication was investigated, but because of the limitations imposed by rain, fog, snow and dust, atmospheric attenuation might be a few dB/Km and this high speed system is economically unattractive. These limitations diverted attention towards using glass fibre as a waveguide but the problem at this time was the optical attenuation in fibre which had a figure of 1000dB/km at the visible wavelengths. By seeking ways to eliminate the absorbing impurities from the fibre, glass manufacturers succeeded in reducing the attenuation to a level of

20dB/km in 1970, 2dB/km by 1975, 0.5dB/km in 1979 and 0.2dB/km in 1979. These later developments allow optical signals to be transmitted over a long distance of fibre.

The losses in the fibres are found to be minimum at three wavelengths, 0.85μm, 1.33μm and 1.55μm; so fibres, light sources and photodetectors, which are the essential elements of a communication system, are fabricated to operate in these regions.

Beside the enormous potential transmission bandwidth of optical fibre systems, they have other advantages over electrical communication systems such as:

1. Immunity to electromagnetic interference because of the dielectric nature of the fibre material.

2. Fibre to fibre cross talk is very low and a high degree of security is afforded.

3. Low attenuation of fibres leads to an increase in the distance between repeaters which brings the cost down.

4. Optical fibres have very small diameter, they are far smaller in size and much lighter than the corresponding copper cables.

5. Silica is the principal material in the fabrication of fibres and it exists abundantly in nature.

Fibre connectors and couplers are now readily available, so that local networks can be built up possessing the above advantages, and are becoming competitive

when compared with coaxial cable networks at high data rates (>100Mbit/s).

1.2 Elements of an Optical Fibre Communication System

The simplest communication system is the point to point transmission link shown in Figure 1.1, which comprises a transmitter at one end of the fibre and a receiver at the other end.

The transmitter consists of light source which launches the optical power into the fibre, and its associated drive circuitry. The light source can be either a light emitting diode (LED) or a laser diode (LD), both of which are dimensionally compatible with the fibre.

The receiver consists of a photodiode plus amplification and signal restoring circuitry. Semiconductor PIN photodiode and avalanche photodiode (APD) are the two principal photodetectors used in fibre optic links, both device types possessing high efficiency and high response speed. The signal restoring circuitry bandlimits the received signal and then compares its magnitude with a decision threshold value.

The optical fibre is contained inside a cable which offer a mechanical and environmental protection to the fibre which can be either a multimode fibre or a single mode fibre.

The point to point transmission link sets the basis for more complex system architecture, and enables certain design parameters to be defined (section 1.3). In many cases the fibre system is a multi-port network, but since only one transmitter can be active at any time, calculations follow those for a point-to-point link (section 1.3).

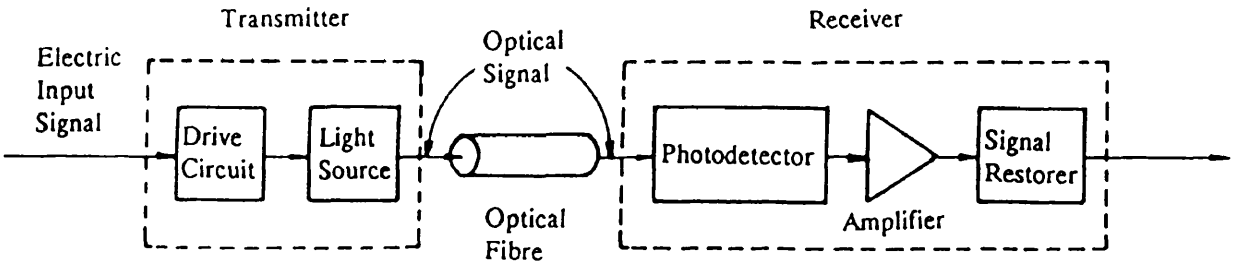

Figure 1.1 Elements of optical fibre communication system

1.3 Optical Fibre Digital Communication System Considerations

In an optical fibre system the digital signals from the information source are suitably encoded for optical transmission, the transmitted signals consist of zeros and ones, randomly distributed, and are used to switch a light source off and on. Light from the source is coupled into the optical fibre, transmitted through it by total internal reflection at the core cladding interface, to emerge attenuated at the far end where it impinges upon a photodetector which converts the light photons to electron-hole pairs in the semiconductor material. These in turn, under the influence of the bias field applied to the detector, give rise to an electric current which then activates a decision circuit whose task is to decide whether the received signal corresponds to a zero or a one.

For a given set of components and a given set of system requirements a power budget analysis is required to determine whether the receiver signal power is adequate or if repeaters are needed. A rise time analysis is required also to verify that the overall system performance requirements are met.

To make more efficient use of the fibre transmission medium, more complex link architectures such as multiterminal data bus networks and multi-channel wavelength division multiplexing systems can be used, which can introduce limitations like crosstalk and reflections that are not present in the simple point to point links.

A coding scheme has to be used that is suitable for digital data transmission over optical fibres. The coding scheme is used to introduce randomness and redundancy into the digital information stream to ensure efficient timing recovery and to facilitate error monitoring at the receiver, as well as minimising the zero frequency component.

In carrying out a link power budget the first thing to be decided is at which wavelength to transmit and then to choose the components operating in this region. If the distance over which the data to be transmitted is not too far it is possible to operate in the wavelength 0.8–0.9μm region, but if the transmission distance is relatively long, it is possible to take advantage of the lower attenuation and dispersion that occurs at wavelengths around 1.3μm. Having decided on the wavelength, the system performance of the three major optical link building blocks, the receiver, transmitter and optical fibre can be interrelated by choosing the characteristics of two of these elements and then computing those of the third to verify the system requirements. The receiver is discussed in section 1.3.1, the transmitter in 1.3.2 and the fibre in section 1.3.3. Link power budget and rise–time budget are then considered in sections 1.3.4 and 1.3.5.

1.3.1 Optical receiver considerations

The functions of an optical receiver are detection of the incoming signal, amplification, pulse shaping (equalisation) if necessary, timing extraction, decision and error detection or correction.

The light detector is a photodiode of either PIN type or avalanche type (APD). A PIN photodiode receiver is simpler, more stable with changes in temperature, and less expensive than the avalanche photodiode receiver. On the other hand, PIN photodiodes may be overruled by the increased sensitivity of the APD if very low optical power levels are to be detected.

Since overall system performance is determined largely by the minimum detectable optical power at the receiver[1.1,1.2,1.3], then in choosing a particular photodetector, it is required to determine the minimum detectable optical power that must fall on the photodetector to satisfy the bit error rate requirement at the

specified data rate. The input optical power required at the receiver is a function of the detector combined with the electrical components within the receiver structure, and is strongly dependent upon the noise associated with the receiver. There are three main noise sources in the system: thermal noise, quantum noise and dark current noise. Thermal noise arises from the photodiode load resistor and the amplifier which follow it; quantum noise arises from the random fluctuation in the rate at which photons arive at the photodiode; and the dark current is the small reverse leakage current that flows from the photodiode terminals when there is no optical power incident on it.

Although the transmitted signal consists of two well-defined light levels, in the presence of noise the signal at the receiver is not as well defined. Figure (1.2a) shows a binary signal in the presence of noise, and Figure (1.2b) describes the probabilities that the output voltage (V) of the photodetector has a value within the incremental range dV of the signal in the two transmitted states, namely 0 and 1, indicated by $P_0(X)$, $P_1(X)$ respectively. If the additive noise is assumed to have Gaussian distribution[1.4] where the Gaussian probability density function is P(X) is given by:

$$P(X) = \frac{1}{\sigma \sqrt{2\pi}} \text{EXP} - [(X - m)^2/2\sigma^2] \qquad 1.1$$

where m is the mean value and σ is the standard deviation of the distribution which corresponds to the rms value of the noise voltage. If a decision threshold D is set between the two signal states as indicated in figure 1.2b and if the noise voltage is sufficiently large, it can either decrease a binary one to a zero or increase a binary zero to a one. The error probabilities can be evaluated and related the signal to noise ratio, hence the average optical power required at the receiver to achieve a prescribed bit error rate can be calculated. This average

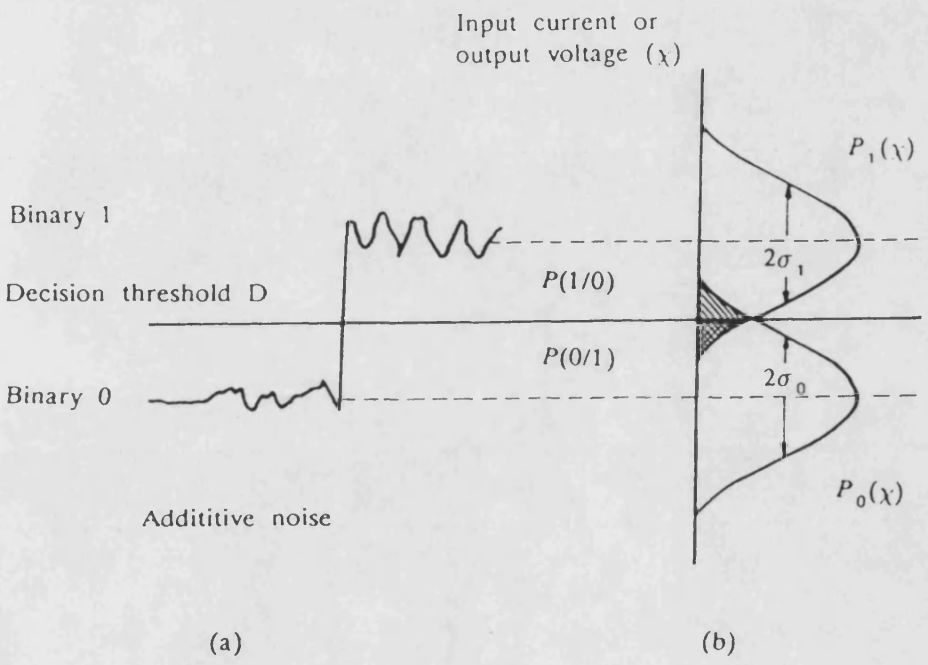

Figure 1.2 Binary transmission:

a) the binary signal with additive noise;
b) probability density functions for the binary signal showing the decision case. P(0/1) is the probability of falsely identifying a binary one and $P(1/O)$ is the probability of falsely identifying a binary zero.

power is given by[1.5]:

$$P_{av} = \frac{q}{2RT}\left[Q^2M^X I_2 + \frac{2Q}{M} Z^2\right] \qquad 1.2$$

where I_2 is a constant depending on the received and desired output pulse shapes normalised with respect to the bit period T [1.1]. The constant Q relates the required signal power to the bit error rate where Q = 6 for a 10^{-9} bit error rate, M is the APD gain (for a PIN photodiode M = 1) while X is the APD excess noise component, R is the primary responsivity of the photodiode and q is the electron charge. Z is a dimensionless parameter representing the signal independent noise of both the receiver pre-amplifier and photodetector.

Since the bit error rate is a sensitive function of the received signal power, it follows that the transmitted power must carefully be controlled to ensure that the required minimum received power is present at all times.

1.3.2 Optical transmitter Considerations

Light emitting diodes and semiconductor injection lasers of various types are the most suitable optical sources; they can be directly modulated and are fairly efficient, particularly the laser.

In deciding between the use of an LED or a laser diode one has to consider the coupled power output, spectral width and signal dispersion, response, data rate, linearity, temperature sensitivity and cost.

Power output is very important in long haul communications, but a high power output is also required in a multi-port fibre network (section 1.4) in order

to overcome the splitting losses.

The laser diode is superior to the LED as it typically has a 10 to 1 advantage in power output with a 4 to 1 improvement in directivity coefficient, representing a difference in coupling efficiency of approximately 15–20dB [1.6]. A pigtail or a connector bushing provides the best way to obtain the highest output coupling efficiency.

A power output ranging from 2mW to 20mW can be launched into pigtail multimode fibre from semiconductor laser, while 100μW can be launched by LED into the same size pigtail fibre.

The optical transmitter is required to emit constant peak power into the fibre during its operating lifetime regardless of operating temperature. Using a semiconductor laser as light source presents problems to the system designers, since the laser is a device that has a threshold current which is a sensitive function of temperature, also the slope of the stimulated emission part of its light–current characteristics may vary due to aging, is not always linear and can exhibit kinks [1.7]. Eventually some control circuit is required to stabilise the optical output power from the laser diode and to compensate for these effects.

The spectral width of the laser output is much narrower than that of an LED, which is important in the wavelength region 0.8–0.9μm where the spectral width of an LED (~50nm) and the dispersion characteristics of silica fibres limit the data–rate–distance to around 150(Mbit/s)Km, for higher values up to 2500(Mbit/s)Km a laser must be used. At wavelengths around 1.3μm, a bit–rate–distance product of at least 1500(Mbit/s)Km is achievable with an LED since most fibres have zero dispersion at 1.3μm. For a laser this figure is in excess of 25(Gbit/s)Km.

Finally, the laser oscillation does not commence at the same time as the drive current pulse is applied but is subject to a switch-on delay period. For high bit rate the device has to be biased near threshold and then a separate current pulse applied to modulate the light output. The advantages of this approach are lower pulse drive currents and lower switch-on delay but the penalty is paid of higher power consumption, higher operating temperature and larger extinction ratio since the device emits significant power into the fibre during the 'off' period [1.8].

Summarising therefore, an LED is the first choice for a low-cost transmission system of any kind; but a semiconductor laser diode is necessary if higher power and/or high data rate is required.

1.3.3 Optical fibre considerations

In an optical fibre system the information is transmitted as a modulated beam of light which propagates through a fibre. Fibre attenuation and dispersion are important parameters that should be considered when choosing the optical fibre but the nature of the fibre also influences the coupling efficiency between light source and fibre.

Attenuation reduces the power margin between transmitter and receiver, hence it limits the amplitude of the signal and determines the distance over which a signal can be transmitted without becoming indistinguishable from noise. The lowest fibre attenuation approaches the limit imposed by Rayleigh scattering which is a function of the variation of molecular density of the fibre material and varies with the reciprocal of the fourth power of wavelength [1.6,1.9]. These attenuation limits are 2.1dB/Km at 0.8μm wavelength, about 0.3dB/Km at 1.3μm and 0.15dB/Km at 1.55μm.

In addition to the fibre attenuation, connector and splice losses, cabling losses as well as environmentally-induced losses should be considered.

Dispersion widens the transmitted pulse along the fibre and consequently generates interference between successive pulses, limiting the bandwidth of the signal and the number of bits of information that can be transmitted[1.10]. The bandwidth of multimode fibre is primarily controlled by two mechanisms. Modal delay spread due to the difference in the group delay of different waveguide modes (rays), where a ray travelling at an angle θ_{int} relative to the fibre axis takes $1/\cos(\theta_{int})$ longer to travel an axial distance than does a ray travelling along the axis.

The maximum delay difference is:

$$\Delta T_{max} = \frac{\Delta n_c}{C} \text{ ns/Km} \qquad 1.3$$

where Δ is the refractive index difference between core and cladding of the fibre, n_c is the core refractive index, C is the speed of light in free space. For Δ = 0.01, n_c = 1.5, ΔT_{max} = 50ns/Km.

Minimising this delay increases the bandwidth of fibre, and can be done by reducing the diameter of fibre core until only one mode will propagate, corresponding to the axial ray through the fibre. These single-mode fibres, have a core diameter of about 5μm for 0.85μm wavelength, and a core of 9μm for 1.3μm wavelength. A less effective method of reducing dispersion is by using graded index multimode fibre which has a refractive index that decreases gradually in a direction perpendicular to the fibre axis such that different modes propagating in such a fibre have nearly equal delay. This fibre has a bandwidth two orders of magnitude greater than that of a step index fibre.

The other factor affecting the bandwidth of a fibre is the material dispersion which is due to the variation of group velocity with wavelength. This causes pulse spreading in fibres driven by incoherent sources such as an LED. At 0.8μm an LED of spectral width 50nm will cause a pulse spreading of 5ns/Km or a modulation bandwidth product of 50-100MHz.Km. There is a null material dispersion near 1.3μm which allows for broad bandwidth transmission over long distance.

The optical power that can be coupled into a fibre depends on the core-cladding refractive index difference Δ, which in turn relates to the numerical aperture. As Δ increases the fibre coupled-power increases correspondingly, however, since dispersion becomes greater with increasing Δ, a trade off must be made between the optical power that can be launched into the fibre and the maximum tolerable dispersion. With LED sources multimode fibre has to be used since very little optical power can be coupled into a fibre from an LED. With an LD either a single-mode or a multimode fibre can be used, and with a single mode fibre a bit rate distance product of 30(Gb/s)Km is achievable. A disadvantage of single mode fibre is that the small core size 5 to 16μm in diameter reduces the coupling efficiency and makes fibre splicing more difficult than for multimode fibre having 50μm core diameter.

1.3.4 Link power budget

In a point to point optical fibre link, the optical power received at the photodetector depends on the amount of light coupled into the fibre, and the losses occurring in the fibre, connectors and splices. The link loss budget is derived from the sequential loss contributions of each element in the link. In addition to the link loss a link power margin is normally provided in the analysis to allow for component aging, temperature fluctuations and losses arising from components that

might be added in the future. The optical power loss (P_T) that is allowed between the light source and the photodetector is given for instance by:

$$P_T = 2L_c + \alpha_F L + \text{system margin dB}$$

where L_c is the connector loss, α_f is the fibre attenuation in dB/Km and L is the transmission distance. The fibre cable is assumed to have connectors only on the ends and none in between. The splice loss is incorporated into the cable loss, and the system margin is nominally taken at 6dB for systems that are not expected to have additional components incorporated into the link in the future. Any reduction in the transmitted power due to poor control, reduces the system margin at the receiver and hence power control at the transmitter is an important part of system design.

1.3.5 Rise time budget

To determine the dispersion limitation of a digital optical fibre link a rise time budget analysis is required to be done. The total rise time of the link t_{sys} is the root-sum-square of the rise times from each contributor (t_i) to the pulse rise time degradation.

$$t_{sys} = \left[\sum_{i=1}^{N} t_i^2 \right]^{1/2} \qquad 1.4$$

The four basic elements that may significantly limit the system speed are the transmitter rise time t_{tx}, the material dispersion rise time of the fibre, the modal dispersion rise time t_{mod} and the receiver rise time. Generally, the total transmission time degradation of a digital link should not exceed 70% of a non-return to zero (NRZ) bit period or 35% of a return to zero (RZ) bit period

[1.11].

The transmitter rise time is attributed to the light source and its drive circuit. The receiver rise time results from the photodetector response and the -3dB electric bandwidth of the receiver B_{rx}. The receiver front end rise time is given by the standard empirical formula[1.12].

$$t_{rx} = \frac{0.35}{B_{rx}} \qquad 1.5$$

For multimode fibre the rise time depends on modal and material dispersion. The rise time due to modal dispersion is given by[1.13]:

$$t_{mod} = \frac{0.44\ L^q}{B_0} \qquad 1.6$$

where L is the link length in Km, B_0 is the bandwidth of 1Km of the fibre cable, $q = 0.7$.

The total system rise time is:

$$t_{sys} = \left[t_{tx}^2 + D^2\sigma_\lambda^2\ L^2 + \left[\frac{0.44\ L^q}{B_0}\right]^2 + \left[\frac{0.35}{B_{rx}}\right]^2 \right]^{1/2} \qquad 1.7$$

where the rise time due to material dispersion = $D\sigma_\lambda L$; σ_λ is the spectral width of the optical source, D is the material dispersion factor of the fibre D = 0.07 ns/(nm.Km) at 0.8μm wavelength but is negligible at 1.3μm region.

1.4 Local Area Networks (LANs)

The wide bandwidth of optical fibre systems makes it possible to multiplex a very large number of channels over a single fibre. Fibre systems were primarily used for point to point links which are suitable for applications where stations can be divided into groups, and stations in one group communicate only with stations in another group. Data generated in one group are then multiplexed at one end and demultiplexed at the other end. If all the stations to communicate with each other then a multi-port network is needed.

A LAN is a communications network connecting a number of users within a local geographical area. The ideal LAN would be an information distribution system that is as easy to use as the conventional ac power distribution system in a building, so that adding a data terminal should require nothing more than plugging it into a conveniently located access port. Once plugged in it should communicate intelligently with any other device on the network.

A number of physically separated terminals can communicate with one another through data bus architectures which are alternatives to point to point links. These architectures can also be used to allow terminals to gain access efficiently to a variety of wide band information services.

There are three general classes of optical data buses, the star or radial configuration shown in Figure 1.3a and the in-line or T-coupler bus in Figure 1.3b and the ring shown in Figure 1.3c.

The choice of a bus network topology (star, ring or open T-bus) depends ultimately on the particular application. Bidirectional T-taps for transmission and reception are difficult to implement with low loss and the passive star configuration

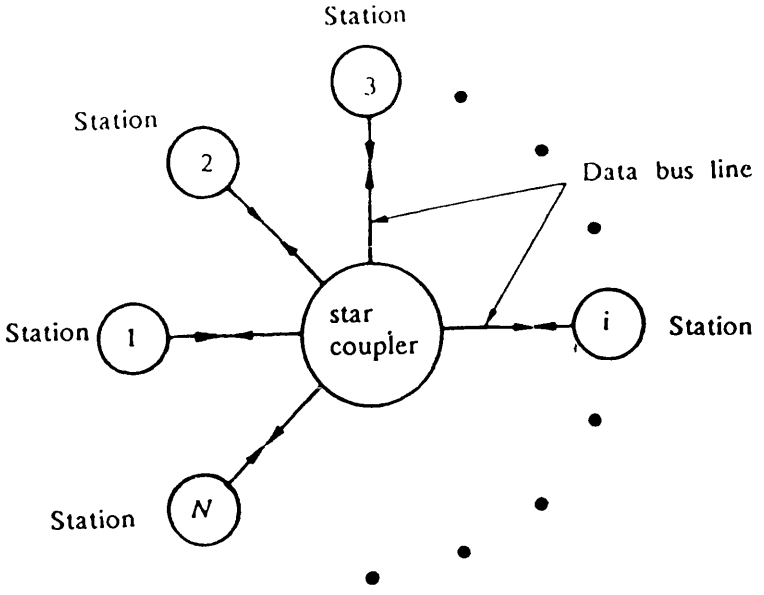

(a)

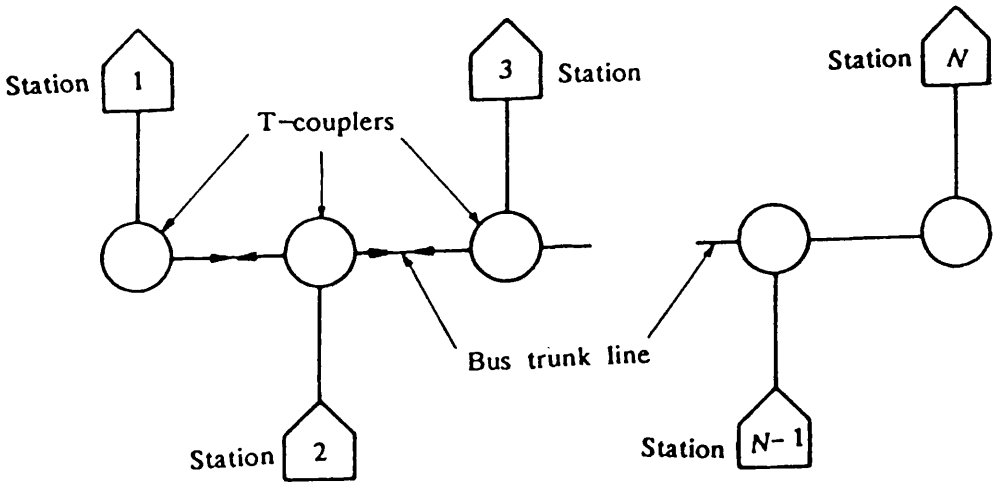

(b)

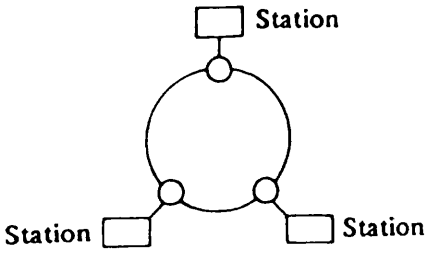

(c)

Figure 1.3 Data buses:

a) Radially- or star-configured data bus
b) In-line or T-coupled data bus
c) Ring topology

offers many advantages[1.14-1.16], including higher reliability, lower terminal to terminal loss and it gives every station signals of approximately equal level from every other station.

1.4.1 Star configuration data bus

A star-configured data bus uses either transmission or reflection star coupler as shown in Figure 1.4a,b, where the optical powers from the input ports are mixed together and divided equally among the output ports. They may be used to combine several signals together, split a signal into a number of parts or to tap optical power out or insert optical power into a fibre optic link. Either type of star coupler is composed of a set of input fibres, a set of output fibres and a mixing region. The transmission star coupler is twice as efficient as the reflection one, where half the light which enters is injected back into the input fibres.

The star coupler introduces an insertion loss L_s which is given by:

$$L_S = -10 \log \left[\frac{\sum_{J=1}^{N} P_J}{P_i} \right] \qquad 1.8$$

where the P_j are the output powers from all the ports, P_i is the input power at one port and N is the number of outputs in the transmission star coupler or the number of inputs plus outputs for reflection star coupler.

Since the optical power that enters a star coupler gets divided equally among the N output ports, so the optical power at any output port is $(1/N)$ of the total optical power emerging from all the coupler outputs which is known as the power

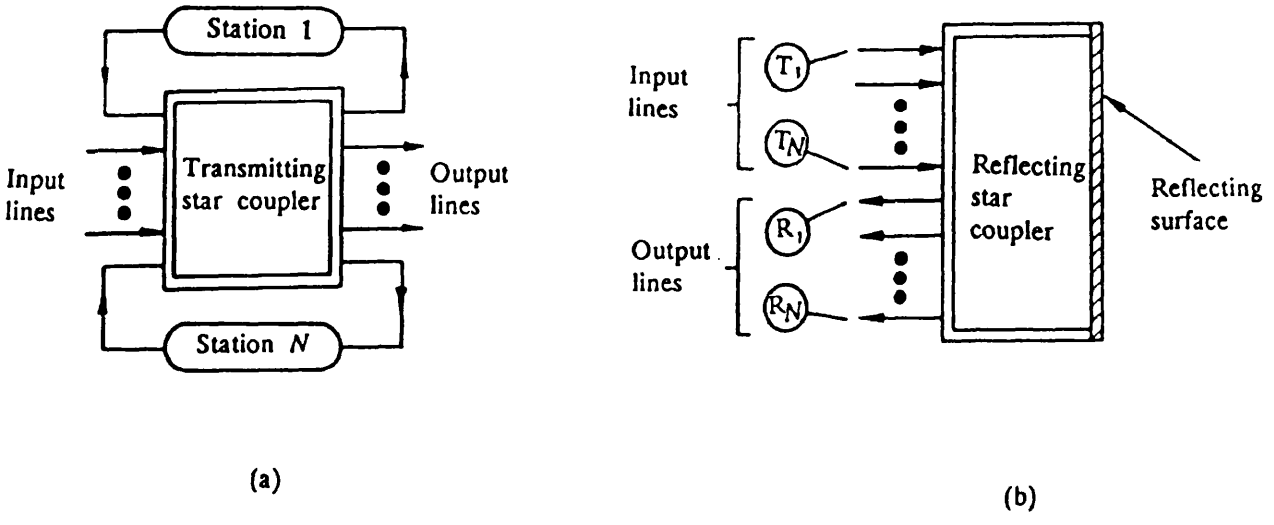

Figure 1.4 Star couplers:

a) Transmitting; b) Reflecting

splitting factor (P.S.F.) and is given in decibels by:

$$P.S.F. = 10 \log N \quad dB \qquad 1.9$$

If P_S is the fibre coupled output power from the source in dBm, P_R is the minimum optical power in dBm, required at the receiver for a specific data rate, α_f is the fibre attenuation, and L_C is the connector loss in dB; then the balance equation for all stations at distance L from the star coupler is:

$$P_S - P_R = L_S + 2\alpha_f L + 4L_C + 10 \log N + \text{system margin dB} \qquad 1.10$$

where a connector loss is assumed at the transmitter, the receiver and the input and output port of star coupler.

All transmitters in a star system have equal access to the network, so each transmission must be in a burst or time-shared mode, and any laser transmitter must have proper power control.

1.4.2 T-coupler data buses

For an in-line data bus, passive T-couplers are used at each terminal to remove a portion of the optical signal from bus trunk line or to inject additional light onto the trunk.

A major problem with the passive T-coupler is the insertion-loss and output loss at each tap plus the fibre losses between taps, which limit the network size to a small number of terminals generally about 10. Figure 1.5 shows a T-coupler which has four ports; two for connecting the device onto the fibre bus, one for receiving tapped-off data and one for inserting data onto the line. If a fraction

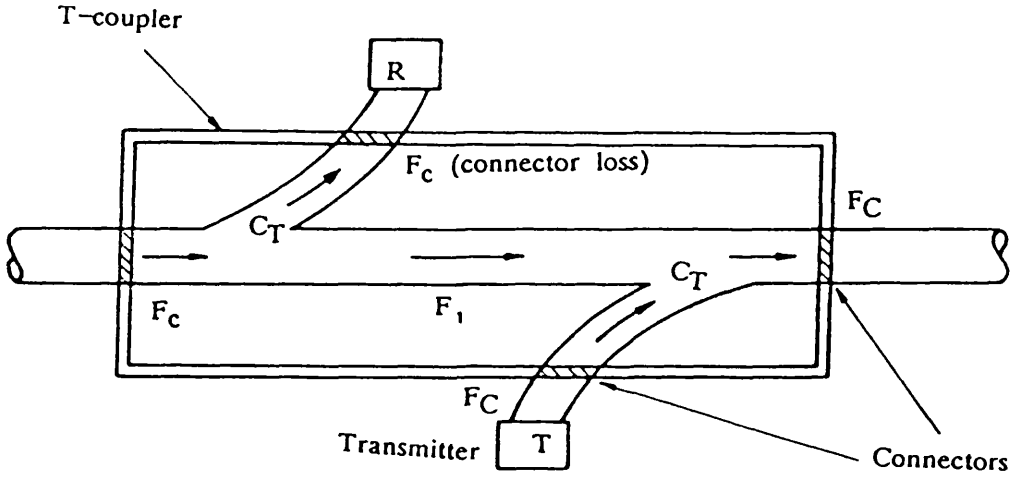

Figure 1.5 Power losses encountered in a passive T-coupler

F_C of optical power is lost at each port of the coupler, then the connecting loss is:

$$L_C = -10 \log (1 - F_C) \qquad 1.11$$

If C_T represents the fraction of power removed from the bus and delivered to the detector port, the actual optical power removed from the line is $2C_T$, since optical power is extracted at the receiving and transmitting ports of the device and the power removed from the transmitting port is lost from the system. The coupling loss is:

$$L_T = -10 \log (1 - 2C_T) \text{ dB} \qquad 1.12$$

There is also an intrinsic loss L_I associated with each T-coupler which is given by:

$$L_I = -10 \log (1 - F_I) \text{ dB} \qquad 1.13$$

where F_I is the fraction of power lost in the fibre.

If an in-line bus of N stations, uniformly separated by distance L, is considered, so the power received at station N from station 1 is given by[1.11]:

$$P_{1N} = A_0^{N-1} (1 - F_C)^{2N} (1 - 2C_T)^{N-2} C_T (1 - F_I)^{N-2} EP_0 \qquad 1.14$$

where P_0 is the optical power launched from a source flylead and E is the coupling efficiency of optical power onto the bus line and A_0 is the fibre attenuation between the adjacent stations:

$$A_0 = \exp [-2.3 \alpha_F L/10] \qquad 1.15$$

The worst case dynamic range is given by[1.11]:

$$D.R = \frac{1}{[A_0 (1 - F_c)^2 (1 - 2C_T) (1 - F_I)]^{N-2}} \qquad 1.16$$

Comparing the star and in-line systems indicates that the difference of the received and transmitted power levels in a star bus varies as log N for N-terminals while for in-line bus the power difference varies linearly with the number of stations and so imposes a much more severe requirement for receiver dynamic range than needed for a star configured data bus.

The star network is therefore preferred where there are a number of participating stations, but in either case the shared transmission medium requires that transmission occur in bursts or packets.

1.4.3 Ring topology

A ring topology consists of a closed loop of point-to-point connections from the transmitter to the receiver of successive stations. Since the transmission is point-to-point between stations, a variety of media including optical fibre, can be used on the separate links.

Repeaters can be installed between stations to extend the topology over several miles. Signal clocking can be passed from station to station around the ring. Most of the error detection, isolation and recovery derive from the fact that every station is down stream from every other station and that a station ultimately receives its own transmissions. The ring is vulnerable to a single node failure and it requires additional protection against failure.

The Ring topology eliminates the problem of T-taps losses, reduces the amount of cabling which is required for a star network, and is widely used. Although each station actively repeats the signal it receives, reliability can be made adequate for safe operation. Each transmitter is operating continuously, so power control is entirely conventional in nature.

1.4.4 Wavelength Division Multiplexing

The information capacity of an optical fibre can be increased dramatically by the simultaneous transmission of, optical signals from many different light sources having different peak emission wavelengths. The integrity of the independent messages from each source is maintained at the receiving end by operating each receiver at a different peak wavelength. This is the basis of wavelength division multiplexing (WDM)[1.17-1.19].

Figure 1.6a shows a unidirectional WDM device used to combine different signal carrier wavelengths onto a single fibre at one end and to separate them into their corresponding detectors at the other end. Figure 1.6b shows a bidirectional WDM scheme sending information in one direction at a wavelength λ_1 and simultaneously transmitting data in the opposite direction at a wavelength λ_2. Insertion loss, channel width and cross talk are three basic performance criteria in WDM. The insertion loss defines the amount of power loss that arises in the fibre optic line from the addition of a WDM coupling device, and in practice insertion loss can be a few decibels at each end. The channel width is the wavelength range that is allocated to a particular optical source. In the case of using laser diodes as sources, channel widths of several tens of nanometers are required to insure that no interchannel interference results from source instability like drift of peak operating output wavelength, while in case of using LED a channel width 10 or 20 times larger is required, because of the greater spectral

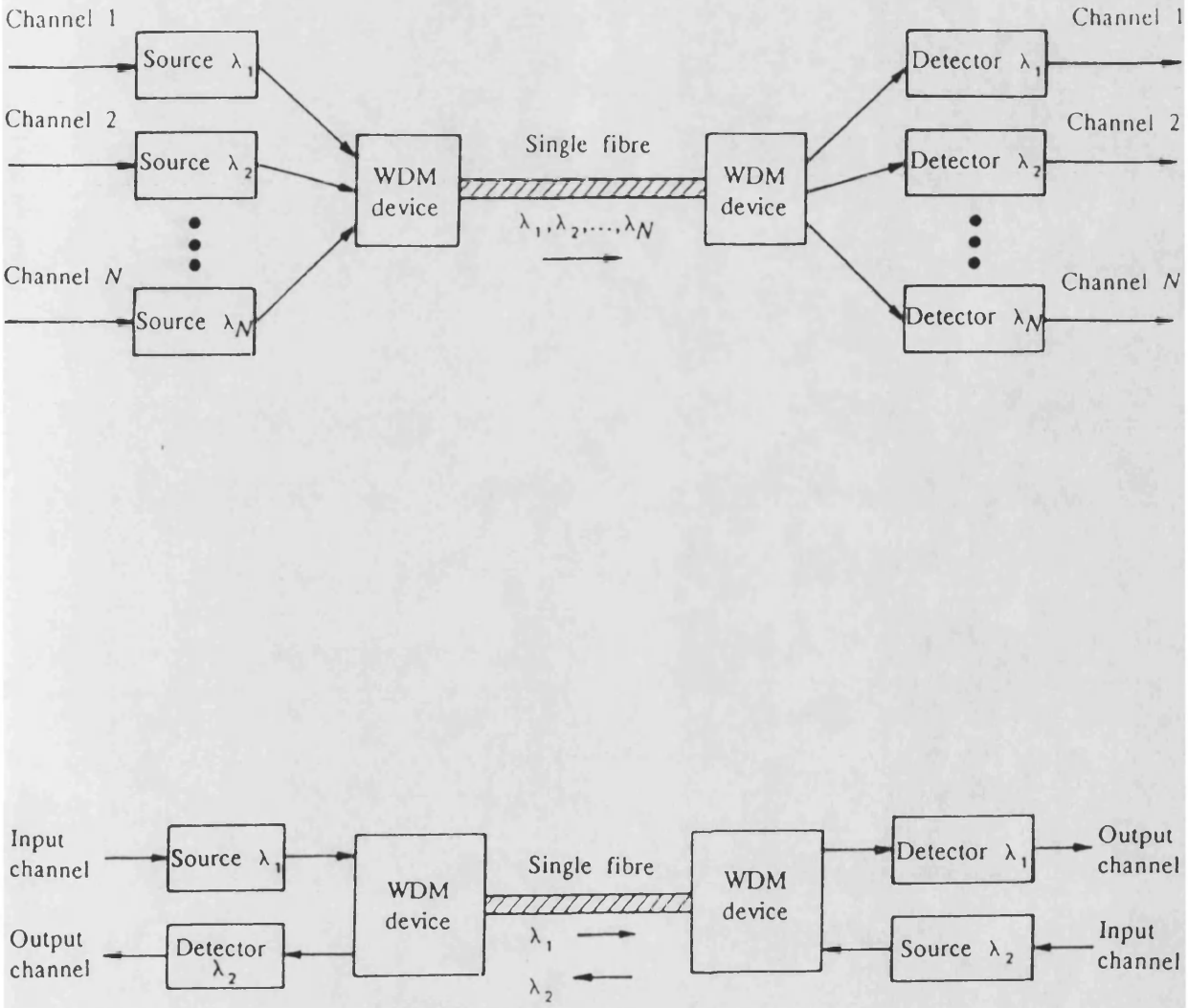

Figure 1.6 WDM Systems:

a) A Unidirectional WDM System that Combines N Independent Input Signals for Transmission over a Single Fibre

b) Schematic representation of Bidirectional WDM system in which two or more wavelengths are transmitted simultaneously in opposite directions over the same fibre.

width of the light emitting diodes.

Cross talk refers to the amount of signal coupling from one channel to another. The tolerable interchannel cross talk levels can vary widely depending on the application.

In implementing unidirectional WDM systems a multiplexer is needed at the transmitting end to combine optical signals from several light sources onto a single fibre and at the receiving end a demultiplexer is required to separate the signals into appropriate detection channels. The multiplexer should provide a low loss path from each optical source to the multiplexer output. The wavelength devision multiplexers used fall into two classes. These are angular dispersive devices such as prisms or gratings and filter based devices such as multilayer thin film interference filter.

WDM is used mostly for point-to-point link although with a wideband star coupler it could be employed over a star network since each path is at a unique wavelength, transmission can be continuous, and laser transmitter power control is conventional.

1.4.5 Ethernet and FibreNet

Ethernet is one of the most important LANs because it represents the first major product offering non-proprietary communication interfaces and protocols. The Ethernet architecture allows multiple distributed devices to communicate with each other over a single channel (coaxial cable); each station being connected to the bus via a bidirectional passive tap. Each station tries to transmit its message when the bus is quiet, and the message sent is a packet of data with a destination address, source address and valid check sums. If a message collision is detected

transmission is stopped and retried a short time later.

Data is encoded using Manchester code. This line code provides a strong timing component for clock recovery because a timing transition occurs in the middle of every bit, and it has the additional property of equal amounts of positive and negative voltages, which prevents the build up of a dc component and simplifies the implementation of decision threshold in the data detectors. Although the data is not transmitted on a carrier, the continuous transmission of Manchester code provides the equivalent of a carrier, so the channel is easily monitored for activity (by carrier sensing).

With fibre optic technology it is difficult to make passive T-couplers without unacceptably high loss, thus restricting severely the number of users attached to the bus (section 1.4.2). To overcome this, FibreNet[1.20] which is the optical version of Ethernet, uses a central passive star coupler to enable 16 users to communicate with each other.

The access protocol of FibreNet is based on the principle of carrier sense multiple access with collision detection CS MACD[1.21-1.22]. Time is slotted into intervals of 2T, where T is the end to end signal propagation delay of the star shaped bus.

A station is ready to transmit if it has a new packet to transmit or if the scheduled waiting period for retransmitting a previously collided packet expires. When it is ready, it senses the bus status to see whether the bus is busy or idle, and transmits the packet only if the bus is idle, that is, no other station is transmitting. If this leads to a collision, that event will be detected within time T + t_d where t_d, ($t_d << T$), is the time needed for a station to detect the collision. A collision occurs when other stations sense the channel as idle and transmit

packets simultaneously. When a collision is detected by a transmitting station, it stops transmitting immediately and chooses a random number, n, such that a retransmission is to be attempted after n slots. FibreNet (and Ethernet) have been proven to be very efficient when T is much less than the packet transmission time T_p. The efficiency of FibreNet drops to the range far below the acceptable levels as the bus data rate increases[1.23]. Another shortcoming of FibreNet is that the delay of a packet is not deterministic. In the worst case, a packet can encounter an unlimited number of collisions. This makes FibreNet unsuitable for real-time (packet-voice) communications. The weak points in FibreNet[1.20] have been overcome in the existing scheme of Express-Net[1.24] and C-Net[1.25]. Also a new scheme, D-Net[1.26] for high data rates optical fibre LAN is disclosed which has the advantage of high efficiency, low bound delay, simple protocol and implementation flexibility. All these implementations of course require the transmitter to be controlled in power during each transmission burst.

1.4.6 Packet Switching Systems

Preallocation and dynamic allocation of transmission bandwidth are two fundamental and competing approaches to communications. The telephone, telex and TWX networks are circuit-switched systems where a fixed bandwidth is preallocated for the duration, either permanently or for single call. On the other hand message, telegraph and mail systems have historically operated by dynamically allocating bandwidth or space after a message is received, one link at a time. Before the advent of computers dynamic-allocation systems were necessarily limited to non real time communications, since many manual sorting and routing decisions were required along the path of each message. In the early 1960s preallocation was so clearly the proven and accepted tecchnique and dynamic allocation techniques had been proven both uneconomic and unresponsive 20-80 years previously. In 1964 computer networks were an important problem for which a

new communication system was required. In 1969 the cost of dynamic allocation switching fell below that of the transmission line, this change made it economically advantageous to build a network of some kind rather than to continue to use direct lines or the circuit switched telephoned network for interactive data communication.

Depending on the nature of data traffic being transferred a packet switching network only allocates bandwidth when a block of data is ready to be sent, and only enough for that one block to travel over one network link at a time. This packet switching approach is 3-100 times more efficient than preallocation techniques in reducing the wastage of available transmission bandwidth resources. To do this, packet systems require both processing power and buffer storage resources at each packet sent.

The bursty nature of the data traffic leads to an inefficient utilisation of the preallocated bandwidth under circuit switching technology. Packet switching, on the other hand, allocates transmission bandwidth among the many active users and data is sent using limited size blocks called packets. The information at the source end is divided into a number of packets and transmitted over the network to the destination where it is assembled to retrieve the original information. In addition, packet switching provides better connect time, reliability, economy and flexibility[1.27]. By its very nature, an optical packet switching network requires burst control of the optical transmitter power.

1.5 Special Problems Introduced by Optical LANs

In the case of the star bus network having several laser transmitters which are biased near threshold, the emitted laser bias power has an effect on the receiver sensitivity[1.6]. It can be treated in the analysis as an equivalent photodiode dark current, in which case the value of Z (equation 1.2) is given by[1.1-1.2]:

$$Z = \frac{T}{q} I_2 M^{2+x} (I_d + I_L) + \frac{T}{q^2} \frac{2K\theta}{R_f} I_2 + \frac{1}{T} \left[\frac{2\pi C_F}{q}\right]^2 \frac{2K\theta\Gamma}{g_m} I_3 \ldots \quad 1.17$$

This is for high impedance and transimpedance input pre-amplifier, where I_3 is a constant depending on the normalised received and desired output pulse shape, I_d is the photodiode dark current, I_L is the effective dark current generated by the laser bias powers, K is Boltzman's constant, θ is the absolute temperature, g_m the FET transconductance, R_F is the transimpedance pre-amplifier feedback resistance. For a high impedance pre-amplifier $R_F = \infty$, C_F is approximately equal to the amplifier input capacitance and Γ is a parameter depending on the type of FET and its bias.

In equation (1.17) the first term represents the signal independent photodiode shot noise, the second term gives the feedback resistance thermal noise, in equation (1.2) the value of M that minimises P_{av} can be found by differentiation. Also for N laser transmitters connected to the star bus network.

$$I_L = RNP_{av} \frac{P_b}{P_s} \quad 1.18$$

where P_b is the laser bias power launched into the fibre, P_s is the average laser signal power launched into one fibre.

From equations (1.2), (1.17) and (1.18) one can evaluate P_{av} and hence evaluate the receiver penalty in case of APD and PIN photodiodes. This shows that the receiver sensitivity for a passive star bus network depends not only on the normal parameters as bit rate and pre-amplifier noise but also on the number of terminals and on the ratio of the launched laser bias power to average launched

signal power. Hence there is a requirement to switch the laser off when there is no data to be sent.

In the case of an optical LAN of the Star or Bus topology, the transmission medium is shared between all stations, and transmission is in bursts or data packets. As shown above, when a laser diode is used as a transmitting device, it must be biased off between transmissions. The laser diode is therefore driven by a current pulse up to threshold, and superimposed on this pulse are the modulation pulses corresponding to the data which is to be sent. The advantage of this is the reduction in power consumption and operation temperature, while also removing the switch-on delay. The drive circuit must therefore allow for two separate pulse functions.

The case has also been made for controlling the ouput power of a laser source, in order to maintain the required system power margin at the receiver. When operating in burst mode, the power control problem is more acute than for continuous operation, and this problem is the one which will be solved in this thesis.

At present, laser diode sources are high-cost, and are used for high speed networks where LEDs are unsuitable. However, the future will see a reduction of cost and a wider use of laser devices in networks.

1.6 The Thesis Format

The first chapter in this thesis is an introductory chapter about the optical fibre communication systems. The factors affecting the choice of essential elements of the system (optical fibre properties, optical receiver and optical transmitter) have been examined generally and the need for packet optical fibre networks has been

introduced.

Each of the essential elements of the optical fibre communication systems, optical fibre, optical receiver and optical transmitter, are now examined in detail in the second, third and fourth chapters respectively. Also in the fourth chapter the design and implementation and results of driving circuitry which can modulate the laser in a packet form have been examined.

In the fifth chapter the heating effects in semiconductor laser and its temperature control, together with a novel practical method to measure the rise in temperature of the LD during the packet duration have been presented, examined and the results have been discussed.

In the sixth chapter power control circuitry for the LD operating in a burst mode, has been designed, analysed and tested. Also the results are given.

The conclusion and any future work have been presented in the final chapter which indicates that the aim of this work has been achieved.

1.7 References

1.1 S. D. Personick: "Receiver design for digital fibre optic communication systems", Bell Sys. Tech. J., 52, pp843–886, 1973.

1.2 D. R. Smith and I. Garrett: "A simplified approach to digital optical receiver design", Opt. Quant. Electron., 10, pp211–221, 1978.

1.3 R. C. Hooper and D. R. Smith: "Receiver amplifier design for digital optical communication system", Third European Conference on Optical Communications, Munich, pp192–194, 1977.

1.4 R. G. Smith and S. D. Personick: "Receiver design for optical fibre communication systems", in H. Kressel (Ed.), Semiconductor Devices for Optical Communications, Topics in Advanced Physics, Vol.39, pp88–160, Springer–VerLag, 1982.

1.5 D. R. Smith, R. C. Hooper and I. Garrett: ibid (10), pp293–300, 1978.

1.6 S. D. Personick: "Review of fundamentals of optical fibre systems", IEEE J. of Sel. Area in Comm., Vol.SAC–1, No.3, pp373–380, April 1983.

1.7 G. Keiser: "Optical Fibre Communications", McGraw Hill, Chapter 4, 1983.

1.8 S. Moustaka, H. H. Witte: "Laser bias effect on the receiver sensitivity of passive fibre optic star bus networks", Optical and Quantum Electronics, 15, pp397–405, 1983.

1.9 G. Keiser: "Optical Fibre Communications", McGraw Hill, Chapter 3, 1983.

1.10 J. E. Fulenwider: "Wideband signal transmission over optical fibre waveguides", Guided Optical Communication Conference, Society of Photo-Optical Instrumentation Engineers, San Diego, California, August 1975.

1.11 G. Keiser: "Optical Fibre Communications", McGraw Hill, Chapter 8, 1983.

1.12 M. S. Ghausi: "Principles and Design of Linear Active Circuits", McGraw-Hill, New York, Chapter 16, 1965.

1.13 J. Midwinter: Optical Fibres for Transmission", Wiley, New York, App. 5, 1979.

1.14 M. C. Hudson and F. L. Thiel: "The star coupler: a unique interconnection component for multimode optical waveguide communication systems", Appl. Opt., 13, pp2540-2545, 1974.

1.15 K. Y. Chang: "Fibreguide systems in the subscriber loop", PROC.IEEE, 68, pp1291-1299, 1980.

1.16 G. Winzer and H. H. Witte, Siemens Forsch, u.Entw.Ber., 10, pp9-15, 1981.

1.17 W. J. Tomlinson: "Wavelength multiplexing in multimode optical fibres", Appl. Opt., 16, pp2180-2194, August 1977.

1.18 K. Ito, Y. Umeda, Y. Sugiyama, K. Nakajima, K. Oshima and M. Nunoshita: "Bidirectional fibre optic loop-structure network", Electron. Lett., 17, pp84-86, January 1981.

1.19 J. Conradi, R. Macieko, J. Straus, I. Few, G. Duck, W. Sinclair, A. J. Springthorpe, and J. C. Dyment: "Laser based WDM multichannel video transmission system", Electron. Lett., 17, pp91–92, January 1981.

1.20 E. G. Rawson and R. M. Metcalfe: "Fibrenet: Multimode optical fibres for local computer networks", IEEE Trans. Commun., pp983–990, July 1978.

1.21 S. S. Lam: "A carrier sense multiple access protocol for local networks", Comput. Networks, Vol. 4, pp21–32, 1980.

1.22 F. A. Tobagi and V. B. Hunt: "Performance analysis of carrier sense multiple access with collision detection", Comput. Networks, vol.4, pp245–259, 1980.

1.23 R. M. Metcalfe and D. R. Boggs: "Ethernet: Distributed packet switching for local computer networks", Commun. Ass. Computer Mach., pp395–404, July 1976.

1.24 L. Fratta, F. Borgonovo and F. A. Tobagi: "The Express Net: A local area communication network integrated voice and data", presented at the Int. Conf. Data Commun. Syst., Performance Applications, Paris, France, September 1981.

1.25 M. A. Marson and G. Albertengo: "C-Net: A local broadcast communication network architecture", Instituto di Elettronica Telecomunicazioni, Politecnico di Torino.

1.26 C. Tseng and B. Chen: "D. Net, a new scheme for high data rate optical local area networks", IEEE J. of Sel. Area in Comm., Vol. SAC-1, No.3,

pp493-500, April 1983.

1.27 L. G. Roberts: "The evolution of packet switching", Proc.IEEE, Vol.66, No.11, pp1307-1313, November 1978.

CHAPTER 2

PROPERTIES OF OPTICAL FIBRES

2.1 Introduction

Light can be guided using thin fibres made of transparent dielectric material. The fibre consists of a central portion or core, made of inorganic glass or plastic dielectric surrounded by cladding, also of either glass or plastic, whose refractive index is slightly lower than that of the core. Light is guided within the core through total internal reflection, and information is transmitted as a modulated beam of light through glass and plastic fibres. Signal loss, attenuation, and dispersion are the most important parameters characterising the optical fibre. Attenuation reduces the power margin between transmitter and receiver; and hence limits the amplitude of the signal and determines the distance over which a signal can be transmitted without becoming indistinguishable from noise. Dispersion widens the transmitted pulses over a given fibre and generates interference between successive pulses; hence, it limits the bandwidth of the signal and determines the number of bits of information that can be transmitted per second[2.1].

Glass fibres offer the lowest achievable loss and dispersion, whereas plastic fibres are characterised by loss and dispersion that are frequently higher by one or more orders of magnitude, hence most currently available plastic fibres have only a limited range of potential application.

The requirement for information transmission is to reduce the attenuation down to a few dB/Km, but advanced technology in the process of fibre fabrication leads to ultra low-loss glass fibres, with a figure of 0.2dB/Km leading to

transmission of information for longer distance without using repeaters.

Light wave communication started with what might be called first generation systems which utilise wavelength in the 0.85μm region, but second generation systems were developed which use a wavelength in the 1.3μm region. A further development is the third generation system using the low loss wavelength of 1.55μm.

The practical implementation of optical fibre systems requires the use of interconnection devices such as splices and connectors. These connectors introduce additional losses which are very significant in the design of fibre optic systems.

Optical fibre systems have significant advantage over existing transmission systems such as high transmission capacity, small cable size, low material cost, complete electrical isolation, high immunity to interference, negligible cross talk and large repeater spacing.

2.2 Fibre Loss Mechanisms

Absorption loss in glass fibres is due to the presence of impurity ions in glass. The presence of water in the glass gives rise to vibration of OH radical which produce absorption losses in the wavelength bands of interest. Many techniques are used in fabrication of glass fibres, such as RF melting and chemical vapour deposition and great care is taken to avoid contamination of the glass.

Rayleigh scattering is due to inhomogeneities of the dielectric material. This inhomogeneity is unavoidable since the molecules in an amorphous material are randomly distributed. Rayleigh scattering loss is inversely proportional with λ^4 so it decreases rapidly with increasing the wavelength λ.

At 0.8μm the Rayleigh scattering limit is about 2.1dB/Km. At 1.3μm it is about 0.3dB/Km. At 1.55μm the limit is about 0.15dB/Km.

The loss in silica fibre is minimised by reducing impurities such as transition metals and the OH radical to the order of parts per billion[2.1]. The major loss of such OH-free silica fibres comes from Rayleigh scattering and the infrared absorption[2.2,2.3].

Mode mixing is a type of scattering due to the irregularities which appear in the core-cladding interface through the fabrication process. These irregularities change the angle of incidence, and hence the angle of reflection will be changed which leads to mixing of different modes. The mixing of modes results in average velocity of the light ray and a corresponding reduction in pulse spreading (dispersion). Dispersion then becomes proportional to $\sqrt{L}$ instead of being proportional to (L) where (L) is the length of fibre, so mode mixing is not disadvantageous[2.4].

Light propagated through the fibre is not confined in the core only, but some power is actually carried outside the core[2.4] through the cladding and this power decays exponentially as a function of distance from the core. When the fibre is bent, the field on the outside of the bend is forced to move faster to keep up with the field in the core. At a certain distance from the core the outside field would be forced to move faster than the velocity of light in the cladding and the light ray will be radiated away. The amount of radiation loss depends on the radius of curvature of the fibre, below a certain threshold radius the loss is negligible but above a critical radius (R) the loss is significant.

$$R = \frac{3n_1^2\lambda}{4\pi(n_1^2 - n_2^2)^{3/2}} \qquad 2.1$$

Typically, for $\lambda = 1\mu m$ $R = 58\mu m$

so the critical radius of curvature is very small and great care should be taken when housing the fibre in a cable to avoid the losses by radiation due to microbending. The bending losses dramatically increase beyond a critical wavelength which depends on the design parameters of the fibre.

Optical fibres are protected against installation and environmental changes by cabling[2.5,2.6], and an additional loss, called cabling loss, is due to random bends introduced in the cabling process[2.7–2.12]. The cabling loss of multimode fibre is inversely proportional to Δ^n, where Δ is the relative difference index.

$$\Delta = \frac{n_1 - n_2}{n_1} \quad \text{and} \quad n = 5 - 8$$

so a slight increase in Δ decreases the cabling loss significantly[2.13].

2.3 Couplers

A coupler is one of the fundamental components in many optical fibre systems. It is used to divide optical power into two or more branches or conversely to combine optical power from two or more branches. It is used in optical data bus multiplexing and power tapping for monitoring, and is an important element in optical fibre sensing systems.

The operation of a simple biconically-tapered star coupler is illustrated in Figure (2.1). In the first converging tapper light guided in the highest order modes is radiated from the core and propagates in guided cladding modes, let K_R

be the fraction of the input light which is so radiated.

In the second diverging taper, this cladding mode light can be recaptured by the core, let K_T be the probability of such recapture. If both tapers are ideally smooth and sufficiently long, all the light is recaptured, that is $K_T = 1$ and the insertion loss is zero. When two or more fibres are joined at the taper point, the cladding mode light can be recaptured equally probable by any of the cores, and the coupling coefficients will be as indicated in Figure (2.1).

The self and cross coupling coefficients are given respectively by[2.14]:

$$C_{i \rightarrow i}' = 1 - K_R + K_R K_T / N \qquad 2.2$$

$$C_{i \rightarrow j}' = K_R K_T / N \qquad 2.3$$

The product $K_R K_T$ is a measure of the cross coupling efficiency. The overall efficiency is given by[2.15]:

$$K_E = C_{i \rightarrow i}' + (N - 1)\, C_{i \rightarrow j}' \qquad 2.4$$

which can be rewritten:

$$K_E = K_R K_T + 1 - K_R \qquad 2.5$$

An excess loss of 1.3dB has been recorded for a 19-fibre fused biconical taper star coupler[2.15], but the splitting loss is 12.8dB. Losses due to couplers and connectors predominant in a Local Area Network due to the relatively short distances between stations.

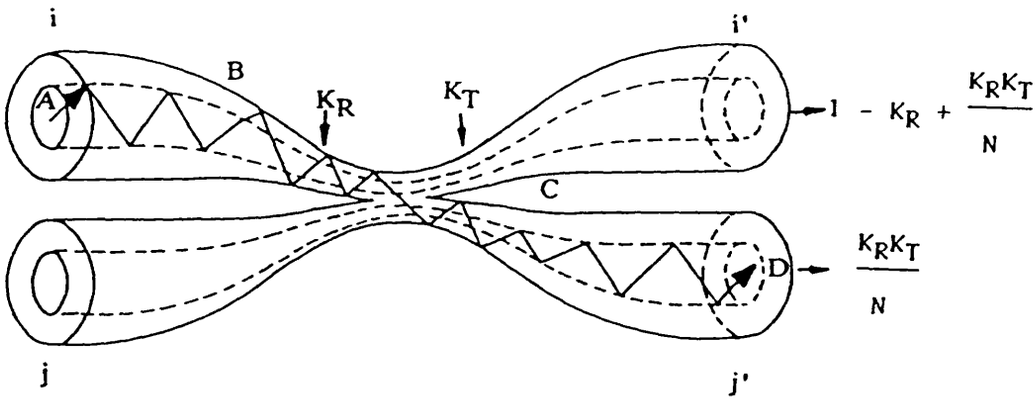

Figure 2.1 The operation of a bi-taper star coupler

2.4 References

2.1 F. Hanawa, S. Sudo, M. Kawachi and M. Nakahara: "Fabrication of completely OH-free VAD fibre", Electron.Lett., Vol.16, No.18, pp699-700, August 1980.

2.2 D. B. Keck, R. D. Mauer, and P. C. Shultz: "On the ultimate lower limit of attenuation in glass optical wavelength", Appl.Phys.Lett., Vol.22, pp307-308, April 1, 1973.

2.3 M. Horiguchi and H. Osanai,: "Spectral losses of low-OH-content optical fibres", Electron. Lett., Vol.12, pp310-311, June 1976.

2.4 E. A. J. Marcatili: "Bends in optical dielectric waveguides", BSTJ, Vol.48, pp2103-2132, 1972.

2.5 N. K. Dutta and R. J. Nelson: "Temperature dependence of threshold of InGa AsP/InP double-heterostructure lasers and auger recombination", Appl.Phys.Lett., Vol.38, No.6, pp407-408, March 1981.

2.6 T. Nakahara and N. Uchida: "Optical cable design and characterisation in Japan", Proc.IEEE, Vol.68, No.10, pp1214-1219, October 1980.

2.7 Y. Katsuyama, Y. Mitsunaga, S. Mochizuki, A. Kawana, K. Ishihara and H. Tsuchiya: Papers on Technical Group meeting of Ins. Electron. Comm.Eng. Japan, OQE378-43, June 1978.

2.8 H. Murata and N. Inagaki: "Low-loss single-mode fibre development and splicing research in Japan", IEEE J.Quantum Electron., Vol.QE-17, No.6,

pp835–845, June 1981.

2.9 D. Marcuse: "Losses and impulse response of a parabolic index fibre with random bends", Bell Syst.Tech. J., Vol.52, pp1423–1437, October 1973.

2.10 R. Olshansky and D. B. Keck: "Pulse broadening in graded index optical fibres", Appl.Opt., Vol.15, pp483–491, February 1976.

2.11 D. Gloge: "Optical fibre packaging and its influence on fibre straightness and loss", Bell Syst. Tech. J., Vol.54, pp245–262, February 1975.

2.12 M. Kubota, K. Furuya and Y. Suematsu: "Random bend loss–evaluation in single–mode optical fibre with various index profiles", Trans.IECE of Japan, Vol.E–63, No.10, pp723–730, October 1980.

2.13 E. A. J. Marcatili: "Modal dispersion in optical fibres with arbitrary numerical aperture and profile dispersions" Bell Syst. Tech. J., Vol.56, pp49–63, January 1977.

2.14 T. Ozeki and B. S. Kawasaki: "New star coupler compatible with single multimode fibre data links", Electronic Lett., 12(6), p151, March 1976.

2.15 E. G. Rawson and A. B. Nafarrate: "Star couplers using fused biconically tapered multimode fibres", Electronic Lett., 14(g), pp274–275, April 27, 1978.

CHAPTER 3

OPTICAL RECEIVER

3.1 Introduction

The optical receiver is an essential element of an optical fibre communication system, and dictates the overall system performance. It consists of a photodetector, low noise amplifier and signal processing circuitry, and has the task of converting the optical energy emerging from the end of a fibre into an electrical signal and then amplifying this signal to a level that can be processed by the electronics following the receiver amplifier. In these processes various noises and distortions will unavoidably be introduced which can lead to errors in the interpretations of the received signal.

In the context of laser-diode power control, the optical receiver is used to monitor the optical output signal of the laser. For the control to be exerted properly, it is necessary to understand the limitations imposed by the sensitivity, bandwidth and noise and how they affect the measurements that are to be made.

The photodetector senses the luminescent power falling upon it and converts the variations of this optical power into a corresponding electric current. Since the optical signal is generally weakened and distorted when it emerges from the end of the fibre, the photodetector must meet very high performance requirements; among the foremost of which are a high response or sensitivity in the emission wavelength range of the optical source being used, a minimum addition of noise to the system, and a fast response speed or sufficient bandwidth to handle the desired data rate. The photodetector should also be insensitive to variations in temperature, be

compatible with the physical dimensions of the optical fibre, have a reasonable cost in relation to the other components of the system and have long operational life.

Among the semiconductor-based photodetectors which have been used almost exclusively for fibre optic systems, are the PIN and avalanche photodiodes. They have been used because of their small size, suitable material, high sensitivity and fast response.

3.2 Noise Considerations in Photodetectors

The sensitivity of the receiver is limited by noise present during detection[3.1-3.3]. The photodetector is required to detect very weak optical signals, which requires that the photodetector and its following amplification circuitry be optimised so that the optical receiver output signal to noise ratio (S/N) is a maximum.

Noise in the photodetector arises from the statistical nature of photon-to-electron conversion and the thermal noise associated with the amplifier circuitry. The signal to noise ratio:

$$(S/N) = \frac{\text{Signal power from photodetector}}{\text{Photodetector noise power + amplifier noise power}} .$$

So, in order to achieve high signal to noise ratio, the following conditions should be met:

1. The photodetector must have a high quantum efficiency to generate a large signal power.

2. The photodetector and amplifier noise should be kept as low as possible.

For most applications it is the noise currents which determine the minimum optical power level that can be detected, since the photodiode quantum efficiency is normally close to its maximum possible value.

The minimum detectable optical power is defined as the optical power necessary to produce a photocurrent of the same magnitude as the root mean square of the total noise current or, equivalently, a signal-to-noise ratio of one. It determines the sensitivity of the receiver.

3.2.1 Noise Sources

Noise appears in optical receiver from several sources, the principal ones being the following:

1. Quantum noise which is simply shot noise in the photon current.

2. Dark current or leakage current, independent of the illumination, it increases shot noise effect.

3. Multiplication noise, or additional shot noise in multiplication[3.4]. It results from the statistical nature of the multiplication process in photodiodes with internal gain.

4. Thermal or Johnson noise in the amplifier - a factor that dominates conventional systems.

In order to examine the different types of noise and their effects on signal to

noise ratio, consider the simple receiver model and its equivalent circuit shown in Figure (3.1). The photodiode has a small series resistance R_s, a total capacitance C_d consisting of junction and packaging capacitances, and a bias (or load) resistor R_L. The amplifier following the photodiode has an input capacitance c_a and a resistance R_a. For practical purposes, R_s is much smaller than R_L and can be neglected. If a modulated signal of optical power P(t) falls on the detector, the primary photocurrent $i_p(t)$ generated is[3.5-3.7]:

$$i_p(t) = \frac{\eta q}{h\upsilon} P(t) \qquad 3.1$$

This primary current consists of a dc value I_p, which is the photocurrent due to the signal average power, and a signal component $i_p(t)$. For PIN photodiodes the mean square signal current is:

$$\bar{i}_s^2 = \bar{i}_p^2(t) \qquad 3.2$$

whereas for avalanche photodetectors:

$$\bar{i}_s^2 = \bar{i}_p^2(t)\, M^2 \qquad 3.3$$

where M is the average of the statistically varying avalanche gain.

Now the sources of noise currents added to the signal current have to be examined.

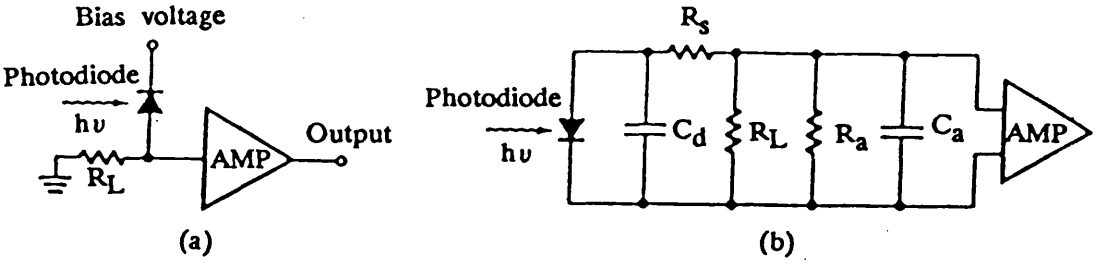

Figure 3.1 a) Simple model of a photodetector receiver, and
b) its equivalent circuit

3.2.1.1 The quantum noise

This noise results from the random time of arrival of the photons, which leads to the statistical nature of the production and collection of photoelectrons. When an optical signal is incident on a photodetector it has been demonstrated that these statistics follow a Poisson process[3.8]. Since the fluctuations in the number of photocarriers created from the photoelectric effect are a fundamental property of the photodetection process, they set the lower limit on the receiver sensitivy when other conditions are optimised. The quantum noise current has a mean square value in a bandwidth B which is proportional to the average value of the photocurrent I_p.

$$\bar{i}_Q^2 = 2qI_p B M^2F(M) \qquad 3.4$$

Where F(M) is a noise figure associated with the random nature of the avalanche process it has been found that to a reasonable approximation:

$$F(M) \simeq M^X, \ (0 \leq x \leq 1) \qquad 3.5$$

where the value of X depends on the material.

For PIN photodiodes M and F(M) are unity. The quantum noise has an important property that it depends on the signal level.

3.2.1.2 Dark current

The dark current is the current flowing through the bias circuitry of the photodiode when no light is incident on the device. This dark current is a

combination of bulk and surface currents. The bulk dark current i_{DB} arises from electrons and/or holes which are thermally generated in the pn junction of the photodiode. In an APD these liberated carriers also get accelerated by the high electric field present at the p–n junction, and are therefore multiplied by the avalanche gain mechanism. The mean square value of this current is given by:

$$\overline{i}^2_{DB} = 2q\, I_D\, M^2\, F(M)\, B \qquad 3.6$$

where I_D is the primary (unmultiplied) bulk dark current.

The surface dark current is referred to as a surface leakage current. It depends on surface defects, clean lines, bias voltage and surface area. The mean square value of the surface dark current is:

$$\overline{i}^2_{DS} = 2q\, I_L\, B \qquad 3.7$$

where I_L is the surface leakage current. The surface dark current is not affected by the avalanche gain since avalanche multiplication is a bulk process.

An effective way of reducing surface dark current is through the use of a guard ring structure which shunts surface leakage currents away from the load resistor.

3.2.1.3 Thermal noise

Thermal noise is due to the spontaneous fluctuations resulting from the thermal interaction between, say, the free electrons and the vibrating ions in a conducting medium, and it is especially prevalent in resistors at room temperature.

The photodetector load resistor (R_L) contributes a mean square thermal noise current:

$$\overline{i_T^2} = \frac{4KTB}{R_L} \qquad 3.8$$

where K is Boltzman's constant and T is the absolute temperature.

3.2.2 Signal to noise ratio

The signal to noise ratio at the input of the amplifier is:

$$\frac{S}{N} = \frac{\overline{i_p^2}\, M^2}{2q(I_p + I_D)M^2F(M)B + 2qI_LB + 4KBT/R_L} \qquad 3.9$$

The thermal noise can be reduced by using a large load resistor R_L but still consistent with the receiver bandwidth requirements.

In APDs the thermal noise is negligible while the photodetector noise is dominant, whereas in PIN photodiodes the thermal noise is dominant. It is to be noted that the surface leakage current is not altered by the avalanche gain mechanism.

In case of using a PIN photodiode the signal to noise ratio will be:

$$\frac{S}{N} = \frac{\overline{i_p^2}}{2qB(I_p + I_d + I_L) + \frac{4KTBF_n}{R_L}} \qquad 3.10$$

where F_n is the noise figure of the amplifier.

3.2.3 Minimum detectable optical power

The minimum detectable optical power is usually limited by the noise level in the receiver. Since the incident power is converted by the photodiode to a current, the signal power at the amplifier is proportional to the square of the optical power. For a full-depth sinusoidal modulation of the optical signal the mean square value of the detector current in terms of the optical power P_{opt} is[3.9]:

$$\overline{i_p^2} = \frac{1}{2}\left[2P_{opt}\frac{q\eta}{h\upsilon}\right]^2 \qquad 3.11$$

and also the mean square value of the quantum noise current in terms of optical power is:

$$\overline{i_Q^2} = 2q\left[2P_{opt}\frac{q\eta}{h\upsilon}\right]B \qquad 3.12$$

so the expression of signal to noise ratio for a PIN photodetector can be written as[3.10]:

$$\frac{S}{N} = \frac{2\left[P_{opt}\frac{q\eta}{h\upsilon}\right]^2}{\left[2qI_D + 4q\left[P_{opt}\frac{q\eta}{h\upsilon}\right] + \frac{4K}{R_L}T_{eff}\right]B} \qquad 3.13$$

where the noise figure of the amplifier (F_n) translates into the effective

temperature $T_{eff} = TF_n$. By setting:

$$\frac{S}{N} = 1$$

in equation (3.13), assuming the thermal noise predominates then the minimum detectable optical power can be obtained:

$$P_{min} = \frac{2h\upsilon}{q\eta}\left[\frac{2K\,T_{eff}\,B}{R_L}\right]^{1/2} \qquad 3.14$$

For the PIN photodiode of the type MF0D1100 responsivity R = 0.35A/W, and for signal bandwidth B = 500MHz, $R_L/F_n = 10^4$, T = 300 ^{0}K, and the quantum efficiency η = 50%, therefore:

$$P_{min} = 0.0713\mu W = -41.5dBm$$

3.2.4 The Bit-Error Rate

In the design of a communication system, the required signal to noise ratio at the receiver is determined by the specification of the desired bit error rate, which has a standard value of 10^{-9} for telecommunications. The relation between specified bit-error rate and the required signal to noise ratio can be calculated from the statistics of signal detection. Two kinds of error are possible. One is that a noise pulse will be mistaken for a signal pulse when in fact no signal occurs. The other is that no signal will be detected when in fact one is present - a 'threshold' error. The correct statistical distribution which describes the arrival rate of the photons in an optical pulse is given by Poisson statistics[3.8]. The central-limit theorem of statistics, however, shows that for a large number of

photons per pulse, the correct Poisson distribution can be approximated by a Gaussian distribution. The number encountered in high bit rate optical communication is $\approx 10^4$ photons per bit, which is large enough to justify using Gaussian statistics to relate the signal to noise ratio and the error rate. In this approximation the probability of an error is:

$$P_e = \text{bit error rate} = \frac{1}{2}\left[1 - \text{erf}\frac{i_p}{< i_N > 2\sqrt{2}}\right]$$

$$= \frac{1}{2}\left[\text{erfc}\frac{i_p}{< i_N > 2\sqrt{2}}\right] \qquad 3.15$$

where erf(x) is the Gaussian error function.

$$\text{erf}(X) = \frac{2}{\pi}\int_0^X e^{-Z^2}\,dZ$$

Figure (3.2) shows the relation between the bit error rate as a function of signal to noise ratio as plotted from equation (3.15). From the figure the required signal to noise ratio for a 10^{-9} bit error rate is = 10.9dB. So in order to achieve a bit error rate of 10^{-9} the optical power needed to be only 12 times larger than the minimum detectable power specified in equation (3.14).

Note the steep rise in BER with reduction in signal power in the region of 10^{-9}. A 1dB change in signal power changes the BER by two order of magnitude. It is therefore important to keep close control of the transmitted power when operating close to the limit.

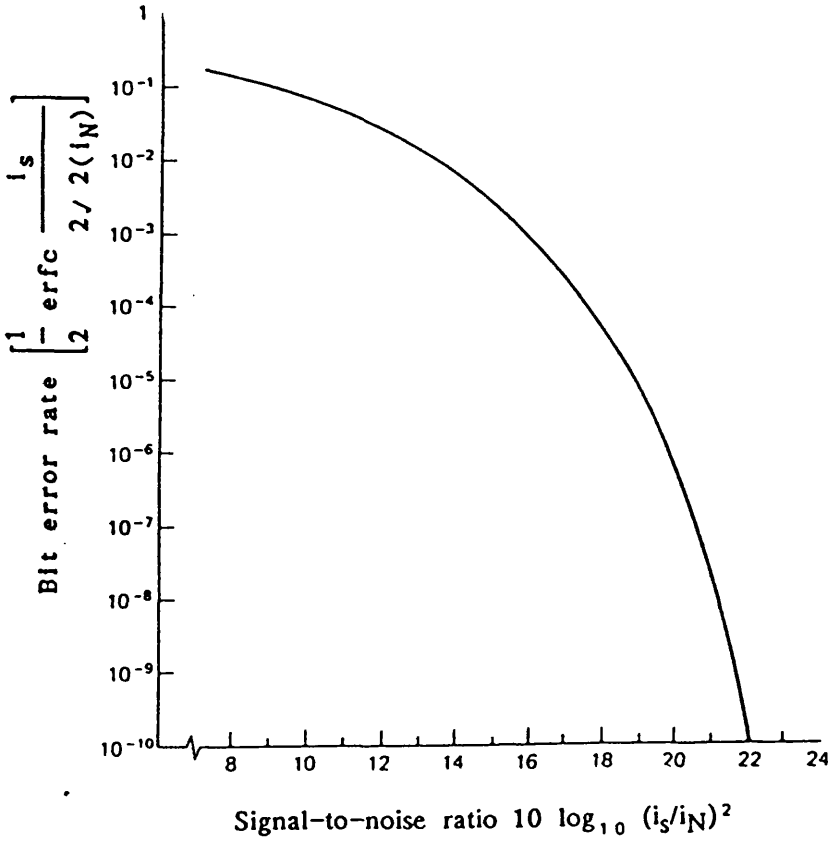

Figure 3.2 The bit error rate as a function of signal-to-noise power at the amplifier. The signal-to-noise power ratio for a 10^{-9} bit error rate is 21.8dB. The optical signal-to-noise ratio is 10.9dB.

3.7 References

3.1 S. D. Personick: "Receiver design for digital fibre optic communication systems", B.S.T.J., 52, p843, 1973.

3.2 D. R. Smith et al: Opt. Quant. Electronic., 10, p211, 1978.

3.3 Y. Okano et al, Rev. Elec. Comm. Labs (NTT), 26, p701, 1978.

3.4 R. J. McIntyre: "Mutliplication noise in uniform avalanche diodes", IEEE Transaction on Electron Devices, ED-13, pp164-168, January 1966.

3.5 P. L. Carni: "Photodetectors" in Optical Fibre Communication, Tech. Staff of CSELT, Pt.II, Chap. 2, McGraw Hill, New York, 1980.

3.6 P. P. Webb, R. J. McIntyre and J. Conradi: "Properties of avalanche diodes", RCA Rev., 35, pp234-278, June 1974.

3.7 B. M. Oliver: "Thermal and quantum noise", Proc.IEEE, 53, pp436-454, May 1965.

3.8 Hans Melchior, F. Arams and M. B. Fisher: "Photodetector for optical communications systems", Proc.IEEE, 58, pp1466-1486, 1970.

3.9 K. Nishida, K. Ishii, K. Minemura and K. Taguchi: "Double epitaxial silicon photodiodes for optical fibre communications", Electron. Lett., 13, pp280-281, 1977.

3.10 Harrison: "RCA Electro-Optics Handbook", RCA Commercial Engineering, pp109-125, 1974.

CHAPTER 4

OPTICAL TRANSMITTER

4.1 Introduction

Communication using electrical signals relies on single frequency oscillators whose output signals are virtually constant in frequency, phase and amplitude. These carriers can variously be modulated by the information signal in frequency, phase or amplitude, and at the receiver it is possible to achieve highly sensitive detectors (demodulators) if the carrier can be regenerated and used for signal demodulation.

With the optical components currently available, it is not possible to modulate or demodulate the optical signal in this way because the spectral width of the output from an optical transmitter is much too large and its frequency stability is much too low for frequency or phase modulation to be practicable. In addition, all multimode fibres greatly distort the transmitted signal due to their multimode transmission (multipath propagation), therefore the type of modulation which can be used for practical application is the intensity (power) modulation of the optical signal. The information to be transmitted in the optical fibre communication system is in the modulation in intensity of the laser beam propagated through the fibre. At the receiving end of the fibre, light detectors are used to transform light signals to electric signals. This simplifies transmitter and receiver designs since the optical source can be directly modulated by the drive current, and photodiodes convert the received optical power directly into an electrical current.

Semiconductor optical sources have been developed to meet the requirements

of optical fibre communication systems. The lowest losses in optical fibre are found to be in the wavelength region 0.8–1.6μm. So, light sources for optical fibre systems should be in the same region. There are some sources based on Gallium Aluminium Arsenide (GaAlAs) which emit light in the 0.8–0.9μm region of the near infrared, and a more recent source based on GaInAsP emits light in the 1.2–1.6μm region. These light sources should have high optical density, minimal beam divergence and high spectral purity. There are two broad categories of semiconductor light sources, the light emitting diodes (LEDs) and lasers. The radiative emission from these semiconductor light sources is achieved by injecting holes and/or electrons across a heavily forward biased p–n junction.

4.2 Laser Diode Characteristics

4.2.1 Optical output power

The electrical power required to operate both injection laser and LEDs is generally similar with typical current levels between 20 and 300mA and voltage drops across the terminals of 1.5–2.5V. However, the injection laser is a threshold device which must be operated in the region of stimulated emission (above the threshold) where continuous optical output power levels are typically in the range of 1–10mW. With lasers much of this output may be coupled into an optical fibre because the isotropic distribution of the narrow line width, coherent radiation is relatively directional; in addition, the spatial coherence of the laser emission allows it to be readily focused by appropriate lenses within the numerical aperture of the fibre. Coupling efficiencies near 30% may be obtained by placing a fibre close to a laser diode mirror, and these can approach 80% with a suitable lens arrangement[4.1,4.2]. Therefore injection lasers are capable of launching several milliwatts of optical power into a fibre, whereas the spontaneous emission of radiation over a wide linewidth from the LED generally exhibits a Lambertian

intensity distribution which gives poor coupling into optical fibres even with appropriate lens coupling, so that only a few to several hundred microwatts can be launched into an individual multimode fibre from an LED.

4.2.2 Switch-on delay

The ability of the laser to respond at high modulation rates is limited by the switch-on delay that occurs before the onset of lasing and by the damped relaxation oscillations of the photon and carrier populations. The switch-on delay results from the finite time that is required for the carrier density to reach the lasing threshold value[4.3]. In a laser operating without a bias current the switch-on delay may be several times the spontaneous carrier lifetime, which is typically 1-3ns. The switch-on delay can be reduced by prepumping with a dc bias current which is set close to the threshold current if the maximum modulation speed is required. If a current pulse of rise and fall time t_1 is presented to the injection laser, the laser will turn-on after a time delay. At first the current takes a time (t) to reach the threshold value (I_{th}):

$$t = \frac{I_{th}}{I} t_1 \qquad 4.1$$

where I is the drive current. After the input current reaches the threshold a time is taken for the carrier population to become inverted, and this lasing delay (t_d) for population inversion is given by[4.4]:

$$t_d = T \ell n \left[\frac{I}{I - I_{th}}\right] \qquad 4.2$$

where T is the carrier lifetime.

Figure 4.1 represents the input current pulse and its corresponding output light pulse for unbiased operation of laser and also represents the total delay which takes place. In order to achieve maximum modulation speed the switch–on delay has to be reduced by prepumping with a dc bias current I_b which is set close to the threshold, then the modulation pulse current I_m is superimposed on this bias current. In this case the lasing delay t_d is given by[4.5]:

$$t_d = T \ell n \left[\frac{I_m}{I_b + I_m - I_{th}}\right] \qquad 4.3$$

It is clear from this equation that the delay time can be eliminated by dc–biasing the laser diode at the lasing threshold current.

4.2.3 Temperature effects

The threshold current (I_{th}) of an LD is sensitive to temperature. Its value increases with increasing temperature as illustrated in Figure 4.2. Because of various complex temperature factors[4.6], it is difficult to have a single equation holding for all devices and temperature ranges. However, the temperature variation of I_{th} can be approximated by the empirical expression[4.7,4.8]:

$$I_{th} = I_{tho} \exp[T/\theta] \qquad 4.4$$

where I_{th} is the threshold current of LD at temperature T, θ is the characteristic temperature which is a measure of the relative temperature insensitivity. Typically the value of θ is in the range of 120 to 165 ^{0}C in the vicinity of room temperature, I_{tho} is constant.

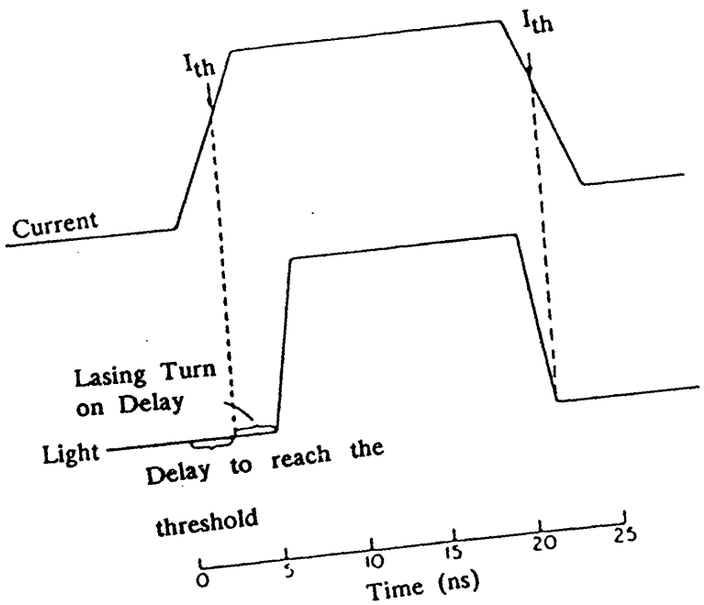

Figure 4.1 Turn-on Delay in Unbiased Laser

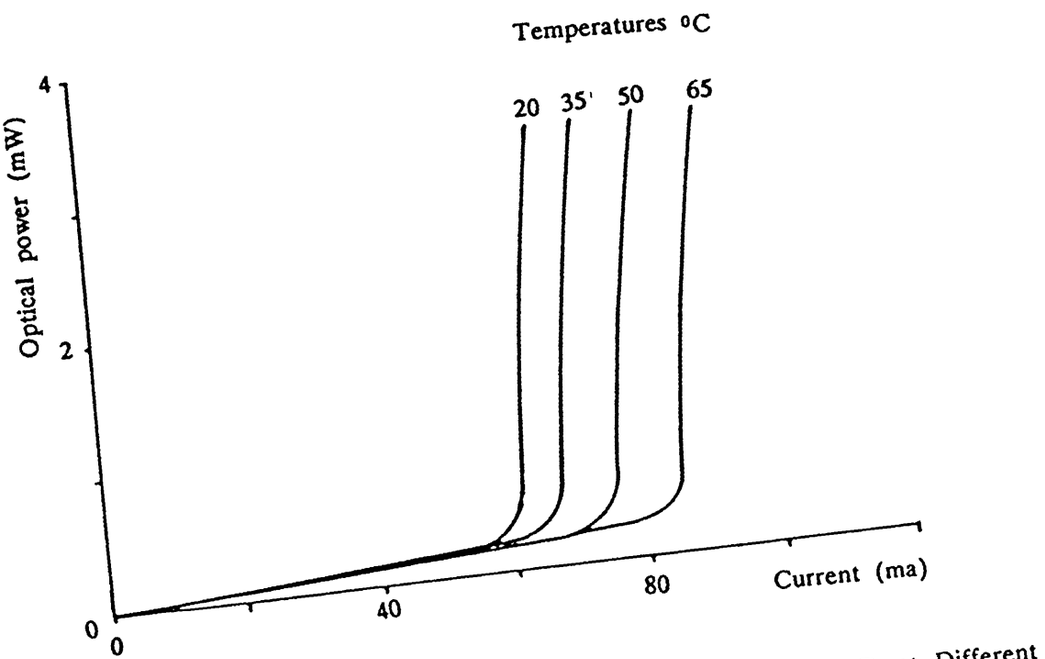

Figure 4.2 Illustration of the Light-Current Characteristic of the LD at Different Temperatures

The slope of the characteristics above threshold is relatively insensitive to temperature changes. A small increase in drive current of the LD causes a considerable increase in the optical output, consequently the threshold current and signal modulation current have to be closely controlled.

4.2.4 Spectral width

Laser diodes are designed such that the optical radiation emitting area matches the optical fibre to which it is to be connected, by altering the stripe width. Reducing the stripe width to 10μm reduces the spectral spread to 1–2nm.

Below threshold the laser diode behaves as an LED emitting spontaneously across a broad spectrum (40–100nm); as threshold approaches, super radiant gain starts to narrow this line and when laser action commences the line width changes considerably into a series of discrete lines (modes) which spread over a smaller range. If the device is pulsed with a random bit stream, every time it turns on, a number of modes or frequencies builds up, and most decay very slowly during the length of the drive pulse. Thus, the emission line width of the device can depend upon how it is biased and driven and on the bit rate of the system.

4.2.5 Relaxation oscillation

The broadening of the laser spectrum under pulsed or transient drive conditions is related to another modulation characteristic of the laser, transient oscillation or ringing[4.9]. If the drive current is raised rapidly from below the threshold current to a value above threshold, a transient oscillation in the light output is frequencly observed[4.10]. This oscillation in the light output corresponds to an oscillating photon density within the laser cavity, and is accomplished by an oscillating carrier inversion, preceding the photon density oscillation in phase. The

decay constant for this transient oscillation is related to the effective carrier lifetime, the photon lifetime and the spontaneous photon density in the lasing mode[4.11,4.12].

Lasers with relatively short carrier and photon lifetimes and large spontaneous photon density in the lasing mode have been made showing no transient oscillation and negligible transient breadening of the spectrum[4.13,4.14].

Undamped self-sustained oscillation[4.15] can occur in a laser even under CW drive conditions, when inhomogeneous pumping of laser mode results in regions of saturable absorption[4.16].

Mode partition noise and effects due to reflected optical power are other possible sources of significant optical power fluctuations. In a fibre transmission system the low level of optical power reflected back into the laser can produce optical power fluctuation and distortion of the modulation response[4.17,4.18]. Measurements at 274Mbit/s of effects resulting from reflected optical power indicate that a penalty as little as 0.7dB would result from the 4% reflection of an air glass interface[4.18]. In systems where the penalties become unacceptably high it may be necessary to use an optical isolator between the laser and the fibre.

4.3 Laser Diode Drive Circuit

A light emitting diode is somewhat restricted in its range of possible applications in comparison with the more powerful, higher speed injection laser. In general, LEDs are far easier to operate than laser diodes, because the LD is a device which has a threshold current and its driving circuit has somewhat different drive current requirements from the LED. Considering digital transmission, the laser is usually given a substantial applied bias often referred to as prebias, in the

off state. Reasons for biasing near threshold in the off state are:

a) It reduces switch-on delay and minimises any relaxation oscillation.

b) It reduces the junction heating caused by the digital drive current since the on and off currents are not widely different for most lasers.

c) It allows easy compensation for changes in ambient temperature and device aging.

However, biasing near threshold causes spontaneous emission of light in the off-state, which may cause an error in case of laser transmitter in a fibre optic network to which several laser transmitters are connected[4.19]. The best spectral behaviour of LD results if the LD is dc biased just above threshold and pulsed from this pedestal. The delay effect is removed and relaxation oscillation reduced, but this is at the expense of consuming more power to bias the laser and so the heat generated by the LD will be greater leading to a higher average temperature of the laser.

If the LD is used to transmit information in a burst mode in a packet switching network, as it is intended to be used for this application, then the LD will be driven by a current pulse close to the threshold value and of width equal to the packet length and data pulses will be superimposed on the top of this pulse. So the laser will be switched-on only when there is data ready to be sent. Using the laser diode in this bursty mode will reduce the power consumption of the laser, reduce the average operating temperature, facilitate getting rid of the heat generated by the LD and will reduce the error rate in a fibre optic network in which several laser transmitters exist.

The laser diode drive circuit used for packet switching consists of two stages; each has the differential amplifier configuration operating in the linear region as shown in Figure 4.3.

The first stage is designed to drive the laser diode by a current pulse up to threshold current, it consists of transistors Q_1, Q_2 and Q_3. The transistor Q_3 and the resistor R_{E_1} are used as a constant current source, where the value of the current I_{E_1} can be adjusted at the required value by suitable biasing of the base of Q_3 using the potential divider R_5, R_6. A zener diode is connected across the potentiometer R_5 in order to minimise the change in current which may occur due to any voltage spike on the supply voltage. The biasing condition in the circuit is adjusted by suitably choosing the values of the resistors of the potential dividers connected to the bases of the transistors Q_1 and Q_2, the values of R_3 and R_4 being chosen such that the current in the branch R_3R_4 is much larger than the current in the base emitter junction of Q_2. The value of the bias voltage V_R applied to the base of Q_2 should be adjusted such that Q_2 remains operating in the active region when the laser diode is on.

$$V_R = \frac{V_E}{R_3 + R_4} \cdot R_3 \qquad 4.5$$

if R_3 is a variable resistance then V_R can be chosen as required.

The values of the resistors R_1 and R_2 are chosen according to the previous conditions of choosing R_3 and R_4 and also to offer a 50Ω input impedance to the circuit that is:

$$\frac{R_1R_2}{R_1 + R_2} = 50 \qquad 4.6$$

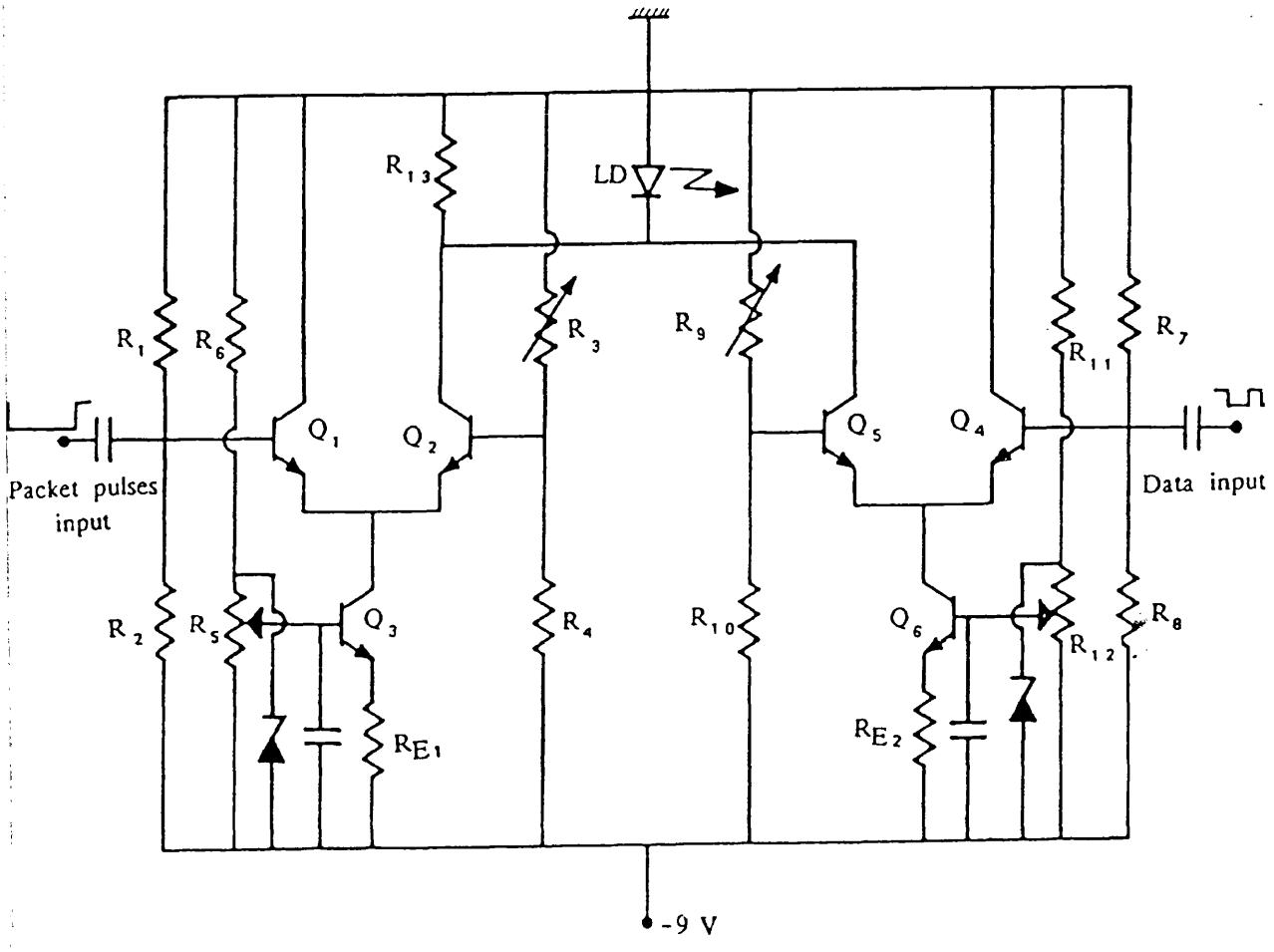

Figure 4.3 LD drive circuit for packet transmission

The value of the resistor R_{E_1} is chosen according to the value of current required to drive the LD, the values of the voltages above which the transistors saturate and to limit the current to a value less than the maximum current required to drive the LD. Also the biasing conditions at the bases of the transistors are adjusted such that they operate in the active region and the current I_{E_1}, through the current source, will be switched through Q_1 when the high level of the EcL input pulse is applied to its base while no current passes through Q_2, and the reverse will occur when the low level of the input pulse is applied. In all cases the transistors Q_1 and Q_2 do not saturate hence providing fast response.

The second stage of the laser drive is used to modulate the output of the LD by superimposing the modulating pulses on top of the pulse obtained by the first stage. This stage is similar to the first but using higher speed transistors, and the value of the resistor R_{E_2} is larger than R_{E_1} to limit the current in this stage to a value less than that of the first stage. The details of this common mode switch have been analysed in Appendix 1 which show the conditions required to operate the circuit in the active region and bias the bases of the transistors Q_1, Q_2 at the midpoint of the transfer characteristics of the switch.

4.3.1 Transient behaviour of the common mode switch

The analysis of nonlinear dynamic system is extremely difficult in practice, the solution cannot be obtained in a closed form and it is necessary to employ numerical techniques and a digital computer to obtain the solution.

The transient behaviour of the common mode switch is characterised by a delay between the excitation and response waveform, and the response rise and fall times. The formulae for these characteristic times are obtained by replacing each nonlinear capacitor by a linear capacitor that is equivalent in the sense that both

capacitors store the same amount of charge when subject to the same voltage excursion[4.20]. Considering the base circuit response of the current mode switch, the response at the common emitter node is much faster than the collector circuit response because with at least one transistor conducting at all times the impedance between the node and ground is small. Recall that there is a depletion capacitance associated with each junction, the effect of the collector–base capacitor of a transistor is multiplied by the non–linear equivalent of Miller effect. Assuming that the emitter junction is abrupt, the collector junction is linearly graded and the logic swing is about 0.8V, the equivalent linear junction capacitance is[4.21]:

$$\bar{C}_j = 1.4C_{BE_0} + 1.62C_{BC_0} \qquad 4.7$$

where C_{BE_0} is the zero bias value of the emitter base junction capacitance and C_{BC_0} is the zero bias value of the collector–base junction capacitance. The input capacitance has a diffusion capacitance component in additon to depletion capacitance. The average value of the base current dependent diffusion capacitance, C_d is:

$$\bar{C}_d = \frac{1}{\alpha_0 R_c \omega_T} \qquad 4.8$$

where ω_T is the gain bandwidth product of the transistor and R_c is the load resistor. The equivalent base circuit is a linear, time invariant single–pole RC circuit with time constant:

$$T_{b_1} = r_b(\bar{C}_j + \bar{C}_d) \qquad 4.9$$

where r_b is the dynamic resistance of the base emitter junction seen from the base terminal. The capacitance of the collector terminal has components due to the collector–base capacitance and the collector–substrate capacitance of the current mode switch transistors.

If the input signal amplitude is larger than $10V_T$, where V_T is the thermal voltage, the rise and fall time of the collector waveform are effectively limited by the collector circuit time constant.

4.3.2 Practical implementation of the LD drive circuit

In the LD drive circuit transistors Q_1 and Q_2 have been chosen of the type BFR96 which has a current gain bandwidth product of 4.5GHz and they can drive the LD with current pulses of amplitudes up to 70ma. Transistor Q_4, Q_5 have been chosen of the type MFR911 which has a current gain bandwidth product of 5GHz and they can modulate the laser diode with a current pulse of amplitude up to 30ma. The current sources transistors Q_3, Q_6 have been chosen of the type 2N3705. The values of the resistors in the circuit have been chosen, according to the previous considerations, to be:

$R_1 = R_6 = R_7 = R_{11} = 68\Omega$

$R_2 = R_4 = R_8 = R_{10} = 195\Omega$

$R_3 < 200\Omega$, $R_9 < 200\Omega$

$R_5 < 470\Omega$, $R_{12} < 470\Omega$

$R_{E1} = 65\Omega$ $R_{E2} = 68\Omega$ and $R_{13} = 1K\Omega$

The circuit has been implemented on double–sided PCB. The layout of the connection between components is shown in Figure 4.4; these connections were reduced to minimum possible length in order to reduce the parasitic inductances

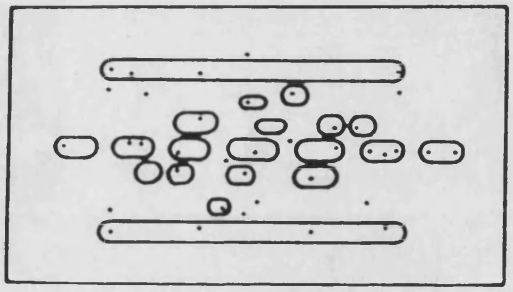

Figure 4.4 Layout of connection between the components, of the LD drive circuit shown in Figure 4.3, on PCB

and capacitances. 0.1μF capacitors are connected between the ground and the bases of transistors Q_3 and Q_6 in order to remove any voltage fluctuation due to spikes which may appear on the power supply line. In testing the circuit, the LD has been replaced by a 20Ω load, which gives nearly the same voltage drop as the laser diode when a similar drive current is used.

4.3.2.1 The dc characteristics of the LD drive circuit

The dc transfer characteristics of both stages of the laser driver have been measured practically and analysed with the microcomputer circuit analysis program Mcapii[4.22]. The results obtained for the stage which drives the laser with current pulse amplitude up to the threshold current ≃ 50mA during the duration of the packet time of 10μsec, is shown in Figure 4.5.a for the theoretical analysis while Figure 4.5.b illustrates the practical transfer characteristic measurement for different values of driving current. Both of the two graphs show that the bias applied to the bases of the transistors Q_1, Q_2 has to be ≃ − 2.4V which is in the mid point of the active region when the driving current is about 50ma. Also, Figure 4.6a,b shows the dc transfer characteristics of the second stage of the LD driver which can modulate the laser with current pulses of amplitude up to 30ma. The theoretically analysed one is in Figure 4.6a while the practically measured one is in Figure 4.6b. Both of the graphs show that the bases of the two transistors Q_4, Q_5 should be biased at about − 2.35V which is in the mid point of the active region when the modulation current is about 20ma.

4.3.2.2 Transient characteristics of LD drive circuit

The transient responses of both stages of the LD drive circuit have been tested both by using Mcapii and practically. The results obtained, when replacing the LD with a 20Ω load and 2pF capacitor in parallel, are illustrated in Figures

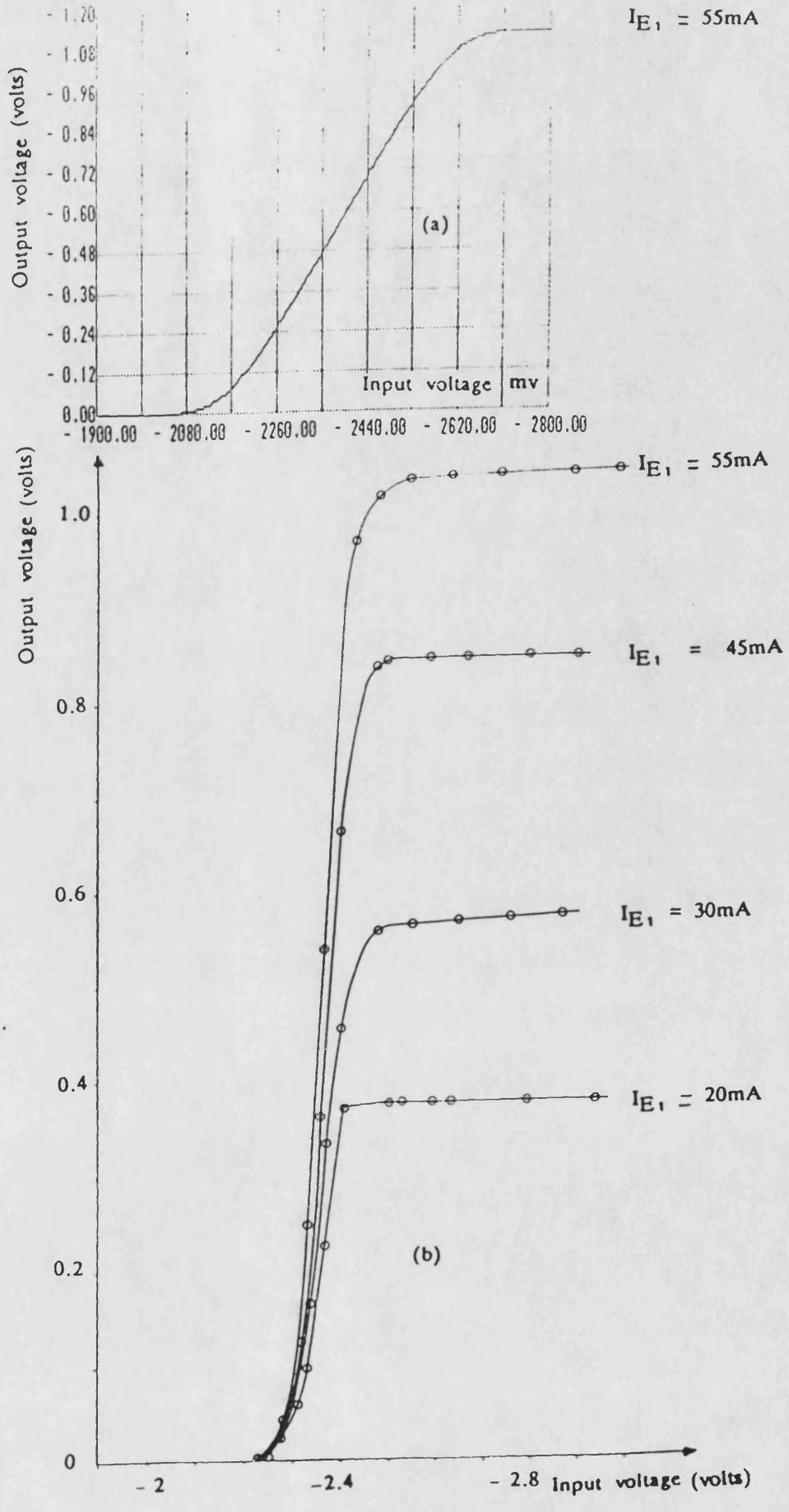

Figure 4.5 DC characteristics of LD packet pulse driving stage for transistors Q_1, Q_2 of the type FR96, using 20Ω load instead of LD

a) using Mcapii

b) practically

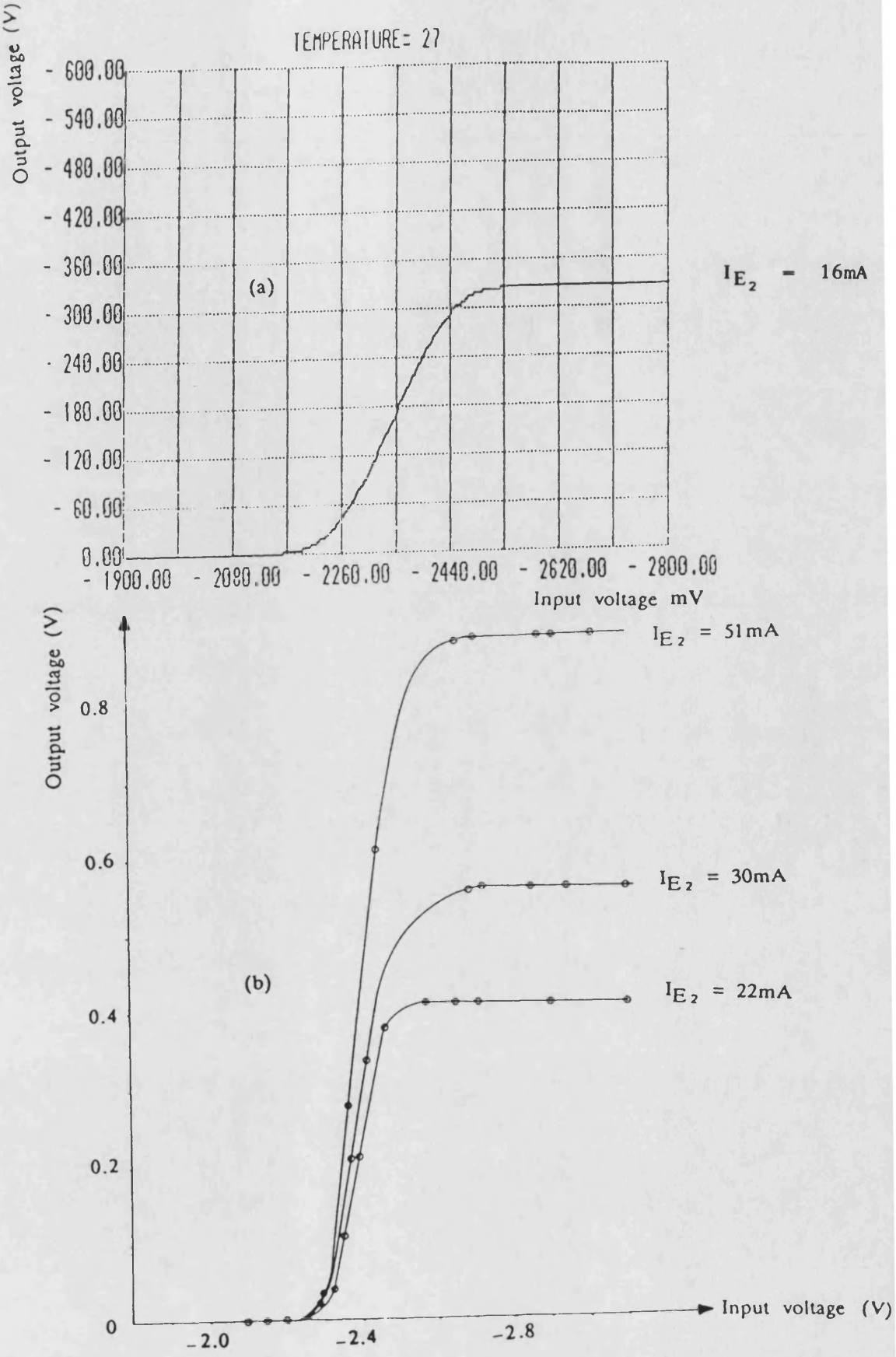

Figure 4.6 DC characteristics of LD modulation driving stage for transistors Q_4, Q_5 of the type MRF911, using 20Ω load instead of LD

a) using Mcapii
b) practically

4.7a,b,c,d and 4.8a,b. Figure 4.7a shows an input pulse of width 10μsec, to the first stage while Figure 4.7b shows the corresponding output voltage which represents a current pulse of 54ma in a 20Ω load. Also, Figures 4.7c,d show the input and output for the same case but when the input pulse has a pulse width of 5nsec and a rise time of 0.5nsec. This has been done in order to evaluate the corresponding rise time and delay of the output pulse. The figure shows that the output pulse has a rise time $\simeq$ 1nsec and a delay $\simeq$ 0.5nsec. Figure 4.8a,b shows the input and output measured practically for this stage using a pulse width of 10μsec. The output pulse amplitude was 1.1 volt in 20Ω load which represents a current of 55ma.

The same experiment has been repeated for the second stage which is used to modulate the LD.

Figure 4.9a shows the input modulating pulse to the second stage, which has a width of 5nsec and rise time of 0.5nsec. The corresponding output voltage pulse across the 20Ω load for a current pulse of 16ma amplitude is shown in Figure 4.9b which shows a rise time $\simeq$ 0.6nsec and a delay of 0.5nsec. Also the practical results obtained for the input and output are shown in Figures 4.10a,b which shows rise and fall times of about 1.6nsec for the output pulses of current amplitude 16ma while the input pulse rise and fall times were about 1.4nsec.

These previous results show that the drive circuit would be able to drive the laser with a current up to the threshold current ($\simeq$50ma) during the packet duration (10μsec) and modulate it with the data pulses of bit rates up to 250Mbit/s.

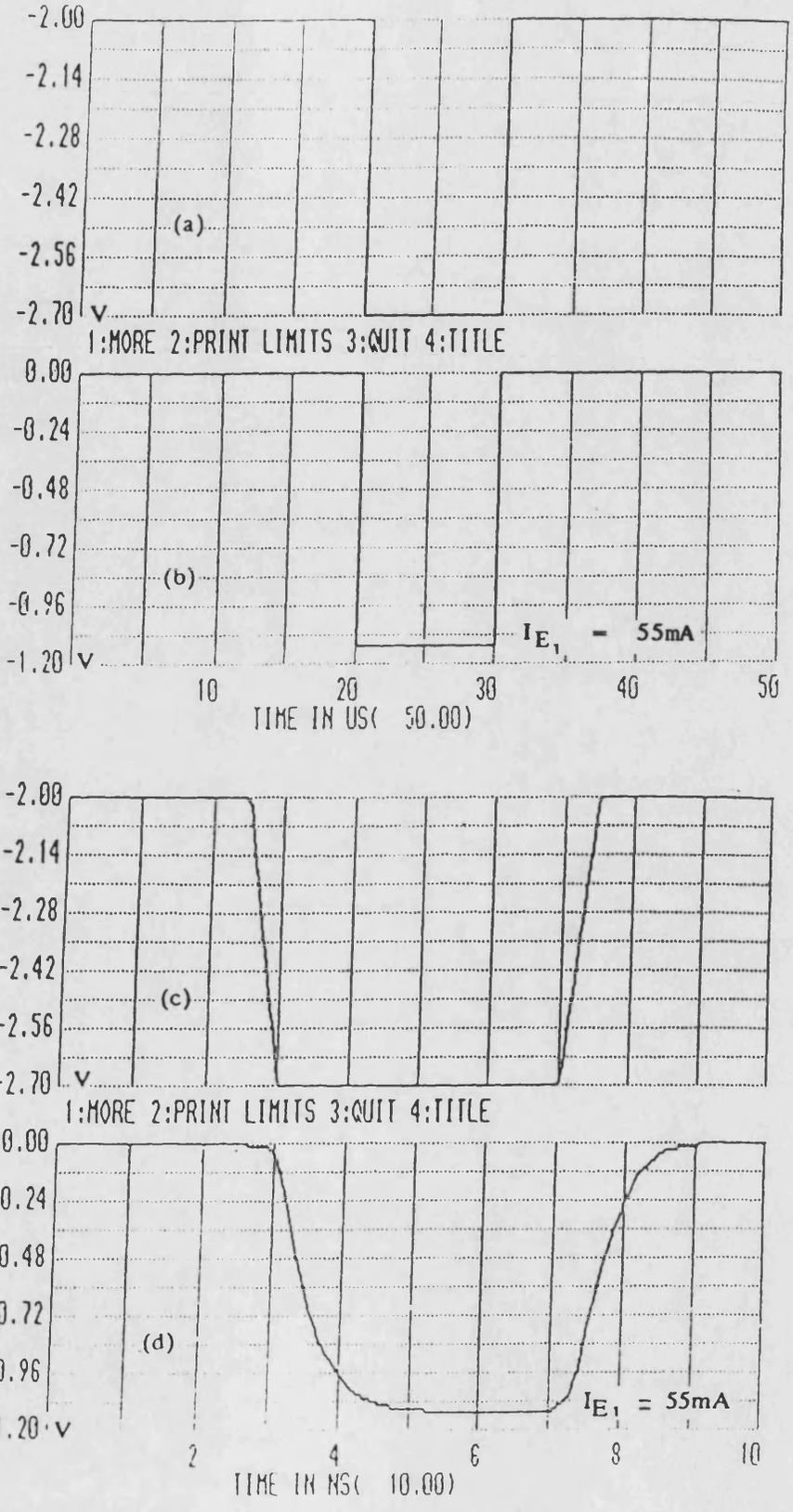

Figure 4.7 Input and output pulses for packet pulse driving stage using transistors Q_1, Q_2 of the type BFR96 by Mcapii

(a),(b) Input pulse of width 10μsec and its corresponding output.

(c),(d) Input pulse of width 5ns and its corresponding output.

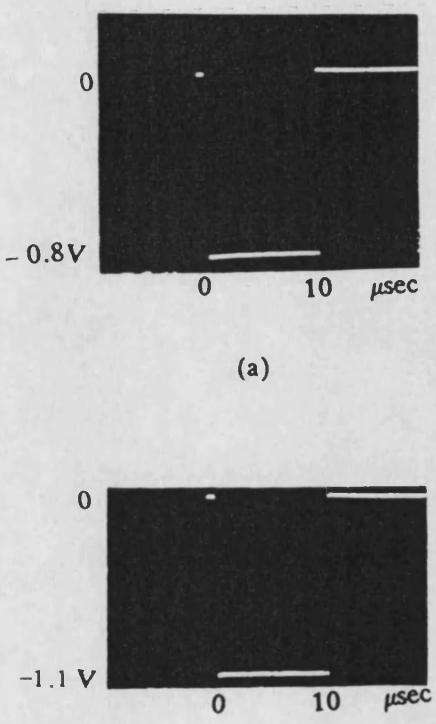

Figure 4.8 The input and output of laser diode packet drive stage (measured using 20Ω load instead of the LD).

a) input
b) output

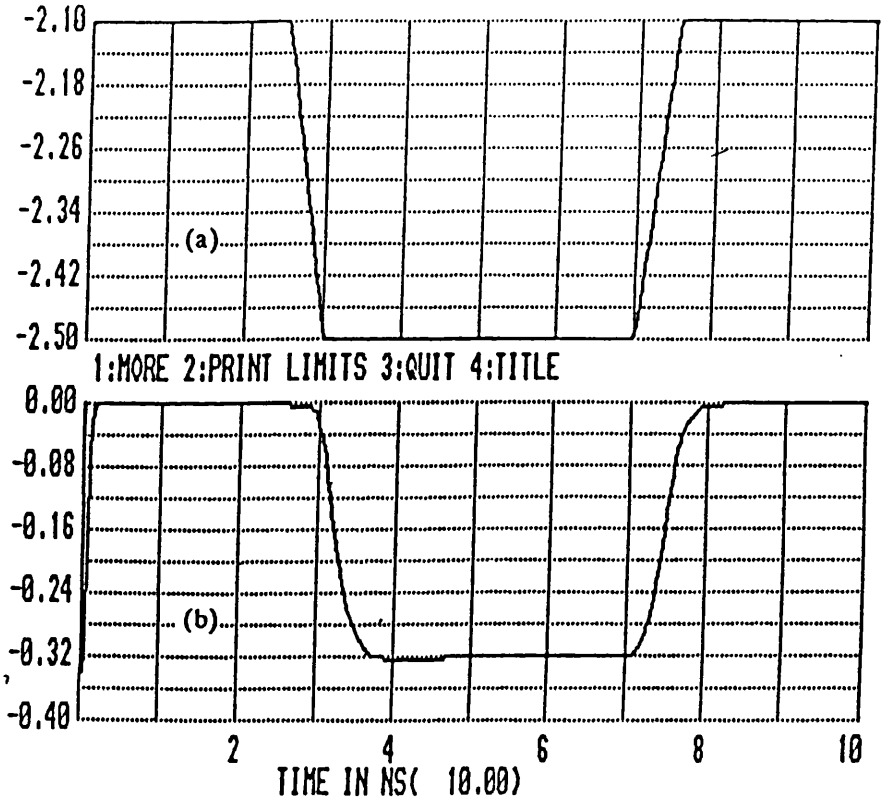

Figure 4.9 Input and output pulses for LD modulation driving stage using transistors Q_4, Q_5 of the type MRF911 by Mcapii. For pulse width 5nsec

a) input pulse
b) output pulse

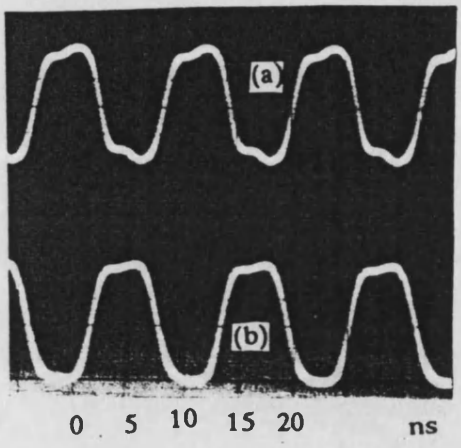

Figure 4.10 The input and output of the modulating stage of the LD drive circuit (measured by 275MHz bandwidth oscilloscope of the type HP8081A).

a) input
b) output

4.3.3 LD protection

The LD has to be protected against voltage spikes which may occur on power supply lines. These spikes can cause a current spike in the laser diode which may increase the driving current more than the maximum limit, leading to damage of the device. To protect the LD against these spikes, a zener diode of low slope resistance is connected across the fixed terminals of the potentiometers such that if a voltage spike occurs on the power supply lines this will have only a slight effect on the voltage applied to the bases of the transistors Q_5, Q_6; hence, reducing the corresponding current spike. The values of the resistances R_{E_1}, R_{E_2} have also to be increased so that the current spike which may occur is minimised. The zener diodes which have low slope resistances and supply a constant voltage of 6.2V are connected across R_5 and R_2, respectively, $R_{E_1} = 65\Omega$ and $R_{E_2} = 68\Omega$. This change leads to the choice of a higher value of −9 volts for the power supply voltage, in order to provide the required protection to the LD.

The amplitude of the spikes which occur on the power supply lines when switching on any device that is connected to the mains, has been measured using a storage oscilloscope and has been found ≃ 2 volt. To evaluate the effect of this spike on the driving current, consider Figure 4.3. V_b is the voltage at the base of the transistor Q_3, and R_x the value of the resistance between the terminals of the potentiometer connected to the base of Q_3 and power supply line. If the power supply voltage is V, then:

$$V_b = \frac{V R_x}{R_5 + R_6} \qquad 4.10$$

so the voltage at the emitter of the transistor Q_3 is:

$$V_E = \frac{V R_X}{R_5 + R_6} - V_{BE(ON)} \qquad 4.11$$

where $V_{BE(ON)}$ is the base emitter voltage required to turn the transistor on. Then the current in the tail resistor R_{E_1} is:

$$I_E = \frac{V_E}{R_E} \qquad 4.12$$

$$I_E = \frac{R_X}{(R_5 + R_6)R_E} V - \frac{V_{BE(ON)}}{R_E} \qquad 4.13$$

so if a relation is drawn between power supply voltage V and I_E a straight line is obtained, its slope is:

$$\frac{R_X}{(R_5 + R_6)R_E} \qquad 4.14$$

This slope gives the rate of change of I_E with respect to V when applying a certain value of V_b. This experiment has been carried out and a slope of −8.5 ma/v has been obtained when the current I_E was initially set at 60ma when the supply voltage was −9v. So if the power supply voltage is affected by −2V spike then it will increase the current I_E by −8.5 x −2 = 17ma which may damage the LD.

Connecting a zener diode, of small slope dynamic resistance r_s = 5Ω and a breakdown voltage V_Z = 6.2V, across the R_5 end terminals will limit the increase in current due to the spike. The previous experiment has been repeated and the slope of the obtained straight line has been found to reduce to a value −1.7mA/V,

so a voltage spike of −2V on the power supply will only increase the current by −1.7 x −2 = 3.4mA. An evaluation of the change in current when the zener diode is connected across R_5 is analysed in Appendix II.

After connecting the zener diodes across both R_5 and R_{10} the laser diode HL8311E is connected with the laser driver, instead of the 20Ω load, and aligned with a PIN photodetector of the type MFOD1100.

The LD has been driven with a pulse of 10μsec width and of current amplitude up to the threshold value and the modulation pulses superimposed on the top of this 10μsec pulse. The optical output of the photodiode has been monitored using 1GHz bandwidth oscilloscope of the type hp54100A. Figure 4.11a shows the input modulation pulses while the corresponding optical output is shown in Figure 4.11b. This shows that the optical pulse has a rise and fall times of about 1ns while the pulse width was 2.6nsec. So the laser driver can be used to modulate the laser diode in a bursty mode up to 250Mbit/sec. The light–current characteristics and its variation with temperature will be examined in the next chapter using this laser driver.

4.4 LD Power Control Considerations

The laser diode has a threshold current which is a sensitive function of temperature, also the threshold level tends to increase as the LD ages, following an increase in internal device losses. So some form of feedback control is required to ensure continuous laser operation and stability of the output of the device. Although the laser may be cooled to compensate for temperature variations, aging is not so easily accommodated by the same process. However, both problems may be overcome through control of laser bias using feedback techniques, so it is usually necessary to monitor the light output from the LD in order to keep some

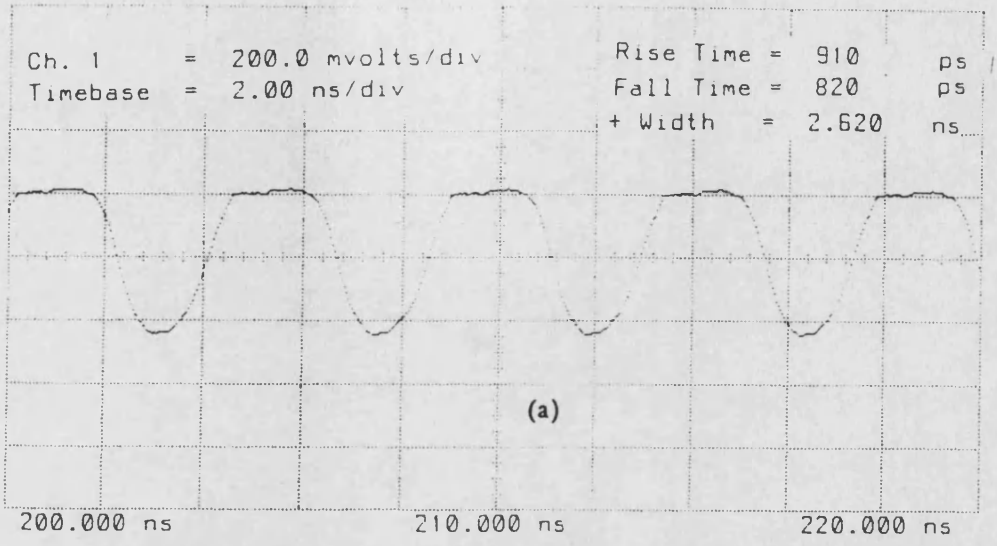

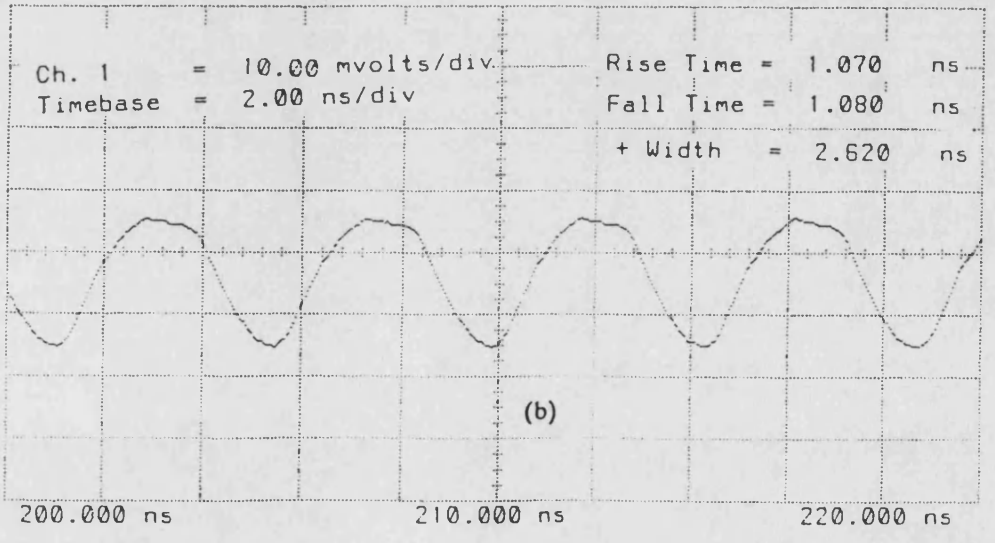

Figure 4.11 The input and optical output of the LD HL8311E (measured using 1GHz oscilloscope of the type HP54100A).

a) Input
b) Optical output

aspect of it constant. Also the laser slope efficiency may change with temperature and aging, in order to compensate for such changes the ac and dc components of the monitored light output must be processed independently.

This is especially important in the case of high bit rate digital systems where control of the on and off levels as well as light level is required.

This power control circuit for LD operating at high bit rate in a burst mode has been designed and examined in Chapter 6.

4.5 References

4.1 C. C. Timmermann: "Highly efficient light coupling from GaAℓAs lasers into optical fibres", Appl. Opt., 15(10), pp2432-2433, 1976.

4.2 M. Maeda, I. Ikushima, K. Nagano, M. Tanaka, H. Naskshima and R. Itoh: "Hybrid laser to fibre coupler with a cylinderical lens", Appl. Opt., 16(7), pp1966-1970, 1977.

4.3 K. Konnerth et al: "Delay between current pulse and light emission of GaAs injection laser", Appl. Phys. Lett., 4, p126, 1964.

4.4 J. E. Riper: "Measurement of spontaneous carrier lifetime from stimulated emission delays in semiconductor laser", J. Appl. Phys., 43, p176, April 1972.

4.5 J. E. Ripper and J. C. Dyment: "Time delay and Q-switching in junction lasers", IEEE J. Quant. Electron. QE-5, pp396-403, August 1979.

4.6 M. Ettenberg, C. J. Neuse and H. Kressel: "The temperature dependence of threshold current for double-heterojunction lasers", J. Appl. Phys., 50, pp2949-2950, April 1979.

4.7 R. Chin, N. Holonyak, B. A. Vojak, K. Hess, R. D. Dupuis and P. D. Dapkus: "Temperature dependence of threshold current for quantum-well heterostructure laser diodes", Appl. Phys. Lett., 36, pp19-21, January 1980.

4.8 G. H. B. Thompson: "Temperature dependence of threshold current in GaInAsP DH lasers at 1.3 and 1.5μm wavelength", IEEE Proc., 128, 37-43,

April 1981.

4.9 T. Ikegai et al, Electron. Comm. (Japan), 51-B, p57, 1968.

4.10 R. Roland: "Spikes in the light output of room temperature GaAs junction lasers", Appl. Phys. Lett., 11, p346, 1967.

4.11 M. Boersp et al: "Dynamic behaviour of semiconductor lasers", Electron. Lett., 11, p206, 1975.

4.12 T. Ikegai: 1st Eur. Conf. on Opt. Comm., London, 1975.

4.13 T. Kobayashi et al, Japan J. Appl. Phys., 15, p2025, 1976.

4.14 M. R. Matthews et al: "Spectral and transient response of low threshold proton-isolated GaAs lasers", Electron. Lett., 14, p649, 1978.

4.15 L. A. d'Asaro et al: "Spikes in the light output of room-temperature GaAs junction lasers", IEEE J. Quant. Electron. QE4, p164, 1968.

4.16 N. G. Basov, Ibid, p855.

4.17 R. J. McIntyre: "Multiplication noise in uniform avalanche diodes", IEEE Trans. Electron. Dev., ED-13, p164, 1966.

4.18 V. J. Mazuczyk: "Sensitivity of single mode buried heterostructure lasers to reflected power at 274 Mbit/s", Electron. Lett., 17, p143, 1981.

4.19 S. Moustakas and H. H. Witte: "Laser bias effect on the receiver sensitivity

of passive fibre optic star bus networks", Optical and Quantum Electronics, 15, pp397–405, 1983.

4.20 T. R. Bashkow: Effect of non-linear collector capacitance on collector current rise time", IRE Trans. on Electron Devices, ED-3, pp167–172, October 1956.

4.21 C. S. Meyer, D. K. Lynn and D. J. Hamilton: "Analysis and Design of Integrated Circuits", McGraw Hill, Chapter 7, 1968.

4.22 "Microcomputer Circuit Analysis Program", Spectrum, Professional Software Products.

CHAPTER 5

HEATING EFFECTS AND TEMPERATURE CONTROL OF SEMICONDUCTOR LASERS

5.1 Introduction

In a laser transmitter, when a constant amplitude current pulse is used to modulate a semiconductor laser, the temperature inside the laser diode will increase as a result of the current, hence affecting strongly the operating characteristics and lifetime of the device. This temperature rise will lead to a change in the emission wavelength and a broadening in the spectral line width, also to an increase of the threshold current, and hence a decrease in optical output power. The heat generated in the active layer of the LD takes some time to be transferred by conduction until reaching the steady state. During the thermal rise time the optical power is decreasing which in case of packet transmission may cause an error in the received data. If this thermal rise time is a few nanoseconds, only the first few pulses in the data will be affected, while if the thermal rise time is long then its effect on the data has to be considered.

The average operating temperature of the LD depends on its construction, material and on its mode of operation. If the diode is biased above threshold and then modulated in a continuous mode then the average rise in temperature will be greater than if it is operated in a bursty mode, as it is intended to be used. In both cases there is a need to stabilise the operating temperature of the device and to get rid of the heat generated, in order to prolong its lifetime. In this chapter a temperature controller has been implemented using a Peltier cooler in order to stabilise the average operating temperature of the laser diode. This temperature

controller has been used together with the laser drive circuit discussed in the previous chapter, to measure the light–current characteristics of the LD at different operating temperatures. A practical method to measure the rise in temperature of the LD and its thermal rise time has been presented, used and the results have been compared with the theoretical predicted values.

5.2 Previous Work

Theoretical and practical research has been done on the temperature distribution and thermal resistance of lasers in order to achieve stable and long life operation of these devices under cw conditions. For instance, the work done by Joyce and Dixon(5.1), Kobayashi and Furukawa(5.2). However, in many circumstances, the laser is required to operate under pulsed condition, for instance, in high power output or in data modulation applications. If a constant amplitude current pulse is used in modulating a semiconductor laser the temperature inside the laser will increase as a result of increasing the current pulse. Engler and Garfinkel(5.3) in 1965 have proposed a very simple model to estimate the transient temperature rise in the active layer of a semiconductor laser. This model assumed a steady heat injection from the active layer to a thick GaAs substrate layer connected to a heat sink. More recently Nakwaski has developed a new model of heat conduction in semiconductor lasers, which is applicable to the broad area of contact double heterostructure laser diodes and it is solved by a transformation technique[5.4,5.5].

Among the works of experimental research on semiconductor laser thermal characteristics, Dyment et al[5.6] estimated the p–n junction temperature, utilising the fact that the peak wavelength (λ_p) of the spontaneous emission spectrum shifts to longer wavelengths as the junction temperature (T) increases. Further, Kobayshir and Furukawa[5.2] have measured the temperature distribution on the

mirror surface of a double heterostructure laser under cw operation, by using a thermal plotter. Suyam et al[5.7] has observed the transient temperature variation of the active region of injection lasers by means of a Michelson interferometer and was able to measure the temperature, T_j, of the active region with an extremely high resolution ($\Delta T_j < 0.01\,^0C$) as a function of time.

5.3 Thermal Characteristics of GaAs Laser Junction

When a laser diode is driven by an injection current, three sources of heat occur inside the diode: i) Joule's heat; ii) absorption of spontaneous and stimulated emission; and iii) the energy dissipated by non-radiative transitions. The first is distributed through the material. The second occurs mainly within the active layer, capping layers and substrate. The third is confined within the active layer, to within a minority carrier diffusion length of the junction. The relative magnitude of these sources depends upon the diode construction, temperature and current density.

As the temperature is increased the threshold current rises and both the internal quantum efficiency and the thermal conductivity fall, so more heat is generated and its removal becomes more difficult.

The threshold currents for a GaAs laser structure run in the order of 10^3–10^4 A/cm^2, even if one ignores any series resistance in the diode and considers only the 1.5 volts drop across the junction, this will represent a power input of 10^3–10^4 W/cm^2 this power input is sufficient to heat the junction and to produce profound effects on the laser diode as follows:

1. The threshold current increases and the optical output power decreases.

2. It degrades the laser diode, thus reducing its useful lifetime.

3. The wavelength of the emitted light changes by approximately $2.8A^0/C^0$ for a reflection feedback laser and by $0.7A^0/C^0$ for distributed feedback laser.

4. The spectral line width is broadened.

5. The current density increases which can lead to thermal runaway that will destroy the device.

The effects of the temperature rise on the light output of GaAs laser structures have been investigated[5.8] and methods of achieving stable output through CW operation have been presented[5.9]. Further, pulsed operation is sometimes desirable, in this case, the temperature rise at the laser diode junction depends on the pulse current, the base temperature and the pulse width. In analysing the problem one has to consider the variation of thermal conductivity and heat capacity with temperature, and also the effect of bulk resistivity and contact resistance have to be included. One of the important assumptions in the analysis is that one end of the diode is kept at a fixed temperature regardless of the heat input to the other end.

In practice there will be a temperature gradient across solder layers, the header and the like. Under short high power pulsed conditions the thermal heat capacity of the diode prevents the heat generated at the junction from diffusing far from it. The solder layers are thus unimportant provided they are sufficiently far from the junction area, i.e. several thermal diffusion lengths away. These solder layers are still important in determining the allowable pulse repetition rates and the effect of series resistance. Figure 5.1 represents the junction of a GaAs laser

diode having an area A, which sits upon a cooled substrate which is maintained at temperature T_B. The p-n junction is at distance L from the substrate current flows in at the top and flows out through the substrate. The heat flux into the junction at X = L is Q_j having the shape shown in Figure 5.2. An expression for temperature at the junction, (i.e. X = L) as a function of time is required. The heat diffuses from the junction region, a portion diffusing up through the p-type material and a portion diffusing down through the n-type material. Figure 5.3 shows the variation of thermal conductivity with temperature for p-type and n-type material of GaAs. They are nearly equal above $100K^0$. In addition to the heat generated at the junction there are two other sources of heat, the heat due to bulk series resistance of the diode and heat due to contact resistance. The heat at the contact will be neglected in the calculation of the junction temperature rise since it occurs many diffusion lengths away from the junction while the heat due to the series resistance will be included in the calculation, they are important only at high current levels.

The equation of heat transfer in the laser diode is:

$$\frac{\partial^2\theta}{\partial X^2} - \frac{1}{D(\theta)}\frac{\partial\theta}{\partial t} = -J \qquad 5.1$$

where J is the heat due to bulk resistivity

$\theta = \int_0^T K(T)dT$ defines a new temperature scale

K is the thermal conductivity

$D(\theta)$ is the diffusion constant

$$D(\theta) = \frac{K}{C}$$

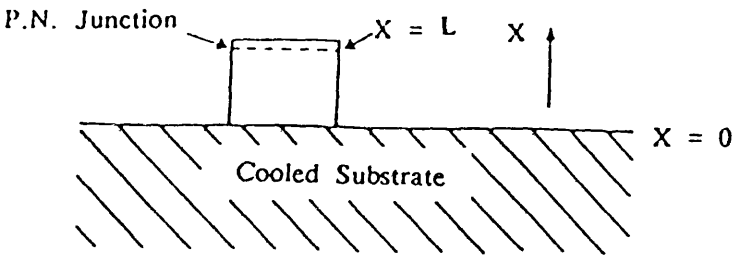

Figure 5.1 Schematic representation of diode

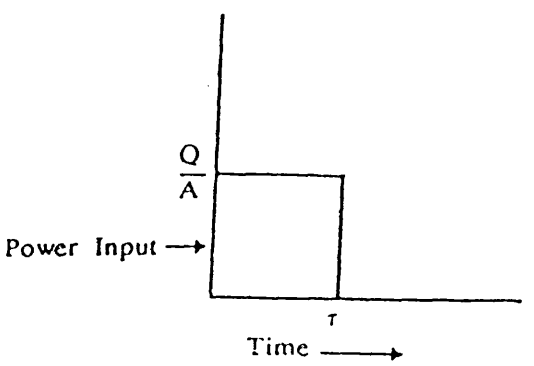

Figure 5.2 Shape of the heat pulse

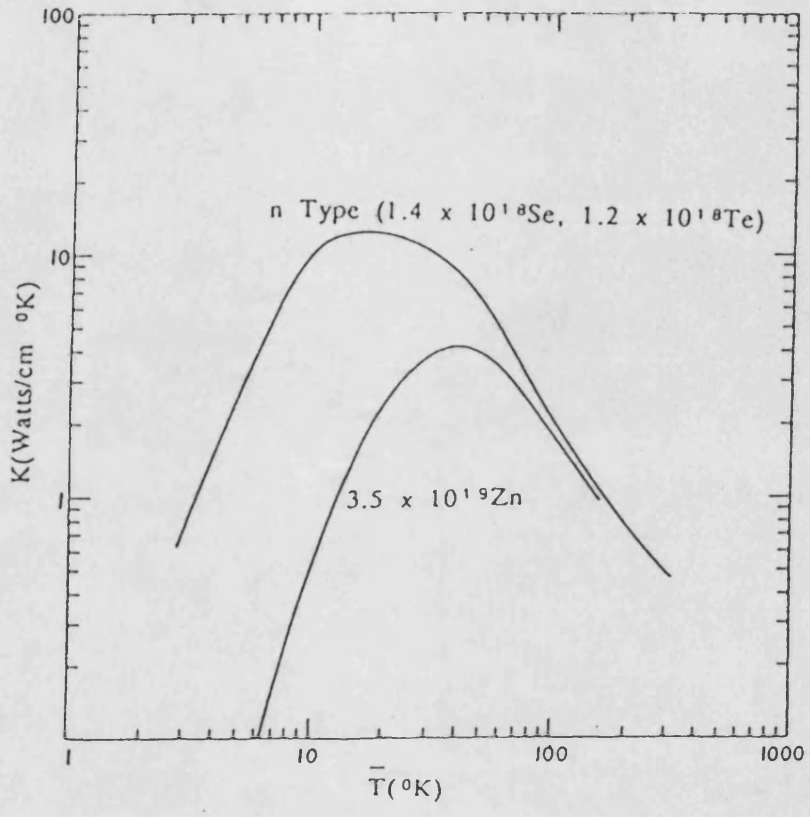

Figure 5.3 Thermal conductivities of GaAs

where C is the heat capacity per unit volume.

Since K,C change with temperature, so $D(\theta)$ changes with temperature, but considering K and C to be constant for a small change in tempterature then $D(\theta)$ can be considered constant D. If J is neglected then the solution of equation (5.1) for times less than the pulse length are given in Carslaw and Jaeger[5.10].

Figure 5.4 illustrates the relation between the junction rise in temperature (ΔT) normalised to the dc value ΔT_∞ (the rise in temperature after a time long enough to reach the steady state) and Dt'^2/L. This figure is drawn from the general solution of equation (5.1). It is to be noted that when the thermal diffusion length is equal to the length of the sample, then the dc temperature T_∞ is reached and any further increase in the length of the heat pulse causes no further temperature rise.

The pulse length for which the temperature rise saturates, t_{dc}, is thus defined by:

$$Dt_{dc} = L^2$$

Only a fraction of the current produces heat Q_j at the junction. Defining the junction quantum efficiency, η, as the fraction of the current which produces light:

$$\therefore Q_j = IV_j \left[1 - \frac{\eta h\upsilon}{V_j}\right]$$

where I is the junction current, V_j is the junction voltage and $h\upsilon$ is the photon energy expressed in volts. The ratio of the heat flow into the n- and p- material depends upon temperature. The value to be used for Q is $Q_j/2$ for temperatures

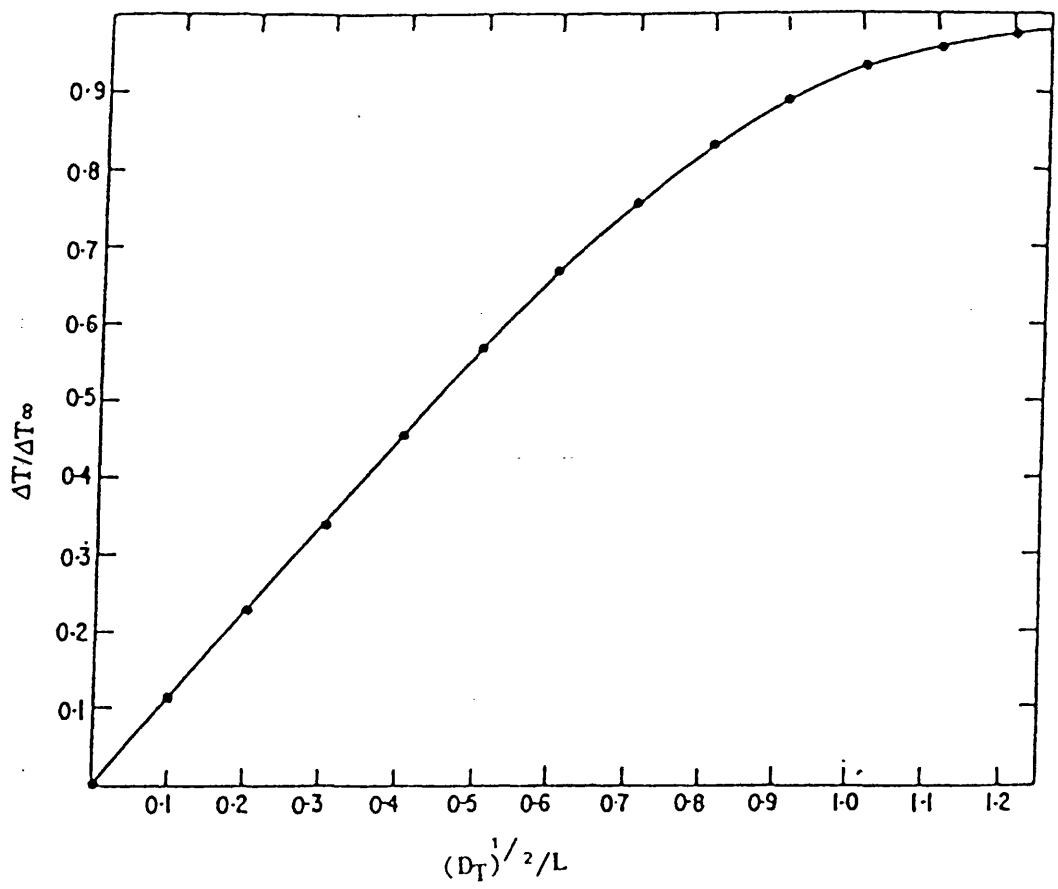

Figure 5.4 Junction temperature rise normalised to the dc value

above 70°K.

5.4 Transient Temperature Effects in a Stripe Geometry Laser

The analysis of the more conventional double heterostructure stripe geometry laser is more complex. Figure 5.5 shows the structure of the stripe geometry laser which has been used by Zhang[5.11] to calculate the temperature rise during a current pulse in the laser diode. For the case of stripe laser all the heat sources are confined within the current stripe path as shown in the figure; a 10-μm stripe laser has been taken as an example to analyse the model. The temperature rise in the ith layer due to heat generated inside the diode can be obtained from the equation:

$$C_i \frac{\partial T}{\partial t} = K_i \left[\frac{\partial^2 T}{\partial x^2} + \frac{\partial^2 T}{\partial y^2}\right] + g_i(y) \quad , \quad t > 0 \qquad 5.2$$

where C_i, K_i, $g_i(y)$ are the specific heat per unit volume, the heat conductivity and the rate of heat generation repsectively for layer i.

The interface condition is:

$$K_i \frac{\partial T}{\partial x} = K_{i-1} \frac{\partial T}{\partial x} \qquad 5.3$$

At the start of the current pulse, the diode is assumed to have a uniform temperature distribution at 20°C. The temperature change in the y-direction is expected to be much slower than in the x-direction because the stripe width is much greater than the active layer thickness and because of the thermal mass of the material beyond the stripe edges. Because of this it is impossible to apply the

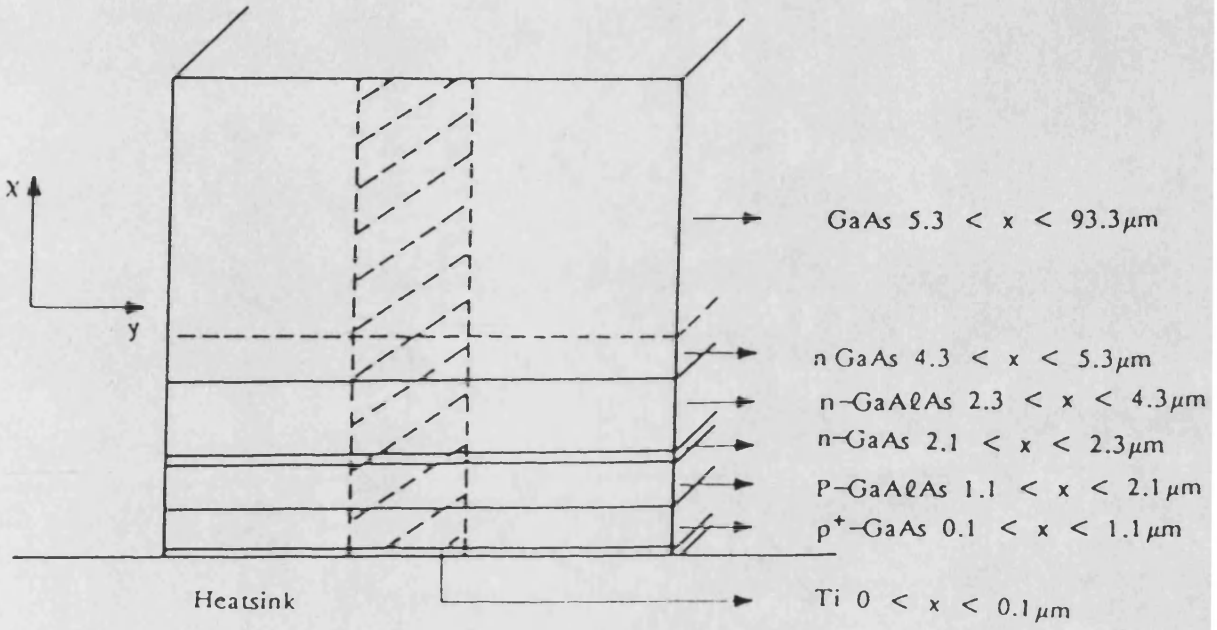

Figure 5.5 The stripe geometry laser structure used in the calculations. The shaded area is the current path in which heat is assumed to be generated. (Not to scale.)

finite difference methods to solution of T in the y-direction[5.12], so the two-dimensional partial differential equation (5.2) can be reduced to a one-dimensional partial differential equation and to a one-dimension heat conduction problem solved numerically. To simplify equation (5.2) the second term of the right hand side can be written as:

$$\frac{\partial^2 T(j)}{\partial^2 y} \cong \frac{T(j+1) - 2T(j) + T(j-1)}{(\Delta y_j)^2} \qquad 5.4$$

in this way a time dependent parabolic equation for each layer can be found which for the ith layer takes the form:

$$C_i \frac{\partial T(1)}{\partial t} = K_i \frac{\partial^2 T(1)}{\partial X^2} + K_i \frac{T(2) - T(1)}{(\Delta y_1)^2}, \quad t > 0 \qquad 5.5$$

$$C_i \frac{\partial T(j)}{\partial t} = K_i \frac{\partial^2 T(j)}{\partial X^2} + K_i \frac{T(j+1) - 2T(j) + T(j-1)}{(\Delta y_j)^2} + g_i, \quad t > 0 \qquad 5.6$$

$$C_i \frac{\partial T(32)}{\partial t} = K_i \frac{\partial^2 T(32)}{\partial X^2} + K_i \frac{T(31) - T(32)}{(\Delta y_{32})^2}, \quad t > 0 \qquad 5.7$$

The coefficient g_i is zero everywhere except beneath the stripe contact area ($100\mu m < y < 110\mu m$). 32 unequal interval points have been taken in the y-direction in the finite difference approximation. A laser diode width of $210\mu m$ in total is taken to be a typical dimension. At the first and last points in the y-direction, T(0) - T(1) = 0 and T(33) - T(32) = 0 in equation (5.4) to represent the adiabatic boundary condition. In the x-direction, the boundary conditions at the top of substrate remains adiabatic. For areas beyond the stripe a good heat

insulator sio^2 exists and so adiabatic conditions apply. The method of Lines and Gear[5.13] has been used to solve the 32x6 one-dimensional time dependent parabolic equations.

Figures 5.6a,b represent the temperature distributions in the x and y direction as obtained by Zhang from the calculated results for 10μm and 6μm stripe-down mounted lasers respectively at an injection current density J = 1000A/cm^2 which is calcualted after 400nsec from the start of the pulse.

For stripe-up mounted laser the method of calculation is precisely the same but the boundary conditions change, in this case the boundary conditions can be written as:

$$T = 20^{o}C \quad , \quad X = 0 \quad , \quad 0 < y < 210\mu m \qquad 5.8$$

$$\frac{\partial T}{\partial X} = 0 \quad , \quad X = 93.3\mu m \quad , \quad 0 < y < 210\mu m \qquad 5.9$$

Figures 5.7a,b are the equivalent to figures 5.6a,b but for the case of stripe-up mounted lasers from these figures it is seen that for stripe-up mounted lasers the temperature at the surface is as high as that in the active layer.

The temperature has been calculated by Zhang at different times for 10μm and 6μm stripes in case of stripe-down and stripe-up mounted lasers. Figure 5.8a shows the variation of temperature in the active region with time for 10μm and 6μm stripe-down mounted laser while Figure 5.8b is the equivalent of Figure 5.8a but for stripe-up mounted laser. It is seen from these figures that stripe-up mounted lasers need a much longer time to reach a steady state temperature distribution than stripe-down mounted lasers and this steady temperature is much

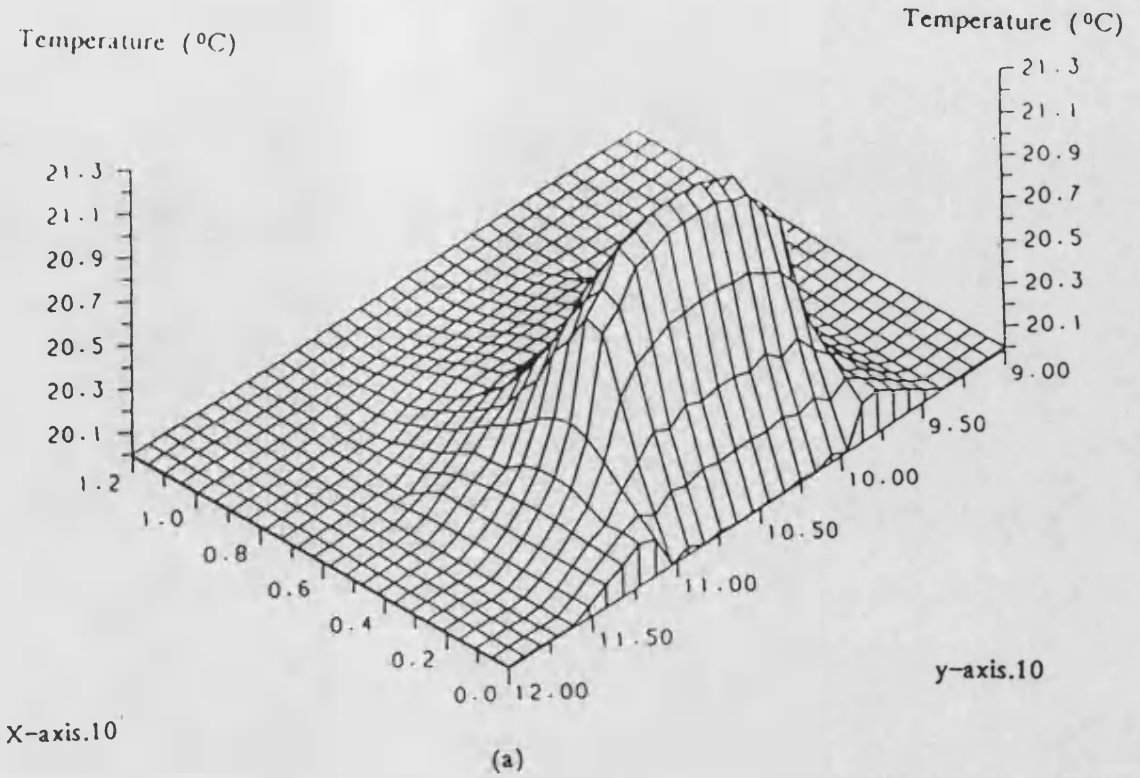

(a)

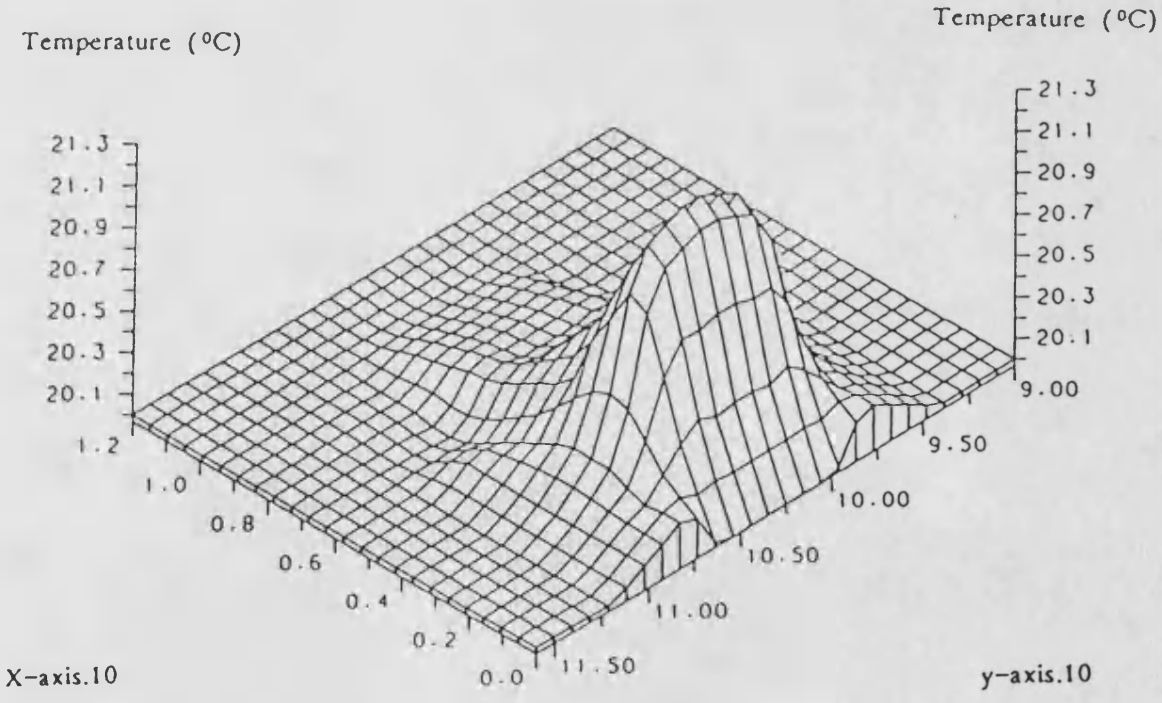

(b)

Figure 5.6 Temperature distribution in X and y directions for stripe-down mounted lasers

a) 10μm-stripe
b) 6μ-stripe

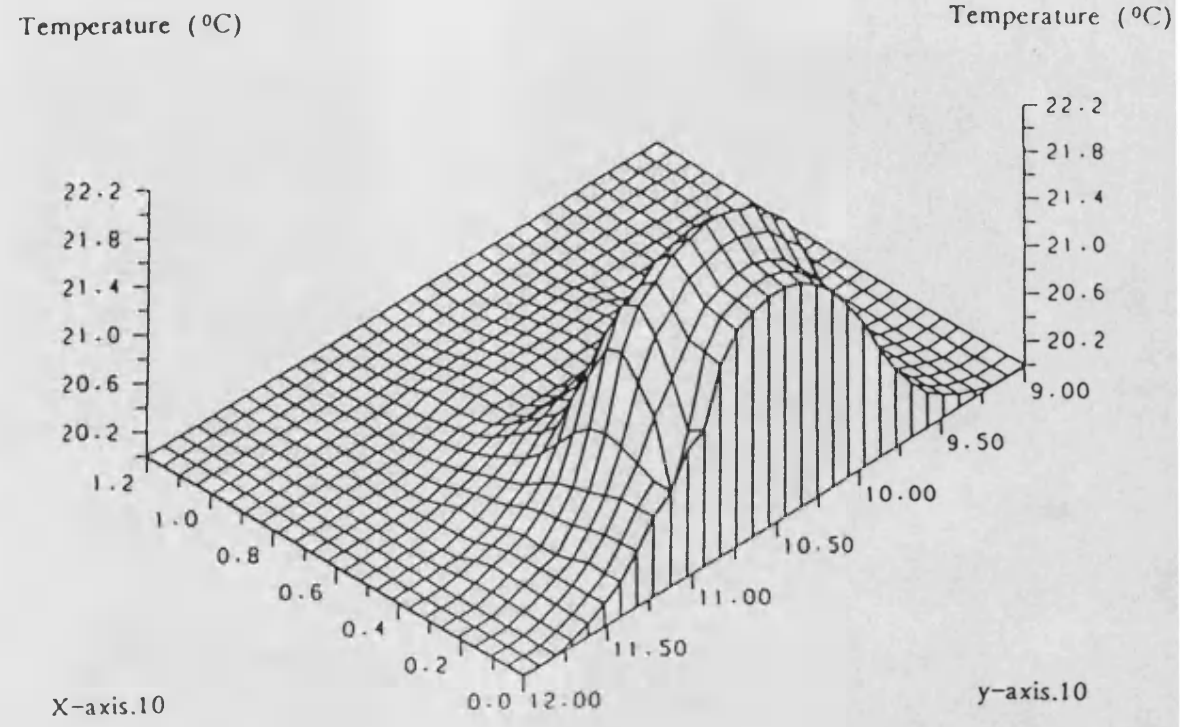

(a)

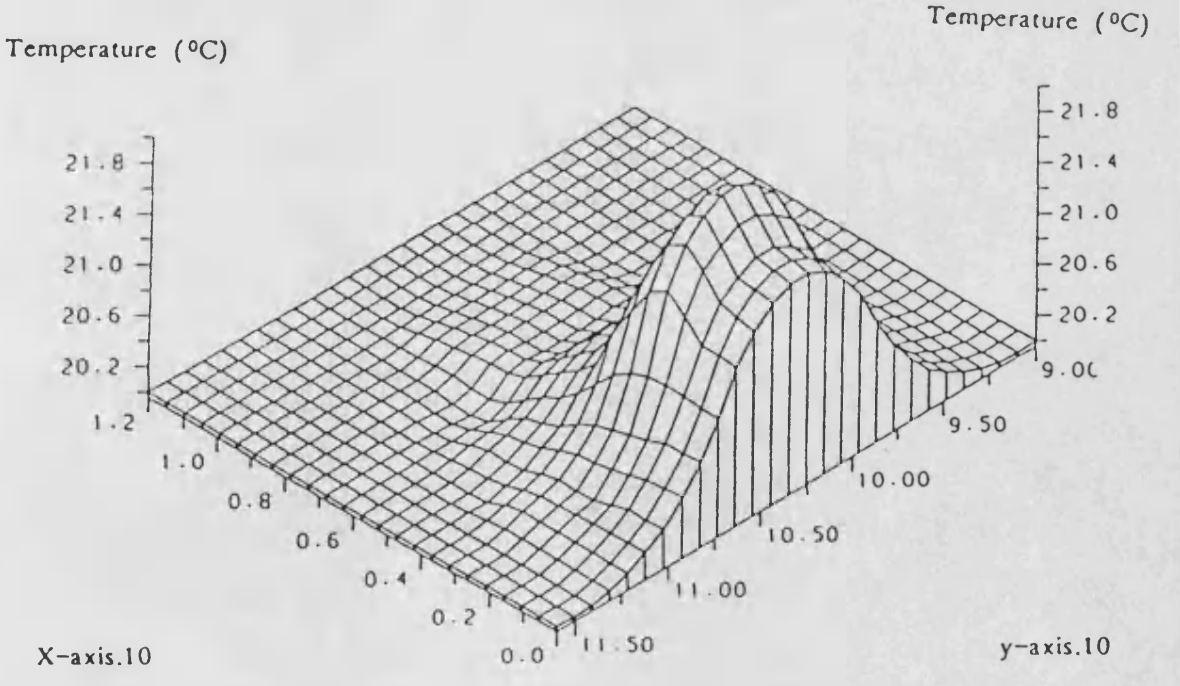

(b)

Figure 5.7 Temperature distributions in X and y directions for stripe-up mounted lasers

a) 10μm-stripe
b) 6μm-stripe

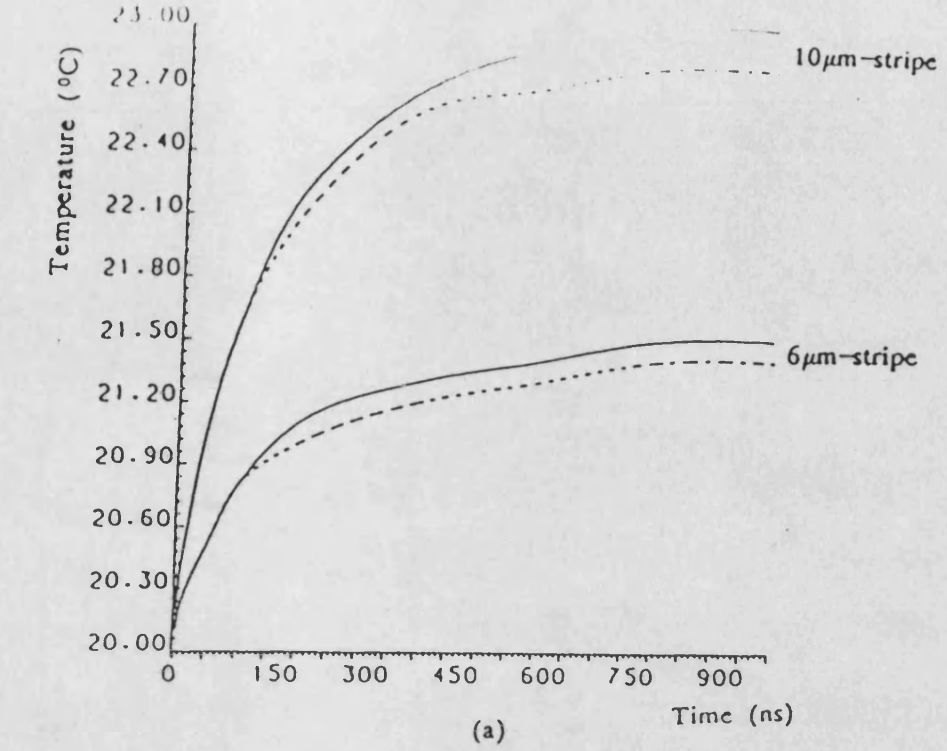

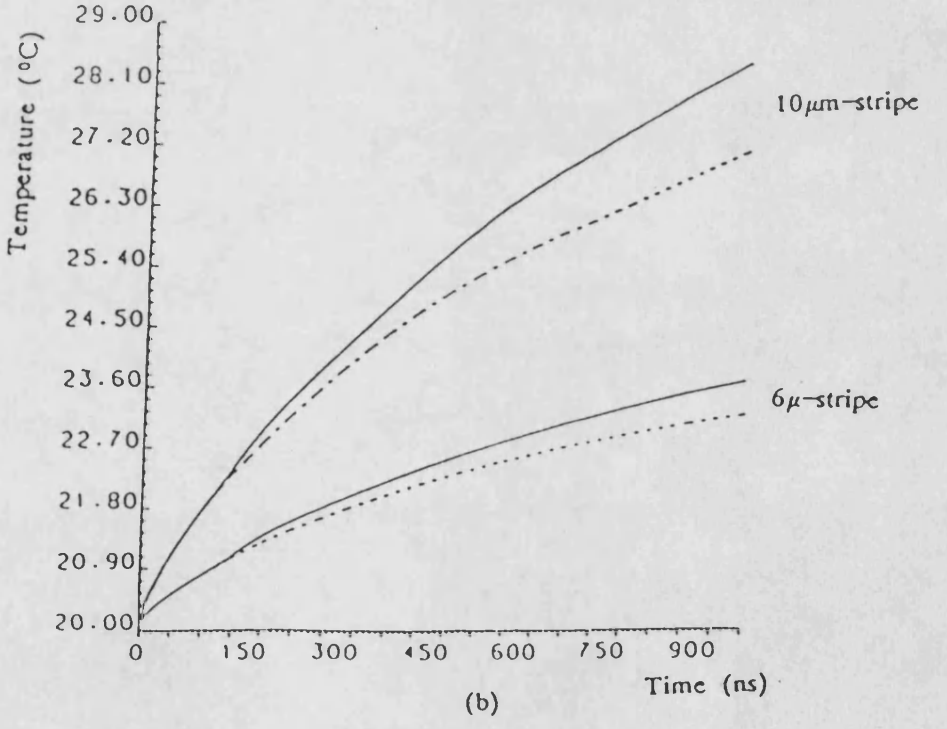

Figure 5.8 Variation of temperature in the active region of LD with time for 10μm and 6–μm at two different values of contact resistances

a) stripe–down mounted lasers
b) stripe–up mounted laser

For lower contact resistance the curves are the dotted ones.

higher. This is illustrated in Figure 5.8a where the temperature in the active region of stripe-down mounted laser remains virtually constant after 200ns, whereas a stripe-up laser does not, as illustrated by Figure 5.8b. The above effects restrict the current pulse width used in stripe-up mounted lasers. Consider the effect of contact resistance (ρ_{con}) on the surface of the substrate, where the solid line curves in Figures 5.8a,b represent the variation of temperature with time for a value of $\rho_{con} = 10^{-4}\Omega/cm^2$ and the dotted curves for a value of $\rho = 10^{-6}\Omega/cm^2$. This illustrates that the contact resistance has no significant influence on the active region temperature for either kind of mounting because of the long time taken for heat conduction from the active layer to reach to the surface of the substrate, which was one reason for not including the Joule heat caused by this contact resistance in the transient model, but the value of the contact resistance has an effect on the temperature at the surface. The analysis shows that the lower contact resistance of $10^{-6}\Omega/cm^2$ gives a lower rise in temperature at the surface. Also Figures 5.8a,b show that the temperature in the active layer of $10\mu m$ stripe laser is higher than that for $6\mu m$ stripe laser, consequently a way of controlling the temperature increase is by controlling the stripe width of the laser diode.

5.5 Semiconductor Laser Temperature Control

5.5.1 Control circuit

The effect of heat on a laser diode limits its use in optical communication applications, and sophisticated heterostructure lasers that have a lower threshold current have been developed in order to lower the junction temperature. The laser junction has to be mounted over a heat sink, through which heat can be extracted via a suitable internal heat transfer to a secondary heat sink, in this case of passive heat transfer via the secondary heat sink, the temperature of the laser diode is principally dependent upon heat flow through this heat sink, and

consequently assumes a temperature determined by it after a certain transient period. Laser diode temperature will then be dependent on the ambient temperature.

Sometimes it is necessary to operate the laser diode at constant temperature in order to achieve a constant radiant power, and in this case active heat transfer can be applied using a thermoelectric heat pump. Such a pump utilises the Peltier effect where a series of alternate P–N and N–P junctions are electrically connected in series, the input and output faces are Beryllium oxide and the junctions are sandwiched between. The P–N junctions are arranged on one face and the N–P junctions on the opposite face; heat is absorbed at the N–P junctions and dissipated at the P–N junctions. The rate at which heat is pumped is approximately proportional to the current applied. The heat pump is reversible, thus allowing the temperature to be controlled both above and below ambient. The circuit shown in Figure 5.9 has been used to operate the laser diode at constant temperature, and has been implemented on double–sided PCB. The laser diode is mounted on a copper block together with a monolithic temperature sensor AD590, the cold face of the Peltier pump is placed in contact with the copper block, while the warm side of the cooler transfers the heat via the wall of a secondary heat sink of thermal resistance 7 ^{0}C/W. The temperature sensor develops a voltage across the resistor R_6 proportional to the absolute temperature. This voltage is compared with a stable reference voltage (V_R) derived from the band gap reference (ZN423), and the error voltage determines the drive current applied to the Peltier pump. A monolithic audiopower amplifier (TDA2030) drives the heat pump. Since a large current may be taken by the circuit, so it is desirable to keep the resistance of the interconnection as low as possible, and good power supply decoupling has also been considered.

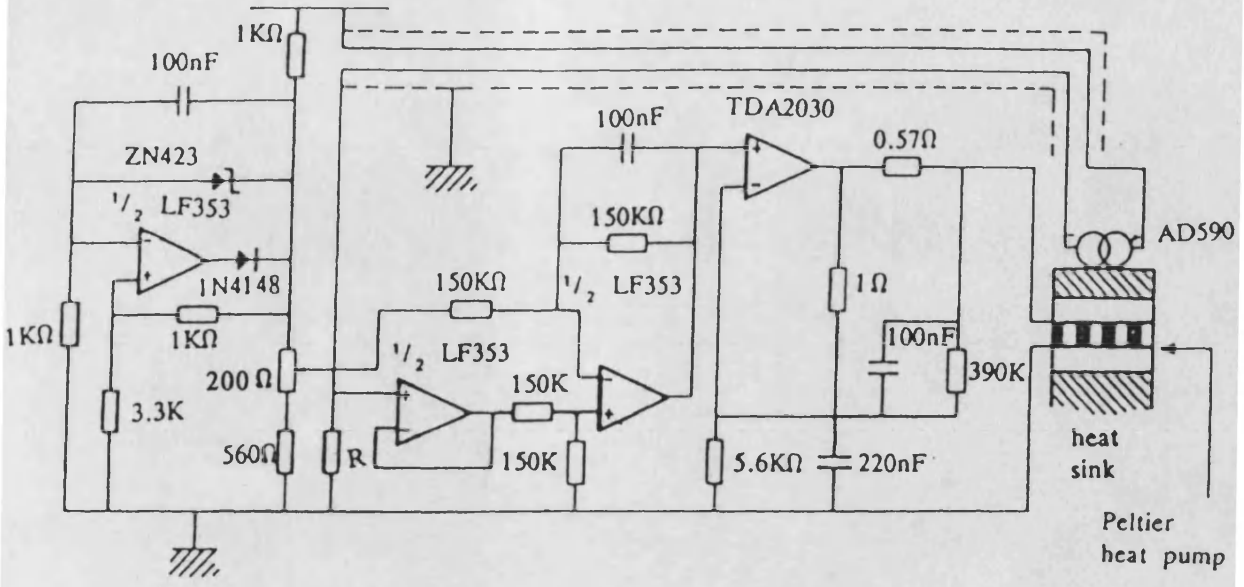

Figure 5.9 LD temperature control circuit

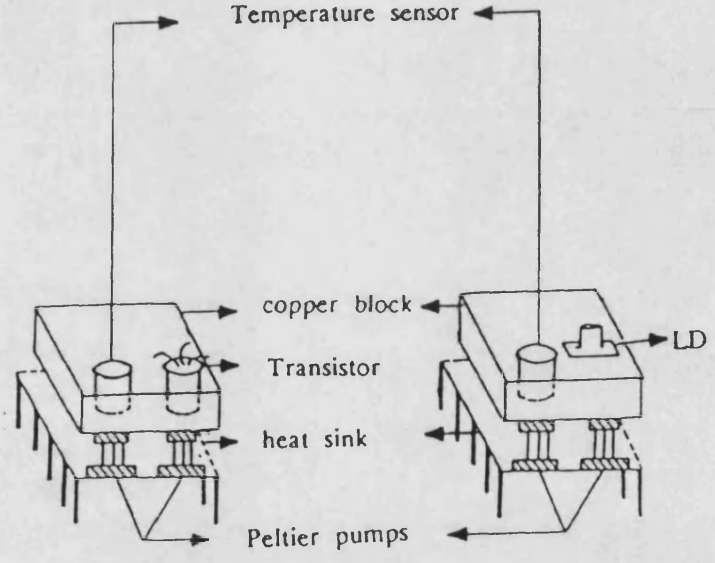

Figure 5.10 Arrangement for fixing, temperature sensor, Peltier heat pumps, on a copper block and heat sink with:

a) metal can transistor
b) LD

5.5.2 Performance of Temperature Control Circuit with Dummy Heat Source

In order to cool the laser diode and monitor its temperature it has to be fixed on a copper block together with the temperature sensor AD590 as shown in Figure 5.10. If a current passes in the LD its temperature rises above the ambient temperature T_a, then the heat is transferred to the copper block by conduction and from the copper block to air by radiation. Because of the heat capacity and thermal resistance of the copper block its temperature rises exponentially above the ambient till reaching the steady state:

$$T(t) = T_a + T_m [1 - \exp(-t/\tau)]$$

where T(t) is the temperature of the copper block at time (t), T_m is the rise in temperature from ambient to steady state and τ is the thermal time constant of the copper block which is the time required for the temperature to reach 0.63 of its final value. It depends on its thermal resistance and its heat capacity.

By rearranging the terms of this equation and taking the natural logarithm of both sides we get:

$$t = -\tau \ln \left[1 - \frac{(T(t) - T_a)}{T_m}\right] \qquad 5.10$$

so if a relation is drawn between

$$\ln \left[1 - \frac{T(t) - T_a}{T_m}\right]$$

and t, a straight line will be obtained. From the slope of this line τ can be

determined. Also if the power input (P) is known then the thermal resistance (R_t) can be determined.

$$R_t = T_m/P \quad {}^0C/watt$$

In testing the performance of the temperature control circuit, a metal can transistor of the type 2N5837 has been used to generate heat in the copper block, instead of the laser diode because it is less prone to accidental damage. The power dissipation in the transistor corresponding to different values of collector current I_c has been calculated and the rate of heat generated in the copper block has been monitored by measuring its temperature T at different intervals of time. Also the voltage V_s developed across the 14.7KΩ resistor connected in series with the temperature sensor has been measured. Figure 5.11 illustrates the variation of the temperature of the copper block with time for different values of power dissipation. From Figure 5.11 a relation is drawn between the power dissipated in the transistor P and the corresponding rise in temperature from the ambient to steady state value (T_m). This relation is illustrated in Figure 5.12 which is straight line of slope R_t = 65 °C/W. It represents the thermal resistance of the copper block between the transister can and the external air.

Also from Figure 5.11 a relation is drawn between t and:

$$\ell n \left[1 - \frac{(T(t) - T_a)}{T_m}\right]$$

as obtained from the curve corresponding to P = 45mw, T_m = 2.9 °C and T_a = 19 °C. The resultant graph is the straight line shown in Figure 5.13. From the slope of this line the thermal rise time is τ = 147 sec.

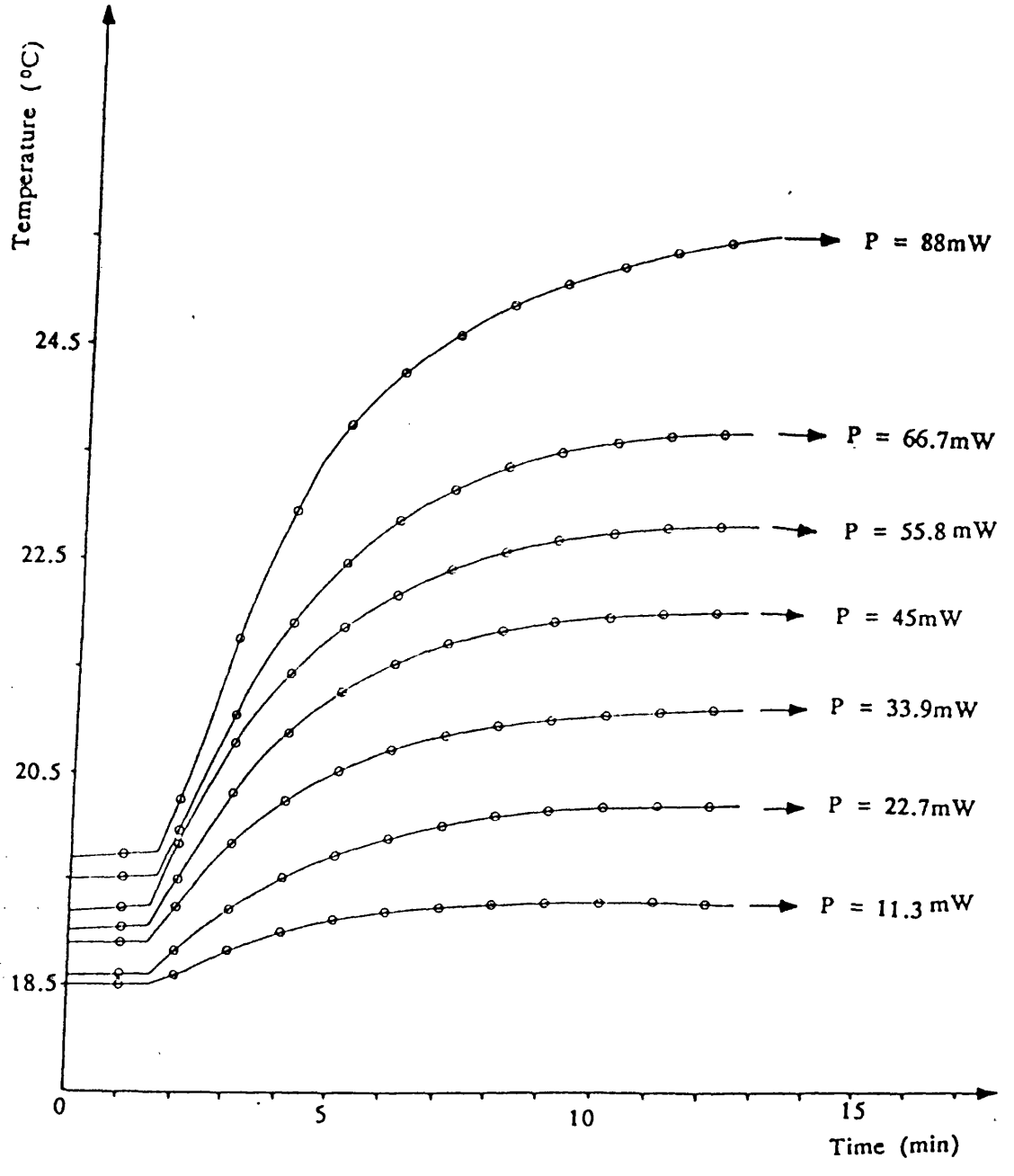

Figure 5.11 Variation of the temperature of the copper block with time for different values of power dissipation in the transistor

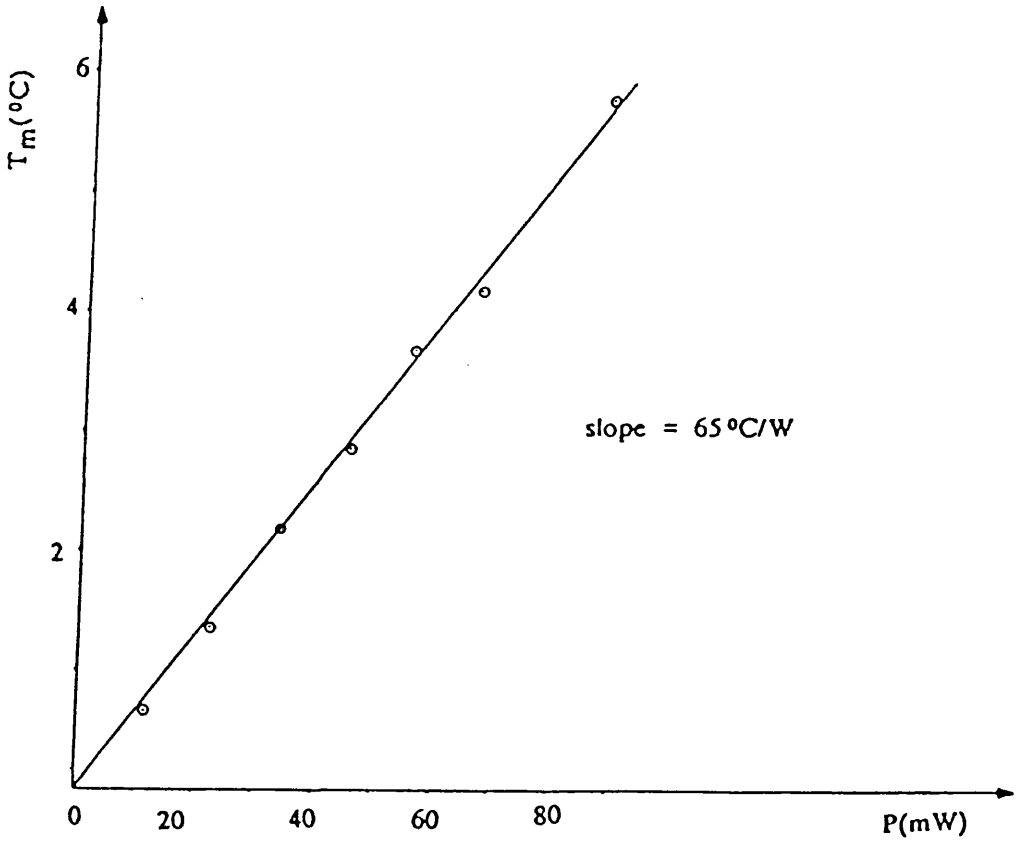

Figure 5.12 Variation of the rise in temperature to steady state value (T_m) with the power dissipation in the transistor

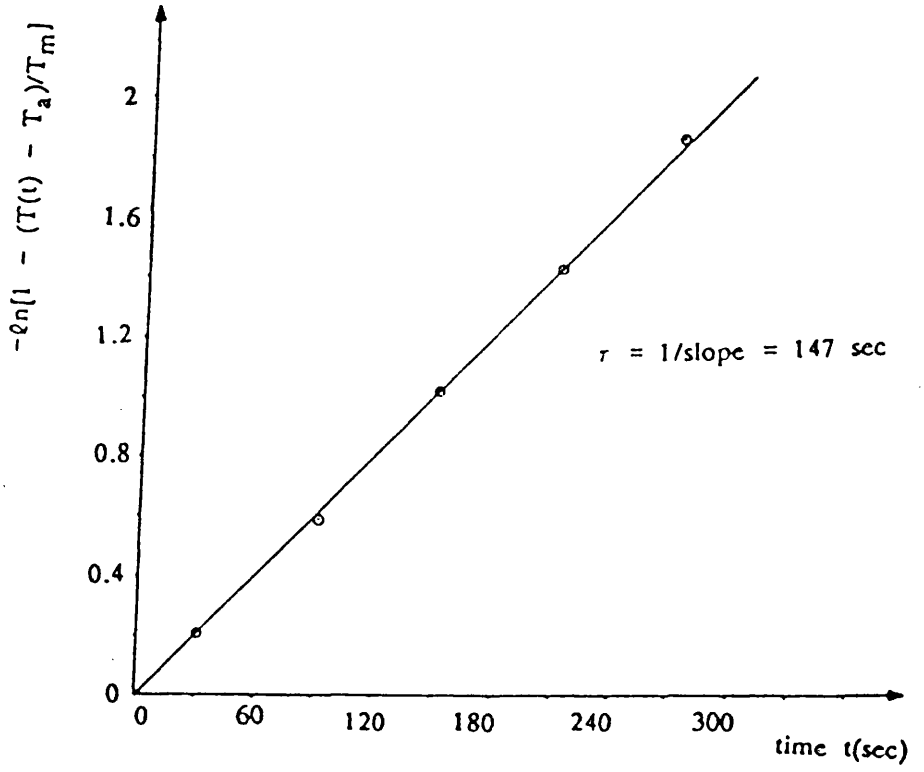

Figure 5.13 Variation of $\ell n[1 - ((T(t) - T_a)/T_m]$ with time (t)

The heat capacity of the copper block is then:

$$\frac{\tau}{\theta} = \frac{147}{65} = 2.26 \text{ Joule/}^{0}\text{C}$$

Figure 5.11 also shows that the initial rates of rise in temperature are ranging from 0.3^{0}C/minute to 1.2^{0}C/minute so to keep the copper block temperature constant the rate of cooling by the Peltier Cooler should be in this range. Two Peltier coolers, of maximum power dissipation 0.29W and has dimensions 2.67mm, 4.06mm and 3.91mm, were connected in series and fixed with their cool surfaces in contact with the copper block and their other surfaces in contact with a heat sink of thermal resistance 7^{0}C/watt. The rate of cooling of the pumps has been measured at different driving currents. Figure 5.14 shows the variation of temperature of the copper block with time when the pumps were allowd to cool the copper block at two different values of driving currents (0.385A and 0.5A).

The figure illustrates that initial rates of fall in temperature ranging down to −3^{0}C/minute were obtained when the Peltier pump driving current was 0.385A, and the thermal time constant was ≈120sec. The rate of fall in temperature is greater than the rate of rise in temperature when the transistor is used to generate heat. Hence, when the transistor is allowed to generate heat in the copper block and the Peltier pumps are allowed to cool the block it is expected that the average temperature of the copper block remains constant.

The transistor 2N3705 has been allowed to generate heat corresponding to power dissipation values of 22.7, 45, 55.8, 66.7, 88mW and in each case the Peltier pumps current and the temperature of the copper block have been monitored. The obtained results are illustrated in Figure 5.15. The figure indicates that the current driving the Peltier pumps is constant at all times as long

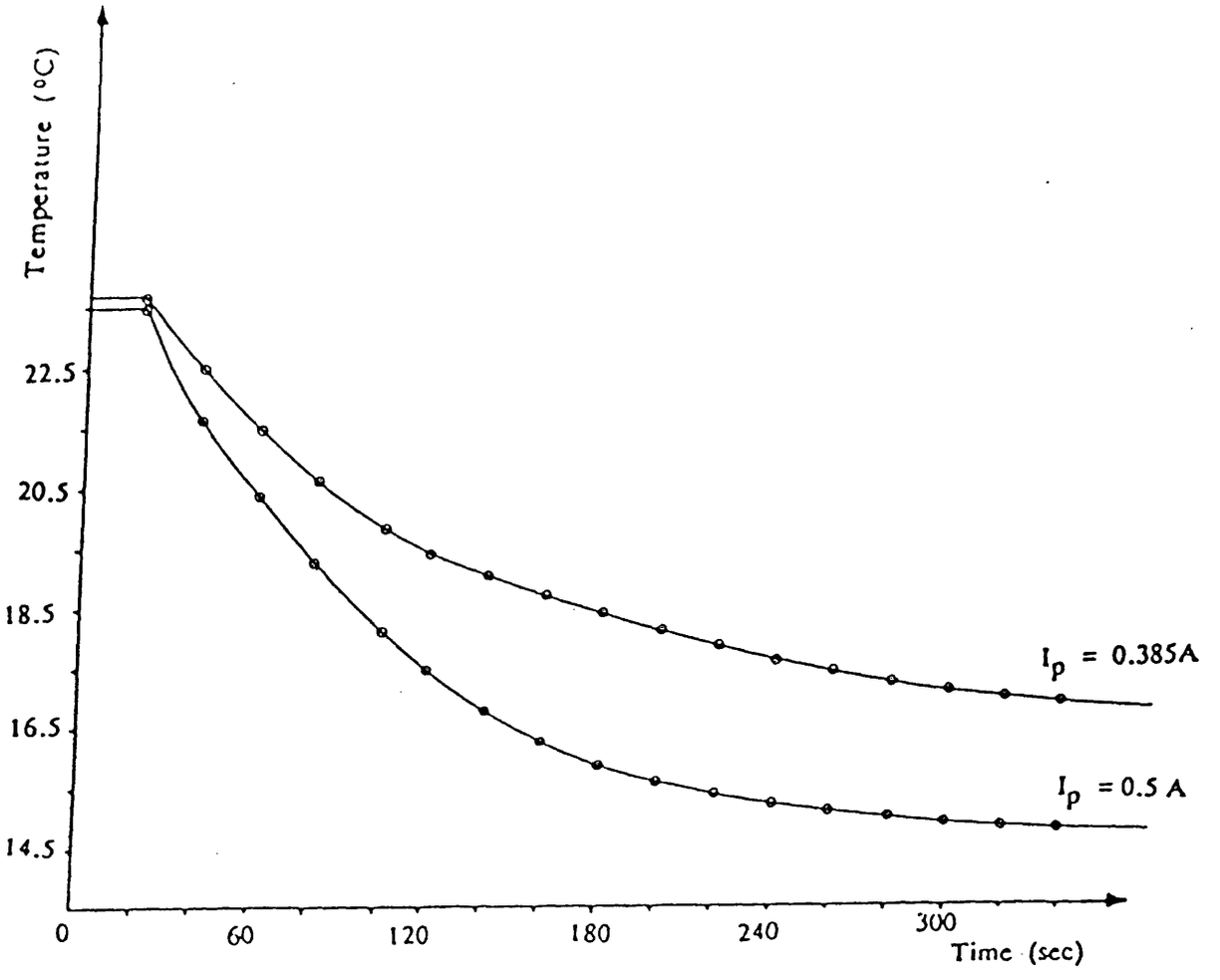

Figure 5.14 Variation of temperature of copper block with time using two different values of Peltier pump current (I_p)

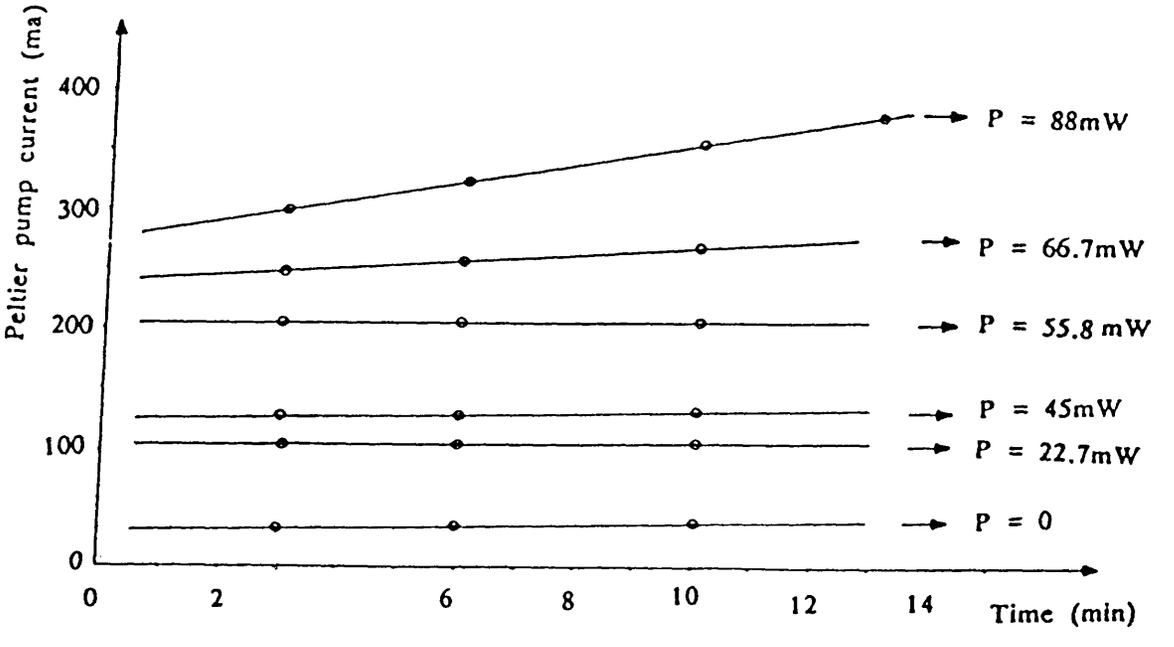

Figure 5.15 Relation between Peltier pump current, driven by the temperature control circuit, and time for different values of power dissipation in the transistor

as the power dissipated in the transistor is less than 55.8mw which means that the temperature remains constant. The monitored temperature was constant to an accuracy of 0.1 ^{0}C, but for powers greater than 55.8mW, the Peltier pump driving current and the monitored temperature showed a slight increase with time which was attributed to heating in the Peltier device and consequently, change of its efficiency.

For an LD operating with pulses of maximum duty cycle of 50% and its threshold current ≈50ma and its junction drop voltage ≈1.7V, the power dissipation = 50 x 1.7 x 0.5 = 42.5mw. This indicates that the temperature control circuit will maintain the average temperature of the laser diode constant when it replaces the transistor.

To maintain the average operating temperature of the LD constant below room temperature one has to adjust the value of the reference voltage. Figure 5.16 shows the relation between the temperature of the copper block and Peltier pump driving current required to keep the temperature of the block constant below the ambient temperature, when there is no heat generation. A line of slope -100mA/ ^{0}C has been obtained.

Figure 5.17 shows the variation of the voltage (V_S) developed across the 14.7KΩ resistor connected in series with the temperature sensor and the operating temperature and also the variation of the reference voltage. The first relation is a line of slope = 22.7mV/ ^{0}C which indicates that the temperature sensor develops a 22.7mv/C^{0} in the 14.7KΩ resistor (i.e. 1.54 μA/C^{0}) whereas the second relation is a line of slope = 33.5mV/ ^{0}C which indicates that an increase in the reference voltage of 33.5mv is required to maintain the temperature of the copper block 1 ^{0}C below the ambient temperature.

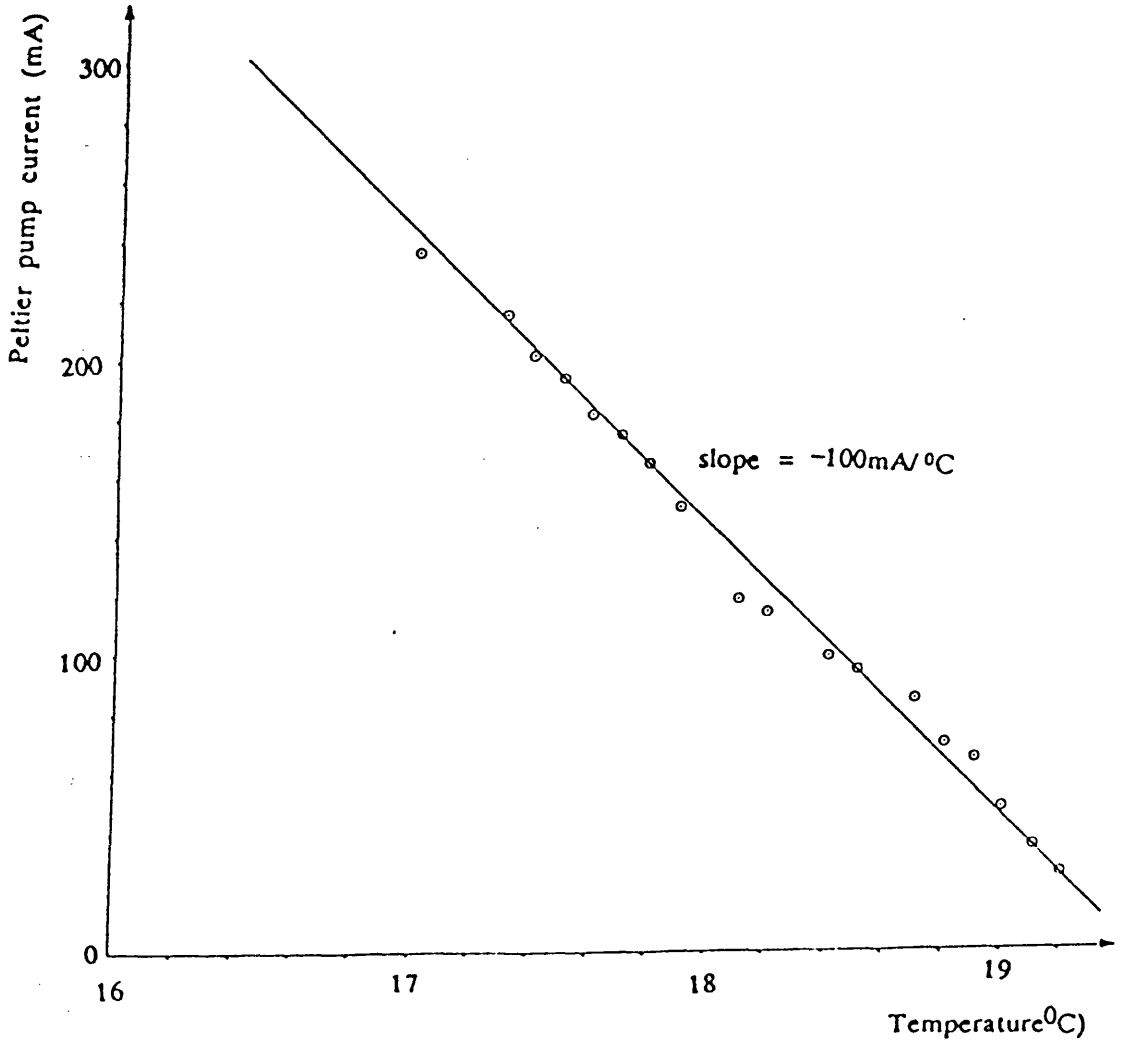

Figure 5.16 Relation between Peltier pump driving current and the temperature of the copper block below ambient without any h eat generation by the transistor

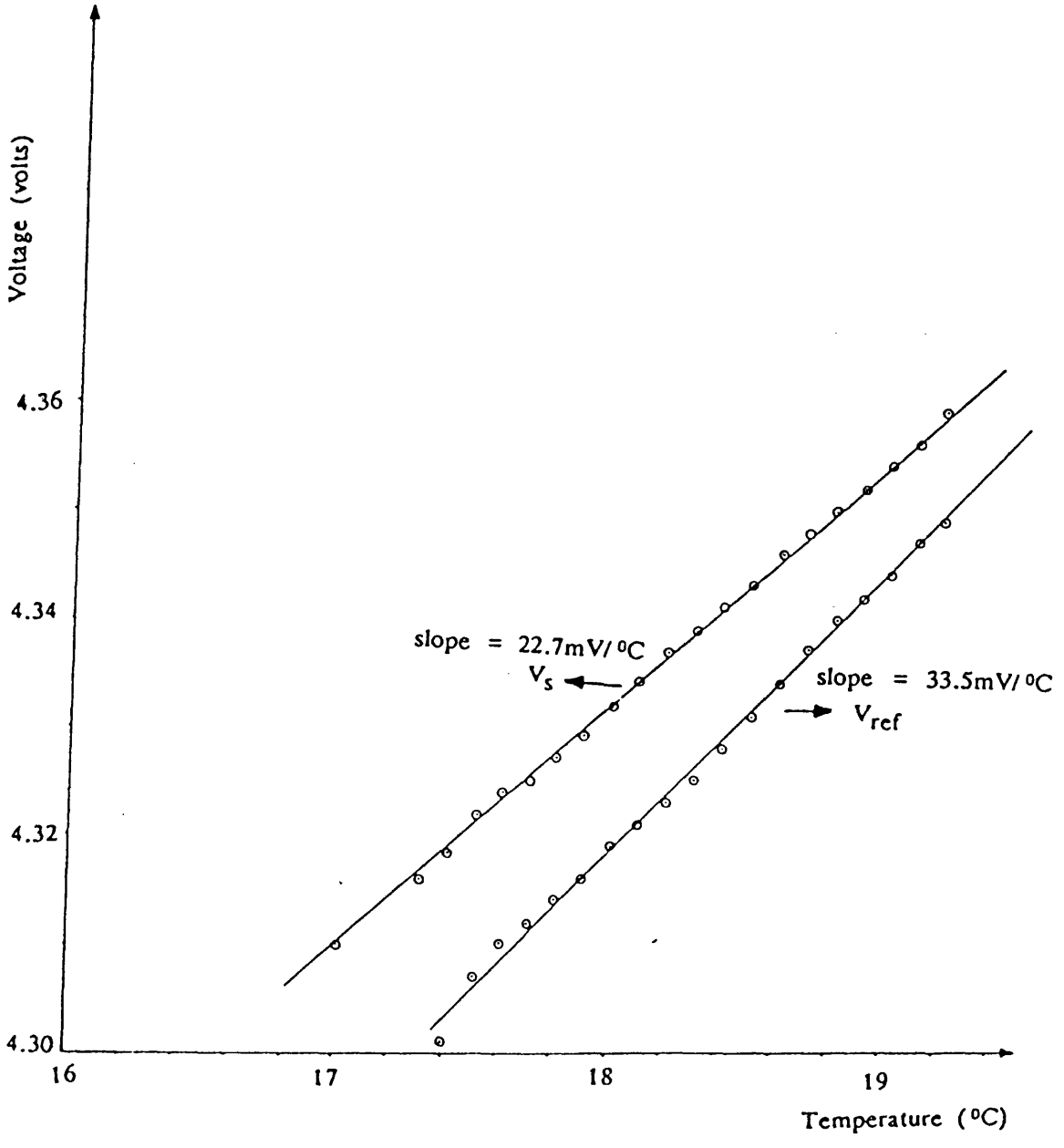

Figure 5.17 Relation between the temperature and the voltage developed across the 14.7KZ resistor connected in series with the temperature sensor AD590 (V_s) and also with the reference voltage (V_{ref})

In the course of these artificial tests on thermal control of the LD monitoring block, the operation of the circuit has been verified and the various parameters determined. The closed loop stability of this temperature controller is examined in Appendix III, which shows that it has a first order response and a time constant of about 2.5sec. It has been established that the Peltier device has sufficient heat pumping capacity to keep the LD at constant temperature.

5.5.3 Performance of laser diode temperature control

In order to determine the rate of temperature rise of the laser diode HL7801E, it was fixed in the copper block keeping a good thermal contact between them and it was then driven with current pulses near to threshold. The threshold current of this LD ≃42mA at 18°C, and its junction voltage drop ≃1.76V. It has been driven with current pulses of width 140ns and duty cycle 27.3%, just above its threshold current.

The power dissipation in the LD ≃0.042 x 1.76 x 0.274 ≃20.2mW.

The duty cycle has been changed to be 23.3% and 18.9% which is equivalent to power dissipation of 17.2mW and 14mW respectively, in each case the rise in temperature of the copper block has been recorded with time. The results obtained are illustrated in Figure 5.18 which shows the variation of the copper block temperature with time, at different values of power dissipation (20.2mW, 17.2mW and 14mW). The figure indicates a rate of rise in temperature of up to 0.4°C/minute, a thermal resistance ≃ 4/0.0202 ≃ 198°C/W and a thermal time constant ≃450 sec. The thermal time constant of the copper block is greater than in the case of using a transistor as a dummy heat source because the thermal contact between the LD and the block is different which is shown by the higher thermal resistance of the block, also the direction of flow of heat in this case is different.

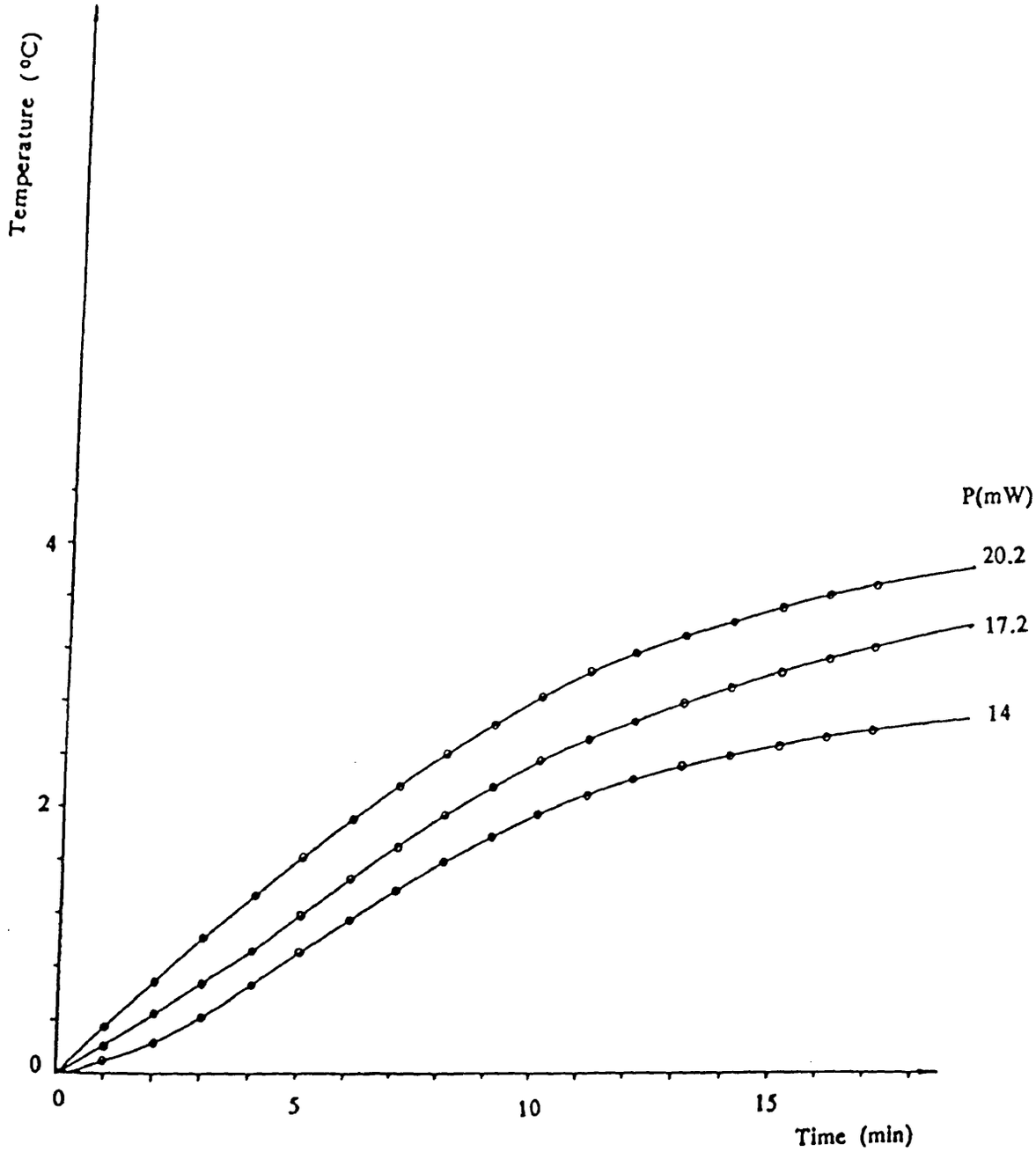

Figure 5.18 Relation between the time and the rise in temperature of the copper block at different values of power dissipation by LD HL8311E

To draw the light-current characteristics of the LD, the required operating temperature is achieved by adjusting the value of the reference voltage in the temperature control circuit. After driving the laser with current pulses and monitoring its temperature it is found that it has been stable to ±0.1 °C.

5.6 Light-Current Characteristics of Laser Diodes and Their Change with Temperature

An important factor to consider in the application of laser diodes is the temeprature dependence of the threshold current $I_{th}(T)$. This parameter increases with temperature (T) in all types of semiconductor laser because of various complex temperature-dependent factors[5.14]. The complexity of these factors prevents the formulation of a single equation holding for all devices and temperature ranges. However, the temperature variation of I_{th} can be approximated by the empirical expression[5.15,5.16]:

$$I_{th}(T) = I_{th_0} e^{T/\theta} \qquad 5.11$$

where θ is a measure of the relative temperature insensitivity and I_{th} is a constant. For a conventional stripe geometry laser diode θ is typically 120 to 165 °C in the vicinity of room temperature.

From equation (5.11):

$$\ell n\ I_{th} = \frac{T}{\theta} + \ell n\ I_{th_0} \qquad 5.12$$

By drawing a relation between $\ell n\ I_{th}$ and T a straight line will be obtained, and from the slope of this line θ can be determined. The value of I_{th} at any

temperature, or the rise in temperature corresponding to a certain shift in I_{th} can then be predicted.

5.6.1 Practical Measurement of Light-Current Characteristic of a Laser Diode and its Change with Temperature

The light-current characteristic of the laser diode HL7801E Appendix (IV) has been measured at different temperatures using the laser diode drive circuit (section 4.7), the temperature control circuit and an APD photodiode of the type LR103 Appendix (IV). The laser diode driving circuit drives the laser diode with flat top current pulses obtained by applying pulses at ECL levels, from the pulse generator HP8082A to the input of laser driving circuit. The value of the current pulse amplitude has been measured using a current probe and the temperature of the laser diode has been kept at constant values by using the previously described temperature control circuit where a feedback technique has been used to keep the temperature of the LD monitoring block stable to $\pm 0.1\,^{0}C$ accuracy. A lens has been used to collimate the laser beam on the sensitive area of the photodetector.

The light-current characteristic of the LD at certain temperatures has been measured by pulsing the laser diode with current pulses of width 140nsec and period 200μsec, then the amplitudes of the pulse and its corresponding optical response have been measured. This step has been repeated by changing the amplitude of the driving current pulses, and in each case the optical receiver pulse amplitude has been measured at the leading edge and the trailing edge of the pulse and also after certain time intervals from the start of the pulse.

The previous experiment has been carried out at operating temperatures of 14, 16, 18, 20, 22, 24, 26, 28, 30 and $32\,^{0}C$. All the previous experiments have been repeated when changing the period of the pulse to 160μsec and 120μsec, in order

to investigate the effect.

Figure 5.19 represents the light current characteristics drawn from these results when the optical pulse amplitude was measured at the leading edge of the pulse, the pulse width was 140nsec and the pulse period was 200μsec; while Figure 5.20 shows the same characteristic but with the optical pulse amplitude measured at the trailing edge.

Figures 5.21 and 5.22 show similar characteristics respectively when the pulse period is 160μsec. The values of threshold currents, measured from these characteristics at different values of temperatures, have been tabulated in Table 5.1 where I_{th} and I'_{th} represent the values of the threshold currents measured from the light-current characteristics at the leading and trailing edges of the optical pulse respectively.

From Table 5.1 it is seen that I_{th} and I'_{th} increase with temperature. Also, $I'_{th} > I_{th}$ at the same operating temperature which indicates a shift in the threshold current value due to the increase in temperature of the laser chip with time during the pulse duration. It is also to be noted that both I_{th} and I'_{th}, at a particular average temperature, do not change when the period of the pulse is changed, which is expected because the average operating temperature is maintained constant by the action of the temperature control circuit.

To predict the threshold current at any temperature or to predict the rise in temperature corresponding to a shift in threshold current, one has to draw the relation between log I_{th} and T. Figure 5.23 illustrates this relation for LD HL7801E. It is drawn from the results obtained in Table 5.1, the relation is a straight line of slope = 2.12×10^{-3} from the slope:

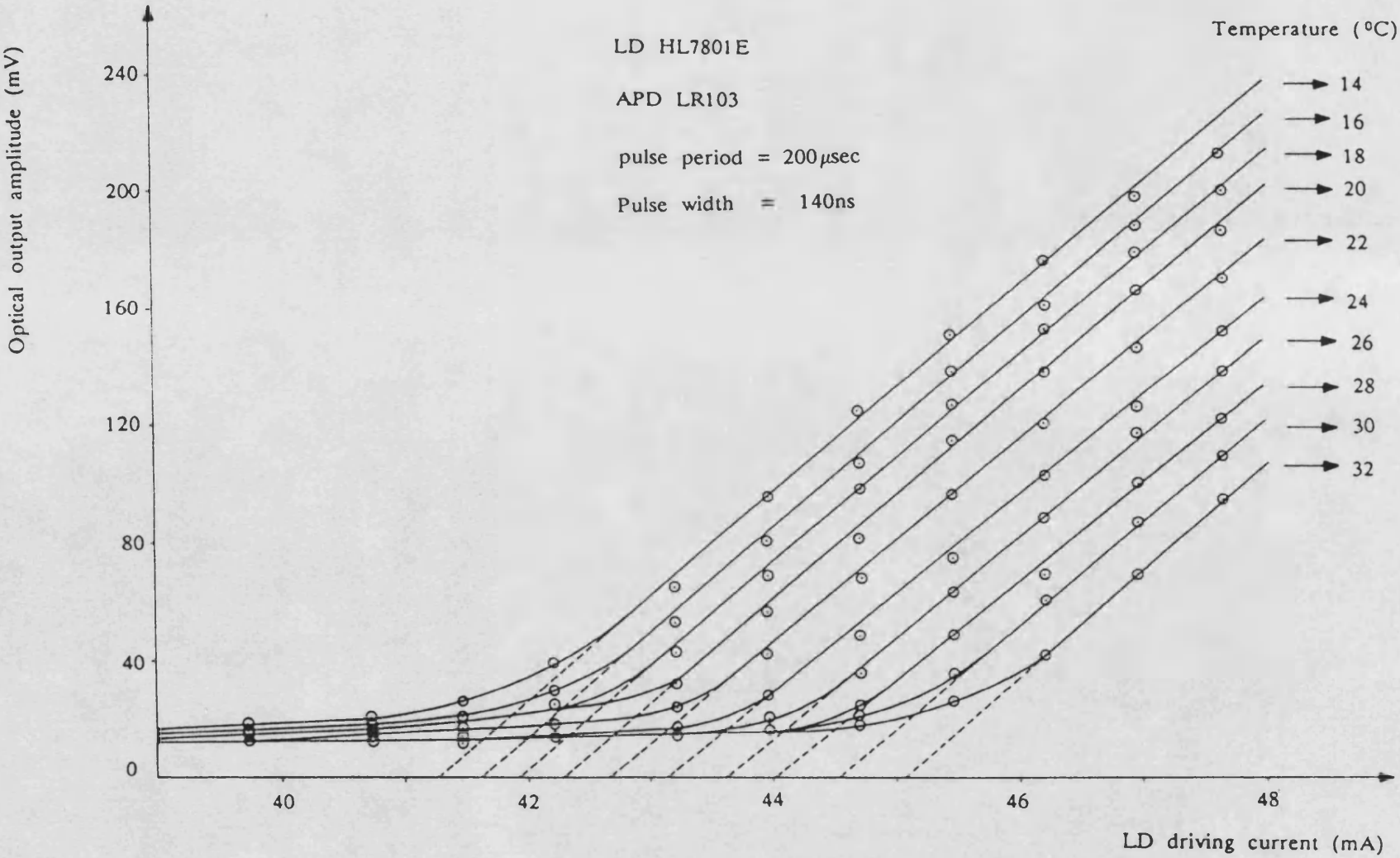

Figure 5.19 Light-current (L-I) characteristics of LD HL7801E. With the optical output amplitude measured at the leading edge of the pulse

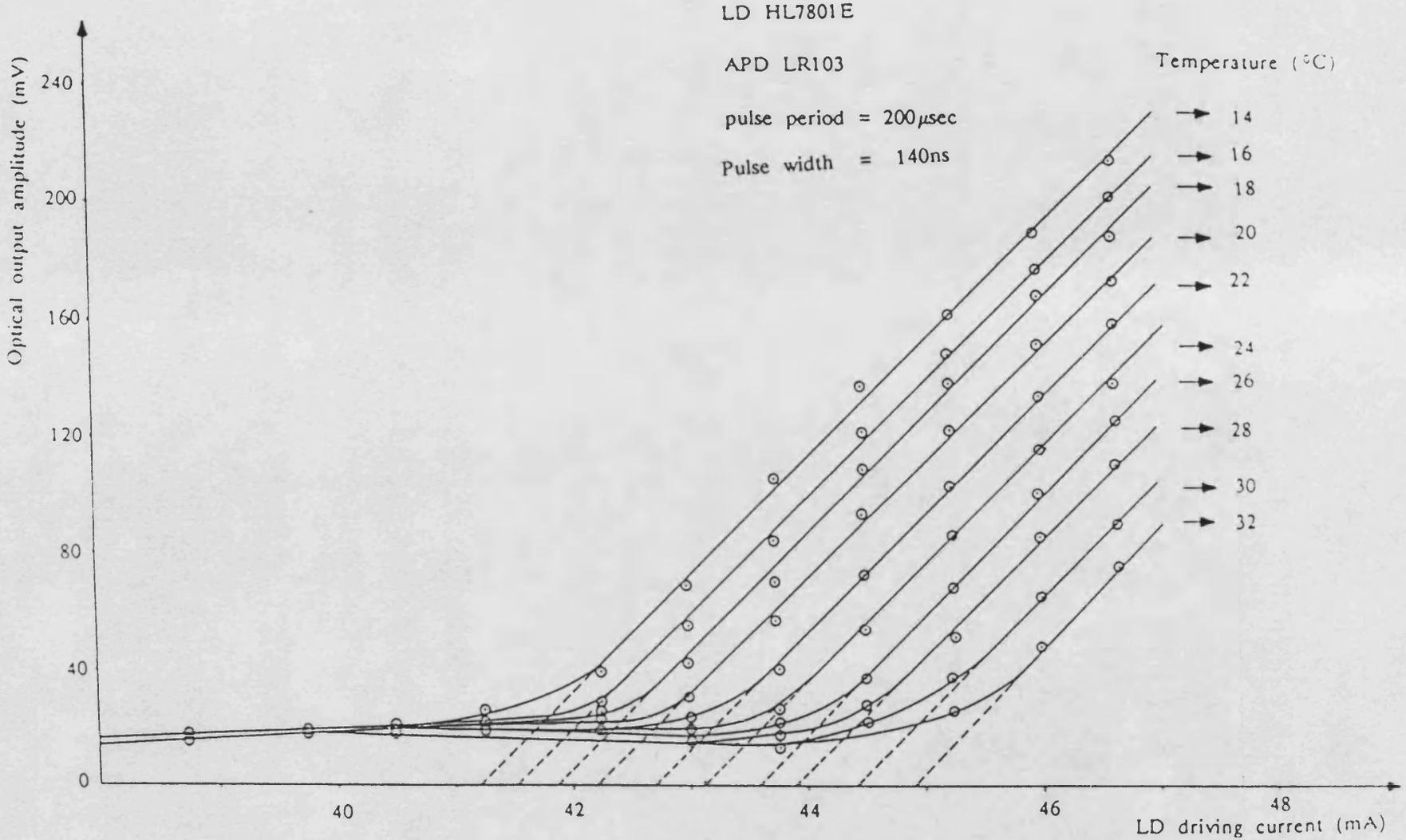

Figure 5.20 Light–current (L–I) characteristics of LD HL7801E with the optical output amplitude measured at the trailing edge of the pulse

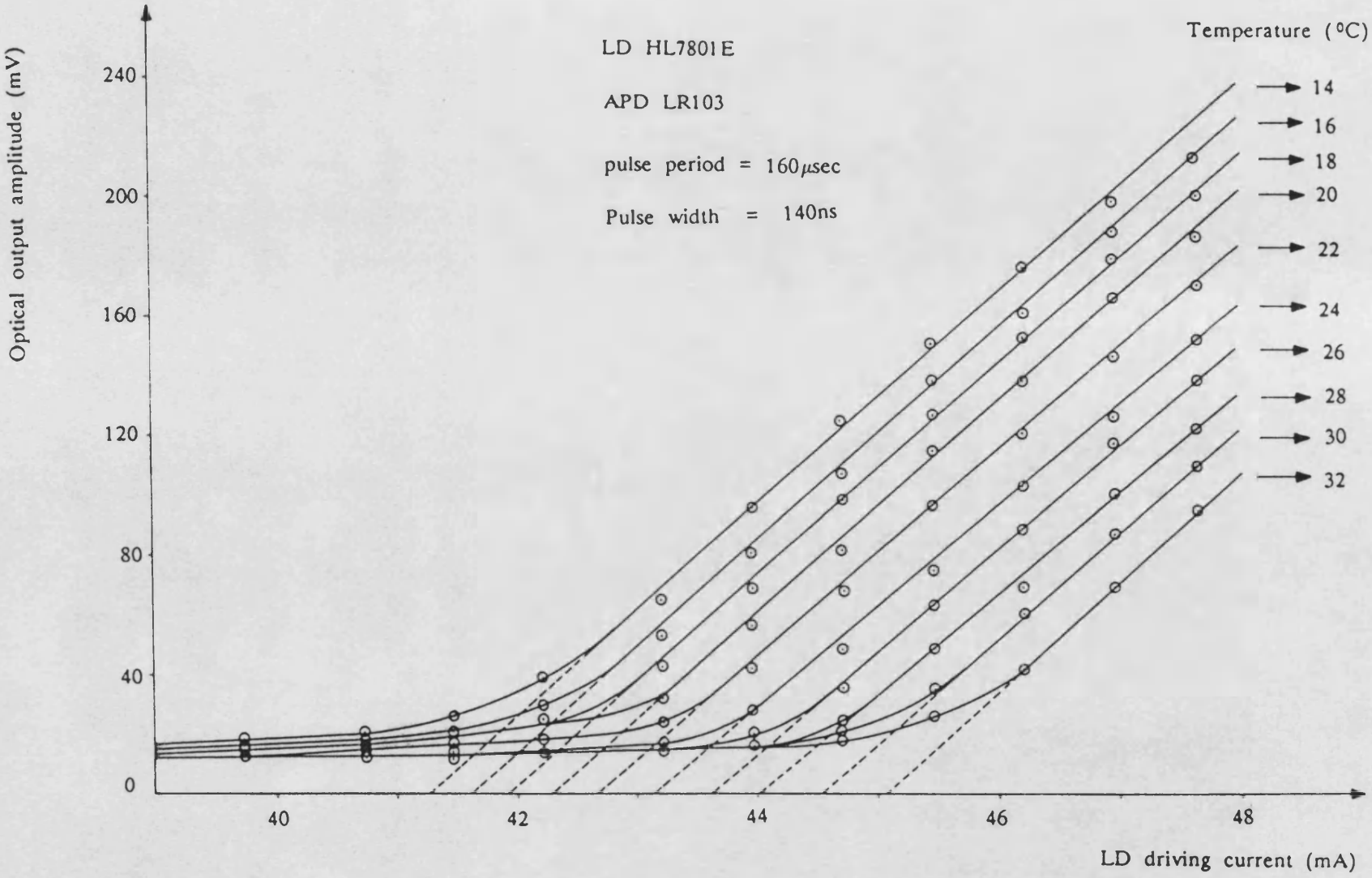

Figure 5.21 Light–current (L–I) characteristics of LD HL7801E. With the optical output amplitude measured at the leading edge of the pulse

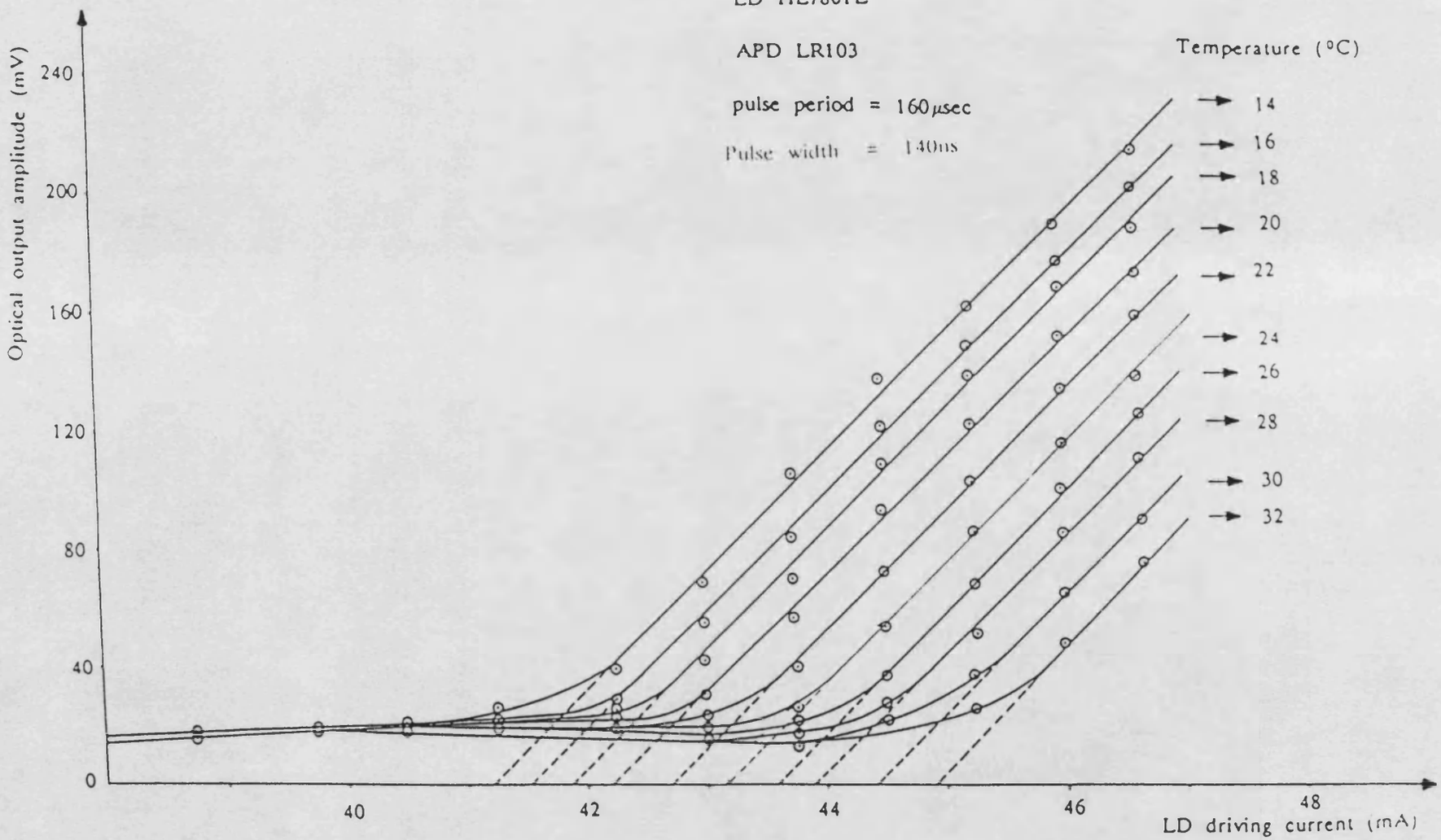

Figure 5.22 Light–current (L–I) characteristics of LD HL7801E with the optical output amplitude measured at the trailing edge of the pulse

Temperature °C	Pulse Period 200μsec		Pulse Period 160μs		Pulse Period 120μsec	
	I_{th}(mA)	I'_{th}(mA)	I_{th}(mA)	I'_{th}(mA)	I_{th}(mA)	I'_{th}(mA)
14	41.3	42.2	41.3	42.2	41.3	42.2
16	41.6	42.5	41.6	42.5	41.6	42.5
18	41.9	42.9	41.9	42.9	41.9	42.9
20	42.3	43.2	42.3	43.2	42.3	43.2
22	42.7	43.7	42.7	43.7	42.7	43.7
24	43.1	44.0	43.1	44.0	43.1	44.0
26	43.6	44.6	43.6	44.6	43.6	44.6
28	44.0	44.9	44.0	44.9	44.0	44.9
30	44.6	45.6	44.6	45.6	44.6	45.6
32	45.0	45.9	45.0	45.9	45.0	45.9

Table 5.1 The Threshold Currents Measured from Figure 5.19 – 5.22

LD : HL7801E

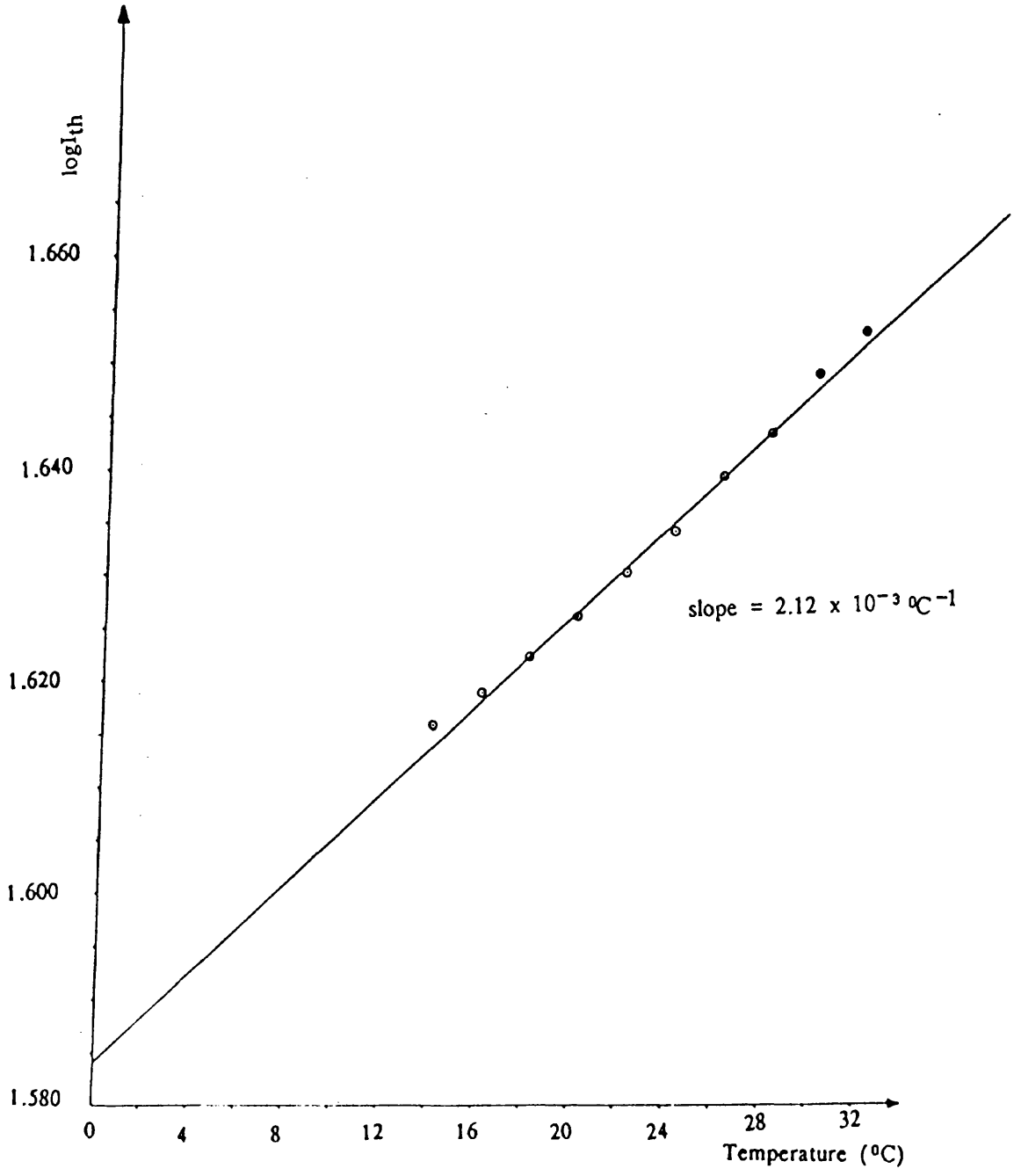

Figure 5.23 Relation between $\log I_{th}$ and operating temperature (T) for LD HL7801E

θ = 205°C

From this line the rise in temperature of the laser diode ΔT during the duration of the pulse, can be predicted by finding the rise in temperature corresponding to the shift of I_{th} to I'_{th}. Table 5.2 summarises the obtained results at different operating temperatures. The average rise in temperature during the pulse duration of 140nsec is found to be ΔT = 4.6°C.

This rise in temperature is in the LD chip itself, since the monitoring block has a much greater time-constant than the length of one pulse. The diode temperature reaches to within 5% of the final value in a time of 120ns.

5.6.2 Evaluation of Thermal Rise Time of LD from its Light-Current Characteristics

The light-current characteristics of an LD can be used in calculating its thermal rise time. Assume the heavily drawn curve in Figure 5.24 represents the light-current characteristics of the LD at an average operating temperature T. If the LD is driven by a current pulse of amplitude I where $I > I_{th}$; heat is generated because of the increase of current and the laser chip rises in temperature until reaching a steady state. This will lead to a shift in threshold current and a reduction in the amplitude of the optical pulse until the steady state temperature is reached. If the maximum amplitude of the received optical pulse which corresponds to the lowest temperature of the LD during the pulse time, is L at instant of time (t), after an interval of time Δt the temperature of the LD increases by ΔT and the received optical pulse amplitude decreases by ΔL. The light-current charcteristic curve, at this instant of time $(t+\Delta t)$, can be obtained by drawing the dotted line shown in Figure 5.24 parallel to the line representing the stimulated emission part of the light-current characteristic curve at temperature (T),

Temperature °C	Pulse Period = 200μsec, pulse width = 140nsec					
	I_{th}(mA)	ℓnI_{th}	I'_{th}(mA)	$\ell nI'_{th}$	Rise in temp = change from $I_{th} \rightarrow I'_{th}$ ΔT(°C)	Average rise in temp ΔT(°C)
14	41.3	1.616	42.2	1.6253	5.4	
16	41.6	1.619	42.5	1.6283	4.8	
18	41.9	1.6222	42.9	1.6325	4.8	
20	42.3	1.6263	43.2	1.6355	4.2	
22	42.7	1.6304	43.7	1.6405	4.6	4.6
24	43.1	1.6344	44.0	1.6435	4.0	
26	43.6	1.639	44.6	1.6493	4.8	
28	44.0	1.6435	44.9	1.6522	4.2	
30	44.6	1.649	45.6	1.659	5.4	
32	45.0	1.653	45.9	1.6618	4.7	

Table 5.2 The Values of I_{th} and I'_{th} and its Corresponding Rise in Temperature as Evaluated from Figure 5.23

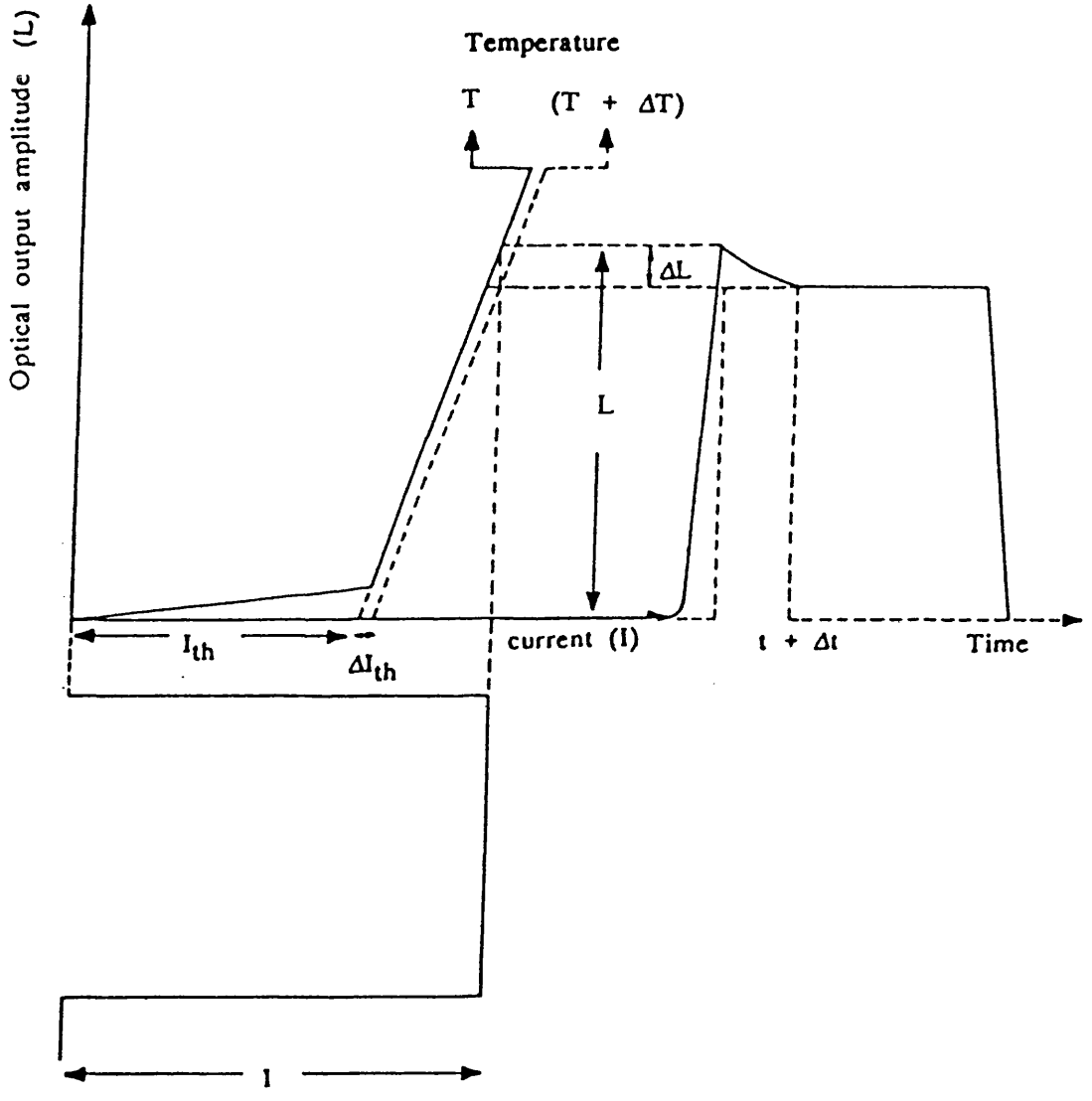

Figure 5.24 Illustration of the reduction in optical output amplitude due to the rise in temperature of the laser chip during the pulse duration

and passing by the point of co-ordinates (I, L-ΔL). This dotted line will represent the stimulated emission part of the characteristics at temperature (T + ΔT). A shift in threshold current of value ΔI_{th} has taken place. From Figure 5.24 the slope efficiency of the stimulated emission part of the light-current characteristics is:

$$\eta = \frac{\Delta L}{\Delta I_{th}} \quad \text{and}$$

$$\Delta T = \theta \ln \left[1 + \frac{\Delta I_{th}}{I_{th}}\right] \qquad 5.13$$

By measuring η and ΔL, the shift in threshold current ΔI_{th} can be determined. Knowing $\log(I_{th} + \Delta I_{th})$ and using Figure 5.23, the rise in temperature ΔT which causes the shift in threshold current ΔI_{th}, can be determined. Similarly, by determining ΔT at different instants of time where Δt equals 20, 40, 60, 80 and 100nsec, a curve showing the rise in temperature of the LD versus time can be drawn.

Table 5.3 shows the values of ΔI_{th} and its corresponding rise in temperature ΔT at different instants of time for the laser diode HL7801E while Figure 5.25 illustrates the relation between ΔT and time along the pulse using the results obtained in Table 5.3. From this figure the thermal rise time of the laser diode HL7801E has been found to be about 41nsec.

Figure 5.26 shows a photograph for the received optical pulse at the photodetector for a flat top current pulse used to drive the LD. It shows the effect of temperature on the pulse amplitude and its change with time, along the pulse, for a current pulse of amplitude $>I_{th}$. Also the same effect has been observed using two pulses of width 40nsec each and separated by 40nsec

Operating temperature = 18°C		$\eta_{stim.}$ = 35mV/mA		
LD drive current (I) = 44.75mA		pulse width = 140nsec		
$I_{th}(18°C)$ = 41.9ma		pulse period = 200μsec		
Time nsec	ΔL (mV)	$\Delta I_{th} = \frac{\Delta L}{\eta_{stim}}$ (mA)	$\log(I+\Delta I_{th})$	Rise in temperature °C
20	10	0.286	1.6251	1.2
40	18	0.514	1.6275	2.4
60	25	0.714	1.6295	3.4
80	28	0.8	1.6304	3.8
100	29	0.83	1.6307	4.0

Table 5.3 The Shift in Threshold Current Values due to Rise in Temperature at Different Instants of Time Along the Pulse

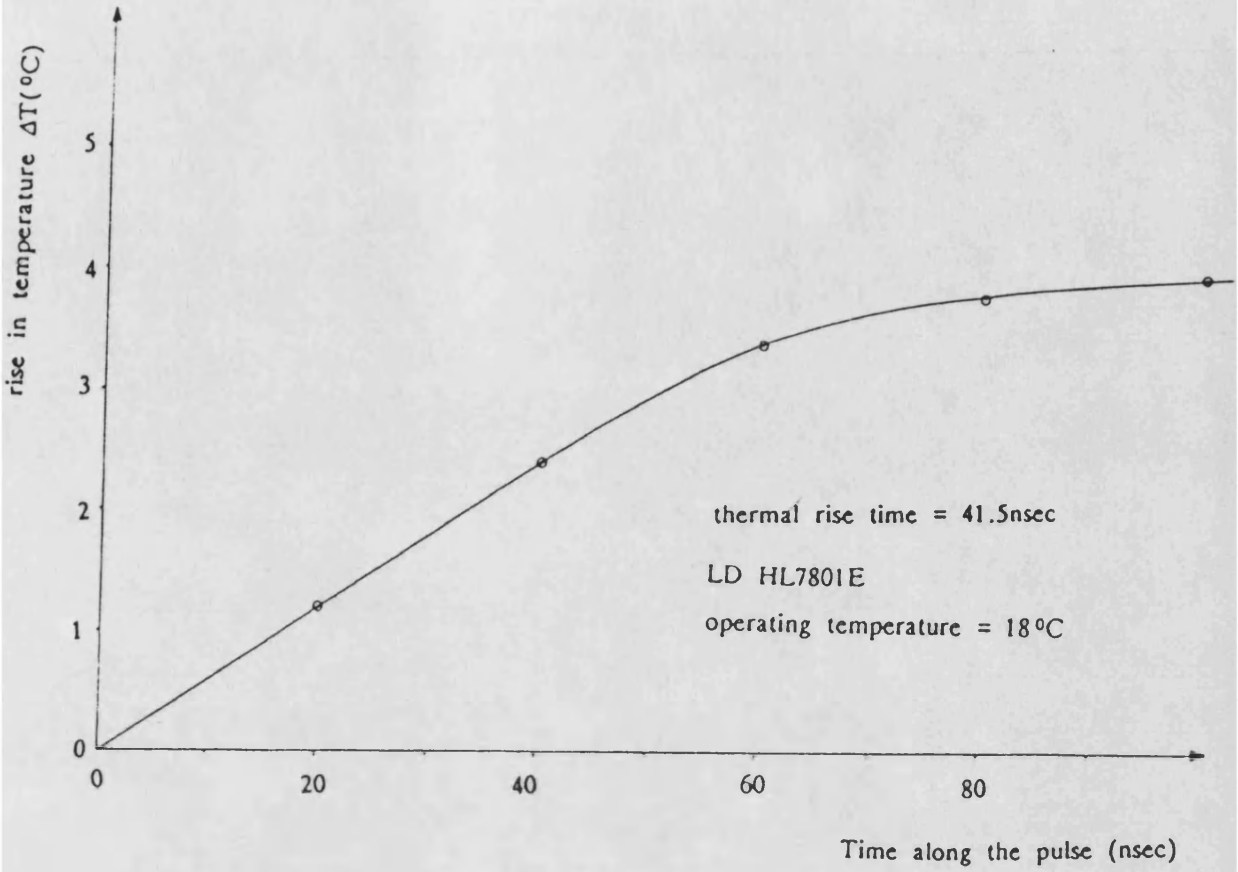

Figure 5.25 Relation between the rise in temperature of the laser chip (ΔT) and the time along the pulse

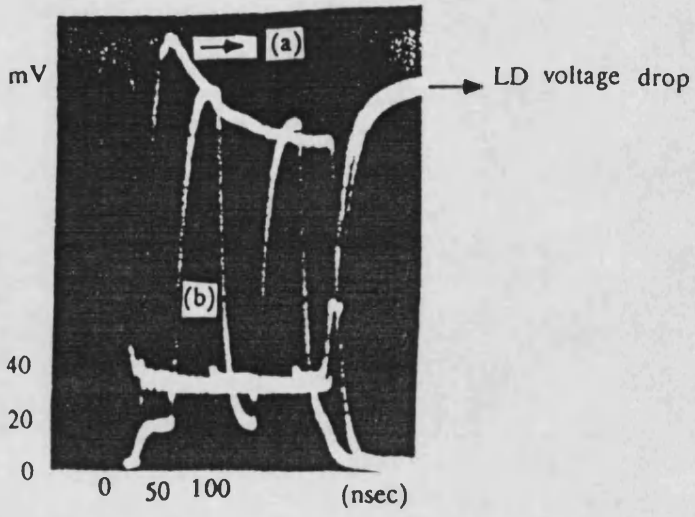

Figure 5.26 Photograph of the optical output of LD HL7801E driven by a flat topcurrent pulse and received by APD LR103

a) LD drive current $I > I_{th}$
b) LD drive current $I = I_{th}$ and modulation current (I_m) superimposed on I

superimposed on a current pulse of width 140nsec and of amplitude $\simeq I_{th}$. It is to be noted that the second pulse has an amplitude less than the first pulse due to the effect of temperature as shown in Figure 5.26.

5.6.3 Light–Current Characteristic of the Laser Diode HL8311E and its Change with Temperature

In order to determine the thermal rise time and to investigate the light–current characteristics of the laser diode HL8311E, Appendix (IV), which has faster response and higher value of threshold current than HL7801E, the experiments have been using the laser diode HL8311E as a light source instead of HL7801E, and using PIN photodiode of the type MFOD1100, Appendix (IV), in the photodetector circuit. PIN photodiode has been used with this LD because it is intended to be used in the optical power feedback control circuit of this LD.

Figure 5.27 shows the light–current characteristics of this laser diode at temperatures 16 °C, 18 °C, 20 °C, 22 °C, 24 °C, 26 °C, 28 °C, 30 °C and 32 °C when the optical pulse amplitude is measured at the leading edge of the pulse, while Figure 5.28 shows the equivalent characteristics when the optical pulse amplitude is measured at the trailing edge of the pulse.

The values of the threshold current at different temperatures as determined from these figures, have been tabulated in Table 5.4 and the average value of rise of temperature ΔT has been found to be 17.3 °C, calculated as previously described in the case of the LD HL7801E.

Also the relation between $\log I_{th}$ and temperature (T) has been drawn in Figure 5.29 using Table 5.4. It is a straight line of slope = $2.5 \times 10^{-3}\,^{\circ}C^{-1}$, from which the characteristic temperature of this laser diode is θ = 174 °C. The rise in

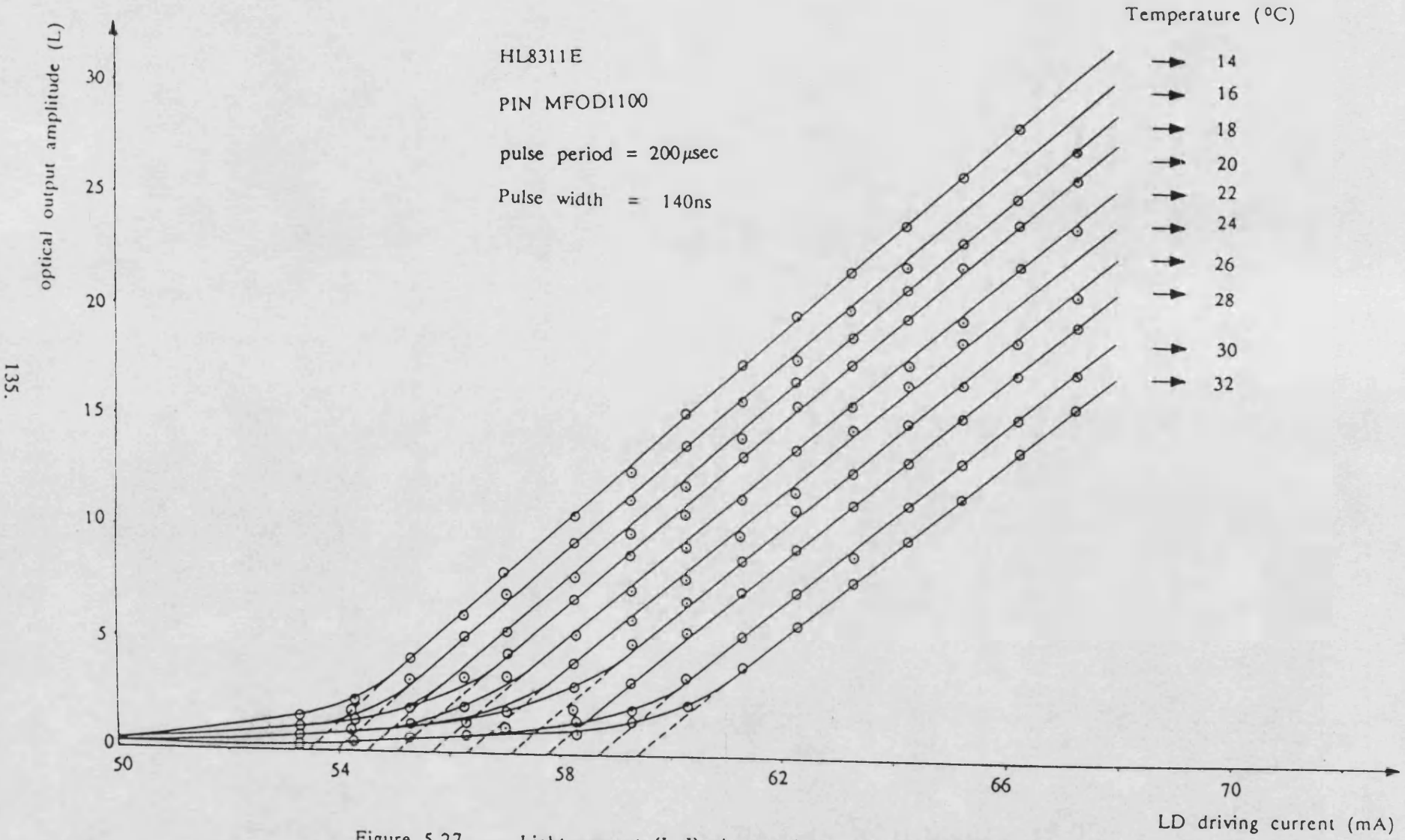

Figure 5.27 Light–current (L–I) characteristics of LD HL8311E with the optical output amplitude measured at the leading edge of the pulse

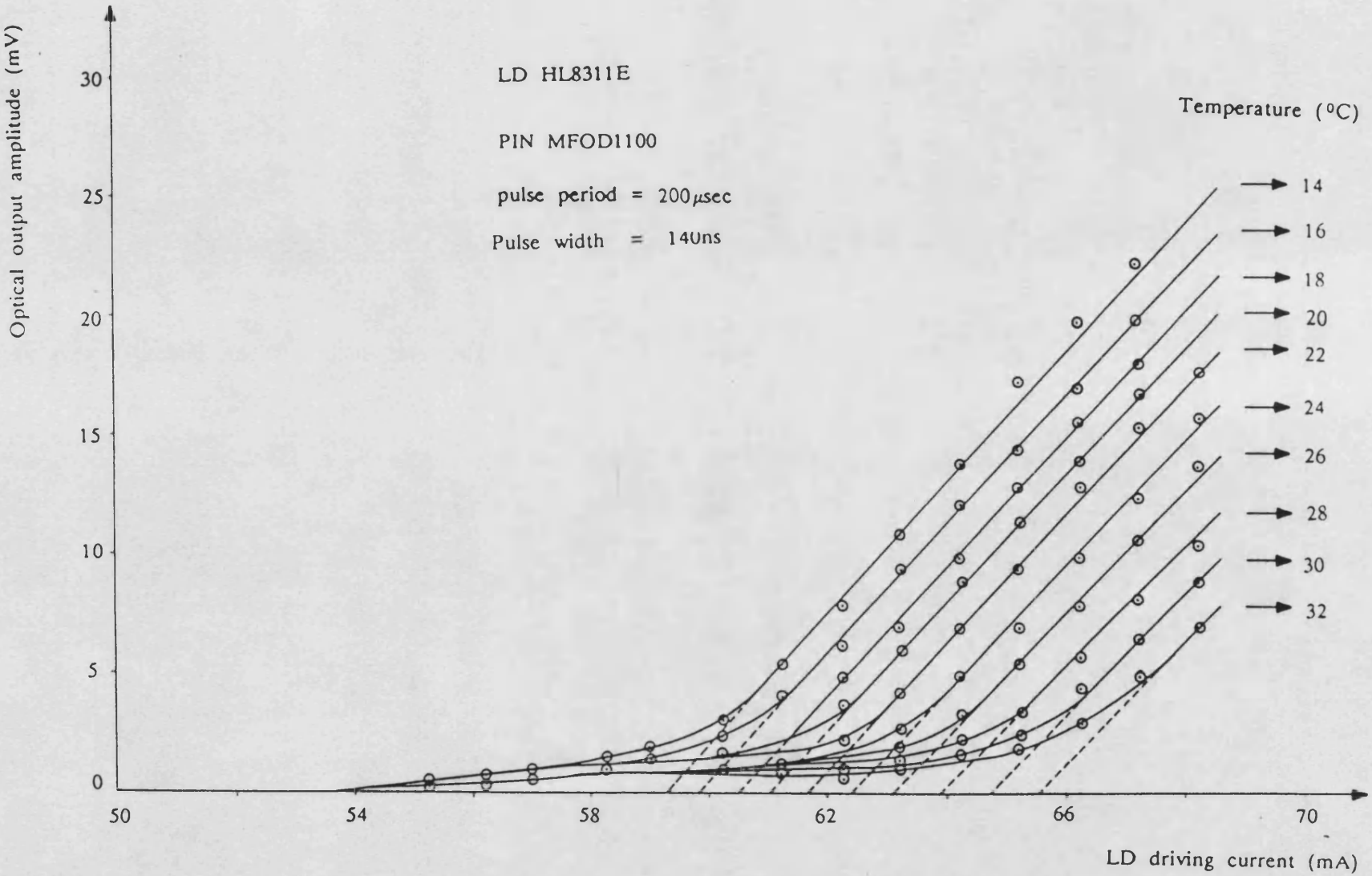

Figure (5.28) Light-current (L-I) characteristics of LD HL8311E with the optical output amplitude measured at the trailing edge of the pulse

Temperature ^{0}C	I_{th}(mA)	$\log I_{th}$	I'_{th}	$\log I'_{th}$	ΔT Increase in temp (^{0}C)	ΔT Average rise in temp (^{0}C)
14	53.5	1.7284	59.50	1.7745	18.8	
16	54.0	1.7324	59.75	1.7763	17.2	
18	54.5	1.7364	60.55	1.7821	17.5	
20	55.1	1.7412	60.85	1.7843	16.3	
22	55.65	1.7455	61.75	1.7906	16.7	17.3
24	56.35	1.7509	62.25	1.7941	16.0	
26	57.1	1.7566	63.10	1.800	16.2	
28	57.8	1.7619	63.75	1.8045	18.0	
30	58.6	1.7679	64.75	1.8112	18.2	
32	59.4	1.7738	65.50	1.8162	18.5	

Table 5.4 Variation of Threshold Current with Temperature

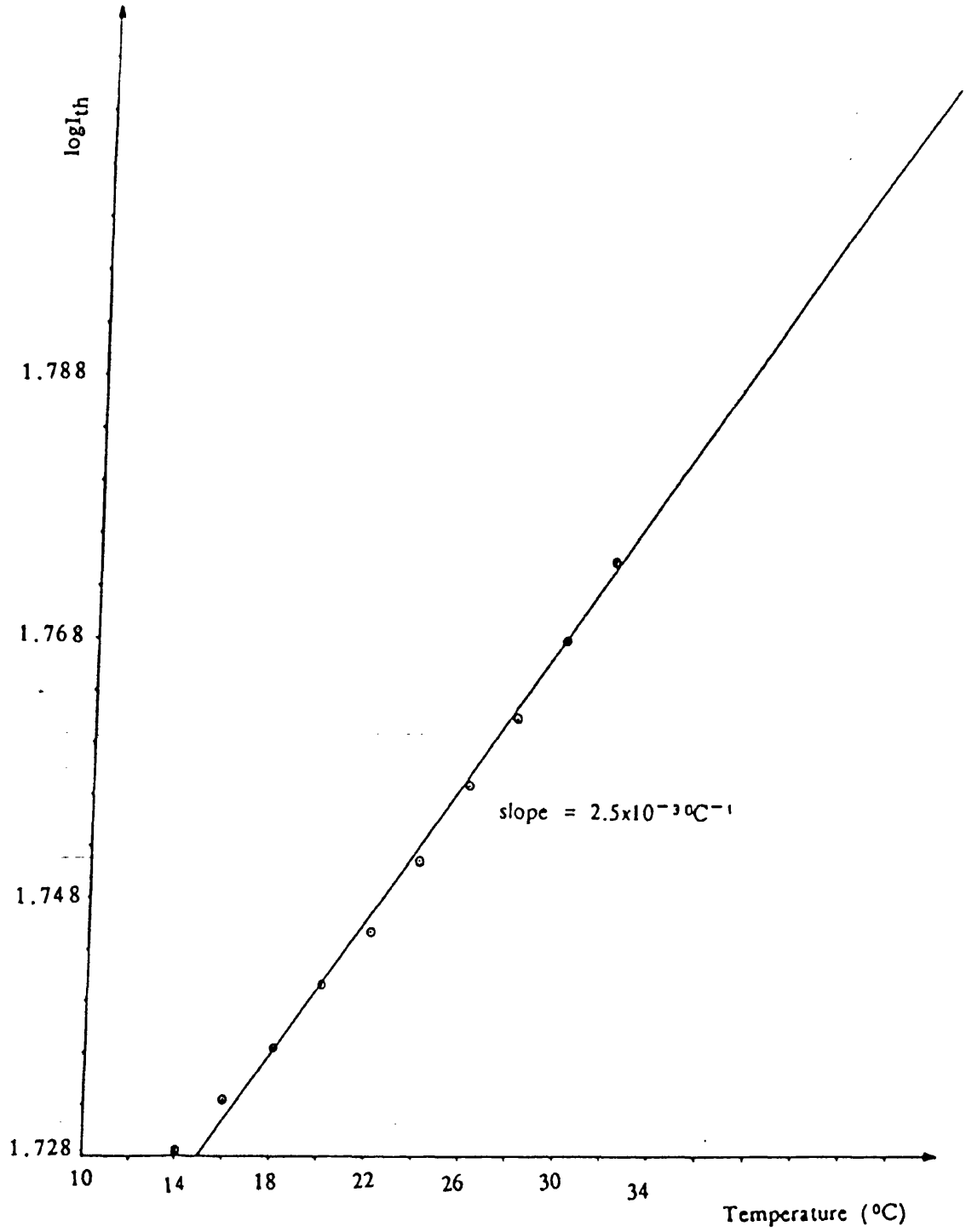

Figure 5.29 Relation between $\log I_{th}$ and operating temperature (T) for LD

LD HL8311E

temperature during the pulse time and its change with time have been illustrated in Table 5.5 while the variation of temperature with time along the pulse has been drawn in Figure 5.30 which shows a thermal time constant of about 9.8nsec. The diode temperature reaches to within 5% of the final value in a time of 30ns.

Time (nsec)	Reduction in optical output amplitude mv	Shift in threshold current ΔI_{th}(mA)	The instant-aneous threshold current (mA)	$\log I_{th}$	ΔT rise in temp (^{0}C)	$\log \Delta T$
6	1.5	0.7	56.35	1.7509	1.6	0.2041
12	7.5	3.5	59.17	1.7720	9.6	0.9822
18	8.25	3.87	59.52	1.7821	10.6	1.0253

Table 5.5 Relation Between the Rise in Temperature of LD and the Time Along the Pulse

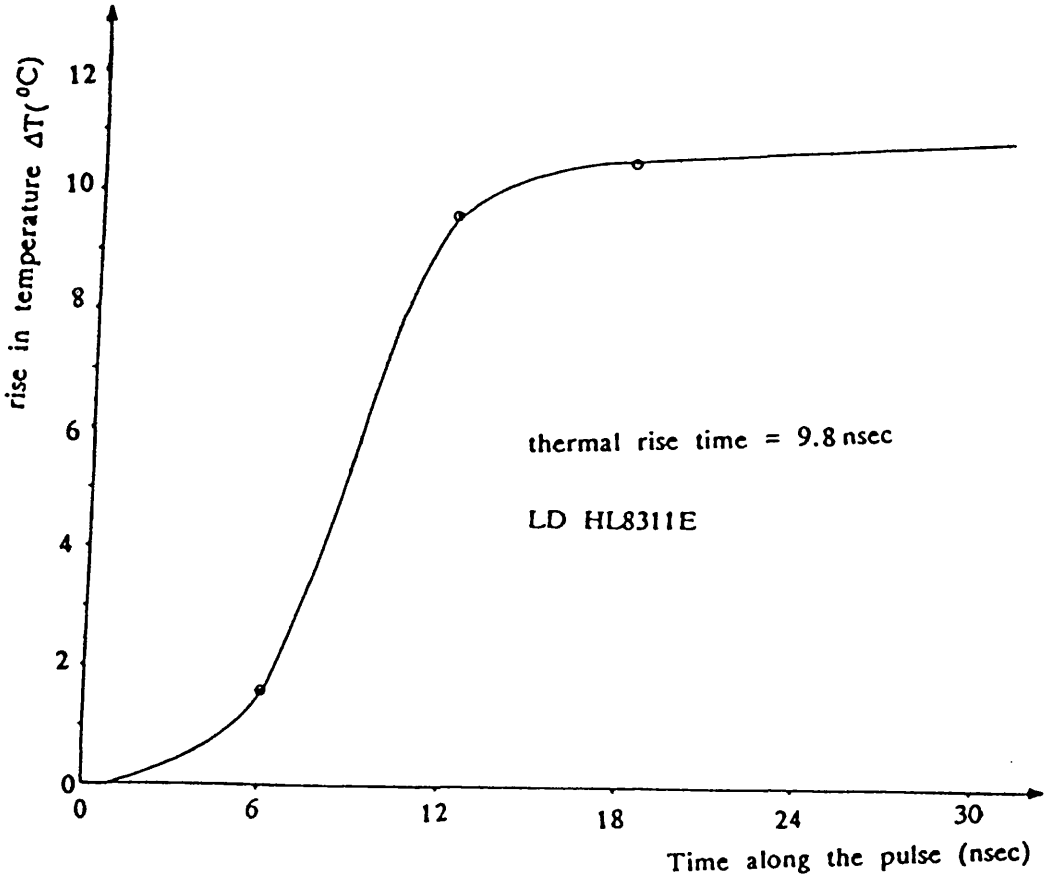

Figure 5.30 Relation between the rise in temperature of the laser chip (ΔT) and the time along the pulse

5.7 Conclusion

In this chapter, the effect of temperature upon the current threshold of a laser has been discussed and measured, and is shown to follow the expected form of an exponential function of temperature. The slope efficiency is not significantly changed. Using a family of light–current curves at different temperatures, it is possible to calculate the slope efficiency and the proportionality constant in the threshold current expression.

Making use of this information, a method has been described which enables the transient thermal response of a Laser Diode to be measured, giving an approximately exponential rise of temperature with time.

Two LDs have been used in measurement. The laser diode HL8311E has a faster response, higher threshold current and shorter thermal time constant than the diode HL7801E, since it is designed for communication use. The measured time constants are about 10ns and 40ns respectively. Assuming an approximately exponential rise of temperature, the diode temperature reaches to within 5% of the final value in a time of about 30ns and 120ns respectively. These figures represent 87 and 30 data symbols respectively, at a data rate of 250Mb/s. Consequently, provided that due allowance is made for the higher signal level at the beginning of a received packet, there is no need to try and carry out temperature control of the laser diode within the packet time.

5.8 References

1. W. B. Joyce and R. W. Dixon: "Thermal resistance of heterostructure laser", J.Appl.Phys., Vol.46, pp855-862, 1972.

2. T. Kobayashi and Y. Furukawa: "Temperature distributions in the GaAs-GaAℓAs double heterostructure laser below and above the threshold current", Japan, J.Appl.Phys., Vol.14, pp1981-1986, 1975.

3. W. Engeler and M. Garfinkel: "Thermal characteristics of GaAs laser junctions under high power pulsed conditions", Solid-State Electronics, Vol.8, pp585-604, 1965.

4. W. Nakwaski: "The thermal properties of a single-heterostructure laser diode supplied with short current pulses", Optical and Quantum Electronics, 11, pp219-327, 1979.

5. W. Nakwaski: "Dynamical thermal properties of broad-contact double-heterostructure GaAs-GaAℓAs laser diodes", Optical Quantum Electronics, 15, pp313-324, 1983.

6. J. C. Dyment, Y. C. Cheng and A. J. Springthorn: "Temperature dependence of spontaneous peak wavelength in GaAs and $Ga_{1-x}A\ell_xAs$ electroluminescant lasers", J.Appl.Phys., Vol.46, pp1739-1743, 1975.

7. M. Suyama, N. Ogasawara and R. Ito: "Transient temperature variation of injection lasers", Jan.J.Appl.Phys., Vol.20, No.6, ppL395-L398, 1981.

8. W. E. Engeler and M. Garfinkel, J.Appl.Phys., Vol.34, p2746, 1963.

9. W. E. Engeler and M. Garfinkel, J.Appl.Phys., Vol.35, p1734, 1964.

10. H. S. Carlson and J. C. Jaeger: "Conduction of Heat in Solids", Oxford University Press, p.10, 1959.

11. X. Zhang: "The Transient temperature effects in GaAs/GaAℓAs stripe geometry semiconductor laser", Internal Research Report, Electrical Engineering Department, University of Bath, September 1986.

12. R. D. Richtmyer, K. W. Morton: "Difference Methods for Initial-Value Problems", Second Edition, John Wiley & Sons, London, 1967.

13. R. M. Sincovec and N. K. Madsen: "Software for nonlinear partial differential equations", Ac.M.Trans.Math.Software, Vol.1, pp232-260, 1975.

14. M. Ettenberg, C. J. Neuse and H. Kerssel: "The temperature dependence of threshold current for double-heterojunction lasers", J.Appl.Phys., Vol.50, pp2949-2950, April 1979.

15. R. Chin, N. Holonyak, B. A. Vojak, K. Hess, R. D. Dupuis and P. D. Dpkus: "Temperature dependence of threshold current for quantum-well heterostructure laser diodes", Appl.Phys.Lettr., Vol.36, pp19-21, January 1980.

16. G. H. B. Thompson: "Temperature dependence of threshold current in GaInAsP DH lasers at 1.3 and 1.5μm wavelength", IEEE Proc., Vol.128, pp37-43, April 1981.

CHAPTER 6

LASER DIODE POWER CONTROL

6.1 Introduction

The laser diode has a threshold current which is a sensitive function of temperature, and the threshold level tends to increase as the LD ages, following an increase in internal device losses. Some form of feedback control is required to ensure the continuous laser operation and stability of the output of the device. Although the laser may be cooled to compensate for temperature variations, aging is not so easily accommodated by the same process. However, both problems may be overcome through control of laser bias using feedback techniques, so that it is usually necessary to monitor the light output from the LD in order to keep some parameter constant. The laser slope efficiency may change with temperature and aging, and in order to compensate for such changes the ac and dc components of the monitored light output must be processed independently. This is especially important in the case of high bit rate digital system where control of the on and off levels as well as average light level is required. Thus for a high bit rate digital system it is required to have two independent control circuits, the first to ensure that the laser diode is biased close to threshold for logical zero condition, so reducing the switch-on delay which causes pulse width narrowing, and the second control loop which ensures that the power in the logical one-condition remains constant even though the laser slope efficiency changes.

A further requirement in a packet transmission system is that this degree of control should be maintained under intermittent operation of the laser diode.

6.2 Previous Work Done for Automatic Power Control of LD

Several strategies to provide automatic power control of semiconductor laser have been followed, with varying complexity and sophistication. They range between those that require a wideband optical detector channel, and those that do not require optical feedback at all.

6.2.1 Power control without an optical detector

A. Albanese[6.1] has used a method to stabilise the optical output of the LD, which depends on monitoring the change of electrical parameters of the diode close to threshold. This method is based on the fact that the laser junction voltage saturates at currents above threshold[6.2–6.8] so an automatic bias control circuit has been designed to monitor the laser junction voltage, to generate an error signal proportional to the degree that the laser junction voltage is not saturated and to increase the bias current in the laser until the error voltage is minimised. The advantage of this circuit is that it does not need a photodetector, but it is used only to adjust the bias current and it does not compensate for any change in slope efficiency and it has been used at frequencies below 100kHz. It can be used at frequencies greater than that if the frequency response of the operational amplifier used to generate the error signal is improved.

M. Ettenberg et al[6.9] have used a simplified technique to compensate for the temperature dependence of the threshold current of the laser diode by employing the temperature dependence of the emitter–base voltage of the driving silicon transistor. This module does not compensate for slope effficiency changes and it is used for unbiased operation of the laser diode so there are some limitations on its modulation capability because of the turn–on delay, and it has been used at a rate of 25Mbit/s.

6.2.2 Power control with a narrowband optical detector

D. W. Smith[6.10] has used an alternative strategy for laser level control that does not (a) require a fast photodiode and its subsequent wideband amplifier, (b) make special demands on the choice of the line code, (c) rely on the correlation between electrical properties of the laser and the onset of the lasing. This circuit used a slow photodiode and a slope detector. The circuit detects the change of slope of the light-current transfer characteristic of the laser diode at threshold to set the 0-level, while the 1-level is set by mean power feedback. The idea is to superimpose a low frequency low amplitude signal on the dc bias and the data pulses to the laser; then the low frequency modulation is detected by a slow photodiode, and the amplitude of the detected signal will indicate if the laser output logical 0-level is above or below threshold. The same photodiode monitors the mean power so that the 1-level can be determined and adjusted. The circuit is capable of providing automatic level control for pulses down to 0.75nsec width and at 300Mbit/s rate. The same goal can be achieved by measuring the slope[6.11] instead of the change in slope[6.12], of light-current characteristics close to threshold. Mean power feedback[6.13] is the most straightforward scheme, where the power is monitored by the photodiode and the time averaged photocurrent is compared to a reference level; the difference signal is amplified and used to control the bias current to the laser. If a laser transmitter containing a mean power feedack circuit has to deal with modulation signals with non-zero average disparity, it is necessary to obtain a reference signal that is proportional to the mean input signal[6.14]. With the mean power feedback featuring bias control, there will be a degradation of the extinction ratio if the effective slope efficiency of the laser decreases during the lifetime of the transmitter[6.13]. Kischi Yamashita et al[6.15] have developed an LD transmitter on an IC which operates at the modulation speed of 300-400Mbit/s. In the transmitter, a bias current sink controlled by an automatic power control circuit is

used to reduce the degradation of modulation speed due to the emission threshold variation with temperature. The automatic power control circuit has an average sensing bias current control technique for constantly maintaining the average magnitude of the optical output power. The average optical output power is monitored by a photodiode coupled to the LD, and then compared with a reference level which is obtained by averaging the input signal, the result is used to adjust the bias current to correct the drift.

The input signal is averaged to produce the reference level, by using an integrator which consists of a limiting amplifier and a resistor–capacitor series circuit, the former reshapes the input signal into a signal with fast rise and fall times. The latter detects the average magnitude of the limiting amplifier output. The photocurrent monitored by the photodiode is also integrated by an integrator which consists of a resistor–capacitor parallel circuit and converted to a voltage V_{eff}, then an amplifier of gain 25dB detects and amplifies the error voltage between the reference and the monitored levels. The amplifier controls the bias current of the LD. The open loop gain of the automatic power control circuit is designed to be more than 45dB, to suppress the optical output power fluctuation to less than ±1dB.

6.2.3 Power control requiring a wideband optical detector

B. R. White et al[6.16] stabilise the output characteristic of the laser by producing an electrical pulse train representative of an optical pulse train of the laser, and then the electrical pulse train is fed to circuitry which monitors the switch–on delay of the laser and controls the bias current of the LD such that the switch–on delay is maintained constant. Alternatively the pulse length can be monitored. The pulse amplitude or the mean pulse energy also has been monitored and maintained constant through controlling the modulation current.

However, measurements of this kind would be difficult to do for wideband lasers. R. E. Epworth[6.17] built a fast feedback system which continuously adjusts both the bias current and the modulation current to ensure normalised optical output levels. The electrical signal from a monitor photodetector is dc amplified and negative and positive peak detected, to give dc voltages which are proportional to the peak and pedestal optical power L_1, L_0, which are then buffered by two voltage followers. L_0 is subtracted from L_1 to give a measure for L_{mod}, the modulation power, then both L_0 and L_{mod} are compared with the demand power values in two comparators. The output of these comparators represent the errors in L_{mod} and L_0, respectively, and are fed back to optimise the modulation current I_M and the bias current I_b. It is also possible to replace the negative and positive peak detectors with sampling gates switched by the data signal, thus synchronously demodulating the values of L_1 and L_0. This sampling method may be extended for use with multilevel data (e.g. ternary) by the addition of an extra sampling gate. This method makes it possible to correct for any laser non-linearities which would otherwise degrade the performance of multi-level system. The main problem of these two previous methods is that the photodetector, the amplifier and peak detectors or sampling gates, need a bandwidth as high as that of the optical receiver, and also the amplifer must be dc coupled.

To avoid the wideband dc amplifier one can use a slow dc amplifier and an additional ac amplifier the output of which is peak detected to give L_{mod}. L_0 is then obtained by subtracting half L_{mod} from the average power L_{av}. The disadvantage of this method is that two terms of nearly equal value are subtracted to obtain a measure for L_0, which needs to be tightly controlled if good system performance is to be maintained. A small gain change in either ac or dc path will have a large effect on L_0. J. Gruber et al[6.18] have used a circuit which controls the dc laser bias current and the modulation current amplitude, stabilising the temporal minimum output level and the modulation amplitude of the light

output power. It is similar to the circuit proposed by Epworth[6.16], and is based on monitoring the light output of the laser diode by a PIN photodiode, then measuring ($L_{av} - L_0$), ($L_1 - L_{av}$). By summing these two quantities a measure of the optical amplitude is found which is then compared with a reference and the result is used to adjust the modulation current amplitude in order to keep the light output amplitude constant. L_0 is compared with a reference and the result is used to adjust the bias current to the laser diode. Measurements have been made with 280Mbit/s RZ-PCM signals with a continuous bit stream and with a single "1" bit within a 16 bit frame. The operation of the circuit does not depend on the 0-1 probability ratio of the PCM laser modulation signal provided that the duty cycle is constant, but if the duty cycle is not constant a signal containing duty cycle information has to be introduced.

F. S. Chen[6.19] designed a circuit which allows regulation of the time average dc optical power L_{av} through control of bias current, and regulation of the optical output amplitude ($L_1 - L_0$) through control of modulation current amplitude. Duty cycle information is derived from the regenerated input signal, which is integrated to provide a reference voltage (V_{ref}) and its complement V_{ref}. These contain information about the duty cycle of the input data and they are compared with L_{av} and ($L_1 - L_{av}$) respectively, and and the results being used to adjust the bias current (I_b) and the modulation current (I_M) respectively. This experiment was performed with a simulated laser which is an LED connected to a series resistance and a shunt resistance so that efficiency as well as threshold current could be altered. The experiment was performed at 20Kbit/s because of the slow response of the simulated laser and the ease of performing it at low bit rate. The circuit can maintain constant peak light output and a large extinction ratio of laser diode in a closed loop manner, regardless of the duty cycle.

A recent laser driver circuit to stabilise the optical output levels independent

of variation in the average output power has been developed[6.20]. The circuit employs balancing compensation of the modulation signal to allow arbitrary on–off ratio. In this circuit three major considerations have been addressed:

1. Whether to bias the laser above or below threshold.
2. Stabilising the optical output levels independent of variation in the average output power.
3. To what degree the output levels can be stabilised.

In this strategy the LD is prebiased near its threshold. Added to this bias is a modulation current which switches the laser between its zero and one light output levels (L_0, L_1). The prebias is stabilised by a negative feedback loop comprising the LD, a photodetector, a reference current, a low pass filter and a current amplifier. The photodetector generates a current (I_D) which is proportional to the optical output of the laser L; a current I_X is added at a summing node S to cancel the influence of alternation of the dc component of the laser output due to the modulation current. The photocurrent is compared with a reference current at the summing node S and the resulting current is low pass filtered and amplified to generate the prebias current. The scheme used in this control strategy leads to a conclusion that if the laser is biased above threshold then as the above–threshold slope efficiency (η_2) drifts as a function of time or change in environment, then L_0, L_1 will exhibit some dependence on the data signal dc component D, and a modulation current control loop is required to stabilise the laser levels against changes in D and η_2.

This control loop generates a signal which is proportional to the difference in levels ($L_1 - L_0$) and uses it in continuous adjustment of the modulation current (I_M) such that $\eta_2 I_M$ remains constant. On the other hand if the laser is biased below threshold the light output levels will exhibit dependence on the data signal

average and they are not stabilised against variation in η and threshold current.

6.3 Analysis of Laser Diode Power Control

The previous section has shown that various schemes have been used to derive the quantities to control bias and modulation currents for a laser diode, and the choice of these is fairly critical. In order to appreciate the choice which is made in this work, it is necessary to analyse the alternatives and to show how the various schemes perform.

The major choice is whether the bias level is near threshold, either just above it or just below it, or whether the bias is set to be midway through the modulation range. Since the laser diode light–current characteristic is non–linear, then this choice is of major importance.

First, the general background to the analysis will be introduced, defining the parameters in use, and then the two cases will be analysed in detail. The aim of the control system is that the two modulation levels of light output should be independent of the temperature–dependent parameters, threshold current I_{th} and slope efficiency η_2. In order to achieve this, two feedback loops are required to fix the bias level and the modulation current swing, and these should also be independent of one another.

6.3.1 Static analysis

Considering the light–current characteristics of an LD shown in Figure 6.1, with the diode biased by a current I_b set above threshold. Consider closed loop control put around the diode as shown in Figure 6.2, then:

$$V_0 = K_L L_0 \qquad 6.1$$

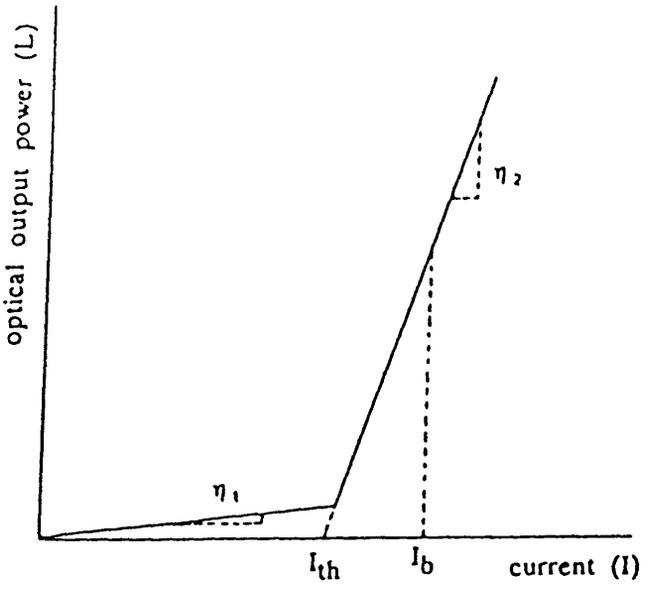

Figure 6.1 Illustration of L–I characteristics of an LD

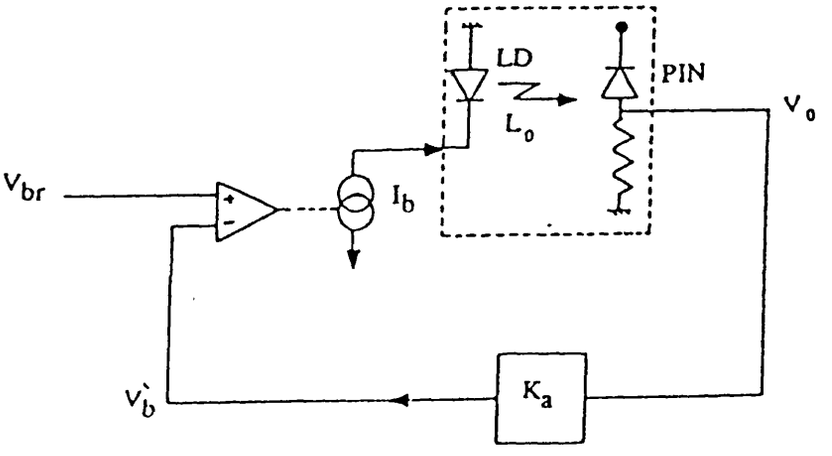

(a)

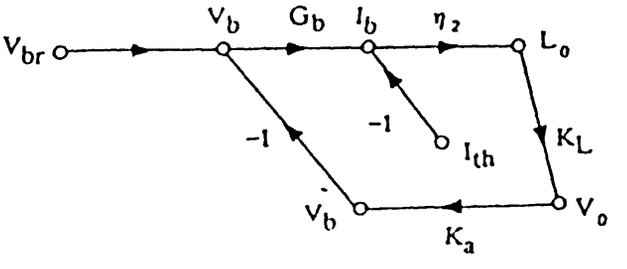

(b)

Figure 6.2 a) Closed feedback control loop around the LD system
b) Signal flow diagram of the system

where L_0 is the diode light output, V_0 is the corresponding electrical output of the monitor PIN photodiode which has efficiency K_L. If K_a is the transfer function of the feedback network, $V_{b'}$ is its output voltage. Then:

$$V_{b'} = K_a V_0 \qquad 6.2$$

$V_{b'}$ is compared with a reference voltage V_{br} through the differential amplifier of conductance G_b, the output of the amplifier controls the bias current (I_b) applied to the LD.

$$I_b = G_b[V_{br} - V_{b'}] \qquad 6.3$$

Assuming that η_1 is the slope efficiency of spontaneous emission part of light current characteristics, that η_2 is the stimulated emission slope efficiency and that I_{th} is the threshold current, then:

$$L_0 = \eta_2[I_b - I_{th}] \qquad 6.4$$

Operating equations of the closed loop are best seen by means of a signal-flow graph shown in Figure 6.2b where nodes represent signals and paths are associated with multiplicative constants. From this signal flow graph:

$$L_0 = \eta_2[v_{br}G_b - I_{th} - L_0K_LK_aG_b]$$

$$(1 + \eta_2K_LK_aG_b)L_0 = \eta_2[v_{br}G_b - I_{th}]$$

$$L_0 = \frac{\eta_2[v_{br}G_b - I_{th}]}{1 + \eta_2K_LK_aG_b} \qquad 6.5$$

η_2 is a variable which is to be eliminated by feedback. This can be achieved if:

$$\eta_2 K_L K_a G_b >> 1 \qquad 6.6$$

Hence, from (6.5) and (6.6):

$$L_0 = \frac{V_{br}}{K_L K_a} - \frac{I_{th}}{K_L K_a G_b} \qquad 6.7$$

Equation (6.7) shows that control has been exerted and L_0 depends mostly on V_{br} if:

$$V_{br} G_b >> I_{th} \qquad 6.8$$

If the feedback loop is broken by mistake the light output in this case is:

$$L_0' = \eta_2 [V_{br} G_b - I_{th}] \qquad 6.9$$

Comparing equation (6.9) with (6.7), we get:

$$\frac{L_0'}{L_0} = \eta_2 K_L K_a G_b$$

since $\eta_2 K_L K_a G_b >> 1$, then $L_0' >> L_0$.

Hence, a current limiting circuit must be used in the driver.

It is to be noted that the control loop cannot compensate for changes in I_{th} or η_2 if normal bias $I_b < I_{th}$. Also, to adjust the bias current exactly to threshold:

$$L_0 = \eta_1 I_{th}$$

$$\therefore \eta_1 I_{th} = \frac{V_{br}}{K_L K_a} - \frac{I_{th}}{K_L K_a C_b}$$

$$\therefore V_{br} = I_{th}\left[\eta_1 K_L K_a + \frac{1}{C_b}\right] \qquad 6.10$$

Equation 6.10 shows the dependence of V_{br} on I_{th} and η_1 which indicate that it will be difficult to keep the bias current exactly at threshold.

6.3.2 Analysis for the case of bias at base of modulation

With the modulation pulse current is superimposed on the bias current the maximum value of the light output is:

$$L_{max} = \eta_2[I_b + I_m - I_{th}] \qquad 6.11$$

where I_m is the amplitude of the modulation pulse current. The average value of the output light is:

$$L_{av} = \eta_2\left[I_b + \frac{I_m}{2} - I_{th}\right] \qquad 6.12$$

The control strategy which is intended to be used in this analysis is to use L_{max} to control modulation current and the minimum value of the light output, L_{min}, to control bias current:

$$L_{min} = L_{av} - \frac{L_{max}}{2} \qquad 6.13$$

In addition to the bias current control loop previously examined, another feedback loop has to be added to control the modulation current, as illustrated in Figure 6.3. If K_m is the transfer function of the feedback network in the modulation current control loop, G_m is the conductance of the modulation current driver and m(t) is the modulation function, [m(t) = 0 or 1], then the average voltage measured at the output of the feedback network of the bias current control loop is:

$$V_{av} = K_a K_L L_{av} \qquad 6.14$$

and the maximum voltage measured at the output of the feedback network of the modulation current control loop is:

$$V_{max} = K_m K_L L_{max} \qquad 6.15$$

By drawing the signal-flow diagram as shown in Figure 6.3b, in this case the light output is now derived from the signal-flow graph to be:

$$L_0(t) = \eta_2\left[V_{br}G_b - \left[V_{av} - \frac{V_{max}}{2}\right]G_b - G_m m(t)(V_{mr} - V_{max}) - I_{th}\right] \qquad 6.16$$

substituting from equations (6.14) and (6.15) into (6.16), we get:

$$L_0(t) = \eta_2\left[V_{br}G_b - K_L G_b\left[K_a L_{av} - K_m \frac{L_{max}}{2}\right] + G_m m(t)(V_{mr} - K_m K_L L_{max}) - I_{th}\right] \qquad 6.17$$

Now $L_0(t) = L_{min}$ when $m(t) = 0$

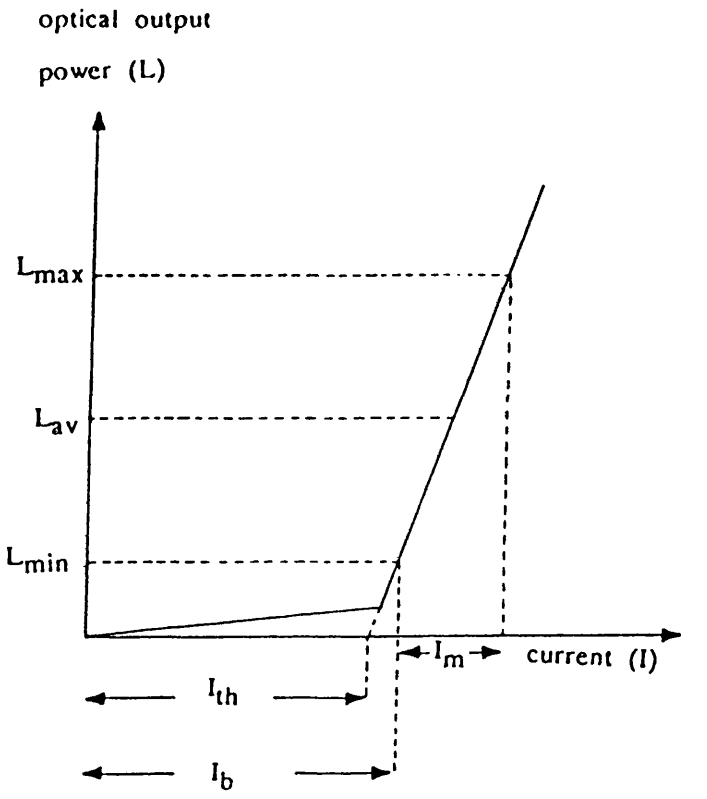

(a)

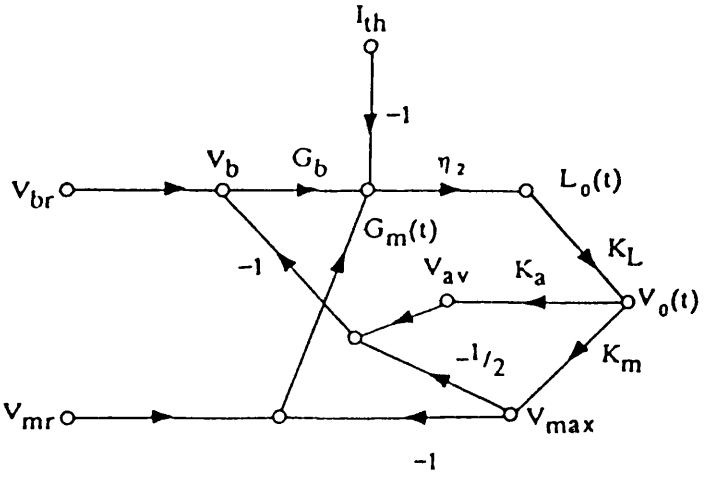

(b)

Figure 6.3 a) (L–I) characteristics of LD illustrating the case when bias is at the base of modulation
b) Signal flow diagram for this case

$$\text{and } L_{av} = L_{min} + \frac{L_{max}}{2} \qquad 6.18$$

$$\text{Hence, } L_{min} = \frac{\eta_2[V_{br}G_b + K_L G_b[K_m - K_a]L_{max}/2 - I_{th}]}{1 + \eta_2 K_a K_L G_b} \qquad 6.19$$

If $\eta_2 K_a K_L G_b >> 1$ which is the control condition, then:

$$L_{min} = \frac{V_{br}}{K_a K_L} + \left[\frac{K_m}{K_a} - 1\right]\frac{L_{max}}{2} - \frac{I_{th}}{K_a K_L G_b} \qquad 6.20$$

also, $L_0(t) = L_{max}$ when $m(t) = 1$.

Then, from equation (6.17) we get:

$$L_{max} = \eta_2\left[V_{br}G_b - K_L G_b\left[K_a L_{av} - K_m\frac{L_{max}}{2}\right] + G_m V_{mr} - K_m K_L G_m L_{max} - I_{th}\right] \qquad 6.21$$

substituting for L_{av} using equations (6.18) and (6.20), we get:

$$L_{max} = \frac{\eta_2[V_{mr}G_m]}{1 + \eta_2 K_m K_L G_m} \qquad 6.22$$

if $\eta_2 K_m K_L G_m >> 1$, then:

$$L_{max} = \frac{V_{mr}}{K_m K_L} \qquad 6.23$$

Substituting back in equation (6.20):

$$\therefore L_{min} = \frac{V_{br}}{K_a K_L} + \left[\frac{K_m}{K_a} - 1\right] \frac{V_{mr}}{2K_m K_L} - \frac{I_{th}}{K_a K_L G_b} \qquad 6.24$$

It is to be noted that the expression for L_{max} in equation (6.23) is very simple and control is unaffected by LD changes, on the other hand the expression for L_{min} in equation (6.24) is not simple, but if $K_m = K_a$ then the control of bias is independent of V_{mr}.

Practical difficulties may arise in getting the bias control signal:

$$\left[V_{av} - \frac{V_{max}}{2}\right]$$

which is very small and errors in gain may make the error signal change in sign. Control with both feedback loops applied simultaneously appears feasible, but controlling the bias at threshold is not practical.

6.3.3 Analysis for the case of bias at mid point of modulation

When the diode is biased at the midpoint of modulation as shown in the L.I. characteristics in Figure 6.4:

$$L_{av} = \eta_2[I_b - I_{th}] \qquad 6.25$$

$$L_{max} = \eta_2[I_b + I_m - I_{th}] \qquad 6.26$$

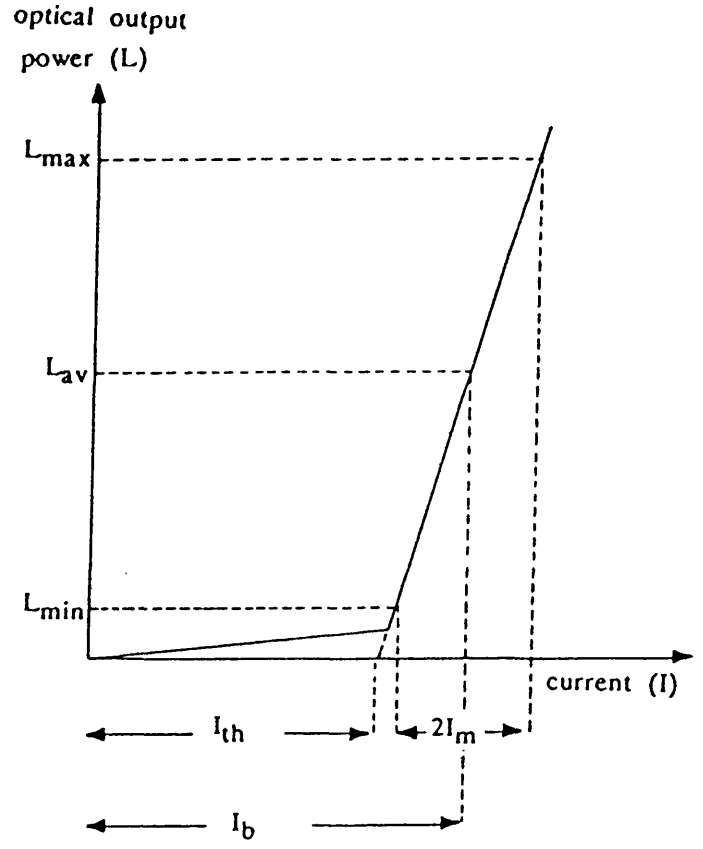

(a)

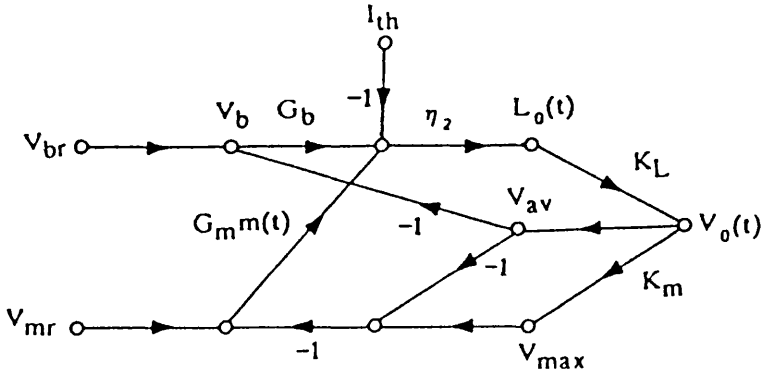

(b)

Figure 6.4 a) L-I characteristics illustrating the case of bias at the mid point of modulation
b) Signal flow diagram for this case

The control strategy is using L_{av} to control bias current and $(L_{max} - L_{av})$ to control modulation current. The signal-flow graph, in this case, is shown in Figure 6.4b, and the equations are similar to those in section 6.3.2, previously described, except m(t) = 0 or 1 or −1. Hence:

$$L_0(t) = \eta_2[V_{br}G_b - V_{av}G_b + G_m m(t)[V_{mr} - V_{max} + V_{av}] - I_{th}] \qquad 6.27$$

Now using the expressions for v_{av} and V_{max} in equations (6.14) and (6.15), then:

$$L_0(t) = \eta_2[V_{br}G_b - K_aK_LG_bL_{av} + G_m m(t)(V_{mr} - K_mK_LL_{max} + K_aK_LL_{av}) - I_{th} \qquad 6.28$$

but $L_0(t) = L_{av}$ when m(t) = 0, so:

$$L_{av} = \frac{\eta_2[V_{br}G_b - I_{th}]}{1 + \eta_2K_aK_LG_b}$$

If $\eta_2K_aK_LG_b >> 1$ then:

$$L_{av} = \frac{V_{br}}{K_aK_L} - \frac{I_{th}}{K_aK_LG_b} \qquad 6.29$$

Also $L_0(t) = L_{max}$ when m(t) = + 1, so:

$$L_{max} = \frac{\eta_2[V_{br}G_b - I_{th} + V_{mr}G_m - K_aK_L(G_b - G_m)L_{av}]}{1 + \eta_2G_mK_mK_L}$$

Substituting for L_{av} from equation (6.29):

$$\therefore L_{max} = \frac{\eta_2[V_{br}G_m + V_{mr}G_m - I_{th}G_m/G_b]}{1 + \eta_2 G_m K_m K_L}$$

if $\eta_2 G_m K_m K_L >> 1$, then:

$$L_{max} = \frac{V_{br} + V_{mr}}{K_m K_L} - \frac{I_{th}}{K_m K_L G_b} \qquad 6.30$$

Equation 6.30 shows that the maximum power control loop is dependent on the average power control loop, hence to achieve independent feedback power control strategy, the control algorithm has to be modified.

6.3.4 Improved algorithm for power control

Suppose that the control algorithm is changed slightly to use L_{av} in controlling bias and L_{max} to control modulation. In this case the signal-flow graph is shown in Figure 6.5 and the equations are similar to the previous section, except that V_{av} is not used in the modulation control, then:

$$L_0(t) = \eta_2[V_{br}G_b - V_{av}G_b + G_m m(t)(V_{mr} - V_{max}) - I_{th}] \qquad 6.31$$

Substituting for V_{av} and V_{max} from equations (6.14) and (6.15):

$$L_0(t) = \eta_2[V_{br}G_b - G_b K_a K_L L_{av} + G_m m(t)(V_{mr} - K_m K_L L_{max}) - I_{th}] \qquad 6.32$$

but $L_0(t) = L_{av}$ when $m(t) = 0$, so:

$$L_{av} = \eta_2[V_{br}G_b - G_b K_a K_L L_{av} - I_{th}]$$

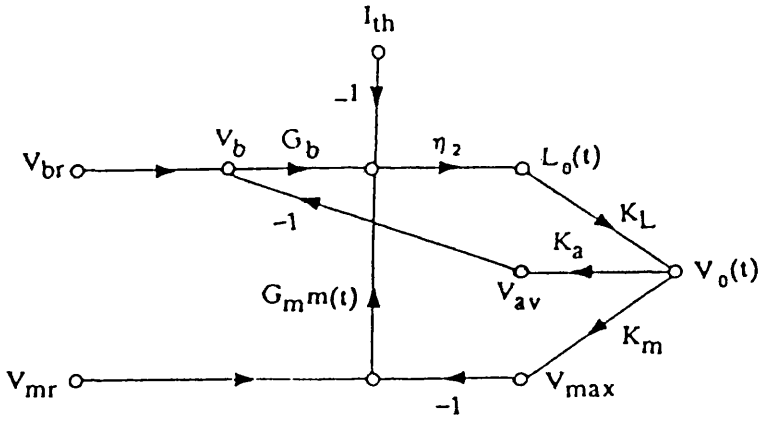

Figure 6.5 Signal flow diagram illustrating the case which uses L_{av} to control bias and L_{max} to control modulation

$$L_{av} = \frac{\eta_2[V_{br}G_b - I_{th}]}{1 + \eta_2 G_b K_a K_L}$$

If $\eta_2 K_a K_L G_b >> 1$, then:

$$L_{av} = \frac{V_{br}}{K_a K_L} - \frac{I_{th}}{K_a K_L G_b} \qquad 6.33$$

which is identical to equation (6.29).

If $V_{br}G_b >> I_{th}$, then:

$$L_{av} = \frac{V_{br}}{K_a K_L} \qquad 6.34$$

Also $L_0(t) = L_{max}$ when $m(t) = +1$, so by substituting in equation (6.32) using equation (6.33):

$$L_{max} = \eta_2\left[V_{br}G_b - G_b K_a K_L\left[\frac{V_{br}}{K_a K_L} - \frac{I_{th}}{K_a K_L G_b}\right] + G_m(V_{mr} - K_m K_L L_{max}) - I_{th}\right]$$

$$L_{max}(1 + G_m K_m K_L \eta_2) = \eta_2 G_m V_{mr}$$

$$L_{max} = \frac{\eta_2 G_m V_{mr}}{1 + G_m K_m K_L \eta_2}$$

If $G_m K_m K_L \eta_2 >> 1$, then:

$$L_{max} = \frac{V_{mr}}{K_m K_L} \qquad 6.35$$

Equations (6.34) and (6.35) indicate that simultaneous control loops operate independently if this algorithm is chosen, also if L_{min} drops below threshold, then the loop will still operate. It is to be noted that control signals are easier to measure and loops always operate in linear region. Although L_{max} is highly controlled by the loop, demand would rise rapidly if the loop is broken, and a current limiting mechanism is essential.

6.4 Requirements for Effective Operation of Power Control Loops

Considering the improved algorithm for power control strategy previously described in section 6.3.3.1 where the LD bias is at the midpoint of modulation, the first requirement to achieve this strategy is to design and implement an LD drive circuit which can drive the laser during the duration of the packet with a current $I > I_{th}$ at the midpoint of modulation, in addition to the modulation drive. The second requirement is to achieve the conditions required for the control to be exerted for both of the two control loops as illustrated in section 6.3.3.1.

6.4.1 Laser Diode Drive Circuit

A modification has been made in the laser diode drive circuit previously described in chapter 4, to allow it to drive the LD above threshold during the packet duration, at the midpoint of modulation. The modulation current must now subtract from the bias current as well as add to it. This has been done as shown in Figure 6.6 where the collector of the transistor Q_4 is connected in series with a resistance $R_{16} = 50\Omega$ and coupled to the LD by a capacitor C.

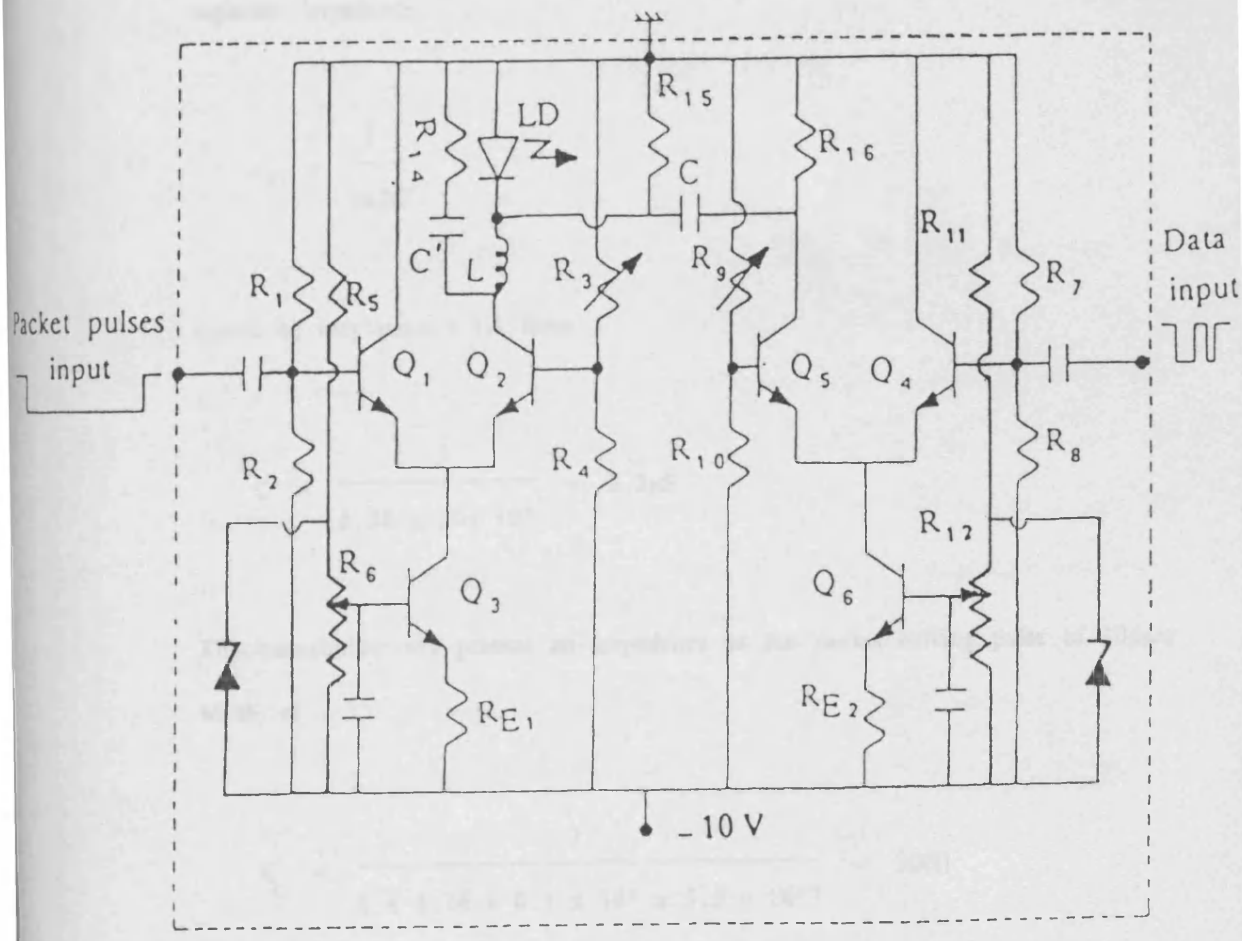

Figure 6.6 Laser diode drive circuit for packet transmission

The value of the capacitor C has to be chosen such that it offers low impedance to the modulating pulse of lowest frequency and high impedance to the driving current pulse of width 10μsec which is equivalent to the duration of the packet. Let the pulse width of the modulating pulses be 3.5nsec. In the case of having a sequence of 9 ones which is equivalent to a pulse width of 31.5nsec, then the lowest frequency for modulation pulses is $\simeq$ 30MHz; and in this case the capacitor impedance:

$$x_C = \frac{1}{2\pi fC}$$

should be very small $\simeq 1\Omega$, then:

$$C = \frac{1}{6.28 \times 30 \times 10^6} = 5.3\text{nF}$$

This capacitance will present an impedance to the packet driving pulse of 10μsec width, of

$$X'_C = \frac{1}{2 \times 3.14 \times 0.1 \times 10^6 \times 5.3 \times 10^{-9}} = 300\Omega$$

The capacitor will present a lower impedance to the higher frequency components of the 10μs pulse so affecting the corners. If the value of C is reduced it will affect the lower frequency component of the modulation pulses. The optimised output is obtained by choosing the value of capacitor 4.7nF and adding the compensating network which consists of a coil and capacitor C' and resistor R_{14} as shown in Figure 6.6. The coil should offer high impedance to modulation pulses of lowest frequency component and low impedance to the packet pulse of width

10μsec.

So for 10μsec pulse the impedance offered to the highest frequency components should be minimum, by choosing L = 0.44μH then:

$$X_L = 2\pi fL = 6.28 \times 10^6 \times 0.44 \times 10^{-6} = 2.7\Omega$$

while for the lowest frequency of modulation pulses X_L = 188Ω.

The value of C' has been chosen practically to optimise the output when replacing the LD with 20Ω load. C' was 1nF and R_{14} = 100Ω. The circuit has been tested first with a 20Ω load instead of the LD, and its input and output at different repetition rates, measured by 275MHz bandwidth oscilloscope of the type HP8081A, are shown in Figure 6.7a,b. It has also been tested with the LD HL8311E and a resistor R_{15} in parallel with it (R_{15} = 300Ω) instead of the 20Ω load. The input and the optical output, measured by 1GHz bandwidth oscilloscope of the type HP54100A, are shown in Figure 6.8a,b. From this figure, the values of the measured rise and fall times were about 1.2ns. There was no distortion in the shape of the pulses at low pulses frequency (30Mbit/s). The circuit was capable of modulating the laser at bit rates from 30-250Mbit/s.

6.4.2 Choosing the loop gain for control loops

For the average optical power control loop the conditions required for the control to be exerted are illustrated by equation 6.34 and inequalities 6.6 and 6.8 where:

$$L_{av} = \frac{V_{br}}{K_a K_L} \qquad 6.34$$

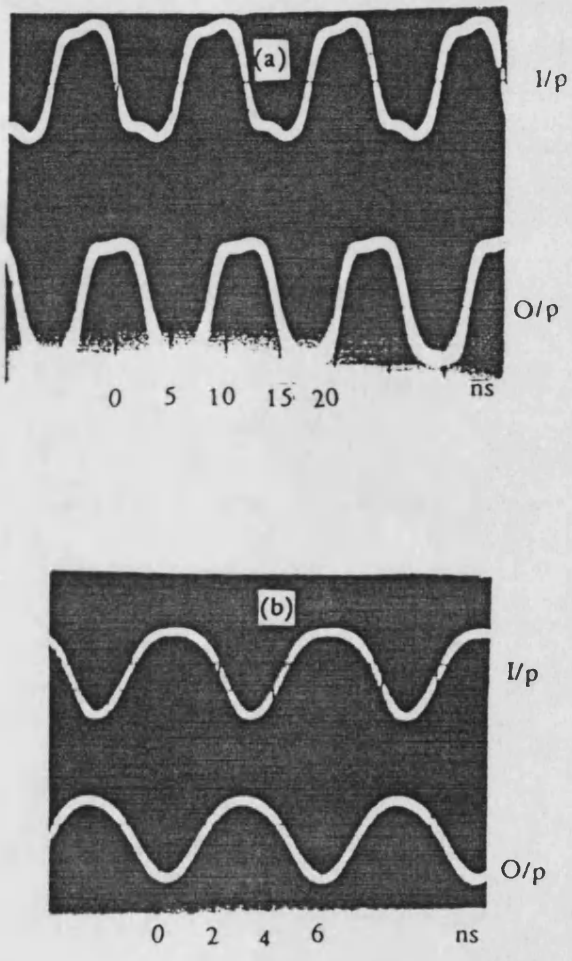

Figure 6.7 Input and output of LD drive circuit of Figure 6.6 using 20Ω load instead of LD at different frequencies

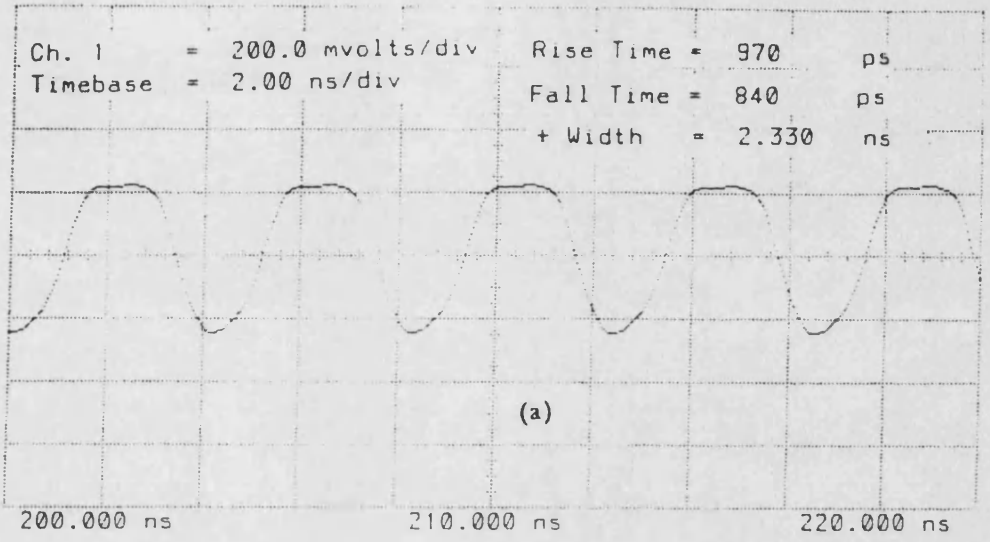

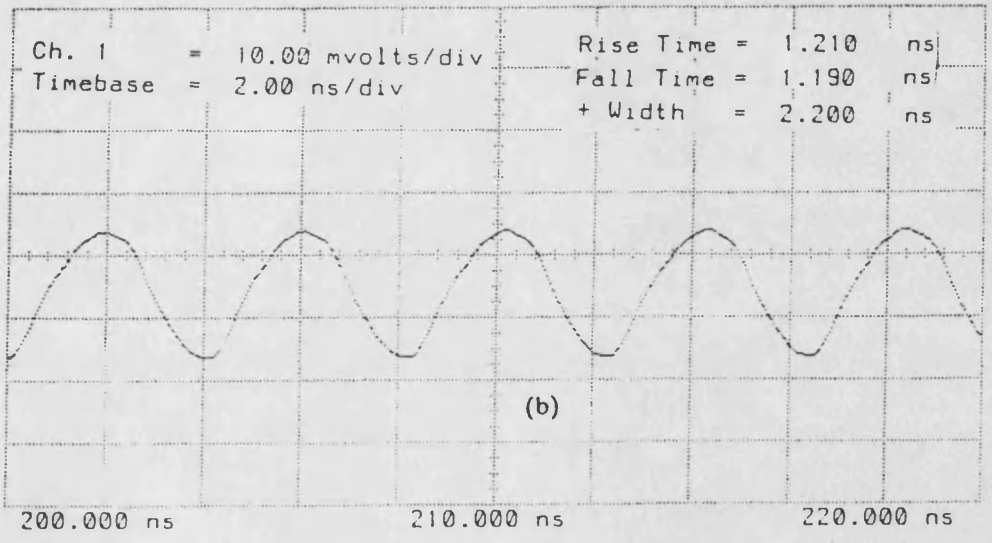

Figure 6.8 Modulating input to the LD drive circuit of Figure 6.6 and the corresponding optical output using LD HL8311E and PIN photodiode

a) Input
b) Optical output

$$\eta_2 K_L K_a G_b \gg 1 \qquad 6.6$$

and $$V_{br} G_b \gg I_{th} \qquad 6.8$$

To satisfy these conditions one has to consider the values of $K_L L_{av}$, $K_L \eta_2$ obtained from the (L.I.) characteristics of the laser diode HL8311E using the PIN MFOD1100 which will be used to achieve this control strategy.

$$K_L L_{av} = 12mV \quad , \quad \eta_2 K_L = 2V/A, \quad I_{th} \simeq 50mA$$

From 6.6:

$$K_a G_b \gg \frac{1}{\eta_2 K_L}$$

therefore:

$$K_a G_b \gg \frac{1}{2}$$

Also from equations 6.8 and 6.34:

$$K_L L_{av} K_a G_b \gg I_{th}$$

$$K_a G_b \gg I_{th}/K_L L_{av}$$

that is:

$$K_a G_b >> \frac{50}{12}$$

so $K_a G_b >> 4$

Choosing $K_a G_b = 100$ will achieve both conditions so by choosing $G_b = {}^1/_3 A/V$ then $K_a = 300$. From equation 6.34:

$$V_{br} = K_L L_{av} K_a$$
$$= 0.012 \times 300 = 3.6V$$

In this case the loop gain $\eta_2 K_L K_a G_b = 200$ which is >> 1 and also:

$$\frac{V_{br} G_b}{I_{th}} = \frac{1.2}{0.05} = 24$$

which is >> 1.

Finally, the requirements for the maximum optical power control loop as illustrated in equation 6.35 is:

$$L_{max} = \frac{V_{mr}}{K_m K_L} \qquad 6.35$$

and $\eta_2 K_L K_m G_m >> 1$

so by taking $\eta_2 K_L K_m G_m = 75$ which is >> 1 and choosing $G_m = 0.2$ A/V then:

$$K_m = \frac{75}{0.2 \times 2} = 187.5$$

From equation 6.35 and from the LI characteristics of the LD where $K_L L_{max}$ = 25mv, then $V_{mr} = 0.025 \times 187.5 = 4.687$ volts.

Practically the values of K_a and K_m will be chosen according to the gain of available components, so if their values have to be changed slightly then one has to change the values of the reference voltages V_{br} and v_{mr} respectively, in order to maintain the average and maximum values of light outputs at the specified levels required.

6.4.3 Sampled nature of the control loops

When operating under packet conditions, it is planned to carry out the measurements of L_{max} and L_{av} during the packet, and then retain the control values for use in the next packet. The control loops are therefore sampled.

However, the controlled parameters are functions of temperature and age of the device, and therefore change very slowly. Under steady operating conditions the environment is not expected to change significantly between packets, and so the control will work just as if the system was continuous. When the system is starting up, temperature will be changing steadily and since the loop gains are large, some transient conditions will be expected.

Sampled-data control loops can become unstable, particularly when the loop gain is large. However, including a simple low pass filter in the loop can prevent instability as is shown in Appendix V. Such solution imposes a limit on the maximum time duration between successive packets to be 200μs in this application.

6.5 Description of the Average Optical Power Control Loop

If the optical output of an LD operated in burst mode is received by a PIN photodiode, the output of the photodiode will be as in Figure 6.9. The figure illustrates that the LD is driven by a current pulse of width equal to the packet duration, and of amplitude $I > I_{th}$ which is at the midpoint of modulation pulses of amplitude $2I_m$, so the net drive current of the LD is $I \pm I_m$.

Figure 6.10 shows a block diagram for the average power control loop.

The control strategy for the average optical power during the packet duration, is based on measuring the average value of the received packet, through low pass filtering, amplifying and integrating the output of the monitor photodiode.

Referring to Figure 6.2a, for a packet duration T sec:

$$V_b' \alpha \frac{1}{T} \int_0^T V_0(t)\, dt \qquad 6.36$$

The output of the low pass filter (LPF) will be a pulse whose amplitude represents the average value of the light output during the packet duration. There are ripples on the top of this pulse; the amplitude of these ripples depending on the order of the filter and on the data bit rate. Therefore the output of the amplifier following the LPF will be integrated using an operational integrator, the output of the integrator is a ramp whose maximum amplitude is proportional to the average value required. This maximum amplitude corresponds to the instant of time at the end of the packet. To avoid the effect of integrator drift on the measured average value, a peak to peak detector is used to hold the maximum

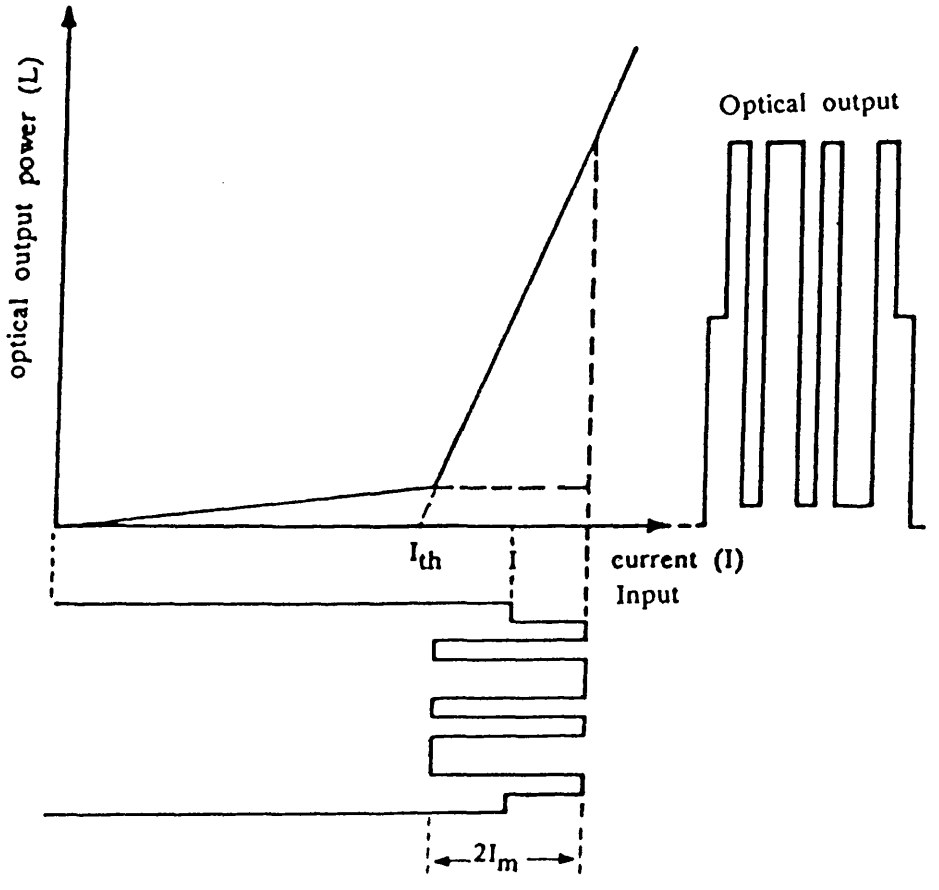

Figure 6.9 Illustration of the modulated optical output for LD operating in a burst mode

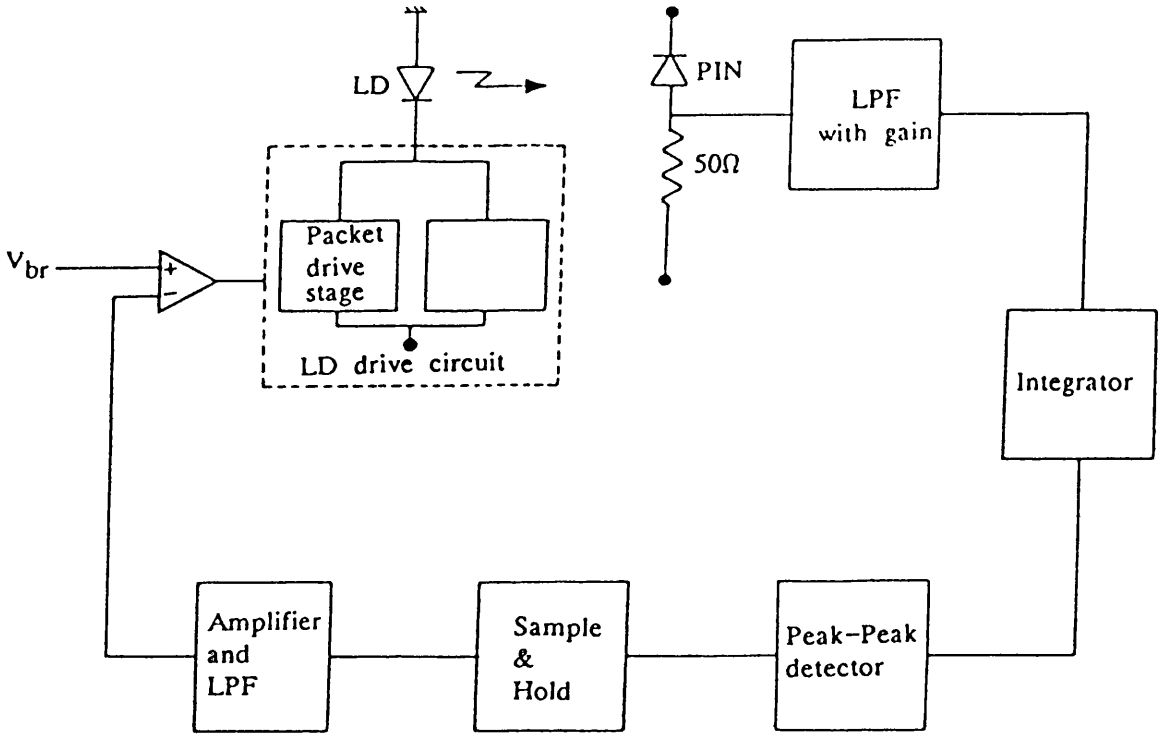

Figure 6.10 Block diagram of average optical power control loop for an LD operating in a burst mode

amplitude of the ramp, then the output of the peak to peak detector is sampled and held to be compared with a reference V_{br}. Using the differential amplifier A_9, the output of the amplifier will drive the transistor Q_3 which will adjust the value of the driving current of the laser for the next packet.

The sample and hold has been used to avoid the effect of delay introduced by the different components of the loop, hence using the hold value to adjust the drive current for the next packet. The capacitors in integrator and peak to peak detector need to be reset after the sample is held by the sample and hold. The output of the LPF needs to be inverted before integration, the reason for that will be discussed when dealing with resetting the peak to peak detector capacitors.

6.5.1 Low pass filter

If data of average duty cycle 50% is sent in a packet of duration 10μsec by the laser diode, and the minimum pulse width of the data pulses is 4nsec, a low pass filter is required to allow signals of frequency 0.1MHz and its harmonics to pass and at the same time attenuate the modulation frequencies of 250MHz and its harmonics. Alternatively, if we have a maximum sequence of 10 ones in the data, that is corresponding to pulse width of 40nsec, then a frequency of 25MHz and its harmonics should be attenuated.

The corner frequency of the filter is chosen to be 0.5MHz to allow the harmonics of 0.1MHz to pass. If the detected modulation pulse amplitude is 26mv and it is required to be attenuated by a factor α in order to achieve a percentage error of 10% relative to the packet pulse amplitude which $\simeq$ 12mv, then for a first order low pass filter which gives an attenuation of 20dB/decade:

$$\frac{26 \times \alpha}{12} = .1$$

$$\alpha = 0.046 = -26.7\text{dB}$$

A first order low pass active filter with gain = −2 and corner frequency 0.5MHz as shown in Figure 6.11 will provide the required attenuation of modulation pulse and at the same time invert and amplify the packet bias pulse.

The advantage of using an active filter over a passive RC network is that the output voltage of the filter is available at the low impedance output terminal of the operational amplifier so it is not subject to any loading error; also the circuit can be given gain if required.

The corner frequency of the filter:

$$f_c = \frac{1}{2\pi R_p C_L}, \quad R_p = R' // R_L \qquad 6.37$$

$$f_c = 0.5\text{MHz}, \quad R' = 10\text{K}\Omega, \quad R_L = 20\text{K}\Omega, \quad R_3 = 6.6\text{K}\Omega$$

$$C_L = \frac{1}{6.28 \times 6.6 \times 10^3 \times 0.5 \times 10^6} = 48\text{PF}$$

6.5.2 Operational integrator

The basic circuit of the operational integrator is shown in Figure 6.12. It performs integration by using an operational amplifier to force the same current through the resistor (R) and the capacitor (C_F). Considering that the operational

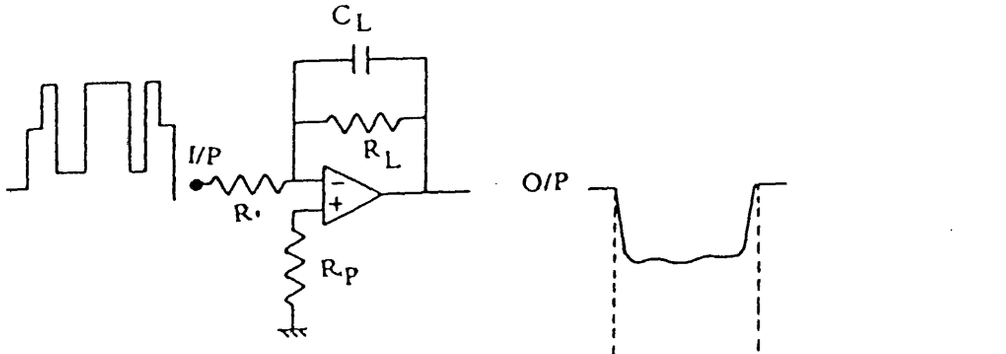

Figure 6.11 low pass filter with gain

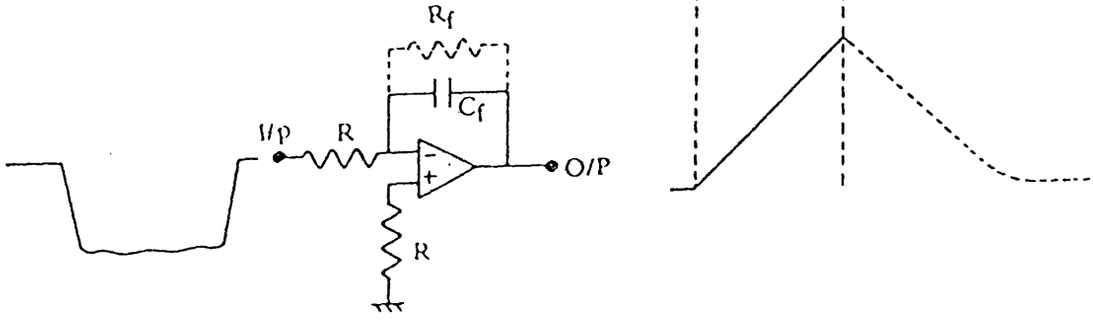

Figure 6.12 Operational integrator

amplifier has infinite gain and infinite input resistance, then the voltage across the feedback capacitor is related to the capacitor current (i_F) by:

$$V_c = -\frac{1}{C_F} \int i_F \, dt \qquad 6.38$$

but the circuit causes the feedback current i_F to equal the input current (i_i), and the output voltage of the integrator is:

$$V_o = V_c = -\frac{1}{C_F} \int \frac{V_i}{R} \, dt$$

$$V_o = -\frac{1}{RC_F} \int V_i \, dt \qquad 6.39$$

From this equation it is seen that the output voltage is equal to the average value of the input voltage and that the output voltage of the ideal integrator is proportional to the integral of the input, i.e. it is proportional to the area under the input waveform.

6.5.2.1 Sources of errors in the operational integrator

The errors in the operational integrator arises from:

1. The operational amplifier input offset voltage and input offset current.

2. The finite open loop gain, finite input impedance and finite bandwidth of the operational amplifier.

3. The capacitor leakage current.

4. The temperature coefficients of capacitance and resistance.

5. The phase advance introduced by the feedback with an ultimate maximum of $+90^{0}$.

a) The operational amplifier input offset voltage and input offset current errors

The input offset voltage V_{io} and the input offset current I_{io} introduce errors to the output of the ideal integrator represented by equation (6.36). The integrator requires very careful offset adjustment otherwise it will integrate its own input offsets and the output will be:

$$V_0 = -\frac{1}{RC_F}\left[\int V_i dt \pm \int V_{io}\, dt\right] \pm \frac{1}{C_F}\int I_{io}\, dt \pm V_{io} \qquad 6.40$$

It is to be noted that the input offset voltage causes a small step voltage $\pm V_{io}$ and $\pm$ a ramp with gain $1/RC_f$, I_{io} causes a ramp of gain $1/C_f$ which can be reduced by increasing C_F while reducing R such that the value of the characteristic time constant RC_F remains constant at the required value. However, decreasing the value of R is limited by the input resistance of the amplifier and by leakage current through (C_F), so that R must be decreased in such a way that the leakage current through C_F is less than the bias current of the amplifier.

b) The finite gain, finite input impedance and finite bandwidth of the operational amplifier

In the ideal operational integrator circuit the gain of the operational amplifier

and the input resistance, were considered to be infinite but practically the operational amplifer has a finite input resistance R_i and finite gain. The effect of these factors on the output of the ideal integrator is analysed in Appendix VI. This analysis shows that the output voltage of the integrator as a function of time is for unity constant input given, for small values of time, by:

$$V_0(t) = \frac{1}{RC_F}\left[t - \frac{1}{\omega_T}\right] \qquad 6.41$$

where ω_T is the unity gain bandwidth of the operational amplifier. This equation indicates that $V_0(t)$ runs parallel to the ideal response t/RC_f but shifted in time by $1/\omega_T$ as illustrated in Figure 6.13a. So the output lags by an amount that depends on the unity gain bandwidth of the operational amplifier.

Also at large values of time,

$$V_0(t) = \left[\frac{t}{RC} - \frac{t^2}{2A_0R_pCR_0C}\right] \qquad 6.42$$

where $R_p = R//R_i$.

In this case the second term represents the error due to finite gain and finite input impedance of the amplifier and it is proportional with t^2 as shown in Figure 6.13b).

6.5.2.2 Minimisation of the offset errors in the integrator

The offset of the integrator should be adjusted such that the output of the

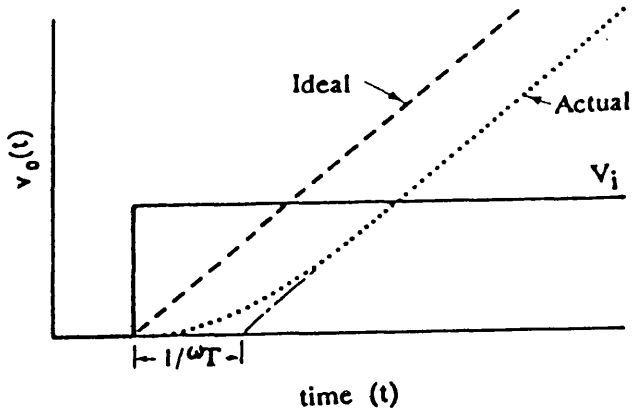

(a)

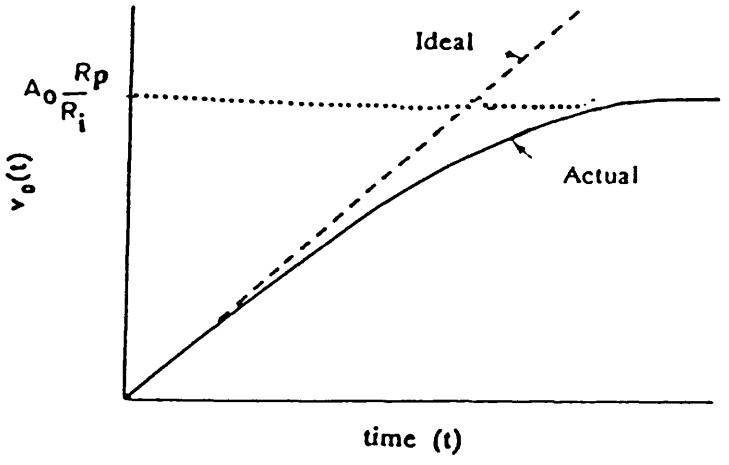

(b)

Figure 6.13 Integrator errors:

a) At high frequency due to finite gain band width of the operational amplifier
b) At low frequency due to finite gain and finite input impedance of amplifier

integrator shows no immediate tendency to creep up or down. It is impossible, in practice, to avoid some slight offset, so the practical circuit will exhibit some drift of the output voltage over a period of time (minutes).

The effect of the input offsets can be reduced by adding a dc "gain stop" resistor R_F in parallel with C_F, as illustrated in Figure 6.12, so reducing the integrator dc gain from the full open loop value to the ratio of this shunt resistor to R. The ratio R_f/R should be as high as the dc considerations allow.

The value of R_FC_F should be $\geq$ 10 RC_F, i.e.

$$R_F \geq 10R$$

The presence of R_f in parallel with C_f allows the discharging of the capacitor, hence resetting the integrator. The optimised size for reset resistor R_F if 0.1% accuracy in starting point is required is given by:

$$R_F = \frac{T_s}{7C_F} \qquad 6.43$$

where T_s is the time required to reset the integrator output to zero.

Under these conditions, the frequency characteristics of the integrator are shown in Figure 6.14. It illustrates that, for frequencies:

$$f > \frac{1}{2\pi R_F C_F}$$

the response approximates that of the ideal integrator. At a frequency a decade

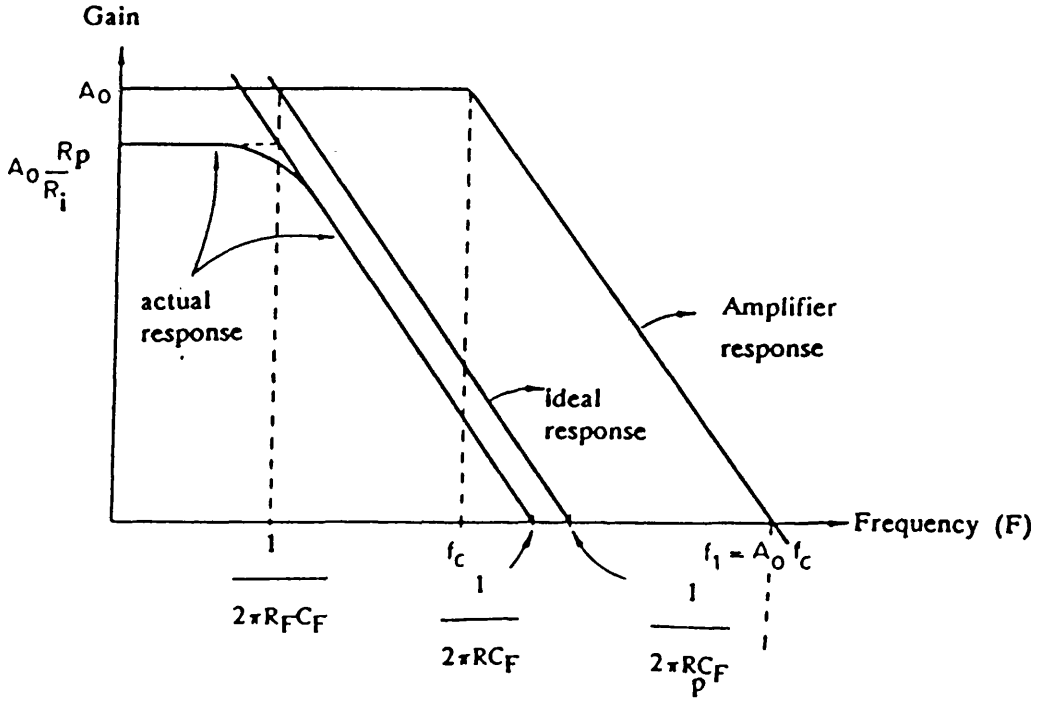

Figure 6.14 Frequency characteristics of integrator

away from:

$$\frac{1}{2\pi R_F C_F}$$

the magnitude error is only 0.5%. The presence of R_F prevents the integrator drift due to amplifier bias current and offset voltage, from causing the amplifier to drift into saturation.

For faster reset of the integrator, the feedback capacitor can be discharged by a low leakage switch formed with two MOSFETs.

6.5.2.3 Design considerations of the integrator

It is required to design an integrator that integrates pulses of width 10μsec. The values of R, C_F and R_F should be chosen such that the performance of the integrator is optimised. The value of R should be chosen on the basis of the value of the input bias current of the amplifier I_B, the voltage drop and to produce a realistic value of C_F.

The voltage drop $I_B R$ should be less than 0.1 of the amplitude of the signal to be integrated. The value of R_F should be $\geq$ 10R. Then from the frequency characteristics of the integrator, the value of:

$$f > \frac{1}{2\pi C_F R_F}$$

$$\text{i.e. } f > \frac{1}{20\pi C_F R}$$

so taking R = 2.7K, then:

$$C_F > \frac{1}{20 \times 3.14 \times 0.1 \times 10^6 \times 2.710^3}$$

$$C_F > 159PF$$

The value of R_F is chosen 100KΩ and C_f = 218PF. This will lead to a time of 152.6μsec to reset the output of the integrator to an accuracy of 0.1% in the starting point.

6.5.3 Peak to peak detector

Although the offset drift of the integrator has been reduced, it is not zero, and will be removed by measuring the peak-to-peak output swing of the integrator. The simple peak detector shown in Figure 6.15a suffers an inaccuracy due to diode voltage drop. The operational amplifier can be used to eliminate this effect as shown in Figure 6.15b.

As long as the input voltage is increasing the diode D_1 is conducting, amplifier A_4 is in the voltage follower mode and the output follow the input. The diode D_1 is always blocking current from flowing out of the capacitor, hence the output voltage is always equal to the maximum value achieved by the input voltage. The diode D_1 must be a low leakage device to maintain the voltage across it during the hold period. A diode D_2 is connected as in the figure to clamp the output of the amplifier A_4 for negative transitions and prevent saturation.

A buffer of high input impedance, that is an FET operational amplifier (A_5)

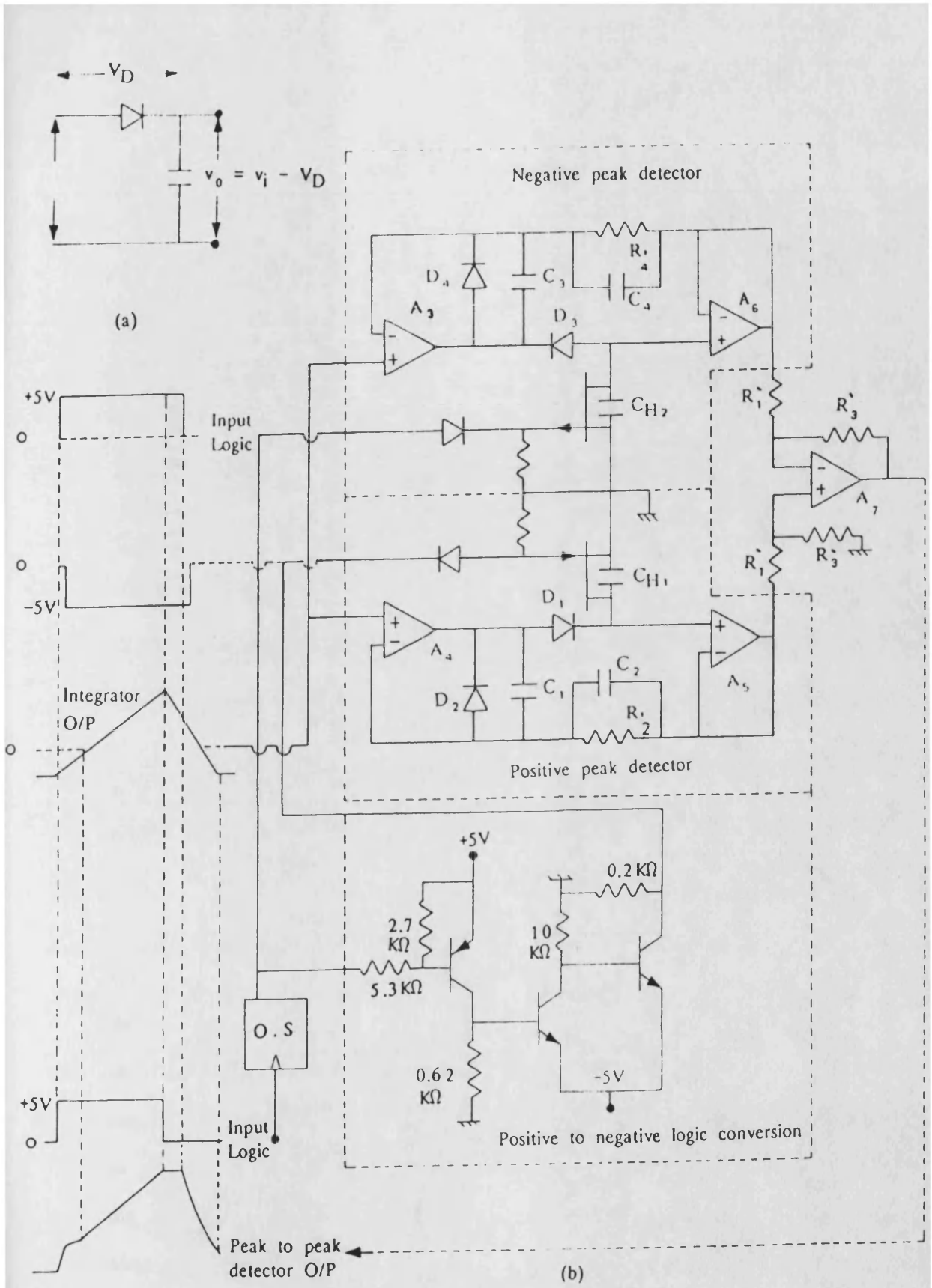

Figure 6.15 Peak detector

a) Simple peak detector
b) Peak to peak detector with gain and its input, output and resetting switches control signal waveforms

in the voltage follower mode is required to read the voltage hold by the capacitor. Direct connection of the voltage follower to the hold capacitor adds another set of offset voltage, input-bias current and gain errors to the peak detector. This is avoided by connecting the follower within the feedback loop so its offset and gain errors are nullified by the feedback action. The buffer A_5 should be significantly faster than the input amplifier A_4. If A_4 were to charge the capacitor C_{H_1} faster than the buffer A_5 could follow, a feedback delay would be introduced that would cause a capacitor C_{H_1} to overcharge; this can be avoided by selecting phase compensation for A_4 that eliminates peak detector overshoot. Also the compensating network C_2 and R_2' is required to improve stability.

For negative peak detector the diodes D_1 and D_2 should be reversed.

A peak to peak detector is obtained by connecting both positive and negative peak detectors to a difference amplifier as illustrated in Figure 6.15, hence gain can be provided.

To reset the peak to peak detector after sampling its output, an FET switch can be used by connecting the drain and source across the capacitor. The source should be connected to ground while the drain is connected to the other terminal of the capacitor. For the positive peak detector the drain should be positive with respect to the source so an N-channel JFET can be used; a negative pulse applied to its gate will switch the transistor off and its absence turn it on so discharging the capacitor. The duration of this pulse should be longer than the packet pulse width by a time that is sufficient for the sample and hold to sample the output of the peak to peak detector and hold it, which is 2μsec in this case. The discharging time can be adjusted by connecting a suitable resistor between the source and drain, on the other hand the negative peak detector will be reset by a p-channel JFET that is switched off and on by applying a positive pulse to its

gate. This positive 5 volt pulse, is obtained by applying a pulse of width equal to the packet width, to the input of monostable multivibrator of the type SN74LS123 and choosing the value of resistance and capacitance connected to it such that it generates the required pulse width, as illustrated in Figure 6.15b.

The negative pulse used for the N-channel transistor is obtained by applying the output of the previous monostable to a circuit which changes the positive logic (0, + 5V) to a negative logic (0, -5V) as shown in Figure 6.15b.

The circuit consists of PNP and NPN transistors, and it introduces some delay on the negative pulse; this is the reason for inverting the input to the integrator such that its positive output starts after a time greater than the delay introduced to the negative logic pulse which used to control the gate of the N-channel transistor as indicated in Figure 6.15b.

All the operational amplifiers are of the type LF353N, all the diodes are of the type HP2835712. The values of the capacitances and resistances used were:

$C_1 = 3.3PF$, $C_2 = 33PF$, $C_3 = 1.8PF$ and $C_4 = 39PF$

$R_1' = 2.7k\Omega$, $R_2' = R_4'' = 20k\Omega$ and $R_3' = 12k\Omega$

The gain given to the peak to peak detector is:

$$\frac{R_3'}{R_1'} = \frac{12K}{2.7K} = 4.44$$

6.5.4 Sample and hold considerations

The circuit of sample and hold is similar to the circuit of peak detector except that the diode D_1 is replaced by an FET switch such that the input can be sampled and held at any instant controlled by the switch. In this case the sample and hold logic control pulse required to sample the output of the peak to peak detector when its output is maximum, then hold it before resetting the peak to peak detector.

The circuit used for the sample and hold of the type LF398 is shown in Figure 6.16; also the figure shows the input and the output together with the control logic pulse. The output of the sample and hold has a glitch during the sampling time which needs to be low pass filtered before the next amplifier stage.

6.6 Description of the Maximum Optical Power Control Loop

The maximum optical power control loop requirements presented in section 6.4, are based on measuring the maximum amplitude of the modulated optical output, this maximum value will be measured through high pass filtering of the optical output of the photodetector which allows the modulation pulse to pass without attenuation and attenuates the packet bias pulse which has a lower frequency content. The output of the high pass filter will include the components of frequency corresponding to the edges of the low frequency packet pulse besides the modulated optical output. The amplitude of the modulation lower frequency pulses might change slightly, so the strategy used here is to measure the average of the maximum amplitudes during the duration of the packet. This has been done using a leaky peak detector. The output of the HPF is amplified using two stages of wide band amplification (0-2GHz) of the type Mar3 and Mar8, to bring the level of signal up to 2volts so that is can be peak detected by a passive peak

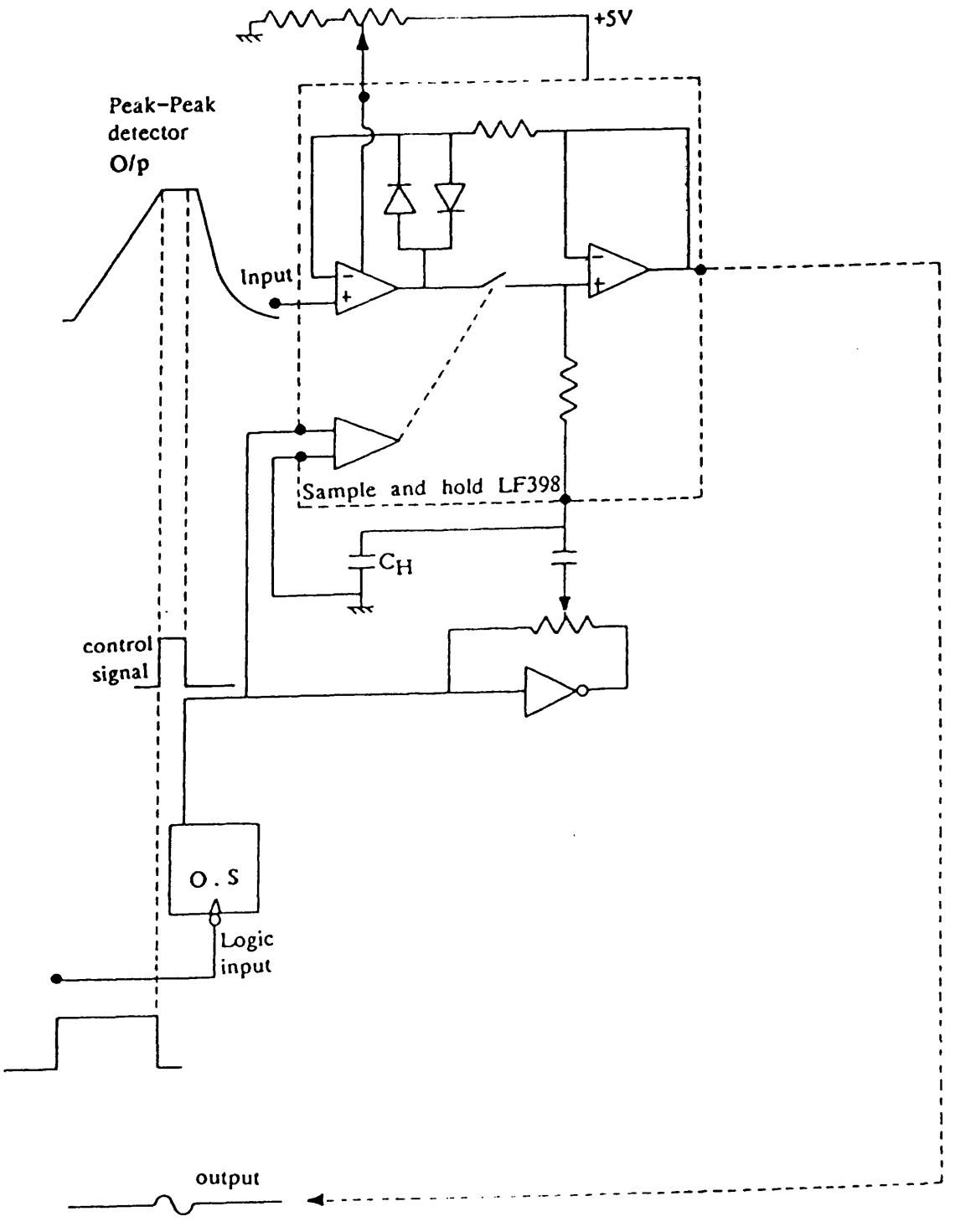

Figure 6.16 Sample and hold LF398 and its circuit. Input, output and control signal waveforms.

detector. The output of this leaky peak detector is proportional to the average maximum amplitude of the modulated optical output. Then the output of the peak detector is sampled during the packet duration and compared with the reference voltage V_{mr} using a difference amplifier whose output adjusts the current in transistor Q_6 to control the modulation current of the next packet.

6.6.1 High pass filter (HPF)

To attenuate the packet pulse of width 10μsec and amplitude 12mv while allowing the modulation pulses of minimum frequency to pass, a high pass filter is required. The attenuation of the filter at the low frequency to achieve an error of 0.1% when compared with the modulation of 26mv is α, and:

$$\alpha \cdot \frac{12}{26} = 0.001$$

$$\alpha = 2.1 \times 10^{-3} = -53.28\text{dB}$$

A third order high pass passive Bessel filter gives an attenuation, 60dB/decade, so it will achieve the required attenuation for packet pulse and allow the modulation pulse to pass.

In order to design this high pass filter, a third order low pass Bessel filter shown in Figure 6.17, has been designed and then transformed to a third order high pass filter using Zeverev's terminology[6.21].

The values of capacitances C_1, C_3 and inductances L_2 are given by:

$$C_1 = \frac{1}{L_1' R_L . 2\pi F_c} \quad , \quad C_3 = \frac{1}{L_3' R_L . 2\pi F_L} \quad , \quad L_2 = \frac{R_L}{C_2' . 2\pi F_c}$$

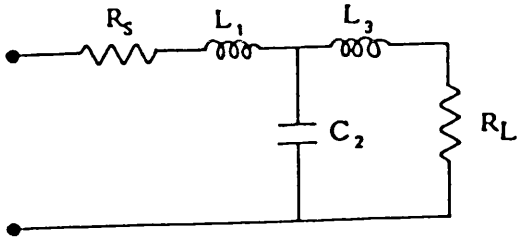

(a)

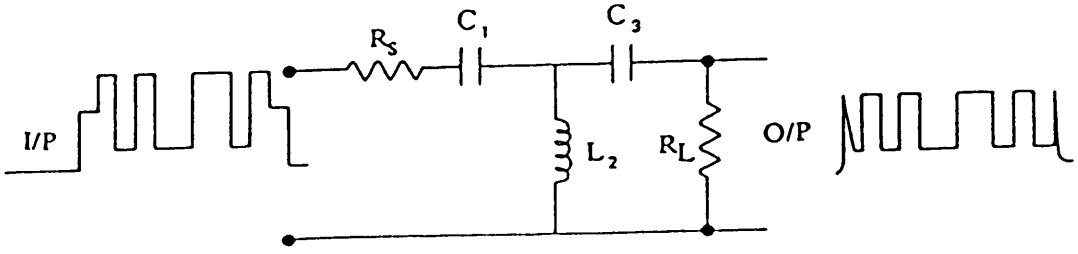

(b)

Figure 6.17 a) Third order low pass Bessel filter
b) Third order high pass Bessel filter

where F_c is the cut off frequency of the filter, R_L is the load resistance and R_s is the source resistance.

$$L_1' = 0.3374 \quad , \quad L_3' = 2.2034 \quad , \quad C_2' = 0.9705$$

then for $F_c = 1.74MH$ and $R_s = R_L = 50\Omega$.

$$L_2 = 4.7\mu H \quad , \quad C_1 = 5.42nF \quad \text{and} \quad C_2 = 0.83nF$$

Using these values will achieve the required response of the filter and the input and output will be as in Figure 6.17.

6.6.2 Leaky peak detector for average maximum optical amplitude detection

The output of the high pass filter is amplified by two wide band amplifiers Mar3 of gain 13dB and bandwidth 0-2GHz, and Mar8 of gain 33dB and bandwidth 0-2GHz.

The average maximum amplitude of the output of the amplifier is detected by a leaky peak detector as shown in Figure 6.18b which consists of fast diode of the type HP2835712 and capacitor C = 680pF, a resistor R = 5.1KΩ is connected in parallel with the capacitor and a resistor R_1 = 100Ω in series with it.

The charging and discharging time of the capacitor can be controlled by the values chosen for R, R_1 and C. The discharging time constant was adjusted to be 3.5μsec and the charging time constant ≃ 68nsec. Hence the output of the peak detector will climb up to the average of the maximum value in a finite time of about 400ns, so the edges of the packet pulse that pass through the high pass filter and are amplified will not affect the average maximum value measured. The

output of the peak detector is buffered by a voltage follower and then amplified using FET operational amplifiers of the type LF353N, Figure 6.18a. The layout of the connection of the circuit, HPF, Mar3, Mar8, the leaky peak detector, the voltage follower and amplifier, has been implemented on a double sided PCB.

Figure 6.18b shows the circuit diagram and the expected output of different components.

6.6.3 Sample and hold considerations

The output of the circuit in Figure 6.18b will be sampled during the duration of the packet pulse then compared with the reference voltage V_{mr}, so any change in the output of the sample and hold during the sampling time will affect the LD driving current, this is why it is important that the output of the sample and hold in this loop has to be low pass filtered to remove any glitch in its output during the sampling mode.

6.7 Testing LD Power Control Circuit and Analysis of its Results

The whole power control circuit is shown in Figure 6.19 while its timing control signal circuit is shown in Figure 6.20.

The power control circuit has been implemented in three separate boxes, one for the logic timing and switching signals and sample and hold circuits, the second for the wide band amplifiers A'_3, A'_4 and the leaky peak detector with gain that follows them. The third is for the rest of the components of the power control circuit components. Figure 6.21 shows a photograph for the whole system which included LD drive circuit, power control circuits and temperature control circuit.

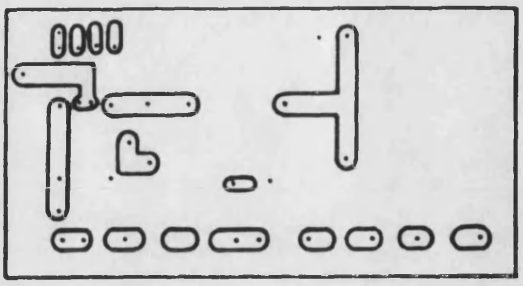

(a)

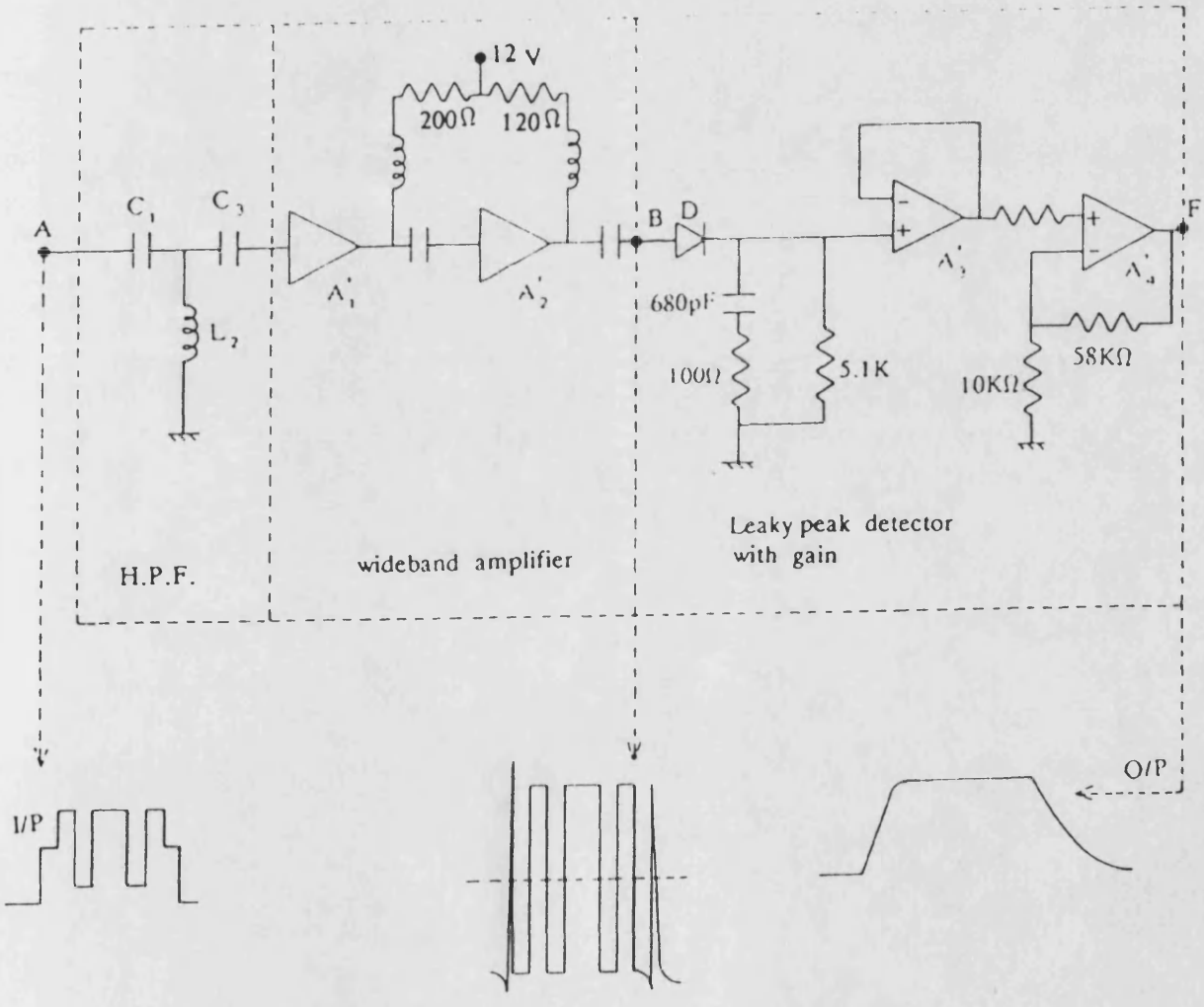

(b)

Figure 6.18 Leaky peak detector with gain

a) Layout of connection between components
b) Circuit diagram, input and output waveforms

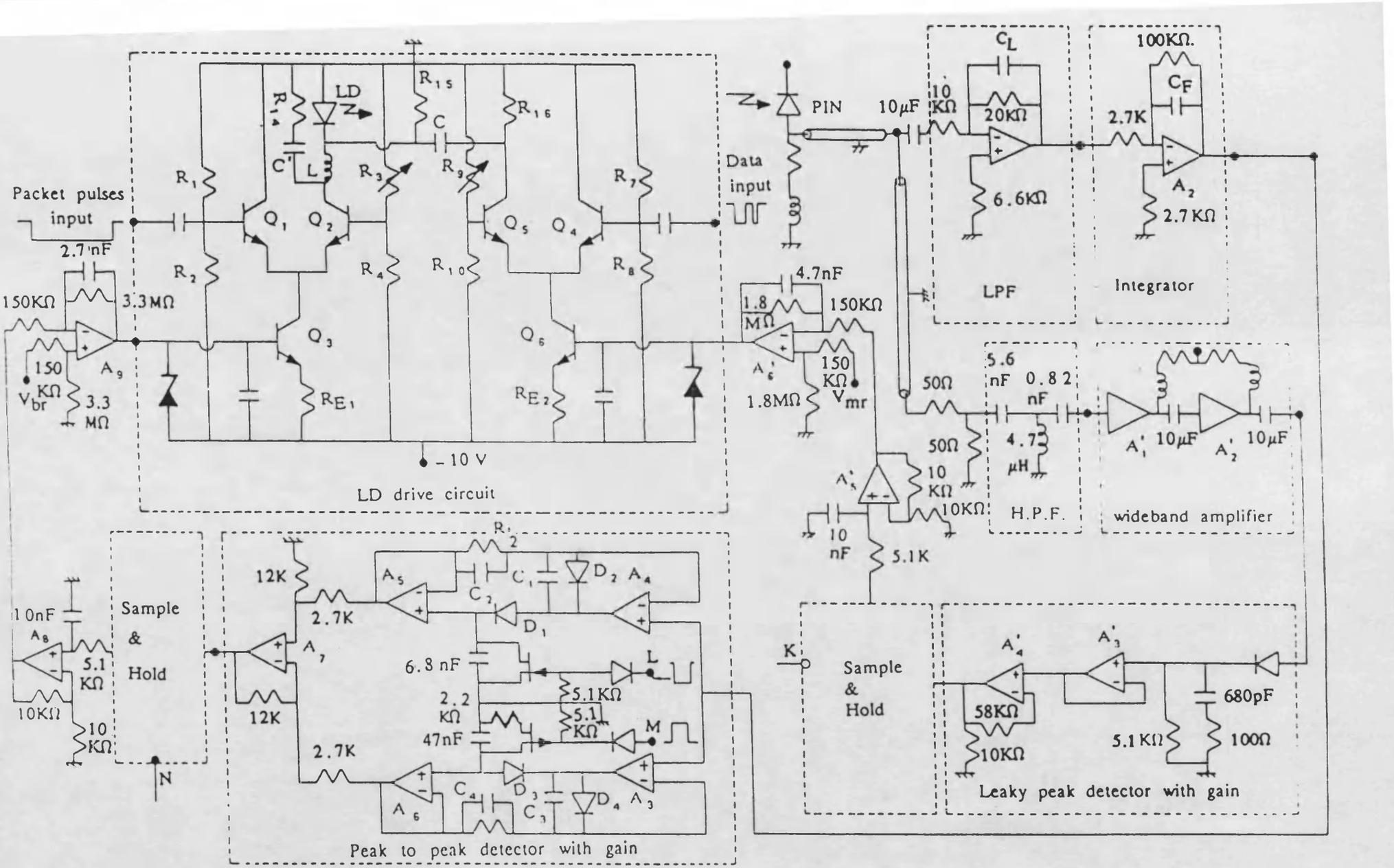

Figure 6.19 LD power control circuit for packet transmission

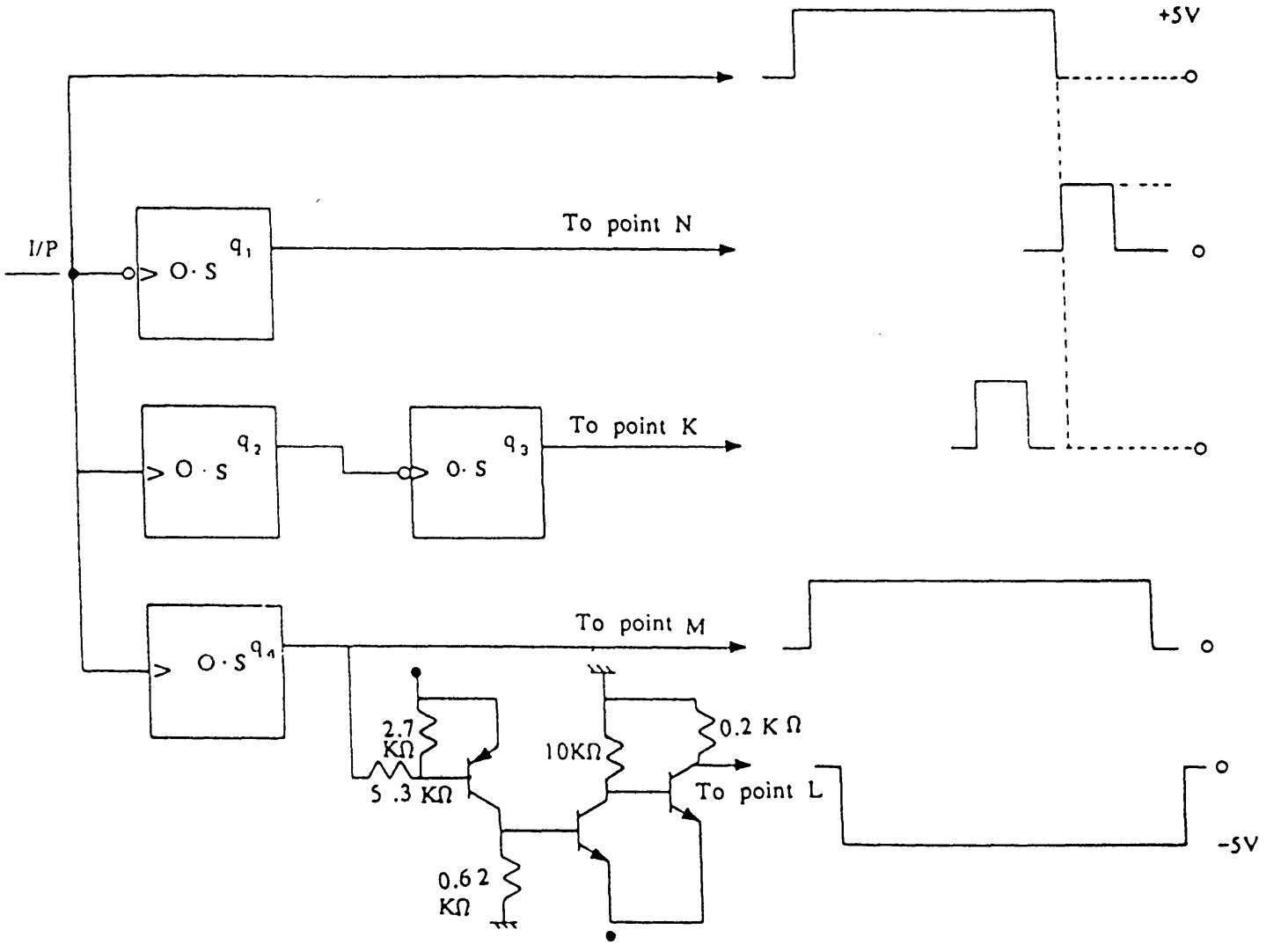

Figure 6.20 Timing circuit and timing control signals to points N, K, M and L in Figure 6.19

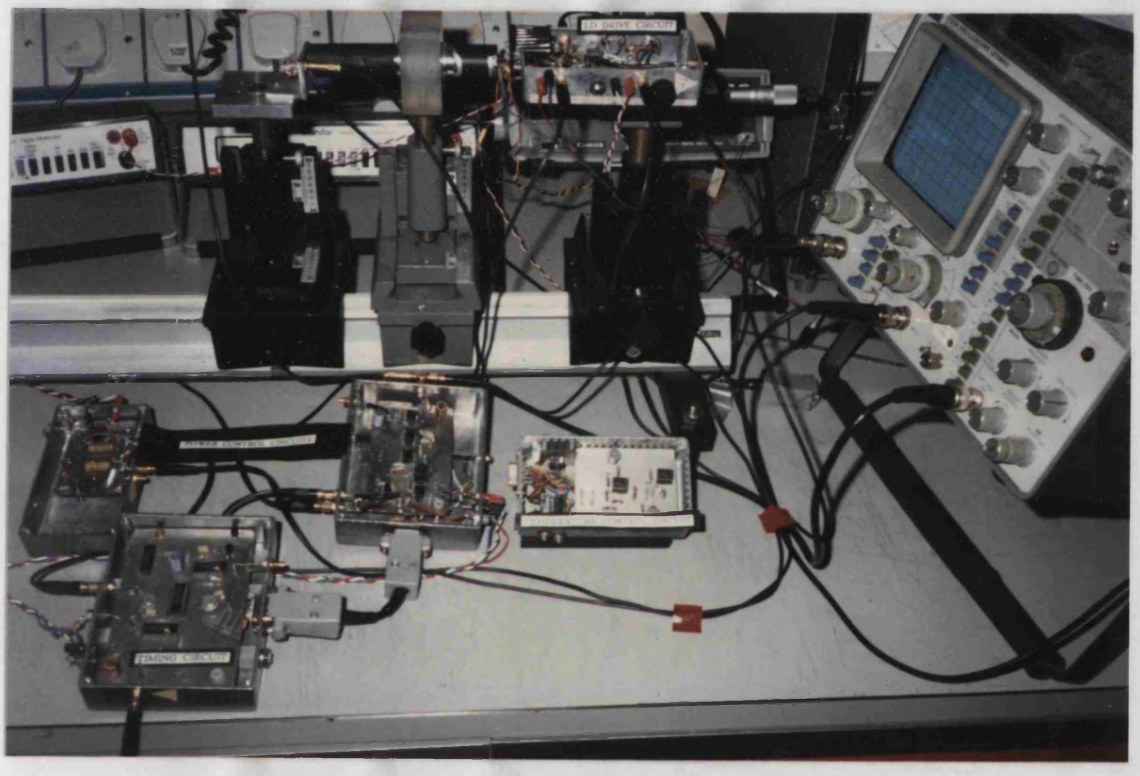

Figure 6.21 Photograph for the whole system used includeing LD drive circuit, power control circuits and temperature control circuit

To test the LD power control circuit, one has to test both of the average and maximum optical power control loops separately when the loops are open. In this case the following steps will be taken:

1. The current in the tail transistor Q_3 and Q_6 of the LD drive circuit will be adjusted by potentiometer arrangement.

2. The output of each component in the loops will be examined and the loop gain will be adjusted to satisfy the requirements for control to be exerted.

3. The values of the reference voltages V_{br} and V_{mr} should be adjusted to give the required values of average and maximum optical power.

4. Zener diodes of breakdown voltages 6.2V and 3V have to be connected between the bases of the transistor Q_3 and Q_6 and the negative power supply line, hence protecting the LD through limiting the current in the two stages of the drive circuit.

5. The potential arrangements which control the current in transistors Q_3 and Q_6 are disconnected and the bases of the two transistors are connected to the average and maximum power control loop respectively.

6. Finally, the control circuit performance as a whole will be examined.

6.7.1 Testing the average optical power control loop and analysing its results

The average power control loop has been examined, first with the loop open. The laser diode HL8311E has been driven by the drive circuit previously described

in section 6.4.1 using a current pulse above threshold of width 10μsec and period 200μsec, which corresponds to the packet pulse. The LD is modulated with modulation current pulse such that the packet pulse current is at the midpoint of modulation. The light from the LD has been received by a PIN photodiode of the type MF0D1100 reversed biased with 5V, and a resistor of 47Ω and a coil 0.22μH are connected in series with the photodiode. The reason for connecting the coil is to increase the speed of response of the photodetector.

The output of the monitor photodetector is low pass filtered, inverted, amplified and then integrated.

The output of the integrator is measured by a peak to peak detector whose output is sampled after the end of the packet; the output of the sample and hold is low pass filtered and amplified, then compared with the reference voltage V_{br}.

The packet pulse driving current has been varied and the output of the loop components has been measured. Figure 6.22 shows the output of the different components of this loop together with the timing pulses which control the sample and hold and reset the capacitors of the peak to peak detector. Figure 6.23 shows the variation of the output of these components with the input to this loop. The input to the loop has been varied by changing the packet pulse driving current of the LD only and without modulation.

Figure 6.23 shows that there is proportionality between the outputs of the different components and the input to the loop, hence the relations between them were straight lines. From the slopes of these lines the gain of each component in the loop can be determined. From the slope of the line which represents the variation of the output of the amplifier (A_s) that follows the sample and hold, and its input one can determine K_a. The value of K_a can be readjusted at certain

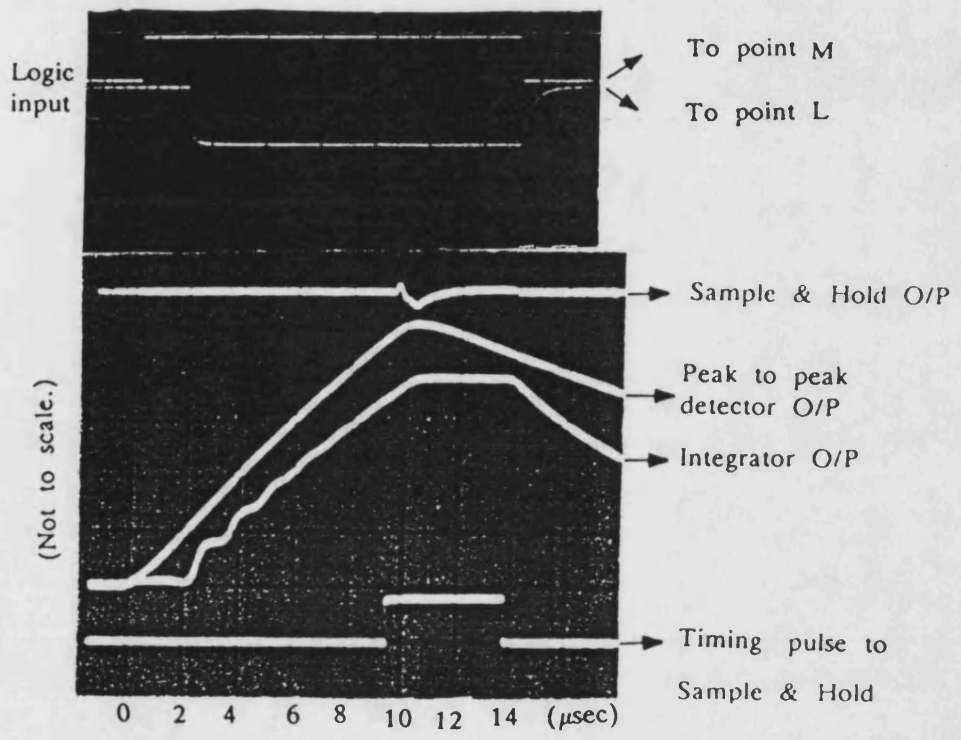

Figure 6.22 Timing pulses and the output of different components in the average power control loop as measured practically

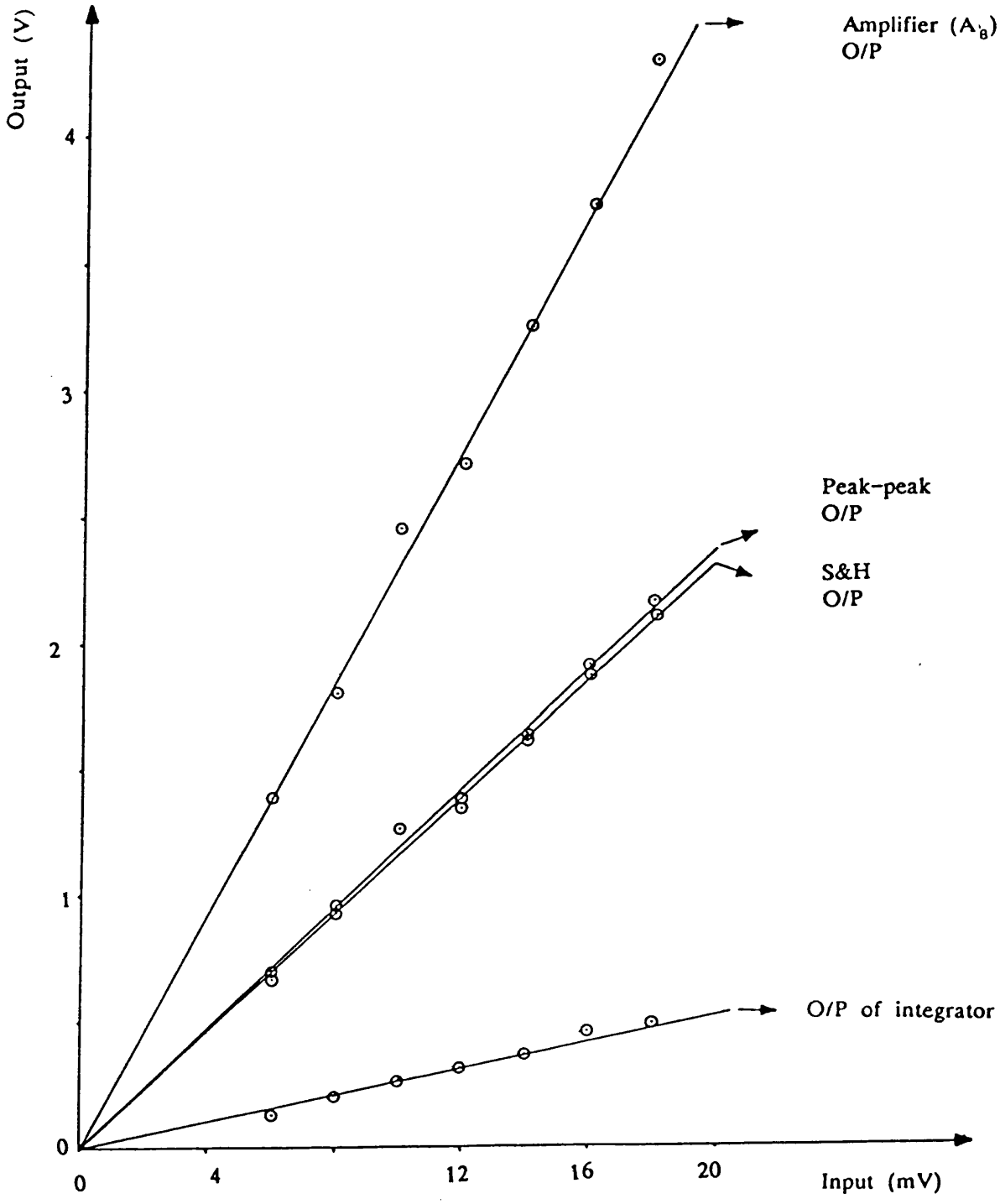

Figure 6.23 Relation between the output of different components in the average power control loop and its input

value by changing the gain of this amplifier or the gain of any other component in the loop. In order to minimise the error in sampling and the effect of the glitch that appears in the output of sample and hold, the gain of the components preceding the sample and hold have been increased to increase the level of signal to be sampled.

The effect of varying the reference voltage V_{br} on the output of driving amplifier A_9 at different values of input voltage to the loop, when it it open, has been examined, and the results are represented by the straight lines obtained in Figure 6.24. The slope of any of these lines gives the value of the gain of the driving amplifier A_9. Also this test has been done when the loop is open and its input is varied by changing the packet pulse driving current only and without modulation.

The effect of changing the packet pulse width on the integrator output and consequently on the output of the driving amplifier has been examined, and the results are shown in Figure 6.25. These results show that the loop is sensitive to change in packet width, which means that if the packet width needed to be changed then the reference voltage V_{br} has to be readjusted. This is because the parameter K_a is a function of packet width due to the effect of integrator.

Finally, the gain of the different components in the average power control loop, as measured from Figures 6.23 and 6.24 was as follows:

The gain of integrator = −26.3/2 = −13.15.

The gain of peak to peak detector = 4.5.

The gain of amplifier (A_8) which follow the sample and hold = 2.

The gain of the driving amplifier = 22.

The gain of the feedback network K_a = 231.5 = 47.3dB.

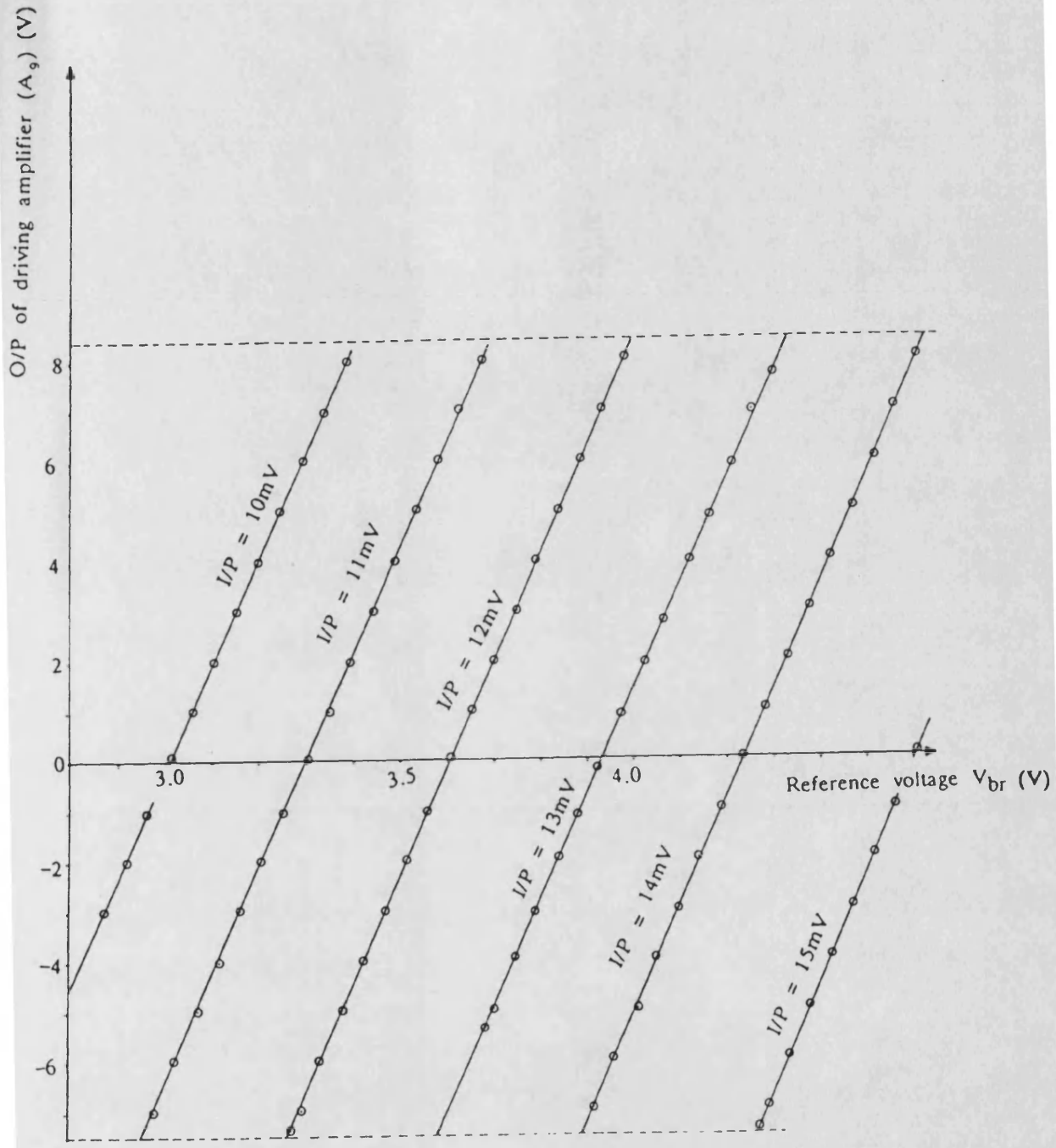

Figure 6.24 Relation between the reference voltage V_{br} and the output of driving amplifier A_9

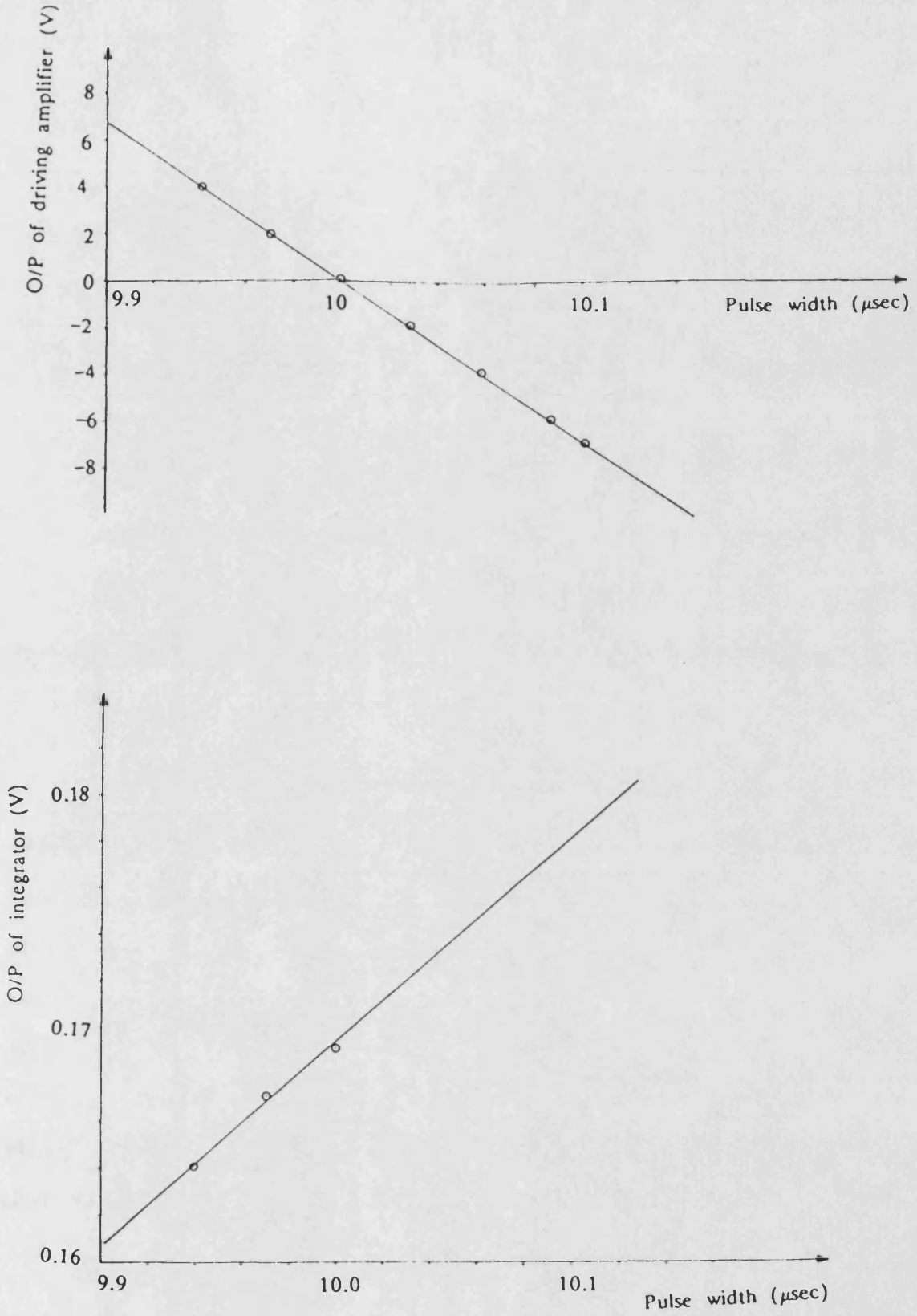

Figure 6.25 Relation between the packet pulse width, of constant amplitude, and the ouputs of integrator and the driving amplifier A_9

The conductance of the driving amplifier (A_9) is:

$$G_b = \frac{A}{R_E} = \frac{22}{65} = 0.33 \quad A/V$$

the loop gain = $\eta_2 K_L K_a G_b$ = 2 x 231.48 x 0.33 = 152.8 = 43.68dB

6.7.2 Testing the maximum optical power control loop and analysis of its results

To test the maximum optical power control loop, the output of the monitor photodiode is connected to the high impedance input of the average power control loop using a 50Ω cable, then the input of the average power control loop is connected through a 50Ω cable to the input of the high pass filter in the maximum power control loop. The end of this 50Ω cable has to be terminated with 50Ω resistors as illustrated in Figure 6.19, otherwise the output of the wide band amplifiers A_1', A_2' will be affected by the reflection which occurs due to the impedance mismatch. The loop has then been examined when it is open. The packet pulse current amplitude was 63mA, the LD operating temperature was 23 °C and the modulation rate was 100Mbit/s. Figure 6.26 shows the outputs of the different components in this loop together with the control signal to the sample and hold. The output of sample and hold shows a glitch during the sampling time which is during the duration of the packet, so it is important to eliminate this glitch by low pass filtering otherwise it will affect the control.

By changing the modulation pulses input amplitude and measuring the output of the different components in the loop one can draw a relationship between the output of different components and the input to the loop. Figure 6.27 illustrates the results obtained. It shows that there is a proportionality between the outputs and the input. The gains of the different components in this loop can be

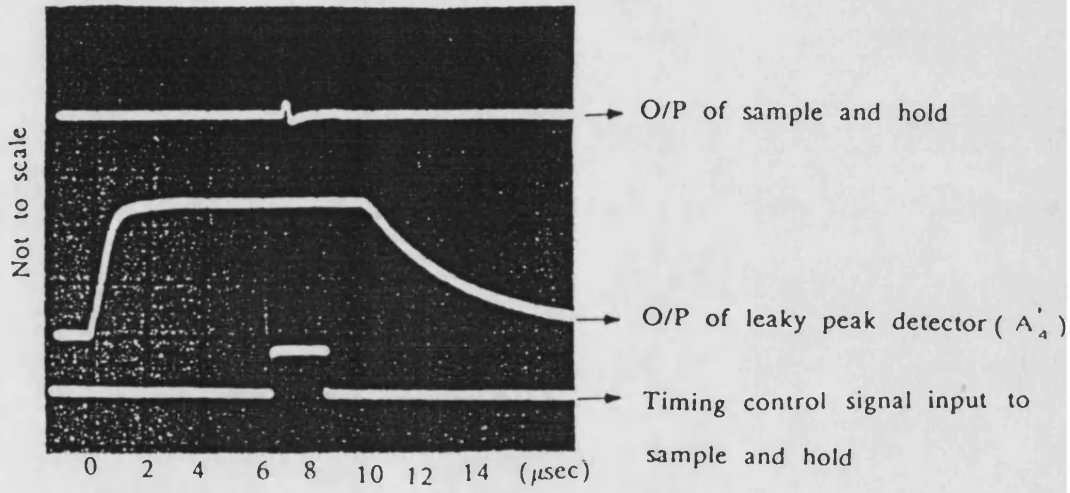

Figure 6.26 The outputs of different components in the maximum optical power control loop and the control signal to the sample and hold

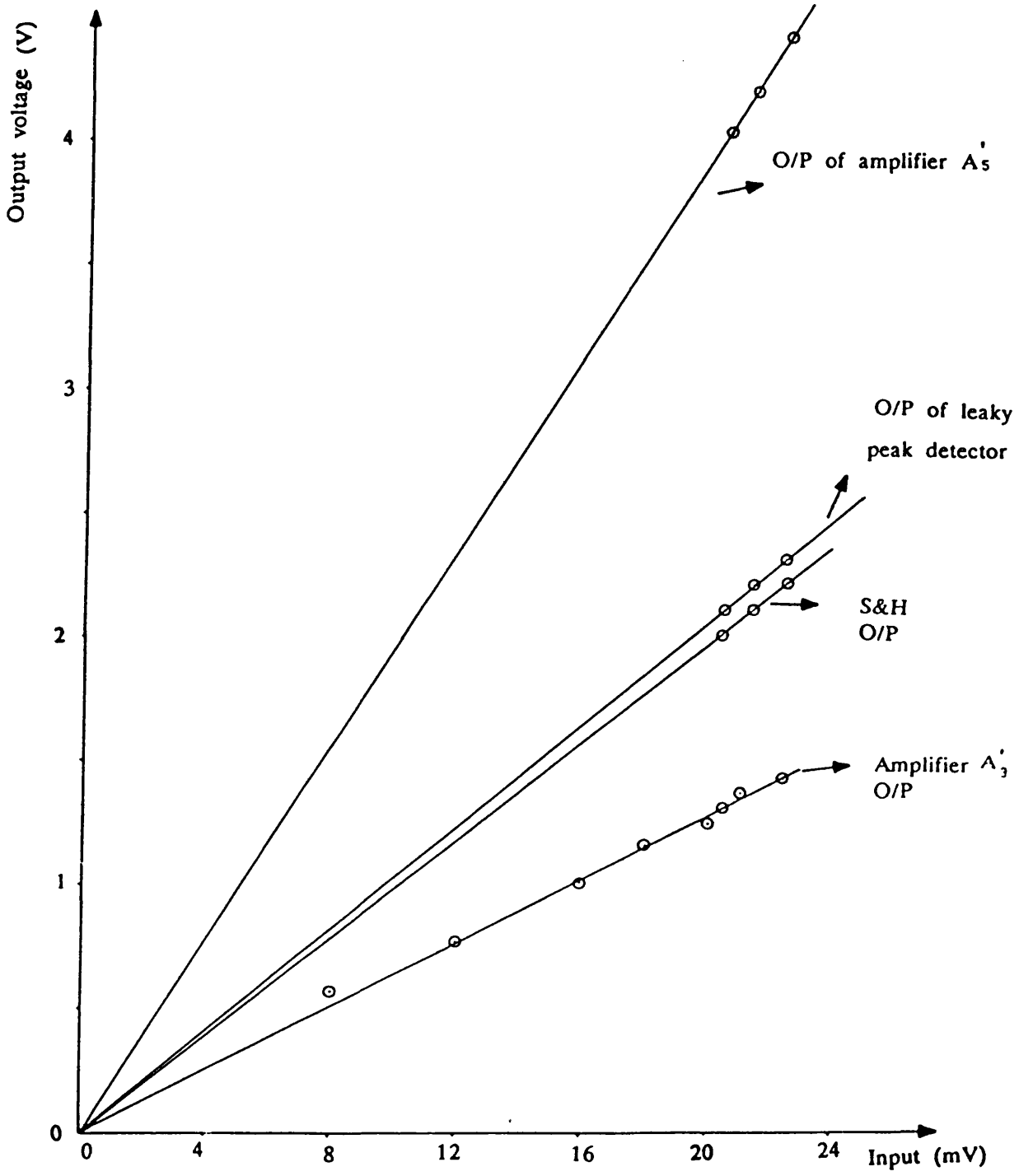

Figure 6.27 Relation between the input to the maximum power control loop and the outputs of different components

determined from the slopes of the lines illustrated in this figure; also the gain of the feedback network in this loop K_m can be determined from the slope of the line representing the output of the amplifier A'_5 which follows the sample and hold. The gain of the loop can be readjusted by changing the gain of the amplifier A'_4 which amplifies the output of the leaky peak detector or the amplifier A'_5 which follows the sample and hold. The effect of the reference voltage V_{mr} on the output of the driving amplifier A'_6 has also been examined. Figure 6.28 shows the variation of the output of the driving amplifier A'_6 with V_{mr} at different values of input. The slope of the obtained lines represent the gain of this amplifier which is found to be = 12. So the conductance of this amplifier is:

$$G_m = \frac{12}{68} = 0.176 \quad A/V$$

The gain of the feedback network K_m = 195.3 = 45.82dB.

The loop gain = $\eta_2 K_L K_m G_m$ = 2 x 195.3 x 0.176 = 68.7 = 36.75dB.

6.7.3 Testing the whole power control circuit and analysing its results

To connect the two power control loops to the LD drive circuit in order to verify that control is exerted, the following steps were taken:

1. The voltage applied to the base of the transistor Q_3 of the LD drive circuit, has been adjusted by the potentiometer arrangement such that the output average optical power required has been obtained. In this case, the average power has been adjusted such that $K_L L_{av}$ = 18.5mv at 20°C.

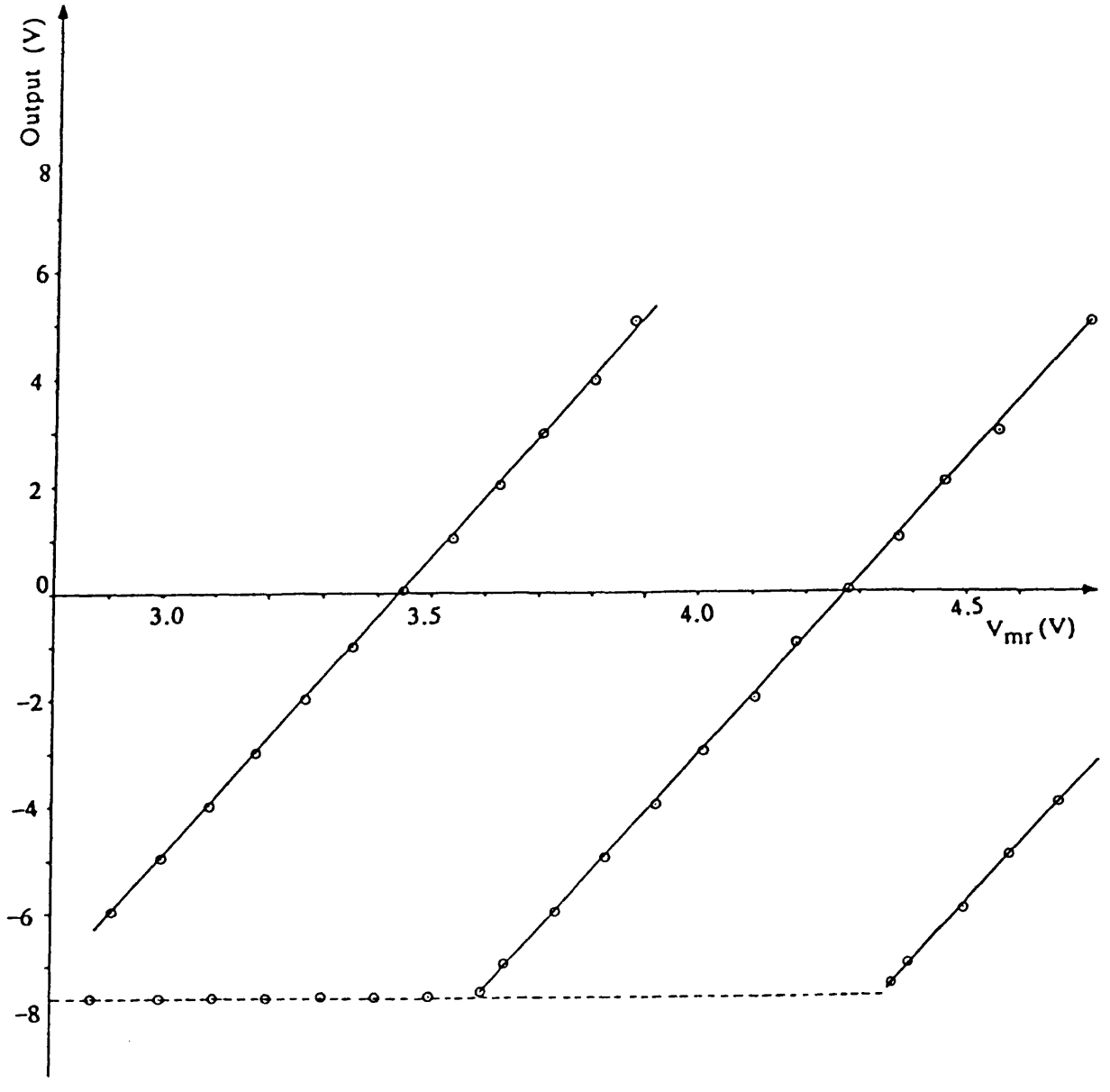

Figure 6.28 Relation between the reference voltage V_{mr} and the output of the driving amplifier A_6^*

2. The reference voltage V_{br} has been adjusted such that the output of the driving amplifier A_9 gives the same value of voltage applied to the base of the transistor Q_3 by the potentiometer. The value of V_{br} was 5.057V.

3. The voltage applied to the base of the transistor Q_6 of the LD modulation drive, has been adjusted by the potentiometer arrangement such that the maximum optical output power required has been obtained. In this case the maximum optical power has been adjusted such that $K_L L_{max}$ = 23.2mv at 20°C and the modulation rate was 100Mbit/s.

4. The reference voltage V_{mr} has been adjusted such that the output of the driving amplifier A_6' gives the same value of voltage applied to the base of the transistor Q_6 by the potentiometer. The value of V_{mr} was 4.158V.

5. The power supply to the LD has been switched off.

6. The bases of the transistors Q_3 and Q_6 have been disconnected from the potentiometer arrangement and a zener diode of breakdown voltage 6.2 volts and 3 volts have been connected respectively between the bases of Q_3, Q_6 and the power supply.

7. The power supply of -10V has been switched on.

8. The output of the driving amplifier A_9 has been connected to the base of Q_3, so the laser diode gives an average optical output power similar to that obtained when the potentiometer has been used.

9. The output of the driving amplifier A_6' has been connected to the base of Q_6, so the laser diode modulated optical output gives a maximum optical power similar to that obtained when the potentiometer has been used. From these previous steps it is found that control has been exerted.

6.7.3.1 Testing the performance of average power control loop

The average optical output power of LD is reduced if the threshold current is increased, but the threshold current increases exponentially as indicated by equation 5.8 in section 5.6.

To test the performance of this loop, the operating temperature of the LD is increased and its effect on the packet pulse drive current, required to keep the average optical output power constant, is investigated through carrying out the following experiment under the conditions in section 6.7.3.

1. The operating temperature of the LD has been increased.

2. The current I_{E_1} in the resistor R_{E_1} connected to the emitter of transistor Q_3 has been measured at different values of operating temperature as recorded by a digital thermometer.

3. The output of the LD has been measured at these temperatures.

4. A relation has been drawn between the operating temperature of the laser diode (T) and log I_{E_1}, as in Figure 6.29 where a straight line has been obtained.

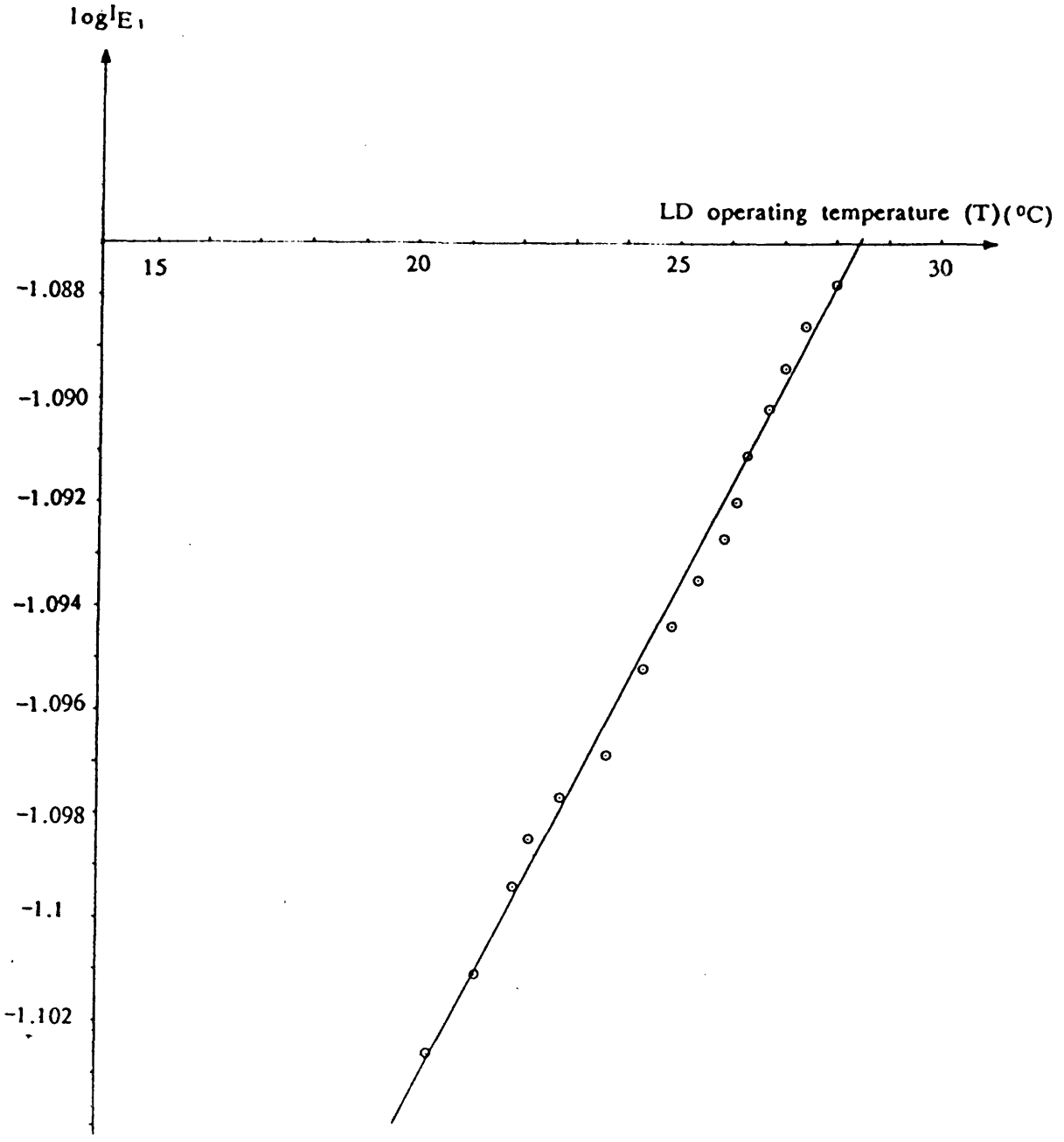

Figure 6.29 Relation between $\log I_{E,}$ and the LD operating temperature (T)

From analysing the results of this experiment it is found that the optical output of the LD is constant while the operating temperature is increasing, which indicates that the loop controls the current I_{E_1} in such a way that it compensates the effect of shift in threshold due to variation in temperature. Also the straight line obtained between log I_{E_1} and T indicates that this control loop drives the LD with a current that tracks the threshold current.

6.7.3.2 Testing the performance of the maximum power control loop

The maximum power control loop has a loop gain = $\eta_2 K_L K_m G_m$ as indicated by equation 6.22 in section 6.3.2. Hence the effect of changing (η_2) the stimulated slope efficiency of the LD can be simulated by changing K_L through changing the gain of the leaky peak detector slightly and investigate its effect on the modulation current. Hence, to test the performance of this loop the following experiment has been carried out, under the conditions described in section 6.7.3.

1. The input and ouput of the leaky peak detector have been measured at different values of reference voltage V_{mr} and in each case the current I_{E_2} in the resistor R_{E_2} connected to the emitter of Q_6 is measured.

2. The gain of the amplifier A_4' in the leaky peak detector is changed slightly and the previous step has been repeated.

3. A relation has been drawn between the input and the output of the leaky peak detector using the results obtained from the two previous steps. The straight lines shown in Figure 6.30 have been obtained. From the slopes of these lines the practical value of change in gain of the feedback network can be obtained.

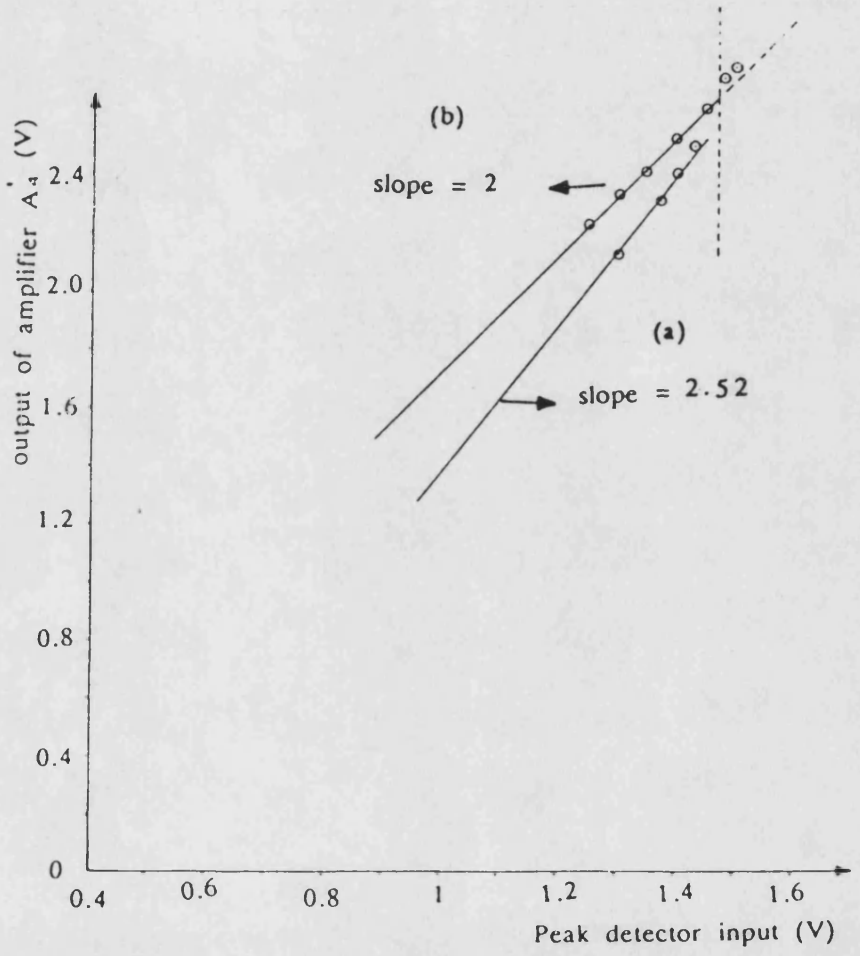

Figure 6.30 Relation between input and ouput of the leaky peak detector at two different values of gain for amplifier A_4'

Figure 6.30 shows that the gain of the leaky peak detector has been changed by a factor of 0.778 i.e. from 2.52 to 2 as indicated by the slopes of the lines (a) and (b) in this figure.

Figure 6.31 shows the variation of the modulation driving current I_{E_2} with the reference voltage v_{mr} at the two values of leaky peak detector gains 2.52 and 2 respectively.

4. A relation between the modulation driving current I_{E_2} and V_{mr} has been drawn at the two different values of gain, where straight lines shown in Figure 6.31 have been obtained.

In analysing the results of this experiment it is found that changing the gain in the loop slightly is similar to changing the value of the laser slope efficiency η_2. Decreasing the gain in the feedback loop gives a similar effect to the decrease of η_2, which makes the control circuit increase the modulation driving current at the same value of reference voltage, such that the maximum optical output amplitude remains constant.

From the lines shown in Figure 6.30 and 6.31 it is seen that decreasing the gain in the loop by a factor of 0.778 leads to the increase of current I_{E_2} by 2.57mA at the same value of reference voltage V_{mr} of 4.158V as seen from Figure 6.31. This increase in modulation current compensates for the simulated change in η_2 and keeps the maximum optical output power constant.

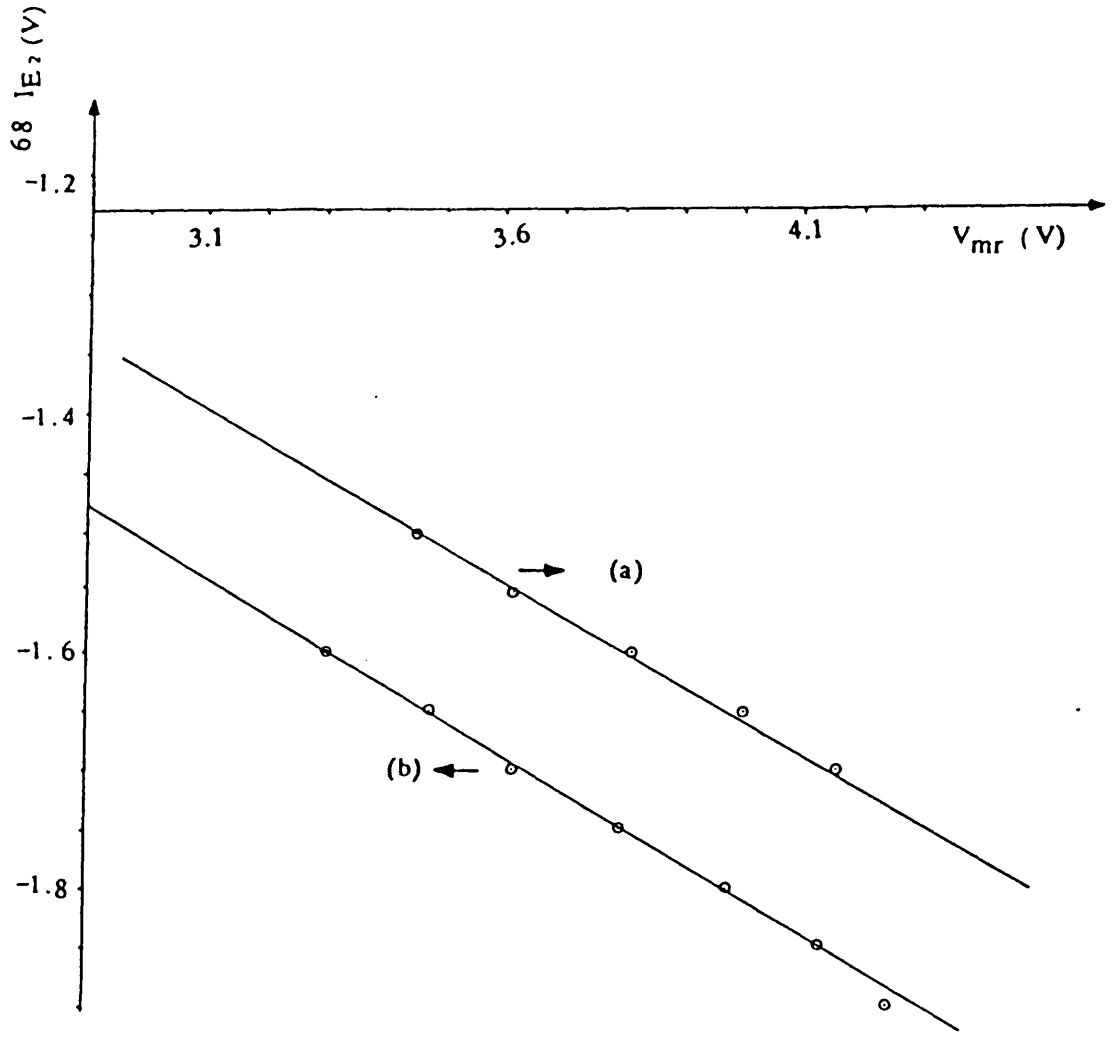

Figure 6.31 Relation between the reference voltage V_{mr} and the modulation driving current I_{E_2} at the two different values of gain of the amplifier A_4'

6.8 Conclusion

From the work done in this chapter a laser drive circuit that can drive the LD in a burst mode, together with the control circuit that stabilises the optical power emitted from the device were successfully designed and operated. Successful control was demonstrated. The control circuit has been tracked the change in threshold current of the LD when operated at different temperatures, and the circuit was shown to be capable of compensating for changes in the slope efficiency of the LD.

The laser drive circuit was capable of modulating the laser at bit rates ranging from 30 to 250 Mbit/s, so it can modulate the laser at a bit rate of 250Mbit/s allowing a maximum of nine consecutive ones in non return to zero code, with average value of 50%.

The optical output power from the LD has been stabilised by two independent feedback control loops. The first stabilises the average optical power through controlling the packet pulse drive current, and has a loop gain of 43.7dB; the second loop stabilises the maximum optical output power through controlling the modulation current and has a loop gain of 36.8dB. There are some limitations imposed on the control circuit concerning the time duration between packets, since there is a time required to reset the capacitors of the integrator, the peak to peak detector and the leaky peak detector which are present in these loops. In this application the time required to reset the integrator output to an accuracy of 0.1% was about 150μsec and the time to reset the peak to peak detector capacitors was adjusted to be of similar value, whereas for the leaky peak detector the discharging time constant was 3.5μsec. These limitations can be reduced by resetting the integrator using fast low-leakage FET switches.

The output of the integrator in the average power control loop is a function of packet length and it varies linearly for packet lengths up to 12μsec. Hence readjustment of the reference voltage in this loop is necessary if the packet length is required to be changed. If the packet length is required to be increased above 12μsec one must readjust the value of the feedback capacitor C_f in the integrator in order to maintain linearity. Also the presence of the high pass filter in the maximum power control loop, limits the minimum packet length to 4μsec.

In the maximum optical power control loop, the wideband amplifiers Mar3 and Mar8 are followed by the passive leaky peak detector which requires a minimum voltage of about 0.6V to turn its diode on, and therefore requires a minimum optical output amplitude of about 6mv. To handle lower level signals, the gain of the amplifier must be increased by choosing both amplifiers to be of the type Mar8 which has higher gain than Mar 3.

Finally, the outputs of the sample and hold in both loops contain a glitch during the sampling time. This glitch may drive the outputs of the difference driving amplifiers into saturation so fast recovery amplifiers must be used. In the maximum power control loop, this glitch affects the control since it is during the packet duration. Low pass filtering on the driving amplifiers has been used to remove the effect of the glitch but it also reduces the bandwidth in the loop.

To overcome this, two sample and hold in series can be used in the maximum power control loop such that the second sample and hold will sample the output of the first after the packet length. Hence removing the effect of the glitch during the packet duration, also fast recovering amplifier should be used.

6.9 References

6.1 A. Albanese: "An automatic bias control (ABC) circuit for injection lasers", Bell Sys. Tech. J., 57, pp1533-1544, March 1977.

6.2 P. G. Elisev, A. E. Krasil, N. Kove, M. A. Man'Ko and V. Pstrakhov: "Investigation of DC injection lasers", Physics of P-n Junctions and Semiconductor Devices, S. M. Ryvkin and Uyv. Skmartsev, eds, New York: Plenum, 1971, p150.

6.3 D. L. Rode and L. R. Dawson: "Differential I/V of heterostructure correlates with laser threshold", Appl. Phys. Lett., 21, pp90-93, 1st Aug. 1972.

6.4 P. A. Barnes and T. L. Paoli: "Current-voltage characteristics of double heterostructure injection lasers", IEEE J. Quant. Elec, QE-12, p633, October 1976.

6.5 S. T. Paoli: "Observation of second derivatives of the electrical characteristics of double heterostructure junction lasers", IEEE Trans. Electron. Devices, ED-23, p1333, December 1976.

6.6 T. L. Paoli and P. A. Barnes: "Saturation of the junction voltage in stripe-geometry (AℓGa)As double heterostructure junction lasers", Appl. Phys. Lett., 28, pp714-717, June 1976.

6.7 R. W. Dixon: "Derivative measurements of light-current-voltage characteristics of (Ga,Aℓ)As double heterostructure lasers", BSTJ, 55, No.7, p973, September 1976.

6.8 W. B. Joyce and R. W. Dixon: "Fundamental and harmonic response voltages of a sinusoidally-current modulated ideal semiconductor laser", J.Appl.Phys., 47, p3510, August 1976.

6.9 B. R. White and D. R. Smith: "injection Laser Stabilisation", United States patent (4,166,985).

6.10 M. Ettenberg, D. R. Patterson and E. J. Delinger: "A temperature compensated laser module for optical communications", RcA Rev., 40, pp103-114, June 1979.

6.11 D. W. Smith: "Laser level-control for high bit rate systems using a slope detector", Electron. Lett., 14, pp775-776, 1978.

6.12 M. Mouthaan and J. R. Schelecte: "140Mbit/s optical transmission system with 8Km repeater spacing and line section lengths of 96Km", presented at the 5th Euro. Conf. Opt. Commun., Amsterdam, The Netherlands, 1979.

6.13 D. W. Smith and T. G. Hodgkinson: "Laser level control for high bit rate optical fibre systems", presented at the 13th Int. Symp. Circuits Syst., Houston, Texas, 1980.

6.14 S. R. Salter, D. R. Smith, R. P. Webb and B. R. White: "Laser automatic level control circuits for optical communication systems", presented at the 3rd Euro. Conf. Opt. Commun., Munich, Germany, 1977.

6.15 F. S. Chen: "Simultaneous feedback control of bias and modulation currents for injection lasers", Electron. Lett., Vol.16, pp7-8, 1980.

6.16 R. E. Epworth: "Subsystems for high speed optical links", Proceedings of the Second European Conference on Optical Fibre Communication, Paris, pp337-382, 1976.

6.17 J. Gruber, P. Marten, R. Petschacher and P. Russer: "Electronic circuits for high bit rate digital fibre optic communication systems", IEEE Trans., 1978, COM-26, pp1088-1098.

6.18 F. S. Chen: "Simultaneous feedback control of bias and modulation currents for injection lasers", Electron. Letts., 16, No.1, pp7-8, 3rd January 1980.

6.19 R. G. Swartz and B. A. Wooley: "Stabilised biasing of semiconductor lasers", The Bell System Tech., J., 62, pp1923-1935, September 1983.

6.20 K. Yamashita et al: "Master-slice monolithic integration design and characteristics of LD/LED transmission systems", IEEE J. of Lightwave Tech., Vol.LT.4, No.3, p353, March 1986.

6.21 A. I. Zverev: "Handbook of Filter Synthesis", J. Wiley, N.Y., 1967.

CHAPTER 7

CONCLUSIONS AND FUTURE WORK

7.1 Conclusions

In a high bit rate laser transmitter, the laser has to be biased to eliminate delay, but biasing the laser in an optical fibre network which has several laser transmitters will introduce errors and impose restrictions on the receiver, so there is a need for a laser transmitter which operates in a burst mode, hence a laser diode drive circuit together with its power control circuitry has been designed, presented and tested and it has successfully provided packets of stabilised optical output. The packets have a width of 10μsec and the information can be sent in these packets at a rate up to 250Mbit/sec.

The laser transmitter which has been designed is suitable for a multiport optical fibre local area network (LAN) where transmitters operate alternately as in the star or bus configuration (chapter 1). A laser drive circuit which can drive the laser in a burst mode has been designed, tested and described in chapter 4. It consists of two stages, one to bias the laser during the packet duration, with a current up to the threshold current of the laser diode and the other to modulate the laser during the packet duration. Microcomputer circuit analysis program Mcapii has been used to perform the dc and ac analysis of the circuit, and it has been compared with the results obtained practically showing that the rise and fall times of the optical output pulse were about 1 nanosecond. Operating the laser in a burst mode requires a consideration of the transient heating effect. At the start of each packet the driving current increases, leading to a transient rise in temperature of the laser chip, and consequently a reduction in the optical output

power during the thermal rise time of the LD; hence, there is a requirement to measure the thermal rise time of the device (chapter 5).

A temperature control circuit has been implemented and tested with a dummy heat source, then used to maintain the LD operating temperature constant to an accuracy of 0.1 ^{o}C. This circuit, together with the laser drive circuit, has been used to draw the light–current characteristics at different temperatures, for the two laser diodes HL7801E and HL8311E.

The effect of temperature upon the current threshold of a laser has been discussed and measured, and I_{th} is shown to follow the expected form of an exponential function of temperature, but the slope efficiency does not change significantly. Using a family of light–current curves at different temperatures, it was possible to calculate the slope efficiency and the proportionality constant in the threshold current expression.

Making use of this information, a method has been described which enables the transient thermal response of a laser diode to be measured, giving an approximately exponential rise with time.

The laser diode HL8311E has a faster response, higher threshold and shorter thermal time constant than the diode HL7801DE, since it is designed for communication use. The measured thermal time constants are about 10ns and 40ns respectively. Assuming an approximately exponential rise of temperature, the diode temperature reaches to within 5% of the final value in a time of about 30ns and 120ns respectively. These figures represent 8 and 30 data symbols respectively, at a data rate of 250Mbit/s. Consequently, provided that due allowance is made for the higher signal level at the beginning of the received packet, there is no need to try and carry out temperature control of the laser diode within the packet time,

but it is very important to stabilise the optical output power of the LD against the effects of temperature and aging.

An automatic power control strategy, that is suitable to control the optical output power of a laser diode operating in a burst mode, has been presented, analysed and used to stabilise the optical output power of the laser diode (chapter 6).

The power control strategy is based on using two independent feedback control loops to maintain the average and maximum optical power L_{av} and L_{max} constant during the packet duration.

In the analysis of power control three strategies have been considered (section 6.3). Firstly, to bias the laser at the base of the modulation, but with this method it is difficult to achieve control and maintain it. Secondly, to bias the laser at the midpoint of the modulation, using the measurement of L_{av} to control the bias current and $(L_{max}-L_{av})$ to control the modulation current. This leads to two control loops which depend on each other. Finally, this last strategy has been improved by using L_{av} to control the packet pulse bias current and L_{max} to control the modulation current. This final strategy has been achieved by designing a drive circuit which can drive the laser in a burst mode with the packet pulse bias current above threshold and at the midpoint of modulation. This circuit has been implemented and tested, and was able to modulate the laser at bit rates ranging from 30 to 250Mbit/s. Hence allowing a maximum of 9 consecutive ones, in non return to zero code, at bit rate of 250Mbit/s to be transmitted.

The automatic power control circuit has been implemented with two feedback control loops. The first loop stabilises L_{av} through controlling the packet pulse drive current. L_{av} is measured through low pass filtering the output of a PIN

monitor photodetector, integrating, then measuring the peak to peak output of the integrator which is proportional with L_{av}. By sampling this value and comparing it with a reference, the result is used to adjust the next packet bias current. This loop has a loop gain of 43.7dB. The second control loop stabilises L_{max} through controlling the modulation current. In this loop a measure for the average maximum optical output power is obtained through wideband amplification, and detecting the average maximum using a leaky peak detector; then by sampling and comparing with a reference, the result is used to adjust the modulation current for the next packet. This loop has a loop gain of 36.8dB.

The power control circuit performance has been tested and proved to be capable of stabilising the average value of optical power during the packet duration and was tracking the changes in threshold current of the LD and compensating for it. Also it proved to be compensating for changes in the stimulated slope efficiency of the LD through stabilising the maximum optical power by controlling the modulation current.

There are some limitations imposed on the circuit concerning the packet duration and the period elapsed between packets.

In the average power control loop the output of the integrator is a function of packet length and it provides a good linearity up to 12μsec. Hence readjustment of the gain in the loop and the reference voltage is necessary if the packet length is required to be changed, but if the packet length is required to be increased above 12μsec one must readjust the value of the feedback capacitor C_f in the integrator in order to maintain linearity. The presence of the high pass filter in the maximum power control loop, limits the minimum packet length to 4μs.

Concerning the time duration between packets, it depends on the time

required to reset the capacitors of the integrator, the peak to peak detector and the leaky peak detector. In this application the integrator has a resistor in parallel with its feedback capacitor C_f, allowing it to reset the integrator output to an accuracy of 0.1% in a time of about 150μsec. A similar time has also been allowed to reset the peak to peak detector by FET switches, whereas the leaky peak detector capacitor discharging time constant was 3.5μs. To reduce the time duration between packets the integrator has to be reset by a low leakage fast FET switch.

In the maximum optical power control loop, the wideband amplifiers are followed by the passive leaky peak detector which requires a minimum voltage of about 0.6V to turn its diode on, and therefore requires a minimum optical output amplitude of about 6mv. In order to handle lower level signals the gain of the wideband amplifiers has to be increased.

Finally, the outputs of the sample and hold in both loops contain a glitch during the sampling time. This glitch may drive the outputs of the difference driving amplifiers into saturation, so fast recovery amplifiers must be used. In the maximum power control loop, this glitch affects the control since it occurs during the packet duration. Low pass filtering on the driving amplifiers has been used to remove the effect of the glitch but this also reduces the bandwidth in the loop.

To overcome this, two sample and hold in series can be used in the maximum power control loop, such that the second sample and hold will sample the output of the first after the end of the packet, hence removing the effect of the glitch during the packet duration. A fast recovery amplifier should also be used.

7.2 Future Work

The aim of this work was to modulate the semiconductor laser in a burst mode, at high bit rates, and investigate the heating effects in this mode as well as stabilising its optical output power against the effects of temperature and aging.

In the course of this work the aim has been achieved, but there are some points which need further investigation and points which need to be tackled to reduce the limitations imposed on the circuit. In any future work these points can be considered:

a) In this work the data is considered to have an average value of 50% using non return to zero code.

   If the duty ratio of the data has to be changed it will produce an error in the average value measured by the integrator in the average power control loop. In this loop the first order low pass filter attenuates the data pulses but still allows some amplitude ripples which increase with long sequences of ones or zeros, consequently affecting the average value measured by the integrator. To overcome this a higher order low pass filter can be used instead of the first order, hence producing more attenuation to the modulation pulses and reducing their affect on the measured average value of optical output power during the packet duration.

b) The extinction ratio of the data depends on the values of average and maximum optical power chosen. To achieve low extinction ratio, the reference voltages in the average and maximum power control loop should be chosen carefully. The effect of changing the stimulated slope

efficiency and the threshold current of the LD on the extinction ratio can be investigated.

c) The performance of the sample and hold circuits in the average and maximum power control loops show that there is a glitch in each output during the sampling time. In the maximum power control loop this glitch is during the packet duration and it will affect the control. In this experimental work the glitch has been removed by low pass filtering on the amplifiers following the sample and hold which reduces the bandwidth in the loop. To overcome this, two sample and hold in series can be used in this loop; the first samples the output of the leaky peak detector and the second samples the output of the first after the packet duration, hence transferring the glitch after the packet length so it will not affect the control, also fast recovery amplifier should be used following the sample and hold.

The sample and hold circuits could also be replaced by A/D and D/A converters which can measure the output of the peak detectors during the packet duration (10μsec).

d) If the laser diode is operated without temperature control, the temperature of the device will rise from cold in the starting up operation leading to a change in the threshold current between packets. These starting up transients need to be investigated.

APPENDIX I

ANALYSIS OF THE CURRENT MODE SWITCH

The current-mode switch shown in Figure I.1 is the decision element in an emitter coupled logic (EcL) gate. It is a difference amplifier used in a large signal mode, where a constant reference voltage V_R is applied to the base of the transistor Q_2 and the input signal V_i is applied to the base of the transistor Q_1. The biasing conditions at the bases of the transistors Q_1 and Q_2 are adjusted such that Q_1 is normally on and Q_2 is off and the transistors operate in the active region, so when the high level of the input pulse is applied it turns Q_3 off and Q_2 on and when the low level of the input pulse is applied it turns Q_1 on and Q_2 off, during this process a current I_E is switched between Q_1 and Q_2; this process is carried out in a very short time because the biasing condition is adjusted such that the transistors operate in the active region and do not saturate. From Figure I.1 the current:

$$I = I_{E_1} + I_{E_2} \qquad I.1$$

$$V_i = V_R + V_{BE_1} - V_{BE_2}$$

$$= V_R + V_T \ell n \left[\frac{I_{E_1}}{I_{E_2}}\right] \qquad I.2$$

where V_T is the thermal voltage.

The current gain of the transistor is assumed to be large so that $I_C \simeq I_E$ and the transistors are not in the saturation region.

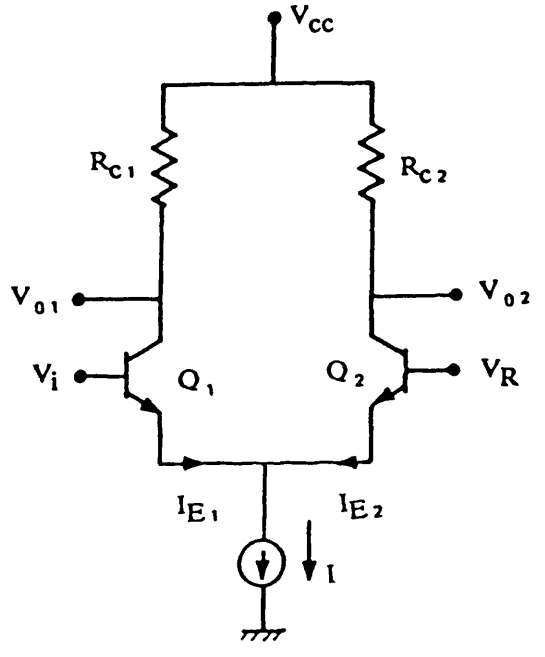

Figure I.1 Current Mode Switch

The output voltage at the collector of the transistor Q_2 is:

$$V_{02} = V_{CC} - I_{C2} R_{C2} \qquad I.3$$

and the output voltage at the collector of Q_1 is:

$$V_{01} = V_{CC} - I_{C1} R_{C1} \qquad I.4$$

From equations I.2, I.3 and I.4 and the relation between V_{BE_1} and I_{E_1}, V_{BE_2} and I_{E_2}, we get:

$$V_{02} = V_{CC} - \frac{\alpha_n I R_{C2}}{1 + \exp\left[\frac{V_i - V_R}{V_T}\right]} \qquad I.5$$

$$V_{01} = V_{CC} \frac{\alpha_n I R_{C1} \exp\left[\frac{V_i - V_R}{V_T}\right]}{1 + \exp\left[\frac{V_i - V_R}{V_T}\right]} \qquad I.6$$

where $I_{C2} = \alpha_n I_{E2}$, $I_{C1} = \alpha_n I_{E1}$.

when $V_i << V_R$, the output voltage V_{02} approaches the lower logic level V_2.

$$V_{02} = V_{CC} - \alpha_n I R_{C2} = V_L$$

and the output voltage V_{01} approaches the upper logic level V_u.

$$V_{01} = V_{CC} = V_u$$

The logic swing, which is the difference between the two logic levels, is:

$$V_l = V_u - V_L \qquad I.7$$

The transistor Q_1 enters its active region as V_i is increased causing I_{C_2} to decrease and V_{02} to increase, because I is constant.

When $V_i = V_R$ the exponentials are unity and if:

$$R_{C_1} = R_{C_2} = R_C$$

$$V_{01} = V_{02} = V_{th} = V_{CC} - \frac{\alpha_n I R_C}{2} \qquad I.8$$

where V_{th} is the output of the current-mode switch at the threshold point. The threshold point for this decision element is equidistant from the two assymptotic output levels and the input voltage swing is symmetric about this point as shown in Figure I.2. In this case the logic swing:

$$V_l = \alpha_n I R_C$$

$$V_{th} = V_{CC} - \frac{V_l}{2}$$

V_{01}, V_{02} can be written in terms of the threshold voltage and the logic swing:

$$V_{01} = V_{th} + \frac{V_l}{2} \tanh \left[\frac{V_i - V_R}{2V_T}\right] \qquad I.9$$

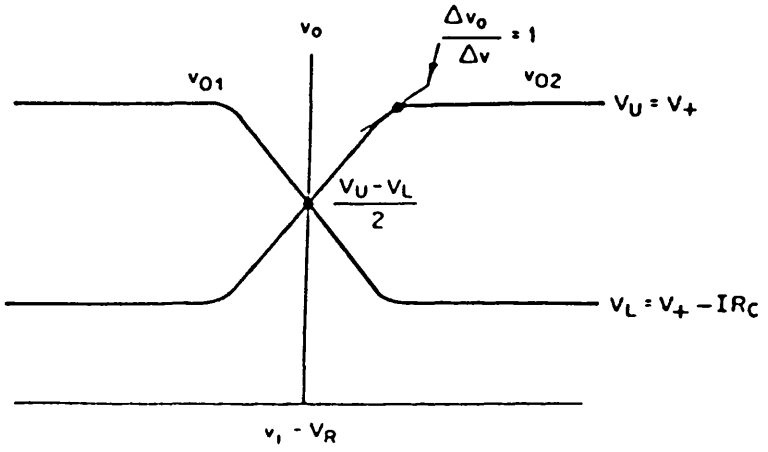

Figure I.2 Transfer characteristic of current mode switch

$$V_{02} = V_{th} - \frac{V_1}{2} \tanh\left[\frac{V_i - V_R}{2V_T}\right] \qquad \text{I.10}$$

The logic swings can differ on opposite sides of the switch if the load resistors are not of equal values. When $V_i = V_R$ both transistors are in the active region so the gain is large and slight changes in V_i result in large changes in V_0. The incremental gain (dV_0/dV_i) is given by:

$$\frac{dV_0}{dV_i} = \frac{V_{12}}{V_T} \cdot \frac{\exp\left[\frac{V_i - V_R}{V_T}\right]}{1 + \exp\left[\frac{V_i - V_R}{V}\right]^2} \qquad \text{I.11}$$

where $V_{12} = \alpha_n I R_{C2}$ is the logic swing at output 2. When V_i is very negative or very positive the incremental gain approaches zero. When the gain is less than unity the circuit is passive, whereas when the gain exceeds unity the circuit is active, therefore the location of the unity gain points is of great interest. To find the unity gain point put the slope of the transfer characteristic curve

$$\frac{dV_0}{dV_i} = 1$$

in equation I.11 so the input voltage corresponding to the unity gain is:

$$V_{ug} = V_R \pm \ell n \left[\frac{V_{12}}{V_T}\right] \qquad \text{I.12}$$

The input voltage difference between the operating point and the nearest unity gain point is the noise margin of the switch.

APPENDIX II

EFFECT OF ZENER DIODE IN SUPPRESSING THE CURRENT SPIKES IN LD DRIVE CIRCUIT

In case of connecting a zener diode of breakdown voltage V_z and dynamic slope resistance r_s, across the terminal of the potentiometer R_5 in the LD drive circuit illustrated previously in Figure 4.8. The current in the resistor R_6 is given by:

$$I = (V - V_z)/R_6 \qquad \text{II.1}$$

where V is the power supply voltage.

If V changes to V' then V_z will change slightly to V_z' and the current becomes:

$$I' = (V' - V_z')/R_6 \qquad \text{II.2}$$

Hence the change in current is:

$$I' - I = \frac{(V' - V)}{R_6} - \frac{(V_z' - V_z)}{R_6} \qquad \text{II.3}$$

but this is nearly the change in current of the zener diode, so:

$$I' - I = \frac{(V_z' - V_z)}{r_s} \qquad \text{II.4}$$

where r_s is the dynamic slope resistance of the zener substituting from II.4 in II.3, then:

$$\frac{(V_Z' - V_Z)}{r_s} = \frac{(V' - V)}{R_6} - \frac{(V_Z' - V_Z)}{R_6} \qquad \text{II.5}$$

Therefore:

$$(V_Z' - V_Z) = (V' - V) \cdot \frac{1}{R_6/r_s + 1} \qquad \text{II.6}$$

the smaller the value of r_s the smaller the change in the zener voltage.

The corresponding change in the voltage of the base of the transistor Q_3 is:

$$(V' - V) \frac{1}{R_6/r_s + 1} \cdot \frac{R_X}{R_5} \qquad \text{II.7}$$

The corresponding change in the current (I_E) in the resistor R_E is:

$$I_E' - I_E = \frac{R_X}{R_5 R_E \left[\frac{R_6}{r_s} + 1\right]} (V' - V) \qquad \text{II.8}$$

so the change in current per volt can be calculated.

APPENDIX III

STABILITY ANALYSIS OF LASER DIODE TEMPERATURE CONTROL CIRCUIT

When the feedback loop of the temperature control circuit in Figure 5.9 is closed, there is a possibility that the transient response may be oscillatory. The following analysis shows that this is not so.

Referring to the circuit of Figure 5.9, the transfer function of the comparator and power amplifier is

$$G_1(s) = \frac{A}{s\tau_c + 1} \qquad \text{III.1}$$

where $1/\tau_c$ is the finite bandwidth of the comparator and A is the gain of the power amplifier.

Also, the transfer function of the thermal block which is driven by the peltier pump is

$$G_2(s) = \frac{g_b}{s\tau_b + 1} \qquad \text{III.2}$$

where g_b is a thermal constant for the block and $1/\tau_b$ is its finite bandwidth. Figure III.1 shows the signal flow diagram of this circuit. From this figure the temperature of the copper block is given by:

$$T = [G_1(s)\ R_p\ G_2(s)]\ [V_R - K_T] \qquad \text{III.3}$$

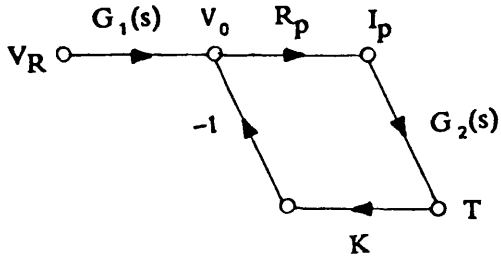

Figure III.1 Signal flow graph for LD temperature control circuit of Figure 5.9

where R_p is the peltier pump resistance and K is the temperature sensor calibration constant.

$$\frac{T}{V_R} = \frac{G_1(s)\, R_p\, G_2(s)}{1 + KG_1(s)\, R_p\, G_2(s)}$$

$$= \frac{A\, R_p\, g_b}{(s\tau_c + 1)(s\tau_b + 1) + 1 + K\, A\, R_p\, g_b} \qquad \text{III.4}$$

From the results obtained in section 5.5.2, τ_c = 15ms, A = 70, R_p = 2Ω, g_b = 10°C/A, τ_b = 120sec and K = 33.5mv/°C. Then the denominator of equation III.4 becomes:

$$s^2 + 66.7S + 26.6$$

so there are poles at −66.3, −0.4 which indicate that the response is first order with a dominant pole at s = −0.4 and a time constant of 2.5sec.

APPENDIX IV

Type	Typical threshold current (mA)	Maximum optical power output (mW)	Peak wavelength (nm)	Rise and fall times (ns)	Maximum reverse voltage (Volts)
HL7801E	60	5	780	-	2
HL8311E	60	15	830	0.5	2

Data of Laser Diodes HL7801E and HL8311E

Type	Reverse voltage (Volts)	Voltage (Volts)	Responsivity	Rise and fall times (ns)	Wavelength (nm)
PIN MFOD1100	5	50	0.35A/W	1	815
APD LR103	156.7	161.3	250V/W	0.050	904

Data of Photodiode of the Type MFOD1100 and APD of the Type LR103

APPENDIX V

LD CONTROL LOOPS STABILITY

Considering the LD average power control loop which is sampled in nature, as shown in Figure V.1, where sampling switch operates when pulse is transmitted. Consider regular pulses of period T_p, then the output occurs at times nT_p. Light output at time $t = nT_p$, depends on the received light output at $t = (n-1)T_p$. Hence:

$$L_0(nT_p) = \eta_2 G_b[V_{br} - K_L K_a L_0(n-1)T_p] - I_{th}\,\eta_2 \qquad V.1$$

and in terms of z transform

$$L_0(z) = \frac{\eta_2[V_{br}G_b - I_{th}]}{1 + \eta_2 G_b K_L K_a . z^{-1}} \qquad V.2$$

Now, for stability, $\eta_2 G_b K_L K_a < 1$ which violates the requirement for good parametric control of laser output as shown in section 6.4.2.

However, placing a simple low pass filter on amplifier A_9 (see Figure 6.19) can control this instability. For the low pass filter of this form (see Figure 6.11) its transfer function

$$H(f) = \frac{R_L}{R'} \frac{1}{1 + j\omega\tau} \qquad V.3$$

where $\tau = R_L C_L$

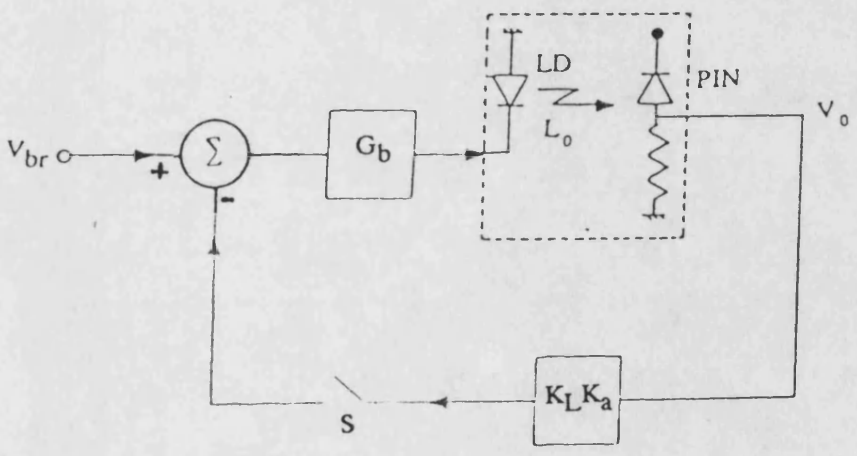

Figure V.1 Illustration of the LD average power control loop

Now, when sampler operates, a step signal is applied to the filter. If $\tau >$ T_p, then the step error signal is reduced by T_p/τ, and the loop gain becomes effectively

$$(\eta_2 G_b K_L K_a) \frac{T_p}{\tau}$$

For $T_p = 200\mu$sec and the values of the capacitor and resistor used practically (see Figure 6.19).

$$\frac{T_p}{\tau} = \frac{200 \times 10^{-6}}{2.7 \times 10^{-9} \times 3.3 \times 10^{6}} = 0.022 \qquad \text{V.4}$$

This leads to an average power control loop gain of $\simeq 3$ and a maximum power control loop gain $\simeq 1.5$.

The values for t were obtained experimentally and seen to agree approximately with those of theoretical calculations, the discrepancy is no doubt due to experimental error, or the combination effects of other capacitors in the closed loop. Although the transient response of the loops has been stabilised in this way, the long term control of LD parameters is still obtained.

APPENDIX VI

EFFECT OF FINITE GAIN, FINITE INPUT IMPEDANCE AND FINITE BANDWIDTH OF OPERATIONAL AMPLIFIER ON INTEGRATOR

Practically, the operational amplifier used in integrator has a finite gain, finite input resistance and finite bandwidth. Considering the circuit of the integrator shown in Figure VI.1:

$$(e(s) - v_i(s))\frac{1}{R} = \left[V_i(s) - V_0(s))\, S'_{CF} + \frac{V_i(s)}{R_i}\right] \qquad \text{VI.1}$$

but the amplifier gain A:

$$A = \frac{-V_0(s)}{V_i(s)} \qquad \text{VI.2}$$

From VI.1 and VI.2:

$$\left[e(s) + \frac{V_0(s)}{A}\right]\frac{1}{R} = \left[\frac{-V_0(s)}{A} - V_0(s)\right] SC - \frac{V_0(s)}{AR_i}$$

$$e(s) = -RSC\left[\frac{V_0(s)}{A} + V_0(s)\right] - \frac{V_0(s)R}{AR_i} - \frac{V_0(s)}{A}$$

Therefore:

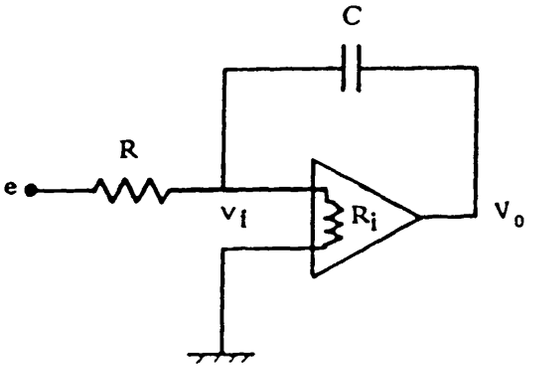

Figure VI .1 Operational Integrator

$$e(s) = -RCS\left[\frac{1}{AR_pSC} + \frac{1}{A} + 1\right] V_0(s) \qquad \text{VI.3}$$

where:

$$\frac{1}{R_p} = \frac{1}{R_f} + \frac{1}{R}$$

$$\frac{V_0(s)}{e(s)} = -\frac{1}{RCS}\left[\frac{1}{AR_pCS} + \frac{1}{A} - 1\right]^{-1} \qquad \text{VI.4}$$

considering the amplifier has a finite bandwidth ($^1/_T$), cutting off at 6dB/octave, and A_0 is the zero frequency gain of the amplifier, then the response of the amplifier can be expressed as:

$$A(s) = \frac{A_0}{1 + TS} \qquad \text{VI.5}$$

substituting from VI.5 in VI.4< then:

$$\frac{V_0(s)}{e(s)} = -\frac{1}{RCS}\left[1 + \frac{1}{A_0} + \frac{1}{A_0R_pCS} + \frac{TS}{A_0} + \frac{T}{A_0R_pCS}\right]^{-1} \qquad \text{VI.6}$$

For $A_0 \gg 1$ and $A_0 \gg \frac{1}{R_pC}$, then:

$$\frac{V_0(s)}{e(s)} = -\frac{1}{RCS}\left[1 + \frac{S}{A_0/T} + \frac{1}{A_0R_pCS}\right]^{-1} \qquad \text{VI.7}$$

putting $\frac{A_0}{T} = \omega_T$ as in Figure VI.2.

$$\frac{V_0(s)}{e(s)} = -\frac{1}{RCS}\left[1 + \frac{S}{\omega_T} + \frac{1}{A_0 R_p C_F S}\right]^{-1} \qquad \text{VI.8}$$

The effect of the finite bandwidth $^1/_T$ may be seen by examining equation VI.8.

At high frequency for $S \gg \frac{1}{A_0 R_p C}$, we have:

$$\frac{V_0(s)}{e(s)} = -\frac{1}{RCS}\left[1 + \frac{S}{\omega_T}\right]^{-1}$$

$$= -\frac{\omega_T}{RCS} \cdot \frac{1}{(S + \omega_T)} \qquad \text{VI.9}$$

If $e_{in}(t) = -U(t)$, the unit step function, and since the transform of U(t) is $^1/_S$, we get:

$$V_0(s) = \frac{\omega_T}{RCS^2} \cdot \frac{1}{S + \omega_T} \qquad \text{VI.10}$$

$$V_0(t) = \frac{1}{RC\omega_T}\left(e^{-\omega_T t} + \omega_T t - 1\right) \qquad \text{VI.11}$$

The relation between $V_0(t)$ and (t) from equation VI.11 is illustrated previously in Figure 6.13a. For small t we get the curved response due to the term

$$(e^{-\omega_T t} - 1)$$

after a time of the order $(1/\omega_T)$ the exponential decays and we have from equation VI.11:

$$V_0(t) = \frac{1}{RC}\left[t - \frac{1}{\omega_T}\right] \qquad \text{VI.12}$$

in this case $V_0(t)$ run parallel to the ideal response,

$$\left[V_0(t) = \frac{1}{RC}\, t\right],$$

so the output lags by an amount dependent on the unity gain bandwidth ω_T but not on R or C.

Also, at low frequency when $S << \omega_T$, equation VI.8 becomes:

$$\frac{V_0(s)}{e(s)} = -\frac{1}{RCS}\left[1 + \frac{1}{A_0 R_p CS}\right]^{-1}$$

$$\frac{V_0(s)}{e(s)} = -\frac{A_0 R_p}{R(1 + A_0 R_p CS)} \qquad \text{VI.13}$$

if we apply a unit step function:

$$V_0(s) = \frac{A_0 R_p}{R(1 + A_0 R_p CS)}$$

$$= \frac{A_0 R_p}{R R_p A_0 C} \cdot \frac{1}{S(S + 1/A_0 R_p C)} \qquad \text{VI.14}$$

or in time domain:

$$V_0(t) = \frac{A_0 R_p}{R} [1 - \exp - (t/A_0 R_p C)] \qquad \text{VI.15}$$

$$= \frac{A_0 R_p}{R} \left[1 - 1 + \frac{t}{A_0 R_p C} - \frac{t^2}{1 A^2 R^2 C^2}\right]$$

$$V_0(t) = \left[\frac{t}{RC} - \frac{t^2}{2A^0 RCR_p C}\right] \qquad \text{VI.16}$$

The first term ($^t/_{RC}$) in equation III.16 represents the ideal response as previously shown in Figure 6.13b, while the second term represents the error due to the finite gain, it increases with the square of time, for a time long compared with $A_0 R_p C$, the exponential term in equation VI.15 becomes negligible and:

$$V_0(t) = \frac{A_0 R_p}{R} \qquad \text{VI.17}$$

as illustrated previously in Figure 6.13b.